Final Report

THE USE OF COMPLEX MODULUS TO CHARACTERIZE THE PERFORMANCE OF ASPHALT MIXTURES AND PAVEMENTS IN FLORIDA

UF Project No.: 4910-4504-784-12

Contract No.: BC-354, RPWO #22

Submitted to:

Florida Department of Transportation
605 Suwannee Street
Tallahassee, FL 32399

UNIVERSITY OF FLORIDA

Bjorn Birgisson
Reynaldo Roque
Jaeseung Kim
Linh Viet Pham
Department of Civil and Coastal Engineering
College of Engineering
365 Weil Hall, P.O. Box 116580
Gainesville, FL 32611-6580
Tel: (352) 392-9537 SunCom: 622-9537
Fax: (352) 392-3394

September 2004

Technical Report Documentation Page

1. Report No.: l Report

2. Government Accession No.

3. Recipient's Catalog No.

4. Title and Subtitle

THE USE OF COMPLEX MODULUS TO CHARACTERIZE THE PERFORMANCE OF ASPHALT MIXTURES AND PAVEMENTS IN FLORIDA

5. Report Date: September 2004

6. Performing Organization Code

7. Author(s)

Bjorn Birgisson, Reynaldo Roque, Jaeseung Kim, and Linh Viet Pham

8. Performing Organization Report No.: 4910-4504-784-12

9. Performing Organization Name and Address

University of Florida
Department of Civil and Coastal Engineering
365 Weil Hall / P.O. Box 116580
Gainesville, FL 32611-6580

10. Work Unit No. (TRAIS)

11. Contract or Grant No.: BC 354, RPWO #22

12. Sponsoring Agency Name and Address

Florida Department of Transportation
Research Management Center
605 Suwannee Street, MS 30
Tallahassee, FL 32399

13. Type of Report and Period Covered: Final Report, August 22, 2000 – Feb 15, 2003

14. Sponsoring Agency Code

15. Supplementary Notes

Prepared in cooperation with the Federal Highway Administration

16. Abstract

The AASHTO 2002 flexible pavement design guide uses complex modulus as an input parameter for its performance models. A comprehensive project was undertaken to develop complex modulus capabilities in compression, torsion, and tension for Florida. Research was performed to evaluate how well the AASHTO 2002 proposed predictive dynamic modulus equation works for Florida mixtures. The results showed that the proposed predictive equation for dynamic modulus appears to work well for Florida mixtures. Potential relationships between the complex modulus and the rutting performance of mixtures were evaluated. No discernable relationship between complex modulus and rutting was established for mixtures of varying gradations and aggregate structure. Methods that can be used to obtain creep properties from complex modulus measurements as input into the Florida Hot Mix Asphalt Fracture Mechanics Model were evaluated. For the range of frequencies typically employed in dynamic modulus testing, it may not be possible to obtain creep compliance and creep compliance parameters accurately from dynamic measurements. However, an approach was developed for determining creep compliance parameters accurately from a combination of complex modulus and static creep tests. The effects of aggregate size distributions on the complex modulus were evaluated. A significant effect of gradation was found on dynamic modulus measurements. In conclusion, the complex modulus should generally neither be used to determine rutting or fracture resistance of mixtures. The primary use for the complex modulus test is to determine the stiffness of mixtures for purposes of determining the response to traffic loading, as per the new AASHTO 2002 flexible pavement design guide.

17. Key Words

Complex modulus, dynamic modulus, hot mix asphalt (triaxial testing, torsional shear testing, tensile testing) creep compliance

18. Distribution Statement

No restrictions. This document is available to the public through the National Technical Information Service, Springfield, VA, 22161

19. Security Classif. (of this report)	20. Security Classif. (of this page)	21. No. of Pages	22. Price
Unclassified	Unclassified	298	

Form DOT F 1700.7 (8-72)

DISCLAIMER

SI* (MODERN METRIC) CONVERSION FACTORS

APPROXIMATE CONVERSIONS TO SI UNITS

Symbol	When You Know	Multiply By	To Find	Symbol
		LENGTH		
in	inches	25.4	millimeters	mm
ft	feet	0.305	meters	m
yd	yards	0.914	meters	m
mi	miles	1.61	kilometers	km
		AREA		
in^2	square inches	645.2	square millimeters	mm^2
ft^2	square feet	0.093	square meters	m^2
yd^2	square yards	0.836	square meters	m^2
ac	acres	0.405	hectares	ha
mi^2	square miles	2.59	square kilometers	km^2
		VOLUME		
fl oz	fluid ounces	29.57	milliliters	ml
gal	gallons	3.785	liters	l
ft^3	cubic feet	0.028	cubic meters	m^3
yd^3	cubic yards	0.765	cubic meters	m^3
NOTE: Volumes greater than 1000 l shall be shown in m^3.				
		MASS		
oz	ounces	28.35	grams	g
lb	pounds	0.454	kilograms	kg
T	short tons (2000 lb)	0.907	megagrams	Mg
		TEMPERATURE (exact)		
°F	Fahrenheit temperature	5(F-32)/9 or (F-32)/1.8	Celcius temperature	°C
		ILLUMINATION		
fc	foot-candles	10.76	lux	l
fl	foot-Lamberts	3.426	candela/m^2	cd/m^2
		FORCE and PRESSURE or STRESS		
lbf	poundforce	4.45	newtons	N
psi	poundforce per square inch	6.89	kilopascals	kPa

APPROXIMATE CONVERSIONS FROM SI UNITS

Symbol	When You Know	Multiply By	To Find	Symbol
		LENGTH		
mm	millimeters	0.039	inches	in
m	meters	3.28	feet	ft
m	meters	1.09	yards	yd
km	kilometers	0.621	miles	mi
		AREA		
mm^2	square millimeters	0.0016	square inches	in^2
m^2	square meters	10.764	square feet	ft^2
m^2	square meters	1.195	square yards	yd^2
ha	hectares	2.47	acres	ac
km^2	square kilometers	0.386	square miles	mi^2
		VOLUME		
ml	milliliters	0.034	fluid ounces	fl oz
l	liters	0.264	gallons	gal
m^3	cubic meters	35.71	cubic feet	ft^3
m^3	cubic meters	1.307	cubic yards	yd^3
		MASS		
g	grams	0.035	ounces	oz
kg	kilograms	2.202	pounds	lb
Mg	megagrams	1.103	short tons (2000 lb)	T
		TEMPERATURE (exact)		
°C	Celcius temperature	1.8C + 32	Fahrenheit temperature	°F
		ILLUMINATION		
lx	lux	0.0929	foot-candles	fc
cd/m^2	candela/m^2	0.2919	foot-Lamberts	fl
		FORCE and PRESSURE or STRESS		
N	newtons	0.225	poundforce	lbf
kPa	kilopascals	0.145	poundforce per square inch	psi

* SI is the symbol for the International System of Units. Appropriate rounding should be made to comply with Section 4 of ASTM E380.

(Revised August 1992)

TABLE OF CONTENTS

LIST OF TABLES

LIST OF FIGURES

EXECUTIVE SUMMARY

The AASHTO 2002 flexible pavement design guide uses complex modulus as an input parameter for its performance models. Therefore, a comprehensive project was undertaken to develop complex modulus capabilities in compression, torsion, and tension for Florida. Additional research was performed to evaluate how well the AASHTO 2002 proposed predictive dynamic modulus equation works for Florida mixtures. Potential relationships between the complex modulus and the rutting performance of mixtures were evaluated. Methods that can be used to obtain creep properties from complex modulus measurements as input into the Florida Hot Mix Asphalt Fracture Mechanics Model were evaluated. The effects of aggregate size distributions on the complex modulus were evaluated. A performance test database was constructed. This summary provides a brief description of accomplishments, key findings, and recommendations resulting from this work.

The primary accomplishments and findings may be summarized as follows:

- A laboratory test system and an associated interpretation method were developed for the triaxial complex modulus test.
- A total of 29 mixtures common to Florida were tested at different temperatures and test frequencies using the triaxial complex modulus test. The results showed that the predictive complex modulus equation used in the new AASHTO 2002 flexible pavement design guide appears to work well for Florida mixtures.
- Potential relationships between the complex modulus and mixture rutting potential were evaluated. The results revealed no discernable relationship between complex modulus parameters and mixture rutting potential for mixtures containing the same

binder type, but varying aggregate types and aggregate structures. However, previous published work has shown that for complex modulus is able to distinguish between the rutting performance of mixtures that consist of the same aggregate type and aggregate structure, but in which the binder properties are varied. In essence, this means that the complex modulus is identifying the effects of mixture stiffness, which may be affected by binder stiffness.

- The effects of aggregate size distribution on the complex modulus were evaluated. A clear effect of gradation was identified, and gradation characteristics that result in high dynamic complex modulus values for both fine-graded and coarse-graded mixtures were established.
- A new torsional shear complex modulus test was developed. A key advantage with this new test is that no on-specimen measurements are needed. The dynamic shear modulus values obtained from the torsional complex modulus test were shown to follow the trends observed in the Superpave Indirect Tension resilient modulus test, and the triaxial complex modulus test.
- Developed the system and interpretation method for obtaining the complex modulus from the Superpave Indirect Tension (IDT) test. It appears that reasonable and rational values of dynamic modulus and phase angle can be obtained in tension using the Superpave IDT test.
- Evaluated the use of the complex modulus test for obtaining creep compliance and creep compliance parameters. For the range of frequencies typically employed in dynamic modulus testing, it may not be possible to obtain creep compliance and creep compliance parameters accurately from dynamic measurements.

- Developed approaches to determining creep compliance parameters accurately from a combination of complex modulus and static creep tests.
- Dynamic modulus tests at multiple frequencies appear to provide the most accurate method to obtain the initial elastic modulus of the mixture. This parameter is primarily useful in that it affects the interpretation of creep compliance data and resulting creep compliance parameters.
- Determined that the creep strain rate and the dissipated creep strain energy per cycle, which are key parameters in the Florida Hot Mix Asphalt Fracture Mechanics model, cannot be obtained from complex modulus test results. The phase angle includes both delayed elastic and creep strain components which cannot be separated.
- The resilient modulus obtained from the Superpave IDT test was found to be highly correlated to the dynamic modulus. A predictive relationship was determined between the resilient modulus and the dynamic modulus. Hence, it may be possible to use the resilient modulus as a substitute for the dynamic modulus.
- Finally, a comprehensive performance test database was developed that allows for the input of complex modulus test results, Superpave IDT test results, compression creep test results, APA test results, and other user-specified performance tests. In addition, the mixture design characteristics for each mixture tested are logged, including asphalt binder type, aggregate type, aggregate gradation, mixture design variables, and key mixture volumetric properties.

The following conclusions may be derived from the accomplishments and findings summarized above:

- The dynamic complex modulus should not be used to obtain creep compliance or creep compliance parameters for mixtures.
- The dynamic complex modulus test should neither be used to assess the rate of damage nor the fracture resistance of mixtures.
- The dynamic complex modulus test should not be used to evaluate the rutting performance of mixtures of varying aggregate type and aggregate structure.
- The primary use for the dynamic complex modulus test is to determine the stiffness of mixtures for purposes of determining the response to traffic loading, as per the new AASHTO 2002 flexible pavement design guide. It may also be possible to use the resilient modulus as a substitute for the dynamic complex modulus.
- The performance database developed should be used as a focal point for maintaining performance test results in Florida.

CHAPTER 1
INTRODUCTION

1.1 Background

The current state-of-practice in Superpave hot mix asphalt design is to rely almost solely on the volumetric composition of asphalt mixtures. The AASHTO 2002 design guide aims to introduce more rigorous measures of performance into hot mix asphalt mixture and pavement design procedures. Research by numerous groups has shown that the complex modulus can be used to characterize temperature dependent mixture stiffness and viscosity characteristics over time. Similarly, the complex modulus has been shown to be a potential measure of the accumulation of damage, including cracking in materials.

In recent years, the Pavement Group at the University of Florida has identified the critical mechanisms associated with longitudinal pavement cracking. On the load side, these include the tire rib and tread effects from modern radial tires that tend to pull the pavement apart in tension. On the material side, the fracture energy has been shown to be an excellent indicator of the likelihood for a given asphalt mixture to develop longitudinal cracks. Other variables that are of importance in predicting the fracture resistance of asphalt mixtures include strength and creep compliance. In this context, it is important to measure the creep compliance at the load amplitudes and frequencies associated with actual traffic. The complex modulus is about the only parameter that allows us to accurately obtain the creep compliance at the load frequencies of interest.

Current national efforts have been focusing on obtaining the complex modulus of mixtures with the cyclic triaxial test, or with the Superpave Simple Shear Test. The triaxial test works well for the characterization of laboratory-prepared mixtures. The Superpave

Simple Shear Test has shown itself to be highly variable. In constant height mode, the applied stress state is also unknown. Therefore, there is a need for a simplified shear test. One option is a torsional shear test, in which gyratory compacted specimens are subjected to torsion at the top of the specimen and the resulting torsional deformation is measured. Similarly, most pavement field cores in Florida are fairly thin, often precluding the use of the triaxial or torsional shear tests. Another alternative is to develop capabilities to measure the complex modulus with the indirect tension test. The indirect tension test developed by Dr. R. Roque has been shown to be both an expedient and a reliable way of obtaining mixture properties from field cores in Florida.

Finally, it is of key importance for Florida to develop complex modulus testing capabilities to remain a part of the national effort currently underway and to start developing a complex modulus database for Florida mixtures, both from the laboratory and the field.

1.2 Objectives

The primary objectives of the proposed research are to:

1. Develop triaxial dynamic complex modulus testing capabilities in Florida.
2. Develop testing and interpretation protocols for torsional shear complex modulus testing capabilities in Florida.
3. Develop a system for obtaining complex modulus from the Superpave Indirect Tension Test.
4. Evaluate how well proposed dynamic modulus predictive relationships work for Florida mixtures.
5. Evaluate any potential relationships between rutting performance and the complex modulus.

6. Evaluate methods that can be used to obtain creep properties from complex modulus testing.
7. Perform a fundamental evaluation of the phase angle in the complex modulus test. In particular, the various testing and material effects that may affect the phase angle will be identified.
8. Perform an evaluation of the effects of aggregate size distribution in asphalt mixtures on the complex modulus.
9. Develop a performance test database for Florida mixtures.

1.3 Scope

To meet the numerous objectives of this research project, multiple studies were performed. The results of each study are presented at the end of each chapter.

Chapter 1 provides background, objectives, and scope for the study. Chapter 2 deals with a literature review of the complex modulus, along with a review of recent model developments, including the AASHTO 2002 pavement design procedure. Chapter 3 describes the materials used in the evaluation of the axial complex modulus. Chapter 4 discusses the testing methodology for the axial complex modulus test. Chapter 5 details the development of the complex modulus interpretation method. Chapter 6 presents the results from the triaxial complex modulus test. Chapter 7 presents an evaluation of potential relationships between the complex modulus and the rutting performance of mixtures. Chapter 8 presents the results of a study on the effects of aggregate size distribution on the dynamic modulus. Chapter 9 presents the development of torsional shear complex modulus test. Chapter 10 discusses the development of a system for obtaining the complex modulus from the Superpave Indirect Tension Test. Chapter 11 presents a detailed evaluation of methods that can be used to obtain creep properties from complex modulus testing. Chapter 12 highlights the results of a fundamental evaluation of the phase angle in the complex modulus test. Appendix A covers the axial complex modulus program and the torsional shear complex modulus program. Appendix B describes the Superpave IDT complex modulus program, while Appendix C contains the performance test database.

CHAPTER 2
LITERATURE REVIEW

2.1 Background and History of Complex Modulus Testing

NCHRP Project 1-37A is producing the new 2002 Design Guide for New and Rehabilitated Pavements. The guide is based on mechanistic principles and requires a modulus to computer stress and strain in flexible pavements. In 1999, the NCHRP Panel for Project 1-27A selected the dynamic complex modulus, |E*|, for this purpose. Complex modulus testing for asphalt mixtures in not a new concept. Papazian (1962) was one of the first to delineate viscoelastic characterization of asphalt mixtures using the triaxial cyclic complex modulus test. He concluded that viscoelastic concepts could be applied to asphalt pavement design and performance. In the late 1960's (Shook and Kallas, 1969), the dynamic complex modulus was selected by the Asphalt Institute as the "Modulus Test of Choice." It subsequently became an ASTM test in the early 1970's, its designation is ASTM D3496.

During the 970' and 1980's, work continued that considered dynamic modulus response under compression, tension, and tension-compression loading. A number of studies indicated differences in dynamic modulus testing obtained from different loading conditions. The differences affect especially the phase angle and tend to become more significant at higher temperatures. Witczak and Root (1974) indicate that the tension-compression test may be more representative of field loading conditions. Khanal and Mamlouk (1995) affirmed this assertion. They performed complex modulus tests under five different modes of loading and obtained different results, especially at high temperatures. Bonneaure et al. (1977) determined the complex modulus from a bending test. The deformation is measured, and the complex modulus is calculated from the results.

In the later 1980's and early 1990's, the International Union of Testing and Research Laboratories for Materials and Structures (RILEM) Technical Committee on Bitumen and Asphalt Testing organized an international testing program (1996). The goal of the program was to promote and develop mix design methodologies and associated significant measuring methods for asphalt pavements. Complex modulus tests were performed by fifteen participating laboratories in countries throughout Europe. Results showed that bending tests and indirect tension tests were in reasonable agreement under certain conditions. The laboratories were able to reproduce the phase angle much better than the dynamic modulus.

Stroup-Gardiner and Newcomb (1997), Drescher et al. (1997), and Zhang et al. (1997a) performed complex modulus tests on both tall cylindrical specimens and indirect tensile specimens. The study resulted in mixed results, showing that tests on the same material with the two different setups sometimes yielded different results for the dynamic modulus and phase angle. The phase angle was especially variable in both test setups.

The most comprehensive research effort started in the mid-1990s as part of the National Cooperative Highway Research Program (NCHRP) Projects 9-19 (Superpave Support and Performance Models Management) and 9-29 (Simple Performance Tester for Superpave Mix Design). This research proposed new guidelines for the proper specimen geometry and size, specimen preparation, testing procedure, loading pattern, and empirical modeling. Some of these key findings have been reported in papers by Witczak (2000), Haifing and Kim (2002), Kaloush and Witczak (2002), Pellinen and Witczak (2002), and Witczak et al. (2002).

2.1.1 Superpave Shear Tester

As part of the SHRP program, the complex shear modulus (G*) was introduced for asphalt binder specifications (AASHTO, 1998), allowing a better characterization of the rheological behavior of asphalt binders at different temperatures. Similar efforts were undertaken on mixtures as a part of SHRP, where testing methods for the complex modulus of mixtures was evaluated by means of a torsional hollow cylinder test. This research led to the development of the SHRP Constant Height Simple Shear Test (CHSST). The complex shear modulus (G*) was the main parameter obtained from the CHSST test. However, a number of issues remain regarding the applicability of the CHSST test. In particular, the adherence to constant height requirements remains controversial at best, resulting in highly variable stress states during testing. Results from the CHSST test have been shown to relate to rutting performance. However, the data from the CHSST tests are highly variable. Several attempts have been made to lower the variation, including reducing the generally accepted specimen air void range of ± 0.5 percent to a tighter tolerance, increasing the number of specimens, and using additional LVDTs.

In the following, an overview of the various stiffness measurements used in flexible pavement characterization will be provided, followed by a summary of the state-of-the-art complex modulus testing of mixtures.

2.2 Modulus Measurement in Viscoelastic Asphalt Mixtures

The resilient modulus (M_r) has long been considered the defining characteristic for HMA layers. It has been used since 1993 in the *AASHTO Design Guide* (AASHTO, 1993). The laboratory procedure for the M_r test is described in AASHTO T 307-99. The test is well defined as a repeated 0.1 second haversine load followed by a 0.9 second rest period, repeated at 1 Hz intervals.

Due to the long history of using M_r in pavement design, many empirical relationships have been developed throughout the years relating M_r to other tests like the California

Bearing Ratio (CBR) and the Marshall stability test (AASHTO, 1993). However, the ability of the M_r to account for vehicle speed effects has lead to a push to develop methods that account fully for the variation of stiffness in HMA pavements with vehicle speeds.

The concept behind the complex modulus test is to account not only for the instantaneous elastic response, without delayed elastic effects, but also the accumulation of cyclic creep and delayed elastic effects with the number of cycles. Hence, the fundamental difference between the complex modulus test and the resilient modulus test is that the complex modulus test does not allow time for any delayed elastic rebound during the test.

The dynamic modulus ($|E^*|$) relates the cyclic strain to cyclic stress in a sinusoidal load test. The dynamic modulus test procedure outlined in ASTM D 3497 uses a standard triaxial cell to apply stress or strain amplitudes to a material at 16 Hz, 4 Hz, and 1 Hz. It also recommends that the test be repeated at 5° C, 25° C, and 40° C (ASTM D 3497). The dynamic modulus is calculated using Equation (Eq.) 2.1 (Yoder and Witczak, 1975):

$$|E^*| = \frac{\sigma_0}{\varepsilon_0} \tag{2.1}$$

where σ_0 = stress amplitude; and

ε_0 = strain amplitude.

This parameter includes the rate dependent stiffness effects in the mixture. However, it does not provide insight into the viscous components of the strain response. The dynamic modulus test can be expanded on to find the complex modulus (E^*). The complex modulus is composed of a storage modulus (E') that describes the elastic component and a loss modulus (E'') that describes the viscous component. The storage and the loss moduli can be determined by the measurement of the lag in the response between the applied stress and the measured strains. This lag, referred to as the phase angle (δ), shown in Figure 2-1. Equations 2.2a through 2.2c describe the relationship between the various components and E*:

$$\delta = \tan^{-1}\left(\frac{E''}{E'}\right) \tag{2.2a}$$

$$E'' = E^* \bullet \sin(\delta) \tag{2.2b}$$

$$E' = E^* \bullet \cos(\delta) \tag{2.2c}$$

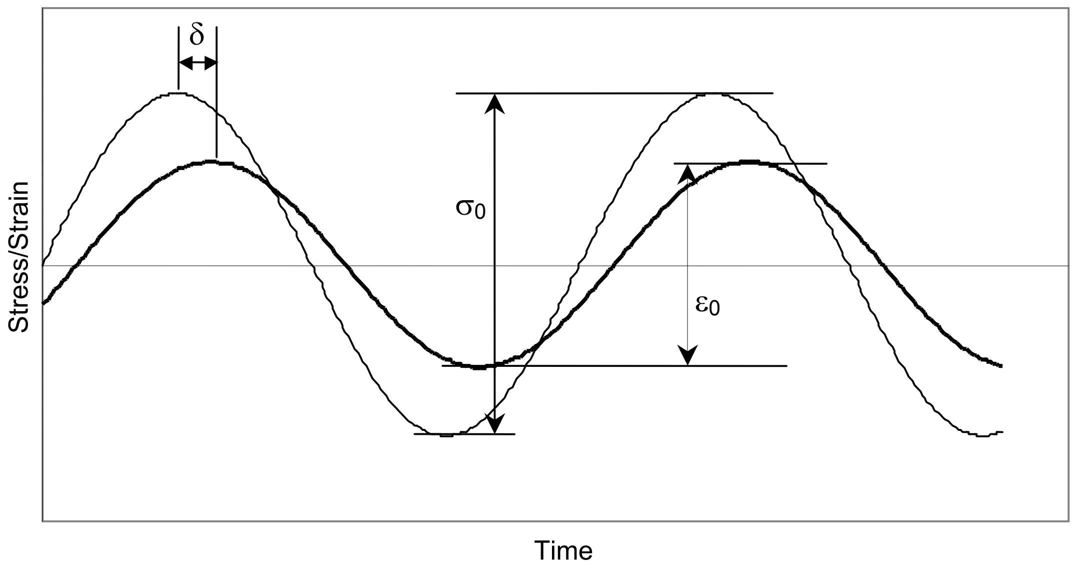

Figure 2-1. The testing components of the complex modulus

The phase angle is typically determined by measuring the time difference between the peak stress and the peak strain. This time can be converted to δ using Eq. 2.3 below:

$$\delta = t_{lag} \bullet f \bullet (360°) \tag{2.3}$$

where f = frequency of the dynamic load (in Hz); and

t_{lag} = time difference between the signals (in seconds).

A phase angle of zero indicates a purely elastic material and a δ of 90° indicates a purely viscous material.

For linear elastic materials, only two properties are required to describe the stress-strain behavior under any loading condition. The Young's modulus is typically used to describe changes due to the normal stresses and the shear modulus (G) describes the change in the material due to shear stresses. Similarly, the inclusion of Poisson effects is captured by the Poisson's ratio (υ). In viscoelastic materials, G* and E* are the most commonly used parameters. The magnitude of G* is calculated using the shear stress amplitude (τ_0) and the shear strain amplitude (γ_0) in Eq. 2.4 (Witczak et al., 1999) below:

$$\left| G^* \right| = \frac{\tau_0}{\gamma_0} \tag{2.4}$$

Similar to the complex modulus, G* has an elastic component (G′) and a viscous component (G″) (Witczak et al., 1999). These components are related through the phase angle (δ) as seen in Eqs. 2.5a through 2.5c (Witczak et al., 1999):

$$\delta = \tan^{-1}\left(\frac{G''}{G'}\right) \tag{2.5a}$$

$$G'' = G^* \bullet \sin(\delta) \tag{2.5b}$$

$$G' = G^* \bullet \cos(\delta) \tag{2.5c}$$

To calculate both the E* and the G* coefficients, it must be possible to measure not only the axial compressive stresses and strains, but also the shear stresses and strains. Harvey et al. (2001) concluded that G* can be related to E* using Eq. 2.6.

$$G^* = \frac{E^*}{2(1+\upsilon)} \tag{2.6}$$

By directly measuring changes in the height and radius of the asphalt sample, Poisson's ratio can be calculated. This is done by calculating ν as the ratio of lateral expansion to the axial compression (Saada, 1989). Equation 2.6 assumes that the Poisson's ratio is constant and some testing has shown that the Poisson's ratio for HMA is frequency dependent (Sousa and Monismith, 1987).

2.2.1 Master Curves and Shift Factors

The master curve of an asphalt mixture allows comparisons to be made over extended ranges of frequencies and temperatures. Master curves are generated using the time-temperature superposition principle. This principle allows for test data collected at different temperatures and frequencies to be shifted horizontally relative to a reference temperature or frequency, thereby aligning the various curves to form a single master curve. The procedure assumes that the asphalt mixture is a thermo-rheologically simple material, and that the time-temperature superposition principle is applicable.

The shift factor, a (T), defines the required shift at a given temperature. The actual frequency is divided by this shift factor to obtain a reduced frequency, f_r, for the master curve:

$$f_r = \frac{f}{a(T)} \quad \text{or} \quad \log(f_r) = \log(f) - \log[a(T)] \qquad (2.7)$$

The master curve for a material can be constructed using an arbitrarily selected reference temperature, T_R, to which all data are shifted. At the reference temperature, the shift factor a (T) = 1. Several different models have been used to obtain shift factors for viscoelastic materials. The most common model for obtaining shift factors is the Williams-Landel-Ferry (WLF) equation (Williams et al., 1955).

When experimental data are available, a master curve can be constructed for the mixture. The master curve can be represented by a nonlinear sigmoidal function of the following form (Pellinen and Witczak, 2002):

$$\log\left(\left| E^* \right|\right) = \delta + \frac{\alpha}{1 + e^{\beta - \gamma \log(f_r)}} \tag{2.8}$$

where $\log(|E^*|)$ = log of dynamic modulus;

δ = minimum modulus value;

f_r = reduced frequency;

α = span of modulus value; and

β, γ = shape parameters.

Note that δ in this equation is not related to the phase angle – it is just the notation chosen by Pellinen and Witzcak (2002) for the minimum modulus value. The sigmoidal function of the dynamic modulus master curve can be justified by physical observations of the mixture behavior. The upper part of the function approaches asymptotically the maximum stiffness of the mixture, which depends on the binder stiffness at cold temperatures. At high temperatures, the compressive loading causes aggregate interlock stiffness to be an indicator of mixture stiffness. The sigmoidal function shown in Eq. 2.8 captures the physical behavior of asphalt mixtures observed in complex modulus testing throughout the entire temperature range (Pellinen and Witzcak, 2002).

2.3 Sample Preparation

Currently, there is much discussion about the shape and size of specimen to be used in complex modulus testing. In NCHRP Project 9-19, Witzcak and his colleagues investigated the proper size and geometry of test specimens (Witzcak et al., 2000). Based on numerous complex modulus test results, they recommended using 100-mm diameter cored specimens from a 150-mm diameter gyratory compacted specimen, with a final saw cut height of 150-mm. This recommendation came from a study by Chehab et al. (2000) that considered the variation in air voids within specimens compacted using the Superpave Gyratory Compactor SGC). The study showed that specimens compacted using the SGC tend to have non-uniform air void distribution both along their diameter and height. SGC-compacted specimens have higher air void content at the top and bottom edges, as well as in sections adjacent to the mold walls, as compared to the interior portion of the specimens. Finally, fully lubricated end plates were found to minimize end restraint on the specimen. Increasing the number of gages used to measure axial strain decreases the number of test specimens necessary.

2.4 Load Level

Since the interpretation of the complex modulus is based on the assumption of linear viscoelasticity of the mixture, it is necessary to maintain a fairly low strain level during testing to avoid any nonlinear effects. Maintaining a stress level that results in a strain response that is close to linear is critical to achieve a test that is reproducible.

The concept of material linearity is based upon two principles. The first principle, proportionality, is described with Eq. 2.9:

$$\varepsilon\left(C \bullet \sigma(t)\right) = C \bullet \varepsilon\left(\sigma(t)\right) \tag{2.9}$$

It implies that if a stress is increased by any factor then the strain will also increase by the same factor. This allows the shape of the stress/strain relationship to be more easily mapped out across the linear range.

The principle of superposition is the other condition that describes linearity. Equation 2.10 describes this concept.

$$\varepsilon\left(\sigma_1(t)+\sigma_2(t-t_1)\right) = \varepsilon\left(\sigma_1(t)\right)+\varepsilon\left(\sigma_2(t-t_1)\right) \quad (2.10)$$

This implies that if it is known how the material will behave under a single loading condition that it will be known how it would behave under multiple loads. Figures 2-2 and 2-3 show graphically the concept proportionality and superposition. The combination of these principles allows the material behavior to be predicted with fewer parameters.

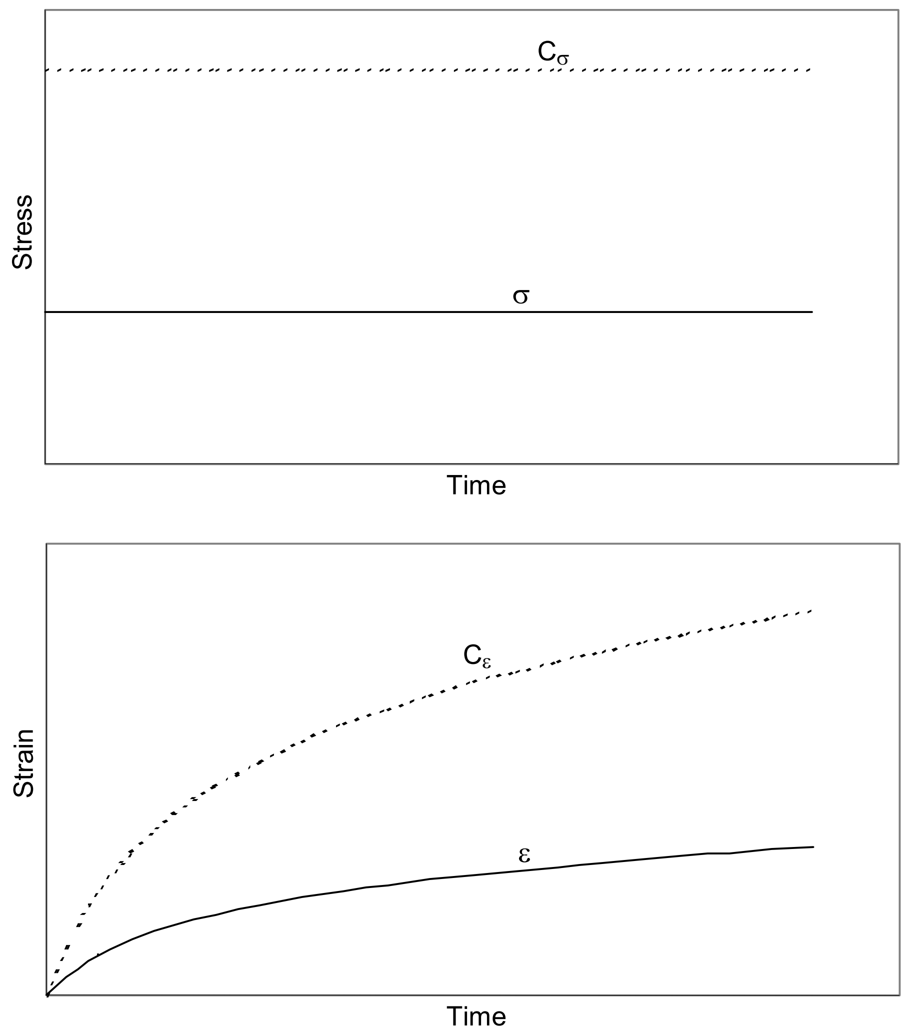

Figure 2-2. Proportionality of viscoelastic materials

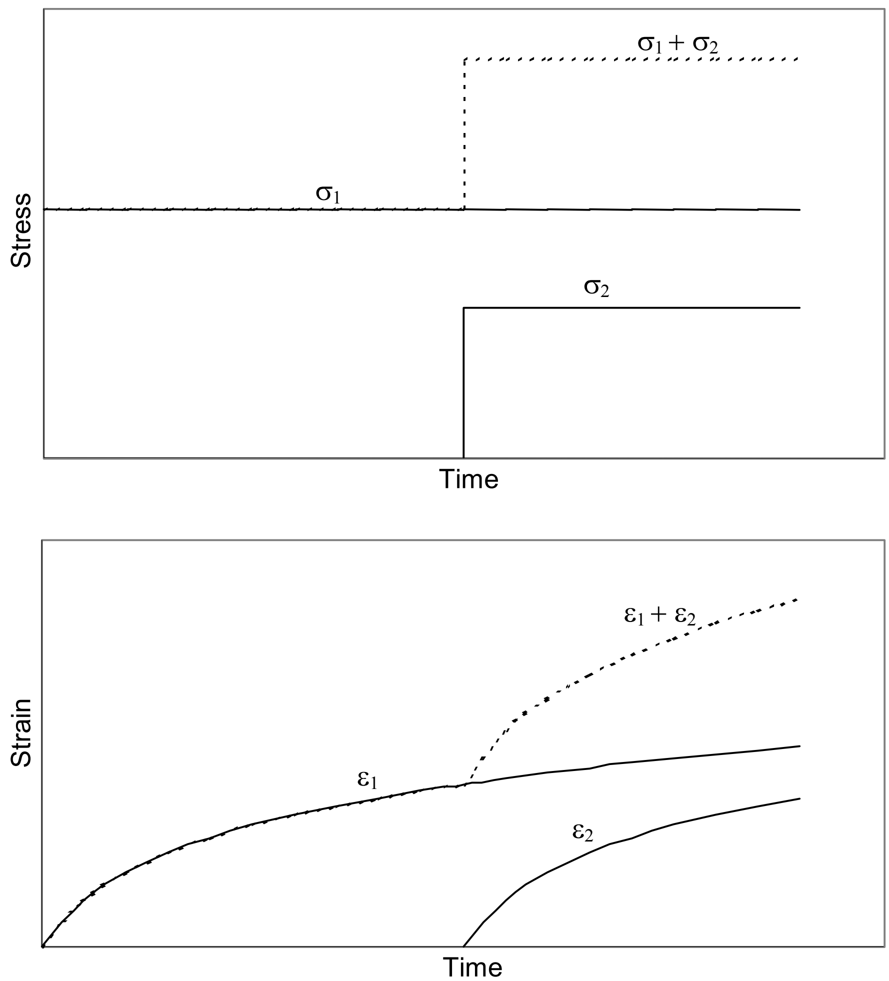

Figure 2-3. Superposition of viscoelastic materials

HMA has been found to behave linearly, but only for specific temperature and strain regions. Mehta and Christensen (2000) describe HMA as linear for low temperatures (–20° C to –10° C) and shear strains under 200 microstrain. For intermediate temperatures (4° C to 20° C) shear strains should be less then 50 microstrain to stay within the viscoelastic limits. However, it should be noted that the determination of linearity may also be affected by the loading mechanism (i.e., compression, tension, torsion).

For dynamic modulus measurements using uniaxial compression testing, the ASTM D 3497 recommends using an axial stress amplitude of 241.3 kPa (35 psi) at all temperatures as long as the total deformation is less then 2500. Daniel and Kim (1998) showed successful triaxial compression testing results with stress levels under 96.5 kPa for 15° C testing. Strain amplitudes of 75 to 200 microstrain have also been suggested to maintain material linearity during triaxial compression testing (Witczak et al., 1999).

2.5 Complex Modulus as a Design Parameter

The *2002 AASHTO Guide for the Design of Pavement Structures* recommends the complex modulus as a design input parameter for the mechanistic-empirical design procedure (NCHRP, 2004). Level 1 Analysis requires actual dynamic modulus test data to develop master curves and shift factor based on Eqs. 2.7 and 2.8. This testing is performed on replicate samples at five temperatures and four rates of loading per temperature. Binder testing must be performed at this level to shift the data into smooth master curves. Level 2 Analysis constructs a master curve using actual asphalt binder test data based on the relationship between binder viscosity and temperature. Level 3 Analysis requires no laboratory test data. Instead, the Witczak modulus equation (NCHRP, 2004) is used with typical temperature-viscosity relationships established for all binder grades.

2.5.1 Witczak Predictive Modulus Equation

The complex modulus test is relatively difficult and expensive to perform. Therefore, numerous attempts have been made to develop regression equations to calculate the dynamic modulus from conventional volumetric mixture properties. For example, a predictive regression equation is proposed as a part of the *2002 Design Guide* to calculate the dynamic modulus, |E*|, based on the volumetric properties of any given mixture. The predictive equation developed by Witczak et al. (2002) is one of the most comprehensive mixture dynamic modulus models available today (Witczak, 2002). The equation is presented below:

$$\begin{aligned}\log\left|E^*\right| = & -1.249937+0.029232\times(p_{200})-0.001767\times(p_{200})^2-0.002841\times(p_4) \\ & -0.058097\times(V_a)-\frac{0.802208(V_{beff})}{V_{beff}+V_a} \\ & +\frac{3.871977-0.0021(p_4)+0.003958(p_{3/8})-0.00017(p_{3/8})^2+0.005470(p_{3/4})}{1+e^{(-0.603313-0.313351\times\log(f)-0.39353\times\log(\eta))}}\end{aligned} \tag{2.11}$$

where $|E^*|$ = dynamic modulus, in 10^5 psi;

η = bitumen viscosity, in 0^6 Poise;

f = loading frequency, in Hz;

V_a = percent air void content, by volume;

V_{beff} = effective bitumen content, percent by volume;

$P_{3/4}$ = percent weight retained on 19-mm sieve, by total aggregate weight;

$P_{3/8}$ = percent weight retained on 9.5-mm sieve, by total aggregate weight;

P_4 = percent weight retained on 4.75-mm sieve, by total aggregate weight; and

P_{200} = percent weight passing 0.75-mm sieve, by total aggregate weight.

The above dynamic modulus predictive equation has the capability to predict the dynamic modulus of dense-graded HMA mixtures over a range of temperatures, rates of loading, and aging conditions from information that is readily available from conventional binder tests and the volumetric properties of the HMA mixture. This predictive equation is based on more than 2,800 different HMA mixtures tested in the laboratories of the Asphalt Institute, the University of Maryland, and FHWA.

2.6 Complex Modulus as a Simple Performance Test

The goal of NCHRP Project 9-19 was to develop a Simple Performance Test (SPT) for asphalt mixtures. Various testing configurations were evaluated from several of the most promising test methods. The potential SPT methods can be categorized as stiffness-related tests, deformability tests, and fracture tests. The stiffness parameters were obtained from compressive complex modulus, SHRP Simple Shear Tester (SST), and ultrasonic wave propagation. Of these three candidates, the complex modulus appeared to be the most promising for relating material properties to rutting and fatigue cracking observed in the field (Pellinen and Witzcak, 2002).

2.6.1 Fatigue Cracking

Witczak et al. (2002) performed numerous complex modulus tests to perfect the recommendations for fatigue and cracking in asphalt mixtures. The results led to the development of a fatigue distress model in which the number of repetitions to failure, N_f, is a function of the horizontal tensile strain, ε_t, which represents the largest of the transverse and longitudinal horizontal strain, and dynamic modulus of the mix, $|E^*|$:

$$N_f = FK_{1\alpha}\left(\frac{1}{\varepsilon_t}\right)^5\left(\frac{1}{|E^*|}\right)^{1.4} \tag{2.12}$$

The adjustment factor, F, that indicates the stress or strain controlled fatigue behavior in the pavement structure, is a function of the dynamic modulus and pavement thickness, h_{ac}:

$$F = 1+\frac{13909|E^*|^{-0.4}-1}{1+e^{(1.354h_{ac}-5.408)}} \tag{2.13}$$

A volumetric adjustment factor, $K_{1\alpha}$, corrects the number of repetitions to failure by taking into account the binder and mix properties. In the following equation, PI is the binder penetration index and V_b is the volume of binder in the mix:

$$K_{1\alpha} = \left[0.0252\,PI - 0.00126\,PI\left(V_b\right) + 0.00673\,V_b - 0.0167\right]^5 \tag{2.14}$$

Equation 2.12 can be reduced to the following equation, where the constants β_n and k_n can be assigned to nationally calibrated fatigue model constants:

$$N_f = \beta_{f1} k_1 \left(\frac{1}{\varepsilon_t}\right)^{\beta_{f2} k_2} \left(\frac{1}{|E^*|}\right)^{\beta_{f3} k_3} \tag{2.15}$$

Finally, it is expected that each state agency will have to develop local calibration factors for Eq. 2.15.

2.6.2 Rutting

The complex modulus test also showed good correlation to permanent deformation of asphalt mixtures. Witczak et al. (2002) performed research on asphalt mixtures similar to the SPT for fatigue cracking. Cylindrical specimens were tested at five temperatures and six frequencies, as well as different level of confining pressure. They come to preliminary findings that warranted a closer look at the dynamic modulus test for rutting susceptibility. Pellinen and Witczak (2002) recommended using dynamic modulus obtained in unconfined compression at 54.4°C and a frequency of 5 Hz. The stress levels must remain small to keep the sample in the linear viscoelastic region. Some other recommendations from this project include (Witczak et al., 2002):

- Prediction of one-dimensional densification, as well as lateral displacement of the mix and tertiary flow.

- Inclusion of temperature as a key factor for permanent deformation modeling.
- Inclusion of HMA layer thickness and total HMA thickness.
- Consideration of pavement type and rehabilitation strategy.

CHAPTER 3
MATERIALS USED IN AXIAL COMPLEX MODULUS TESTING

3.1 Introduction

This chapter provides information on the materials used in the testing of the axial complex modulus. The physical properties of materials used are discussed, such as their aggregate gradation, aggregate physical properties, mixture design procedures, and material preparation.

3.2 Overview of Mixtures Used

Four distinctive groups of mixture were used for the purpose of this research.

1. Eight mixtures of varying gradations with oolitic limestone (Whiterock) from South Florida entitled “Limestone Gradation Study Mixtures” (C and F).
2. Six mixtures of varying gradations with Georgia granite (GA185) identified as “Granite Gradation Study Mixtures” (GAC and GAF).
3. Five field mixtures of varying gradations and aggregate types from Superpave monitoring test sites in Florida entitled “Superpave Field Monitoring Mixtures” (P).
4. Eight mixtures called “Fine Aggregate Angularity (FAA) Mixtures” with different fine aggregates (defined as material passing the no. 4 sieve) and coarse aggregates consisting of oolitic limestone (Whiterock) from South Florida.

3.3 Asphalt Binders Used

The grade of asphalt cement used in mixtures is one factor that can have an effect on the amount of rutting that occurs in the mix. All other things being equal, the stiffer the asphalt cement, the less the rutting that is expected in the mix under a given weight and volume of truck. In this research, only one type of unmodified asphalt cement, AC-30

(PG67-22), which is commonly used in Florida, was used for all mixtures tested except for the modified HVS mixture in which an SBS modified binder (PG 76-22) was used.

3.4 Aggregates

This section describes the type of aggregates, aggregate gradations and combination of various aggregates in this research.

3.4.1 Fine Aggregate Angularity (FAA) Mixtures

The first part of the research was performed using gradations of coarse and fine Whiterock limestone mixtures (C1 and F1, respectively) provided by FDOT for use as the reference mixtures. The nominal maximum aggregate size for these mixtures is 12.5 mm (1/2-in). These Superpave mixtures were selected because they are commonly used FDOT gradations and are known to perform well in the field. Figure 3-1 shows the gradation curves for the C1 and F1 mixtures.

The fine aggregate portions of these mixtures were volumetrically replaced by four other fine aggregate types (passing the No. 4 sieve) to obtain five fine-graded and five coarse-graded mixtures. All materials were washed in accordance with ASTM C-117 and washed-sieve analyses were performed according to ASTM C-136. The fine aggregates used were selected to be of varying angularity, texture, toughness, and historical rutting performance. The designations for the fine aggregates used are as follows:

- Limestone
  - Whiterock (baseline aggregate)
  - Cabbage Grove (Florida, FL)
  - Calera (Alabama, AL)
- Granite
  - Ruby (Georgia, GA)
- Gravel
  - Chattahoochee FC-3 (Tennessee, TN)

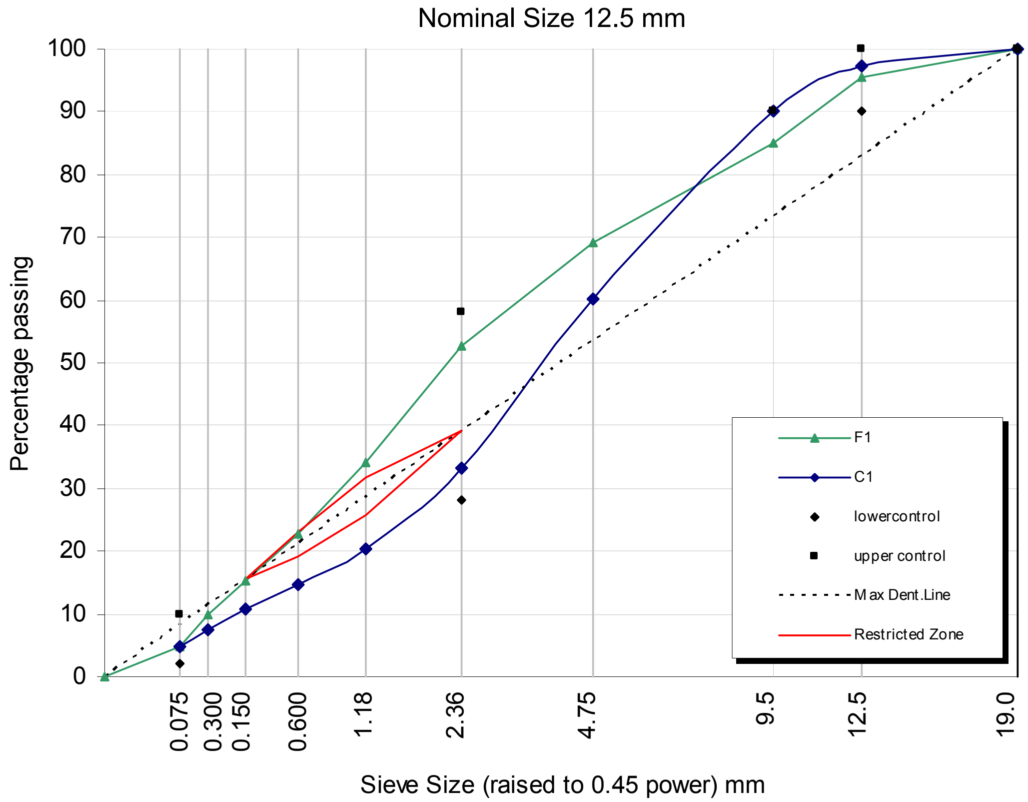

Figure 3-1. Gradation curves for C1 and F1

The aggregates are designated in this project as follows:

- Calera = CAL
- Whiterock = WR
- Cabbage Grove = CG
- Ruby = RB
- Chattahoochee FC-3 = CH

Tables 3-1 and 3-2 show the resulting coarse and fine gradations, respectively.

Table 3-1. Coarse Gradations for Fine Aggregate Effects

Sieve Size (mm)	WRC	CGC	RBC	CHC	CALC
25	100.0	100.0	100.0	100.0	100.0
19	100.0	100.0	100.0	100.0	100.0
12.5	97.4	97.4	97.5	97.5	97.5
9.5	90.0	88.8	89.5	89.4	89.3
4.75	60.2	54.8	57.6	56.9	56.5
2.36	33.1	30.4	31.6	31.3	31.2
1.18	20.3	20.5	21.1	20.9	20.9
0.600	14.7	14.8	15.1	15.0	15.0
0.300	10.8	11.0	11.0	11.0	11.0
0.150	7.6	7.2	7.0	7.1	7.1
0.075	4.8	5.5	5.2	5.2	5.3

Table 3-2. Fine Gradations for Fine Aggregate Effects

Sieve Size (mm)	WRF	CGF	RBF	CALF	CHF
25	100.0	100.0	100.0	100.0	100.0
19	100.0	100.0	100.0	100.0	100.0
12.5	95.5	97.4	95.1	94.9	95.0
9.5	85.1	83.8	85.0	84.6	84.7
4.75	69.3	66.0	68.5	67.6	67.9
2.36	52.7	49.4	51.2	50.6	50.8
1.18	34.0	33.3	34.2	33.9	34.0
0.600	22.9	21.9	22.4	22.2	22.2
0.300	15.3	13.9	14.0	14.0	14.0
0.150	9.6	7.0	6.9	6.9	6.9
0.075	4.8	4.5	4.3	4.3	4.3

Table 3-3 shows the bulk specific gravity and toughness, as well as the surface texture, particle shape, direct shear strength (DST) from a geotechnical direct shear box test, and fine aggregate angularity (FAA) values of the five fine-graded aggregates used. Bulk specific gravity ranged from 2.27 for relatively porous limestone to 2.68 for very non-porous granite. Toughness of the parent rock varied from 18 % as the lowest value to 42 % as the highest value of the Los Angeles (LA) Abrasion Test. Average surface texture values ranged from 1.7 to 4.6, while average particle shape values ranged from 2.4 to 4.3.

Table 3-3. Physical Properties of Fine Aggregates

Material	Bulk Specific Gravity	LA Abrasion[a]	Toughness[b]	Surface Texture[c]	Particle Shape[d]	FAA	DST (psi)
White Rock	2.48	34%	Medium	3.3	3.0	43.4	134.4
Calera	2.56	25%	High	1.7	3.5	42.7	140.8
Cabbage Grove	2.56	41%	Low	4.6	2.4	53.1	106.7
Ruby	2.68	20%	High	2.7	4.3	46.3	120.5
Chattahoochee FC-3	2.60	42%	Low	2.3	3.5	44.0	106.9

[a] Los Angeles Abrasion Test performed on the parent rock. Values provided by the Florida DOT Materials Office.
[b] Definition of toughness based on LA Abrasion: High: < 30; Medium: 30-40; Low: > 40.
[c] Average of 8 evaluations, where 1 = smooth and 5 = rough.
[d] Average of 8 evaluations, where 1 = rounded and 5 = angular.
Source: Roque et al., 2002a

Bulk specific gravities for each material were determined in accordance with ASTM C-128. The FDOT provided LA Abrasion values. The FAA values were calculated using the Uncompacted Void Content of Fine Aggregate Test (ASTM C-1252 and AASHTO TP33), and the Direct Shear Test (DST, ASTM Standard Method D 3080) was used to determine the shear strength of each fine aggregate. Both FAA and DST values were provided by previous research done by Casanova (Roque et al., 2002a).

3.4.2 Determination of Fine Aggregate Batch Weights

To volumetrically replace the fine aggregates in the FDOT Whiterock limestone C1 and F1 mixtures with the other aggregate types, the weight of Whiterock aggregate retained on each sieve (from #8 Sieve to # 200 Sieve) was replaced with an equivalent volume of fine aggregate of the replacement material during the batching process using the following formula:

$$W_r = \frac{G_{mbr}}{G_{mbL}} \bullet W_L \qquad (3.1)$$

where W_L = weight of Whiterock limestone retained on a specified sieve;

W_r = weight of replacement fine aggregate retained on the specified sieve size;

G_{mbL} = bulk specific gravity of Whiterock Limestone; and

G_{mbr} = bulk specific gravity of replacement aggregate.

3.4.3 Limestone Gradation Study Mixture Gradations

The second part of the research was done with an oolitic limestone aggregate identified as “Whiterock” aggregate, which is commonly used in mixtures in Florida. This aggregate was made up of three components: coarse aggregates (S1A), fine aggregates (S1B) and screenings. These were blended together in different proportions to produce ten (10) HMA mixtures consisting of five coarse and five fine gradations, two of which are the same gradations as in the fine aggregate study, namely WRC and WRF. Georgia granite

(GA 185) mineral filler was used in all the above gradations. These gradations were produced and extensively studied in a previous research at the University of Florida (Nukunya, 2001). Tables 3-4 and 3-5 show the gradations for the coarse and fine blends, respectively. These are also displayed in Figures 3-2 and 3-3.

Table 3-4. Gradations for Whiterock Coarse-Graded Mixtures

Sieve Size (mm)	C1	C2	C3
25	100.0	100.0	100.0
19	100.0	100.0	100.0
12.5	97.4	91.1	97.6
9.5	90	73.5	89.3
4.75	60.2	47.1	57.4
2.36	33.1	29.6	36.4
1.18	20.3	20.2	24
0.600	14.7	14.4	17.7
0.300	10.8	10.4	12.9
0.150	7.6	6.7	9.0
0.075	4.8	4.8	6.3

Table 3-5. Gradations for Whiterock Fine-Graded Mixtures

Sieve Size (mm)	F1	F2	F4	F5	F6
25	100.0	100.0	100.0	100.0	100.0
19	100.0	100.0	100.0	100.0	100.0
12.5	95.5	90.8	95.5	95.5	95.5
9.5	85.1	78	85.1	85.1	85.1
4.75	69.3	61.3	69.3	61.3	69.3
2.36	52.7	44.1	52.7	52.7	44.1
1.18	34.0	34.7	40.0	34.0	34.7
0.600	22.9	23.6	29.0	22.9	23.6
0.300	15.3	15.7	20.0	15.3	15.7
0.150	9.8	8.9	12.0	9.6	9.1
0.075	4.8	6.3	6.3	4.8	6.3

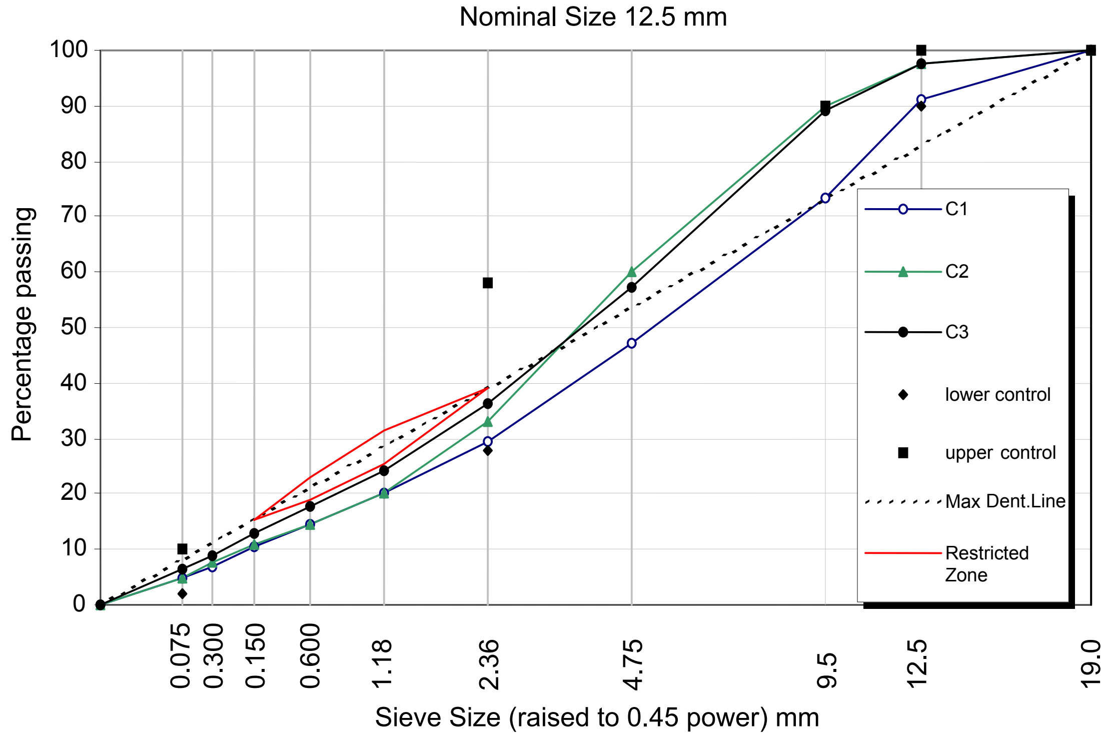

Figure 3-2. Coarse gradations for gradation effects studies

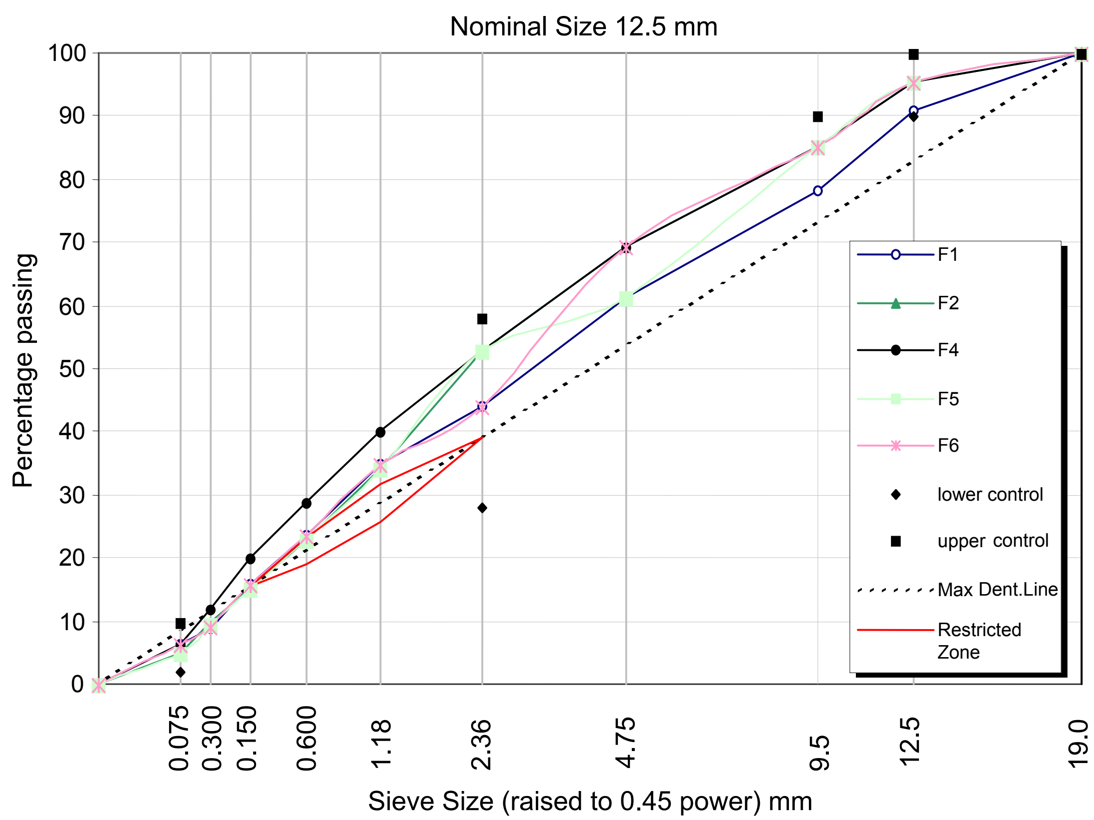

Figure 3-3. Fine gradations for gradation effects studies

3.4.4 Granite Mixtures Used

Three mixtures were prepared by volumetrically replacing the aggregate particles in the GAC1, GAC2, GAC3, GAF1, GAF2 and GAF3 limestone mixtures with the appropriate sizes of Georgia granite (GA185) aggregates from pit #185 (code #7 for 12.5 and 9.5 mm sieves, code #89 for 4.75 mm (#4) sieve and code #W10 for sieves less than #4). Tables 3-6 and 3-7 show the gradations, which are also displayed in Figures 3-4 to 3-7.

Table 3-6. Granite Based Mixture Gradations

Sieve Size (mm)	GAC1	GAC2	GAC3	GAF1	GAF2	GAF3
25	100.00	100.0	100.0	100.0	100.0	100.0
19	100.00	100.0	100.0	100.0	100.0	100.0
12.5	97.39	90.9	97.3	94.7	90.5	94.6
9.5	88.99	72.9	89.5	84.0	77.4	85.1
4.75	55.46	45.9	55.4	66.4	60.3	65.1
2.36	29.64	28.1	33.9	49.2	43.2	34.8
1.18	19.24	18.9	23.0	32.7	34.0	26.0
0.600	13.33	13.2	16.0	21.0	23.0	18.1
0.300	9.30	9.2	11.2	12.9	15.3	12.5
0.150	5.36	5.6	6.8	5.9	8.7	7.7
0.075	3.52	3.9	4.7	3.3	5.4	5.8

Table 3-7. Gradation of Field Projects

Sieve Size (mm)	P1	P2	P3	P5	P7
25	100.0	100.0	100.0	100.0	100.0
19	100.0	100.0	100.0	100.0	100.0
12.5	100.0	98.0	94.0	100.0	95.0
9.5	99.0	89.0	90.0	94.0	88.0
4.75	64.0	45.0	67.0	64.0	70.0
2.36	40.0	28.0	34.0	34.0	57.0
1.18	29.0	22.0	25.0	24.0	41.0
0.600	21.0	17.0	18.0	19.0	30.0
0.300	14.0	12.0	13.0	13.0	19.0
0.150	8.0	7.0	7.0	8.0	9.0
0.075	5.1	4.9	4.4	3.9	4.2

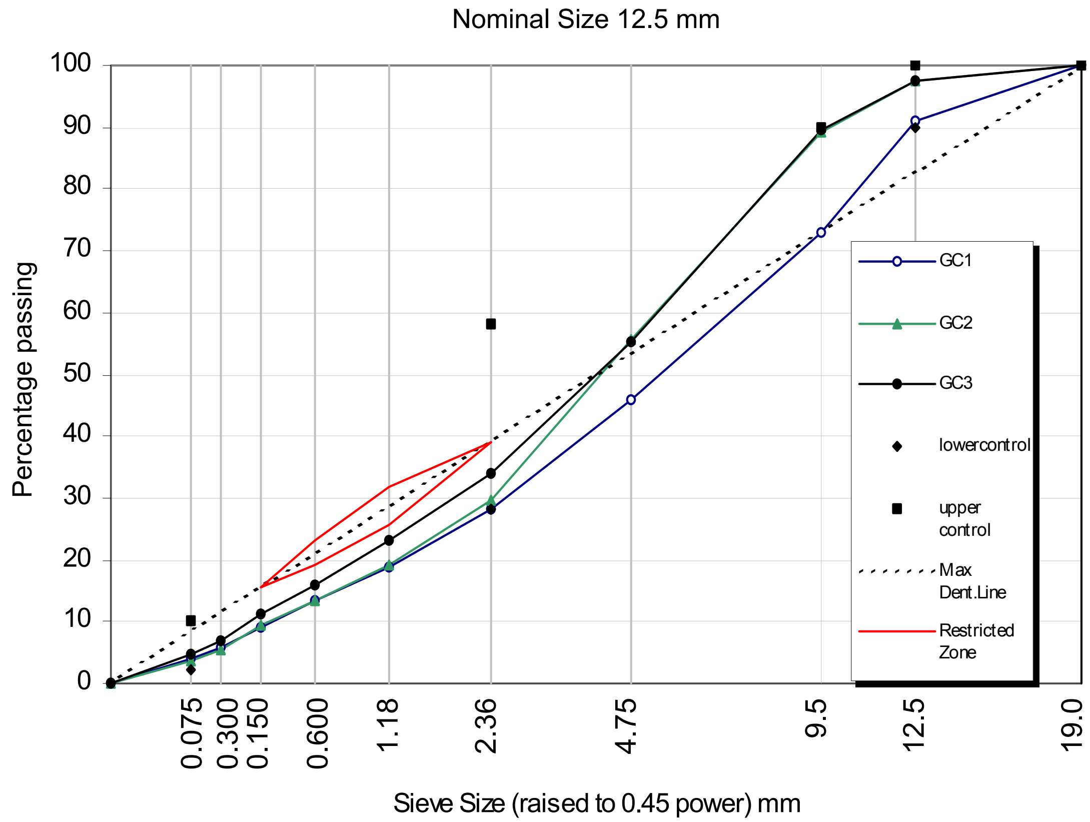

Figure 3-4. Coarse-graded granite aggregate gradations

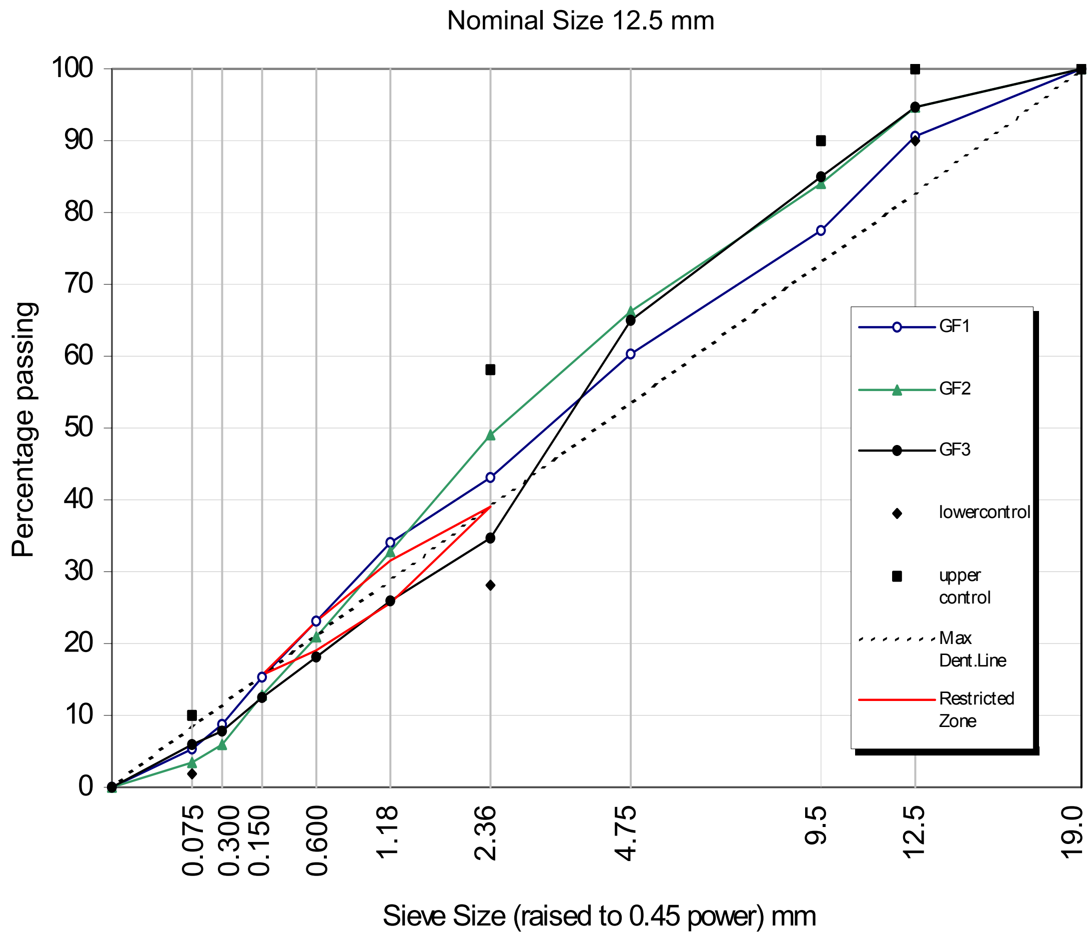

Figure 3-5. Fine-graded granite aggregate gradations

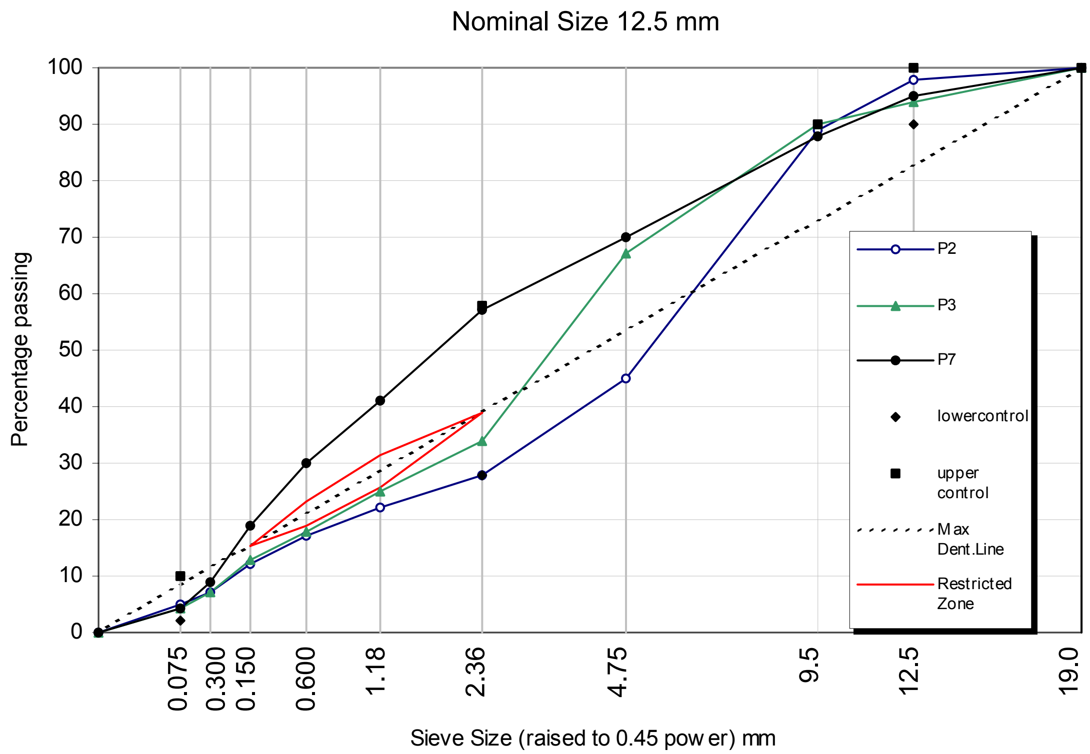

Figure 3-6. Gradations for Superpave project mixture numbers 2, 3, and 7

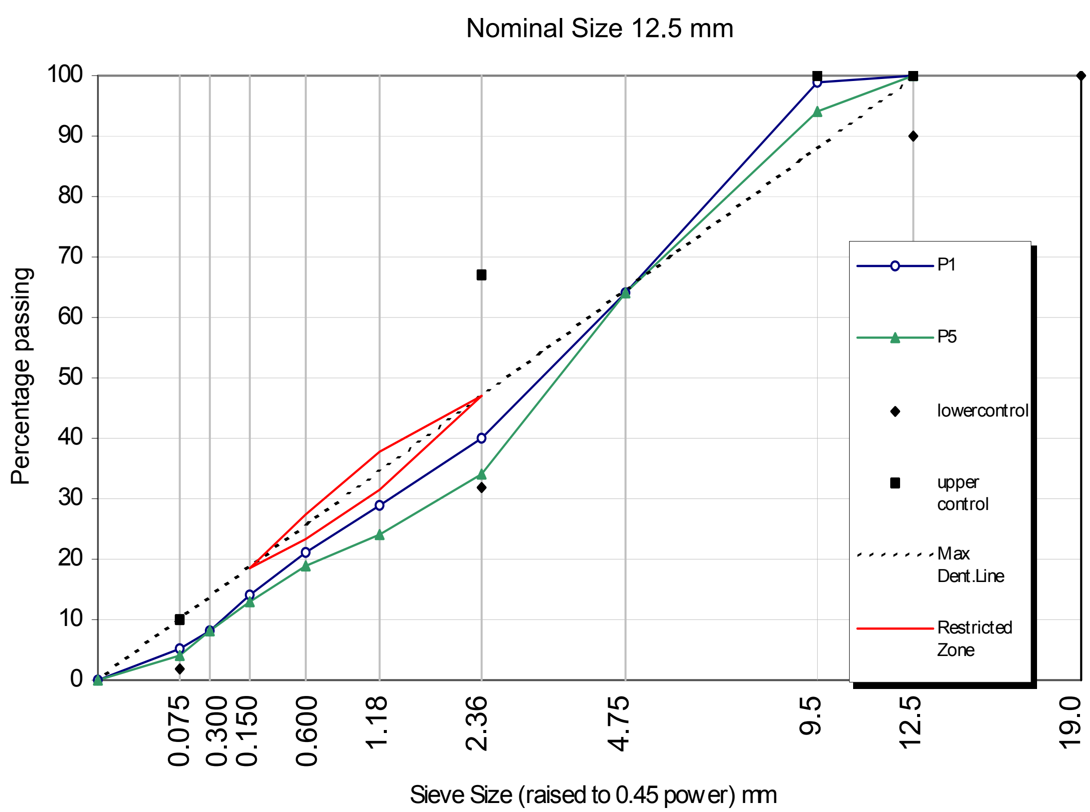

Figure 3-7. Gradations for field projects 1 and 5

3.4.5 Superpave Field Monitoring Mixture Gradations

Five Superpave mixtures from Florida, tested for performance at the University of Florida, were also evaluated (Asiamah 2001). Figures 3-5 and 3-7 display the gradations of these mixtures.

Project 1 (P1) and project 5 (P5) are 9.5-mm nominal gradations while all the other projects are of 12.5-mm nominal size. All the field mixtures are coarse-graded (i.e., the gradations pass below the Superpave Restricted Zone).

3.5 Mixture Design

Before the production of test specimens, the mixture design process was verified for the mixture volumetric properties. The original Superpave design procedure was used for all the mixtures. The Servopac Superpave gyratory compactor (see photograph in Figure 3-8) was used in this process. Table 3-8 displays the Superpave compaction requirements for specified traffic levels as a guide for the design of asphalt paving mixtures. The mixture volumetric properties are calculated based on the design number of gyrations (N_{des}). At this number of gyrations, a specified air voids level of 4% provides the optimum design asphalt content. All mixtures were designed for a traffic level of 10-30 million ESALS, that is, an N_{des} of 109 and N_{max} of 174. The project mixes except project 7, were designed at an N_{des} of 96 and N_{max} of 152. Project 7 has an N_{des} of 84. The Servopac compaction parameters used for the design are 1.25° gyratory angle, 600-kPa ram pressure and 30 revolutions per minute.

For each mixture, two pills were produced at the specified asphalt content. Compaction of the mixtures was made to 109 gyrations with the Servopac gyratory compactor, after which the bulk densities were measured. To verify the volumetric properties of the mixtures, the maximum theoretical specific gravity was measured using the

Figure 3-8. Servopac Superpave gyratory compactor

Table 3-8. Superpave Gyratory Compaction Effort (after Asphalt Institute Superpave Series No. 2)

Design ESALS (millions)	Average Design High Air Temperature < 30°C		
	N_{ini}	N_{des}	N_{max}
< 0.3	7	68	104
03. to 1	7	76	117
1 to 3	7	86	134
3 to 10	8	96	152
10 to 30	8	109	174
30 to 100	9	126	204
> 100	9	143	233

Rice maximum theoretical specific gravity method specified in AASHTO T 209/ASTM D 2041 standards. In this case, the mixtures were allowed to cool down in the loose state. Tables 3.9 to 3.14 show the volumetric properties of all the mixtures used in this research.

Table 3-9. Volumetric Properties of Coarse-Graded Mixtures (FAA Effects)

Property	Symbol	Mixture				
		WRC	CGC	RBC	CALC	CHC
Maximum theoretical density	G_{mm}	2.328	2.386	2.393	2.454	2.394
Specific gravity of asphalt	G_b	1.035	1.035	1.035	1.035	1.035
Bulk specific gravity of compacted mix	G_{mb}	2.235	2.295	2.300	2.353	2.289
Asphalt content	P_b	6.5	6.5	6.25	5.8	5.7
Bulk specific gravity of aggregate	G_{sb}	2.469	2.418	2.576	2.540	2.535
Effective specific gravity of aggregate	G_{se}	2.549	2.625	2.622	2.680	2.601
Asphalt absorption	P_{ba}	1.1	3.0	0.6	1.7	0.7
Effective asphalt content in the mixture	P_{be}	5.3	3.3	5.6	3.7	4.7
Percent VMA in compacted mix	VMA	15.4	11.2	16.1	12.6	14.8
Percent air voids in compacted mix	V_a	4.0	3.8	3.9	4.1	4.4
Percent VFA in compacted mix	VFA	74.0	66.5	77.3	67.4	70.6
Dust/asphalt ratio	D/A	1.0	1.7	0.9	1.4	1.1
Surface area (m^2/kg)	SA	4.2	4.4	4.3	4.3	4.3
Theoretical film thickness	FT	11.2	6.7	11.7	9.8	7.7
Effective VMA in compacted mix	VMA_e	35.4	28.6	38.4	31.7	35.6
Effective film thickness	Fte	39.2	25.1	42.5	27.4	36.0

Table 3-10. Volumetric Properties of Fine-Graded Mixtures (FAA Effects)

Property	Symbol	Mixture				
		WRF	CGF	RBF	CALF	CHF
Maximum theoretical density	G_{mm}	2.338	2.381	2.416	2.480	2.407
Specific gravity of asphalt	G_b	1.035	1.035	1.035	1.035	1.035
Bulk specific gravity of compacted mix	G_{mb}	2.244	2.288	2.327	2.386	2.315
Asphalt content	P_b	6.3	6.7	5.9	5.3	5.5
Bulk specific gravity of aggregate	G_{sb}	2.488	2.403	2.599	2.524	2.549
Effective specific gravity of aggregate	G_{se}	2.554	2.63	2.637	2.691	2.608
Asphalt absorption	P_{ba}	1.1	1.2	1.2	1.2	1.0
Effective asphalt content in the mixture	P_{be}	5.3	3.2	5.7	3.4	4.8
Percent VMA in compacted mix	VMA	15.6	11.2	16.0	10.5	14.1
Percent air voids in compacted mix	V_a	4.0	3.9	3.7	3.8	3.7
Percent VFA in compacted mix	VFA	74.2	65.2	76.8	63.8	73.7
Dust/asphalt ratio	D/A	0.8	1.4	0.7	1.3	0.9
Surface area (m^2/kg)	SA	5.4	4.8	4.7	4.7	4.7
Theoretical film thickness	FT	9.0	6.3	10.2	5.2	8.7
Effective VMA in compacted mix	VMA_e	25.7	21.3	27.3	18.8	24.7
Effective film thickness	Fte	19.3	14.6	22.8	11.7	19.7

Table 3-11. Volumetric Properties of Coarse-Graded Mixtures (Gradation Effects)

Property	Symbol	Mixture		
		C1	C2	C3
Maximum theoretical density	G_{mm}	2.328	2.347	2.349
Specific gravity of asphalt	G_b	1.035	1.035	1.035
Bulk specific gravity of compacted mix	G_{mb}	2.235	2.255	2.254
Asphalt content	P_b	6.5	5.8	5.3
Bulk specific gravity of aggregate	G_{sb}	2.469	2.465	2.474
Effective specific gravity of aggregate	G_{se}	2.549	2.545	2.528
Asphalt absorption	P_{ba}	1.3	1.3	0.9
Effective asphalt content in the mixture	P_{be}	5.3	4.6	4.5
Percent VMA in compacted mix	VMA	15.4	13.8	13.6
Percent air voids in compacted mix	V_a	4.0	3.9	4.0
Percent VFA in compacted mix	VFA	74.1	71.6	70.2
Dust/asphalt ratio	D/A	0.7	0.8	1.2
Surface area (m^2/kg)	SA	4.9	4.6	5.7
Theoretical film thickness	FT	11.2	10.1	8.0
Effective VMA in compacted mix	VMA_e	35.4	35.3	30.4
Effective film thickness	Fte	39.2	39.3	24.1

Table 3-12. Volumetric Properties of Fine-Graded Whiterock Mixtures (Gradation Effects)

Property	Symbol	Mixture				
		F1	F2	F4	F5	F6
Maximum theoretical density	G_{mm}	2.338	2.375	2.368	2.326	2.341
Specific gravity of asphalt	G_b	1.035	1.035	1.035	1.035	1.035
Bulk specific gravity of compacted mix	G_{mb}	2.244	2.281	2.272	2.233	2.244
Asphalt content	P_b	6.3	5.4	5.7	6.7	6.1
Bulk specific gravity of aggregate	G_{sb}	2.488	2.489	2.491	2.485	2.489
Effective specific gravity of aggregate	G_{se}	2.554	2.565	2.568	2.555	2.550
Asphalt absorption	P_{ba}	1.1	1.2	1.2	1.2	1.0
Effective asphalt content in the mixture	P_{be}	5.3	4.2	4.5	5.6	5.2
Percent VMA in compacted mix	VMA	15.6	13.2	14.0	16.2	15.4
Percent air voids in compacted mix	V_a	4.0	3.9	4.0	4.0	4.2
Percent VFA in compacted mix	VFA	74.2	70.1	71.2	75.0	72.8
Dust/asphalt ratio	D/A	0.8	1.4	1.3	0.8	1.1
Surface area (m^2/kg)	SA	5.4	5.7	6.0	6.5	4.1
Theoretical film thickness	FT	9.0	6.9	9.7	8.2	10.8
Effective VMA in compacted mix	VMA_e	25.7	25.8	23.5	26.8	28.9
Effective film thickness	Fte	19.3	17.1	13.2	20.7	20.9

Table 3-13. Volumetric Properties of Granite Mixtures

Property	Symbol	Mixture					
		GAC1	GAC2	GAC3	GAF1	GAF2	GAF3
Maximum theoretical density	G_{mm}	2.442	2.500	2.492	2.473	2.532	2.505
Specific gravity of asphalt	G_b	1.035	1.035	1.035	1.035	1.035	1.035
Bulk specific gravity of compacted mix	G_{mb}	2.442	2.399	2.391	2.473	2.433	2.404
Asphalt content	P_b	6.63	5.26	5.25	5.68	4.56	5.14
Bulk specific gravity of aggregate	G_{sb}	2.687	2.687	2.686	2.686	2.687	2.687
Effective specific gravity of aggregate	G_{se}	2.710	2.719	2.709	2.706	2.725	2.720
Asphalt absorption	P_{ba}	0.37	0.43	0.31	0.28	0.53	0.46
Effective asphalt content in the mixture	P_{be}	6.32	4.85	4.96	5.42	4.06	4.70
Percent VMA in compacted mix	VMA	18.5	15.4	15.7	16.6	13.6	15.1
Percent air voids in compacted mix	V_a	4.0	4.0	4.1	4.0	3.9	4.0
Percent VFA in compacted mix	VFA	78.5	73.8	74.2	75.9	71.2	73.3
Dust/asphalt ratio	D/A	0.6	0.8	0.9	0.6	1.2	1.2
Surface area (m^2/kg)	SA	3.3	3.5	4.2	4.1	5.3	4.9
Theoretical film thickness	FT	19.9	14.3	12.1	13.4	7.7	9.9
Effective VMA in compacted mix	VMA_e	42.9	39.0	35.1	28.4	26.6	33.5
Effective film thickness	Fte	67.3	50.8	35.7	27.3	17.8	28.4

Table 3-14. Volumetric Properties of Field Projects

Property	Symbol	Mixture				
		Proj-1	Proj-2	Proj-3	Proj-7	Proj-8
Maximum theoretical density	G_{mm}	2.509	2.523	2.216	2.334	2.382
Specific gravity of asphalt	G_b	1.035	1.035	1.035	1.035	1.035
Bulk specific gravity of compacted mix	G_{mb}	2.407	2.445	2.122	2.229	2.284
Asphalt content	P_b	5.5	5.0	8.3	6.1	6.0
Bulk specific gravity of aggregate	G_{sb}	2.691	2.694	2.325	2.47	2.503
Effective specific gravity of aggregate	G_{se}	2.736	2.725	2.475	2.573	2.598
Asphalt absorption	P_{ba}	0.6	0.4	2.7	1.7	1.4
Effective asphalt content in the mixture	P_{be}	4.9	4.5	5.7	5.2	4.5
Percent VMA in compacted mix	VMA	15.5	14.8	16.4	16.0	14.0
Percent air voids in compacted mix	V_a	4.1	4.4	4.2	4.5	3.9
Percent VFA in compacted mix	VFA	73.7	70.6	74.1	71.9	72.4
Dust/asphalt ratio	D/A	1.2	0.6	0.6	0.6	1.0
Surface area (m^2/kg)	SA	5.2	3.0	3.7	4.6	4.3
Theoretical film thickness	FT	9.2	8.7	11.3	7.7	8.9
Effective VMA in compacted mix	VMA_e	31.1	38.1	35.4	22.1	34.3
Effective film thickness	Fte	24.4	52.3	48.3	18.6	35.3

CHAPTER 4
TESTING METHODOLOGY FOR AXIAL COMPLEX MODULUS TEST

4.1 Introduction

In this chapter, the methodology used for the testing of complex modulus will be described. The test equipment and experimental setup used will be described, along with test protocol used. Since water was used as a medium for heating and cooling the test specimens, the development of the protocol for heating and cooling is also discussed.

4.2 Description of Servo-hydraulic Test Equipment

The loading frame used for the complex modulus test was an MTS 810 load frame, with a closed-loop servo-hydraulic controller attached. The applied force was measured and controlled using a 100-kN (22-kips) load cell. The MTS system was controlled by a Teststar IIm controller system, which is capable of controlling up to four loading frames and eight actuators at the same time. The Teststar IIm controller program has the capacity of simultaneously recording up to 12 output signals. The output and input signals can be viewed during the test with the meter option in the controller program.

The complex modulus test sequences described below were automated through user-defined programs using the Teststar IIm multi-purpose MTS 793.10 tool. This program is capable of creating complex test procedures that include command, data acquisition, event detection and external control instructions.

4.3 Testing Frequencies and Temperatures

Since the NCHRP 1-37A Draft Test Method DM-1: Standard Test Method for Dynamic Modulus of Asphalt Concrete Mixtures (Witczak, 2002) had not been developed at the onset of the testing program, the older ASTM D 3497 testing procedure for dynamic modulus testing was followed, with major modifications, summarized by Witczak et al. (1999; 2002). Most of the key features of the NCHRP 1-37A Draft Test Method DM-1 were followed, with the exception of:

- the heating/cooling system, discussed below; and
- frequencies and temperatures of testing, discussed below.

The load levels used provided strain amplitudes between 75 and 150 microstrain to maintain linearity with a seating load of about 5 percent of the dynamic load applied to the specimen. These strain levels were deemed within the linear viscoelastic range based on prior testing (Witczak, 2000; Pellinen and Witczak, 2002). The testing frequencies (16 Hz, 4 Hz, and 1 Hz) were recommended in ASTM D 3497. In addition, testing was performed at 10 Hz frequency as well, in order to obtain a better distribution of testing frequencies.

In order to obtain a measure of the temperature dependency of the complex modulus for typical Florida mixtures, test temperatures were selected at 10° C, 25° C, 30° C, and 40° C. Most mixtures were tested at three temperatures, with some of the mixtures only being tested at two temperatures, as discussed in Chapter 5.

Finally, the duration of testing at each frequency was determined. At the beginning of testing, the samples were preconditioned with 200 cycles at 25 Hz. After the preconditioning phase, preliminary testing showed that the dynamic modulus becomes stable state very soon. For example, in Figure 4-1, the dynamic modulus remains almost constant after second or third points. Therefore, the duration of the test does not need to be long. For the complex modulus test, a test duration of 50 cycles was found sufficient for all frequencies tested. However, to be consistent with recommendations by Witzcak et al. (2002), Table 4-1 was used to determine the duration of testing at each frequency.

Table 4-1. Number of Cycles for the Test Sequence for Dynamic Modulus Testing

Frequency (Hz)	Number of Cycles
16	200
10	200
4	100
1	20

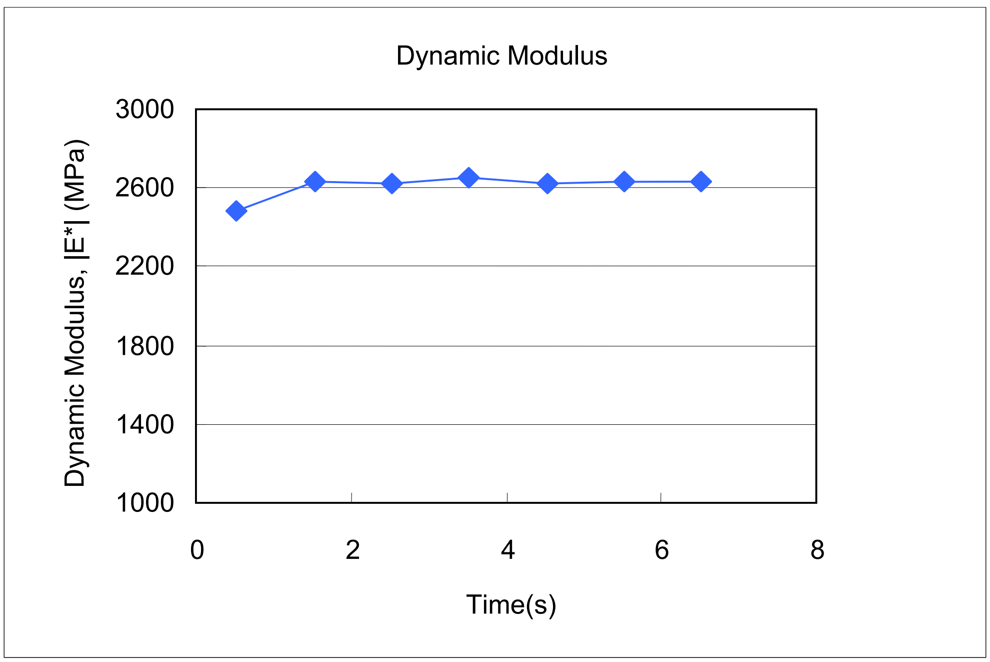

Figure 4-1. Typical dynamic modulus results

Similarly, the calculation of modulus as an average of 10 test cycles resulted in less variability in the dynamic modulus than an average of 5 test cycles. Figure 4-2 shows the dynamic modulus calculated as an average modulus of 10 cycles versus 5 cycles. It was shown that the results is less scattered if we calculate the modulus for average of 10 cycles than that of 5 cycles.

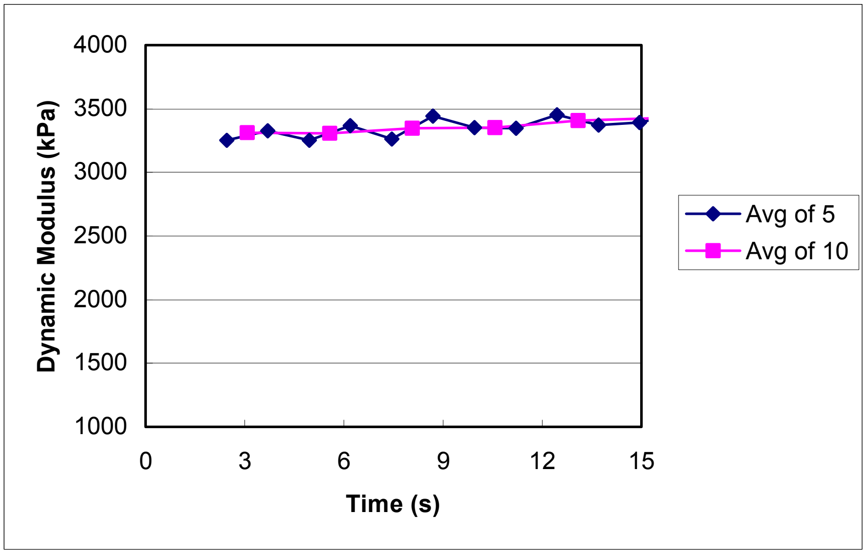

Figure 4-2. Calculation of modulus, average of 10 cycles versus 5 cycles

Finally, for each testing frequency, the number of samples per cycle of loading was set at 50 to ensure high quality sampling of results.

4.4 Specimen Preparation

Currently, there is much discussion about the shape and size of specimens to be used in complex modulus testing. In NCHRP project 9-19, Witzcak and his colleagues investigated the proper size and geometry of test specimens (Witzcak et al., 2000). They designed full factorial experiments using nominal maximum aggregate size, aspect ratio, and diameter as the controlled variables. The results were analyzed using ANOVA and graphical techniques. Another consideration was the repeatability of test results. Based on numerous complex modulus test results, they recommended using 102-mm diameter cored specimens from a 150-mm diameter gyratory compacted specimen, with a final cut (sawed) height of 150-mm. Fully lubricated end plates (by use of Teflon paper or other methods) were found to minimize end restraint to the specimen. Increasing the number of gages used to measure axial strain decreased the number of test specimens necessary.

The recommendation for coring a 102-mm diameter sample out of a 150-mm diameter sample came from a study by Chehab et al. (2000) that considered the variation in air voids within specimens compacted using the Superpave Gyratory Compactor (SGC). The study showed that specimens compacted using the 150-mm SGC mold tended to have non-uniform air void distribution both along their diameter and height. Compared to the interior portion of regular SGC-compacted specimens, the sections at the top and bottom edges, as well as the sections adjacent to the mold walls, tend to have higher air void contents.

To evaluate the variation in air voids along the diameter in 102-mm diameter compacted SGC-compacted specimens, two typical mixtures were studied. The first one was a coarse-graded 12.5-mm nominal maximum aggregate size Whiterock oolitic limestone mixture (WR-C1), and the second one was a fine-graded 12.5-mm nominal maximum aggregate size Georgia granite mixture (GA-F1). Both mixtures are described in Chapter 3. For each mixture, digital x-ray tomographic images were obtained for a 100-mm diameter Servopac SGC-compacted specimen, and the air voids in each imaging slice were calculated radially away from the center of the specimen. In order to not bias the calculation of air voids, care was taken to split the specimen into disks of approximately equal areas. Each tomographic imaging slice had a finite thickness of 0.5-mm. The air voids versus radius in all slices were summed, and the resulting distribution of air voids was plotted in Figure 4-3. The results show that there is a gradient in air voids toward the edge of the compaction mold. However, the maximum difference in air voids across each specimen is only about 0.2-0.3 percent. Based on these relatively small differences in the lateral distribution of air voids, the use of 102-mm diameter gyratory compaction molds for sample preparation appeared to be justified. Recent work by Azari et al. (2004) confirmed that the dynamic modulus is insensitive to much greater sample inhomogeneity than those introduced by the current sample preparation technique.

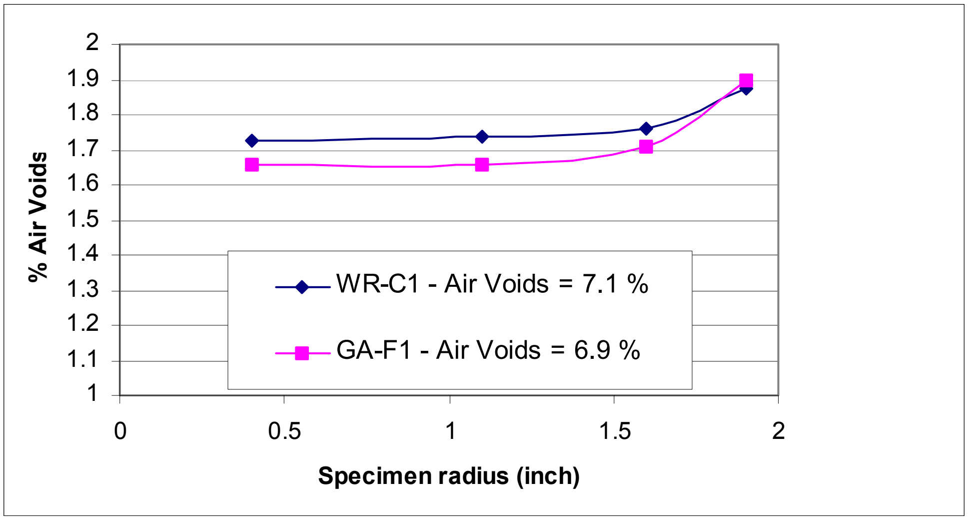

Figure 4-3. Radial distribution of air voids from x-ray tomographic imaging for typical coarse-graded and fine-graded mixtures

Similarly, Figures 4-4 and 4-5 show the distribution of air voids versus depth along the vertical axis for WR-C1 and GA-F1. Consistent with published results (e.g., Chehab et al., 2000), a very sharp gradient in the air voids is present for both mixtures in the top 10 to 20 mm of the sample. Hence, this confirms that it is important to trim the ends of testing samples.

Based on these findings, it was decided for expediency of testing and preparation, to use the following settings and procedures for sample preparation:

- SGC compaction mold diameter: 4.0 in (102-mm);
- compacted specimen height: 170-mm to 180-mm; and
- trim (saw) ends of specimens to obtain 102-mm diameter samples that are 150-mm tall.

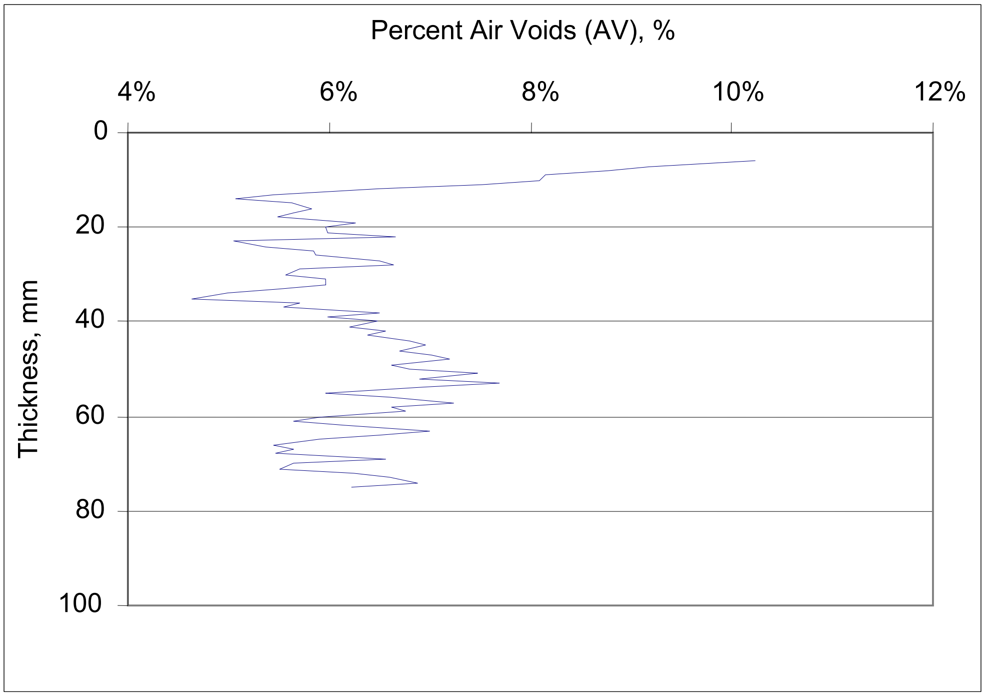

Figure 4-4. Vertical distribution of air voids from x-ray tomographic imaging for the WR-C1 coarse-graded 12.5-mm nominal aggregate size mixture

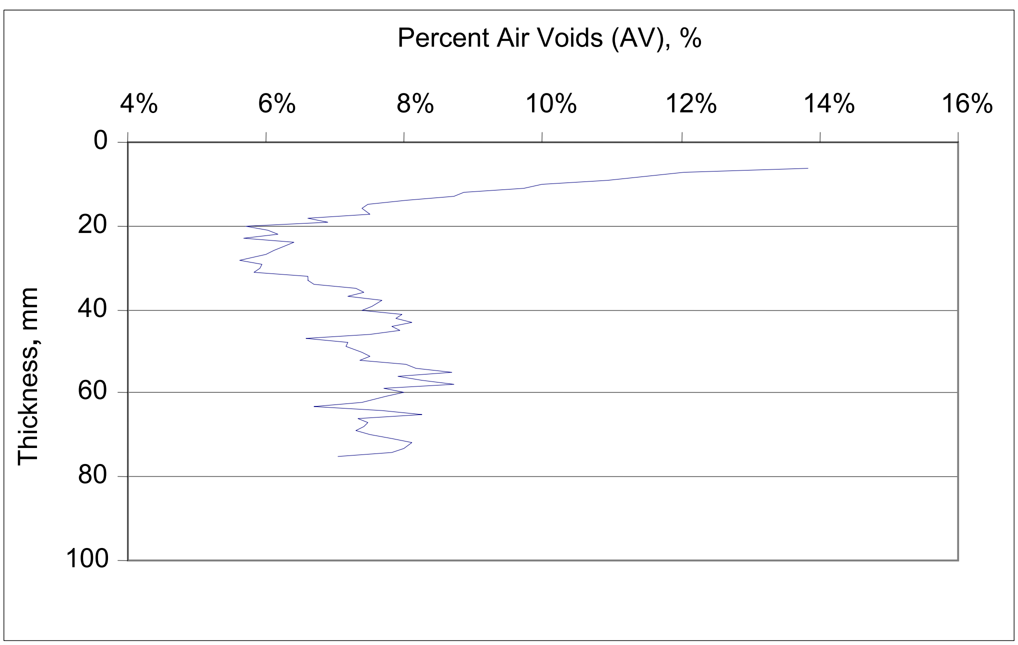

Figure 4-5. Vertical distribution of air voids from x-ray tomographic imaging for the GA-F1 fine-graded 12.5-mm nominal aggregate size mixture

Figure 4-6 depicts a specimen ready to be tested. In order to reduce end effects during testing, the two 0.5-mm (0.02-in.) latex sheets were placed between the ends of the specimen and the loading platens, and a lubricating agent (silicone grease) was applied between the membranes.

Figure 4-6. A sample ready to be tested

In order to minimize the variability in measurements, four LVDTs were used to measure vertical deformation. Each LVDT had a range of 0.5 mm (0.02 in.). The gage length of each LVDT was set at 2 inches (51.0 mm).

4.5 Description of LVDT Holder Design

The LVDTs are positioned such that they are normal to the cylindrical surface of the specimen in 90° increments. A holder was designed that allows for the installation of four

LVDTs in this configuration. Machined from aluminum and anodized for corrosion resistance, the holder contains four "through" holes that allow the holder to be integrated with the struts of the cell. Slightly oversized, these through holes enable the holder to travel to any position along the length of the struts. Once positioned, the holder is affixed to the struts via eight nylon-tipped, stainless steel setscrews. The nylon tip prevents marring of the strut and is intended for applications where the setscrew is continuously re-engaged. The LVDTs are placed into the holder via thru holes and restrained with stainless steel set screws. This simple configuration allows for rapid positioning of the devices at any position along the length of the specimen. Figure 4-7 illustrates the LVDT holders used, as well as the preparation of test specimens.

4.6 Temperature Control System

Fluid was used for temperature control. This required the specimen to be sealed with a 3.048×10^{-4}-m (0.012-in.) thick latex membrane during testing. For temperatures above 2° C, circulating water was used for temperature control. The water delivery system can be connected to either a heater or chiller unit. The heater and chiller are each capable of pumping water through the water delivery system and into and out of the cell cavity prior to returning in a closed-loop path. Conditioning in this manner utilizes the principle of conduction as the mode of energy transference. Figure 4-8 depicts a schematic of the heating/cooling system used.

Figure 4-7. Preparation of a sample complex modulus test

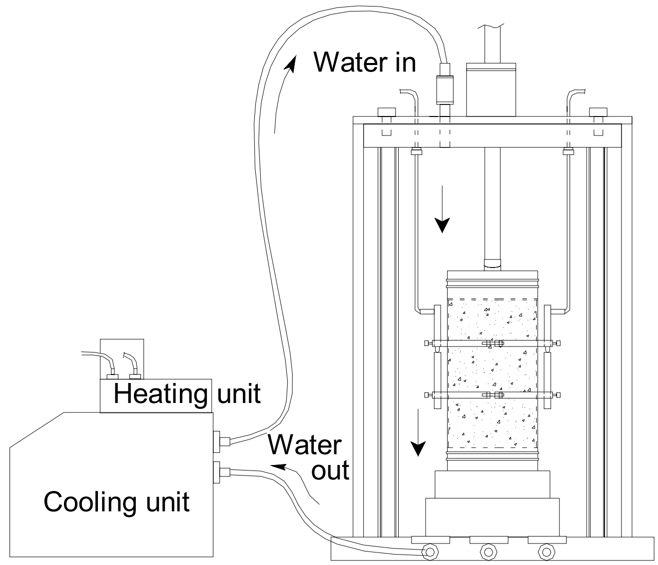

Figure 4-8. Temperature control by circulating water

The combination of the heating and chiller units allows the test specimen to be controlled within the range of 2º C to 75º C. Unlike other systems, which use indirect conditioning methods (e.g., a closed conduit running through a temperature bath), this configuration has proven very responsive and capable of conditioning a specimen from room temperature to the aforementioned range limits in less than 90 minutes.

At the time the specimen is first placed into the system, it is stabilized at room temperature. The specimen is surrounded about its circumferential perimeter by confining water. This water acts as a medium for temperature conditioning of the specimen. As the temperature-conditioned water surrounding the membrane-encased specimen is cycled through the system, thermal energy is either drawn from the specimen, as occurs during cooling, or added to it, as occurs during heating. During the cooling process, heat is conducted from the specimen to the "colder" confining water; the opposite is true for the heating process. As this process continues, concentric layers of the cylindrically shaped specimen reach thermal equilibrium starting from the outer layer and migrating towards the central core (Çengal, 1997).

The transfer of energy from more energetic particles to less energetic adjacent particles through interactions is the thermodynamic process of conduction. The equation for the rate of heat conduction is defined as:

$$Q_{cond} = kA \frac{\Delta T}{\Delta x} \tag{4.1}$$

where Q_{cond} = rate of heat conduction, (W);

k = thermal conductivity of the layer, (W/(m·K));

A = area normal to the direction of heat transfer, (m^2);

ΔT = temperature difference across the layer, (K); and

Δx = thickness of layer, (m).

The "layer" referenced in the variable definition, Δx, is the latex membrane that encapsulates the specimen. Thermal conductivity of the latex membrane is approximately 0.13 W/m · K with a thickness, Δx, of 3.048×10^{-4} m (0.012 in.). A circumferential surface area of approximately 0.045 m^2 simplifies Eq. 4.1 to:

$$Q_{cond} = 19.19 \cdot \Delta T \text{ (W)} \tag{4.2}$$

As can be seen from Eq. 4.2, the larger the difference in temperature across the layer, the greater the rate of heat conduction. Additionally, it can be inferred that, as the temperature on either side of the layer approaches equilibrium, the rate of heat conduction decreases. Therefore, to achieve a specimen target temperature rapidly, the temperature difference between the specimen and the circulating water must be as large as possible to maximize the rate of heat conduction without surpassing the target temperature.

4.6.1 Specimen Set-up for Temperature Calibration

The final portion of the specimen to reach temperature equilibrium is the central core. Therefore, it is this region of the specimen that controls the length of conditioning time prior to the establishment of thermal equilibrium. Since the testing protocol for specimen temperature conditioning relies upon conductance for specimen heating or cooling, it was necessary to plot the change in temperature of the confining water and the core of the specimen versus time.

Although both the heater and chiller units used with the system digitally report the water temperature within their fluid reservoirs, thermal losses or gains that occur along the fluid distribution panel can vary from the reported temperature by several degrees. A series of trials were conducted for both cooling and heating to determine the most time conservative sequence to rapidly achieve the target temperature. Since the rate of heat conduction is directly proportional to the temperature difference across the layer (latex membrane), initially set temperatures were significantly lower (in the case of cooling) or higher (in the case of heating) than the target temperature to expedite thermal equilibrium. The large combined mass of the triaxial cell, water, and components of the distribution panel required a large rate of energy exchange be implemented in order to achieve the target temperature.

Two type-K thermocouple probes connected to digital gages were used to report the temperature of the confining water and the core of the specimen throughout a series of heating and cooling sequences. The thermocouples used were bare-tip and were connected to digital gages that had a recording tolerance of ±0.1° C. Prior to implementation, the thermocouples were calibrated using a certified laboratory grade mercury thermometer. From these calibrations, offsets were determined across the anticipated range of temperatures. These offsets were applied to the raw recorded data to derive a time versus temperature relationship.

The calibration of the specimen in conditions as close as is possible to those anticipated during testing is extremely important to fully account for variables of energy transference. These variables are present due to thermal sources and sinks (metal cell components), as well as insulators (latex membrane). Thermocouple 1, used to monitor the confining water temperature, was installed through one of the accessory ports located at the base of the triaxial cell. In order to avoid false readings that may have occurred by contact between the probe and metal components of the cell, the end of the probe was suspended within the volume of the cell with cotton thread. Thermocouple 2, which was required to be inside of the specimen, was more difficult to install. To simulate testing conditions, the specimen was required to be wrapped in the latex membrane thereby preventing routing of the thermocouple into the cell like that of the formerly discussed probe. Routing of the thermocouple wire through the cell's piston was eventually decided as the only viable option to achieve placement of the probe even though it required dismantling of active components of the system. The specimen used for calibration was prepared by first cutting the ends to facilitate contact between the specimen and the end platens. To allow for the installation of the probe into the specimen, a 0.25-inch diameter hole was drilled into the specimen, parallel with the longitudinal axis, starting centered on the end of the specimen and terminating at a depth equal to ½ the length of the specimen. The thermocouple was then inserted through the cell's piston and into the void in the specimen. In order to affix the thermocouple in its position and prevent energy transfer from the air-filled void to the end of the piston, the end of the specimen was sealed with silicone. The specimen was then set aside for 24 hours to allow the silicone to cure. Following the 24-hour cure time, the specimen was positioned between the end platens, wrapped with latex membrane, and secured to the end platens with O-rings.

As previously discussed, the installation of the thermocouple into the specimen required partial dismantling of the piston assembly. The removal of components used to conduct water through the specimen prevented a saturation sequence as is typical with test specimens. Therefore, it was decided to calibrate the heating and cooling times of the specimen in a dry condition. Water is a more efficient conductor of thermal energy than is air, 0.613 W/(m · K) and 0.026 W/(m · K), respectively, therefore testing with a dry specimen yields conservative calibration times for thermal equilibrium.

4.6.2 Method of Cooling and Heating Calibration

At the commencement of the cooling conditioning process, both the specimen and the conditioning water were approximately 25° C which was the typical ambient temperature of the room in which testing occurred. A multitude of chiller set temperature combinations were run to determine the most expedient sequence for equilibrium with a target end temperature of 10° C ± 0.1° C for the specimen. Owing to the efficiency of the chiller unit, care was taken not to allow the chiller to run lower than the target temperature for too long. Once the specimen temperature is achieved in the cooling process, any increase in temperature can only occur due to thermal conduction from the surrounding warmer environment.

The heating conditioning sequence began with the specimen at approximately the target temperature of the cooling process (10° C). This was done in order to allow for future nondestructive testing of specimens at low and high temperatures progressively. As with the temperature combination iterations with the cooling process, those for the heating process followed the same logic. The target end temperature was set at 40° C ± 0.1° C for the specimen.

Initially, 60 minutes of conditioning time was the target for achievement of thermal equilibrium within the specimen. This target conditioning time was used as a basis for sizing of the heater and chiller used with the system. After several calibration sequences, it was validated that this limited conditioning time was sufficient to achieve the target temperature but that an additional 30 minutes would allow for further stabilization. Although the specimen may be at the target temperature, the entire mass of the system may not. Therefore, the additional energy exchange can help to bring more of the system to the target temperature, which acts as a thermal blanket around the specimen.

4.6.3 Cooling Calibration Results

For the target temperature of 10° C, the chiller was initially set at 7° C. Initial conditions for the specimen and circulating water were 27.1° C and 25.0° C, respectively. The chiller set temperature was held for 40 minutes at which time the set temperature was increased to 8° C and maintained for an additional 50 minutes. The specimen reached the target temperature of 10° C after a total of 61 minutes of conditioning time. Further conditioning was conducted for 29 minutes at which time the specimen stabilized to 10.0° C. The chiller was then turned off thereby terminating the flow of conditioned water through the system. The specimen core temperature was monitored for an additional 30 minutes wherein the end temperature of the specimen was 10.1° C. This range of temperature (10° C ± 0.1° C) was considered acceptable for the anticipated testing. Water circulation was maintained throughout testing.

As is shown in Figure 4-9, the chilled circulating water achieved the set temperature very rapidly. Prior to stabilizing at the initial set temperature of 7° C, the water temperature is shown to drop to a temperature lower than the set temperature. This is attributed to the response sensitivity of the chiller itself. In order to rapidly lower the temperature of the circulating water, the chiller maximizes the amount of energy that it can draw from the fluid. As the circulating water approaches the set temperature, the chiller decreases the rate of energy transference, thereby decreasing the change in temperature per time. As was observed in all cooling sequences conducted, a ΔT of 18° C (initial temperature of 25° C to a set temperature of 7° C) was large enough that the efficiency of the chiller exceeded its ability to decrease the rate of heat conduction. As a result, the chiller "overshot" its target temperature. Additionally, it is shown that for the maintenance of the target temperature inside of the specimen, the chiller must be set to a lower temperature. For a specimen target

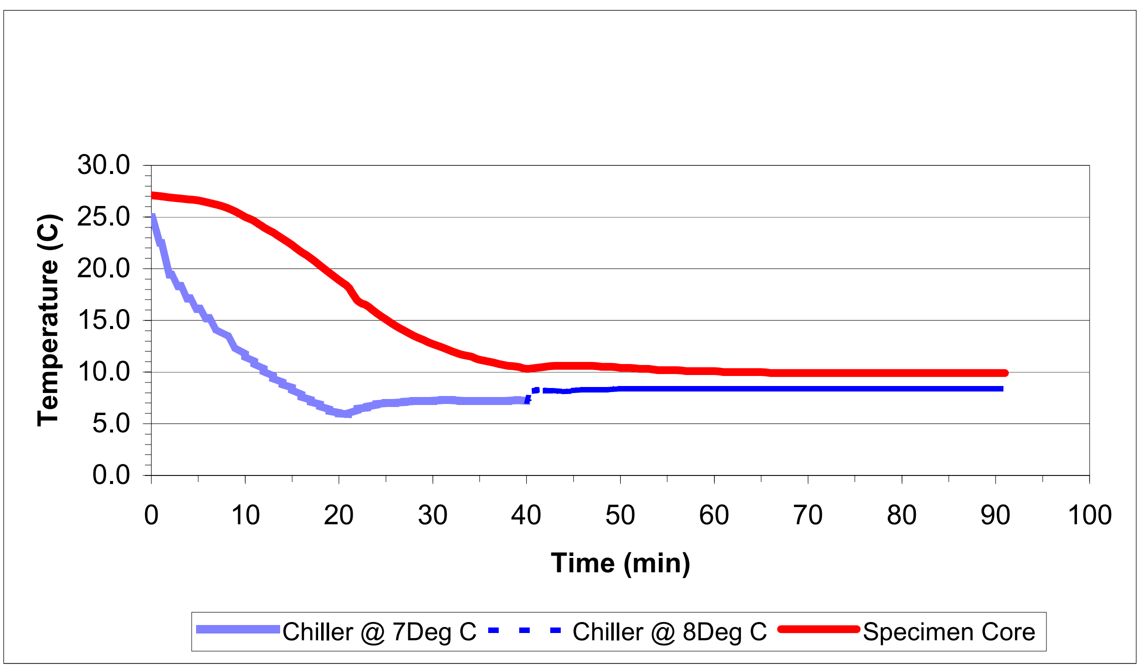

Figure 4-9. Typical time vs. temperature-specimen to 10° C (GA-C1)

temperature of 10° C, the chiller is required to be set to 8° C. This loss of 2° C from the time the fluid left the chiller to reaching the interior of the cell is attributed to the conditioning water gaining energy from the ambient temperature room as the fluid is conducted through the distribution lines and the cell itself.

The prescribed protocol for cooling the specimen to 10° C is summarized as:

1. Set chiller to 7° C and run for 40 minutes;
2. Change chiller set temperature to 8° C and run for 50 minutes; and
3. Perform complex modulus testing.

4.6.4 Heating Calibration Results

Initial conditions for the specimen and circulating water at the commencement of the heating process was 10.2° C and 26.5° C, respectively. For the target temperature of 40° C, the heater was initially set at 45° C. The heater set temperature was held for 55 minutes at which time the set temperature was decreased to 40° C and maintained for an additional 35 minutes. At the end of the total 90 minutes of conditioning, the specimen core temperature had reached 40.0° C. The heater was then turned off thereby terminating the flow of conditioned water through the system. The specimen core temperature was monitored for an additional 30 minutes wherein the end temperature of the specimen was 39.9° C. This range of temperature (40° C ± 0.1° C) was considered acceptable for the anticipated testing. During anticipated testing, the heated water circulation is maintained throughout testing.

As is shown in Figure 4-10, the circulating water achieved the set temperature very rapidly at which it was allowed to stabilize while the specimen core temperature increased. Also notable is the near parallelism of the rate of temperature increase in specimen and heater from 0 to 35 minutes of test time. This parallelism is consistent with the equation for the rate of heat conduction.

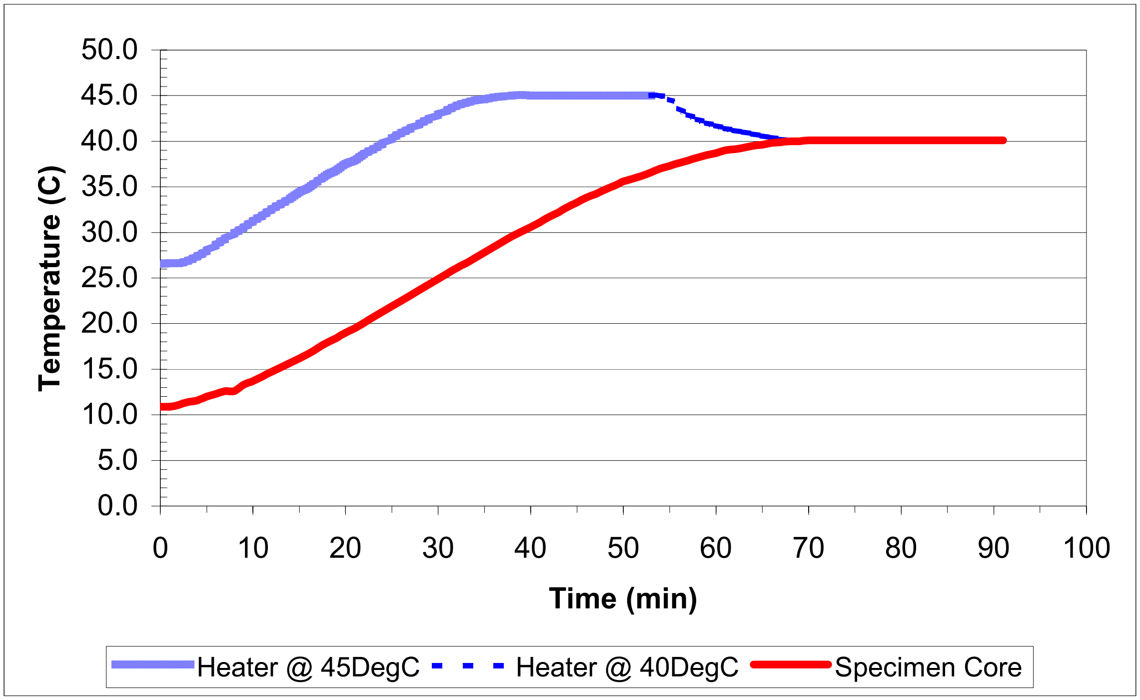

Figure 4-10. Time vs. temperature-specimen to 40° C (WR-C1)

The prescribed protocol for cooling the specimen to 40° C is summarized as:

1. Set heater to 45° C and run for 55 minutes;
2. Change heater set temperature to 40° C and run for 35 minutes; and
3. Perform complex modulus testing.

The protocols for cooling and heating were initially developed using both the GA-C1 and WR-C1 mixes with percent voids of 7.0% ± 0.5%. It is recommended that this protocol be used with the mixes used in this research and other coarse mixes with approximately similar air void percentage. For other mixes, a baseline should be developed using the same methodology as presented herein to ensure the amount of time and temperature to stabilize the core of the specimen.

4.7 Summary

In this chapter, the experimental setup and the testing protocol used for the complex modulus test was described. This includes the determination of testing frequencies and temperatures, temperature control protocols, determination of seating loads and strain magnitudes, and number of loading cycles for each frequency. The resulting test protocol follows closely the recommendations of NCHRP 1-37A Draft Test Method DM-1: Standard Test Method for Dynamic Modulus of Asphalt Concrete Mixtures (Witczak, 2002).

CHAPTER 5
DEVELOPMENT OF COMPLEX MODULUS DATA INTERPRETATION METHOD

5.1 Introduction

The data obtained from the complex modulus test is quite extensive. For a single temperature and frequency combination, there are potentially thousands of lines of data for just one specimen. There are also a number of possible interpretation methods available for analyzing the complex modulus data. It is not immediately clear which method is optimal in terms of consistency and robustness. For example, axial stress and strain measurements include some noise, which shows up as a scatter around a trend. The strain measurements also include a creep strain component that could possibly affect the determination of the phase angle. In the following, a study was performed on a set of potential interpretation methods to determine the most robust complex interpretation method. Based on the evaluation of available methods, a method based on least squares linear regression analysis was selected for determining dynamic modulus and phase angle.

5.2 Hand Calculations

According to ASTM D 3497 - Specification for Dynamic Modulus Testing, the amplitudes of the stress and strain signals are to be measured off of a scale diagram. However, this was designed for a testing system that uses a mechanical signal reading system to draw the signals directly on chart paper. With increased technology, this method is no longer optimal.

To measure the amplitudes by hand with the computer data recorded, the simplest way is to graph the results in a spreadsheet program and measure them from a printed copy. This method is fairly straightforward but it asks for the judgment of the operator.

It was assumed with the hand calculations that the amplitude of the signal was constant. This allows the signal to be enclosed by two parallel lines. Using mechanical drafting tools, these lines were drawn on the graph such that the average amplitude is directly readable. The amplitudes are to be carefully measured only in the vertical direction of the graph. If the amplitude is measured perpendicular to the creep lines drawn, an error may be induced.

In order to calculate the phase angle (δ) of the material, the time between the peaks and valleys of the signals is measured. The phase angle is measured for at least 3 cycles on the peaks and the valleys and an average is calculated. The lag time is converted to a phase angle using the following equation:

$$\delta = t_{lag} \bullet f \bullet (360°) \tag{5.1}$$

where f is the frequency of the dynamic load (in Hz); and

t_{lag} is the time difference between the signals (in seconds).

Often due to the small strains and noise in the data acquisition system, it can be difficult to isolate these points. Smoothing techniques have often been used to help identify measurement points. Any permanent deformation due to cyclic creep must also be corrected before locating the peaks and valleys. The phase angle should be measured using a combination of peaks and valleys to eliminate problems if the signal is not a perfect sinusoid.

This method is very operator dependent. The operator is required to use his judgment in order to draw the parallel lines. Phase angle measurements provide even more sources of error when an operator's decision is required to locate the peak or valley. The precision of the measurement instruments can also affect the accuracy as well.

5.3 Iterative Curve Fit Method

At the University of Minnesota, proposed that the stress and strain functions were of the following form:

$$F(t) = A + B \bullet t + C \bullet \cos(\omega \bullet t - \delta) \tag{5.2}$$

The parameter C is half of the amplitude of the wave and δ is a phase shift. The angular frequency (ω), in rad/s, is found based on the test frequency (f), in Hz, as presented below:

$$\omega = f \bullet (2 \bullet \pi) \tag{5.3}$$

The phase lag in Eqs. 5.1 and 5.2 can be calculated in Eq. 5.4 by determining the best-fit curves for both the stress and the strain as follows:

$$\delta_{Lag} = \delta_{\varepsilon} - \delta_{\sigma} \tag{5.4}$$

In order to match the predicted equation to the data, a non-linear least squared error regression technique is used. Since the phase lag is unknown and inside the trigonometric operator, a standard linear regression cannot be used to calculate all of the variables. In order to determine the optimal signal, the δ was guessed at many points through out the possible range until the error was minimized.

Zhang et al. (1997a) employed a bracketed search technique where they would guess δ at regular intervals. They would then find out which range the lowest error was in and search the system again in that reduced range. For every guess of δ, the set of matrices shown in Eq. 5.5 below were used to solve Eq. 5.2:

$$\begin{bmatrix} n & \sum t_i & \sum \cos(\omega \bullet t - \delta) \\ \sum t_i & \sum t_i^2 & \sum t_i \cdot \cos(\omega \bullet t - \delta) \\ \sum \cos(\omega \bullet t - \delta) & \sum t_i \bullet \cos(\omega \bullet t - \delta) & \sum \cos^2(\omega \bullet t - \delta) \end{bmatrix} \bullet \begin{bmatrix} A \\ B \\ C \end{bmatrix} = \begin{bmatrix} \sum F(t_i) \\ \sum t_i \bullet F(t_i) \\ \sum \cos(\omega \bullet t - \delta) \bullet F(t_i) \end{bmatrix} \quad (5.5)$$

After the least squared error values for A, B, and C were found, the least squared error was compared to the other guesses of δ. A minimum number of four guesses must be used per iteration to reduce the scope of the search. The search algorithm used is:

Step 1: Set $\delta_{start} = 0$, $\delta_{end} = 180$, $\Delta\delta = (\delta_{start}-\delta_{end})/M$ (M is an integer, M > 1)

Step 2: Calculate $\delta_j = \delta_{start} + j*\Delta\delta$ (j = 1, 2, 3, …, M)

Step 3: Solve for A, B, and C using Eq. 5.5 (j = 1, 2, 3, …, M)

Step 4: Calculate the squared error for all values of j (j = 1, 2, 3, …, M)

Step 5: Select the value d that provided that least squared error (δ_k)

Step 6: Check Convergence:

If $\Delta\delta$ > Tolerance, then update the range of d and repeat

$$(\delta_{start} = \delta_k - \Delta\delta, \delta_{end} = \delta_k + \Delta\delta), \Delta\delta = (\delta_{start} - \delta_{end})/M$$

If $\Delta\delta$ < Tolerance, then stop.

By repeating this system several times, showed that the δ could be roughly predicted. A recursive computer subroutine allows a simple error criterion to make sure that the range of the phase angle was narrowed to an acceptable level. This technique involves calling a subroutine within itself until the tolerance criteria is met. This technique requires more computer memory, but it is a much more elegant way to perform the task then a standard loop function.

This method should also be applied to the known stress signal as well. It is a good check to verify the applied stress amplitude and the data acquisition.

There are several problems and issues associated with this method. The first is that it is not very flexible. It is only designed to read the signal of a sinusoid on a straight line. It was designed for the secondary phase of creep, so it does not work as well early in the test. It also requires a perfect sinusoid and frequency. In cases where the testing machine is not tuned properly for higher frequency testing, controlling the signal based on load can lead to small variations from a perfect sinusoid, thus affecting the results obtained by this method. Also, since this is an iterative method, it can be very time consuming. Hence, the user must balance the acceptable error with the time restraints.

To verify that this method works correctly, it is recommended that the regression coefficients obtained from Eq. 5.5 be input back into Eq. 5.2 and graphed with the original signal. This allows a visual comparison of the raw data and the modeled signal.

5.4 Linear Regression Method

In order to improve upon some of the issues with the iterative curve fit method, a method based on linear regression techniques was developed. The only reason that the iterative method uses a nonlinear curve fit technique is that the δ value in the trigonometric function in Eq. 5.2 cannot be obtained directly. However, Eq. 5.2 can be rewritten using a series of trigonomic identities to obtain the following form:

$$F(t) = A_0 + A_1 \bullet t + B \bullet \cos(\omega \bullet t) + C \bullet \sin(\omega \bullet t) \qquad (5.6)$$

This allows for the use of a least squared error linear regression approach to determine all of the coefficients. The amplitude of the sinusoid can then be calculated using Eq. 5.7 and the phase angle can then be obtained with Eq. 5.8 as follows:

$$\text{Amplitude} = \sqrt{B^2 + C^2} \tag{5.7}$$

$$\text{Phase Angle} = \tan^{-1}\left(\frac{C}{B}\right) \tag{5.8}$$

Hence, there is no need for an iterative curve fitting technique anymore. Another major advantage of this method is that this linear regression technique can be expanded to allow a sinusoid oscillating around a higher order polynomial, rather then just a straight line. This potentially allows for a better representation of data earlier in the test when the material is still experiencing significant delayed elastic behavior. For a polynomial of degree m-1, the signal would then resemble Eq. 5.9:

$$F(t) = A_0 + A_1 \bullet t + A_2 \bullet t^2 + \ldots + A_m \bullet t^{m-1} + B \bullet \cos(\omega \bullet t) + C \bullet \sin(\omega \bullet t) \tag{5.9}$$

In order to solve for the best-fit solution, an algorithm based on least squares minimization of error is used. For simplicity, a linear example of these matrices is described by Eq. 5.10 below:

$$A \bullet x = B \tag{5.10}$$

where

$$A = \begin{bmatrix} n & \sum t & \sum \cos(\omega \bullet t) & \sum \sin(\omega \bullet t) \\ \sum t & \sum t^2 & \sum t \bullet \cos(\omega \bullet t) & \sum t \bullet \sin(\omega \bullet t) \\ \sum \cos(\omega \bullet t) & \sum t \bullet \cos(\omega \bullet t) & \sum \cos^2(\omega \bullet t) & \sum \cos(\omega \bullet t) \bullet \sin(\omega \bullet t) \\ \sum \sin(\omega \bullet t) & \sum t \bullet \sin(\omega \bullet t) & \sum \cos(\omega \bullet t) \bullet \sin(\omega \bullet t) & \sum \sin^2(\omega \bullet t) \end{bmatrix}$$

$$x = \begin{bmatrix} A_0 \\ A_1 \\ B \\ C \end{bmatrix}$$

$$B = \begin{bmatrix} \sum F(t) \\ \sum t \bullet F(t) \\ \sum \cos(\omega \bullet t) \bullet F(t) \\ \sum \sin(\omega \cdot t) \cdot F(t) \end{bmatrix}$$

The matrix values are found by summing up all of the relevant terms for each time step. Once the known elements in the matrix formulation are calculated, the unknown coefficients in the column vector x can be determined. The last two entries in the solution matrix then represent the coefficients B and C, respectively, in Eq. 5.9. The remaining coefficients in the matrix represent the polynomial coefficients.

The big advantage of this method is that it is a lot more efficient then the iterative curve fit method because it does not require the procedure to be repeated with several iterations. The increased matrix size is still significantly faster to process then several iterations of the smaller matrix.

5.5 Discrete Fourier Transform Method

A Fourier transform is an integral transformation that translates a complex signal in the time domain to be represented as sinusoids of varying amplitudes at all frequencies. The Fourier transform in its integral form is designed for continuous signals. The time history of stress or strain is recorded at a specified time interval. This makes it possible to use the more practical Discrete Fourier Transform (DFT). This is a computer algorithm that transforms a complex signal in the time domain into a series of sinusoids at discrete frequency intervals.

A typical 4 Hz axial strain signal, shown in Figure 5-1, is depicted as a transformed signal in Figure 5-2.

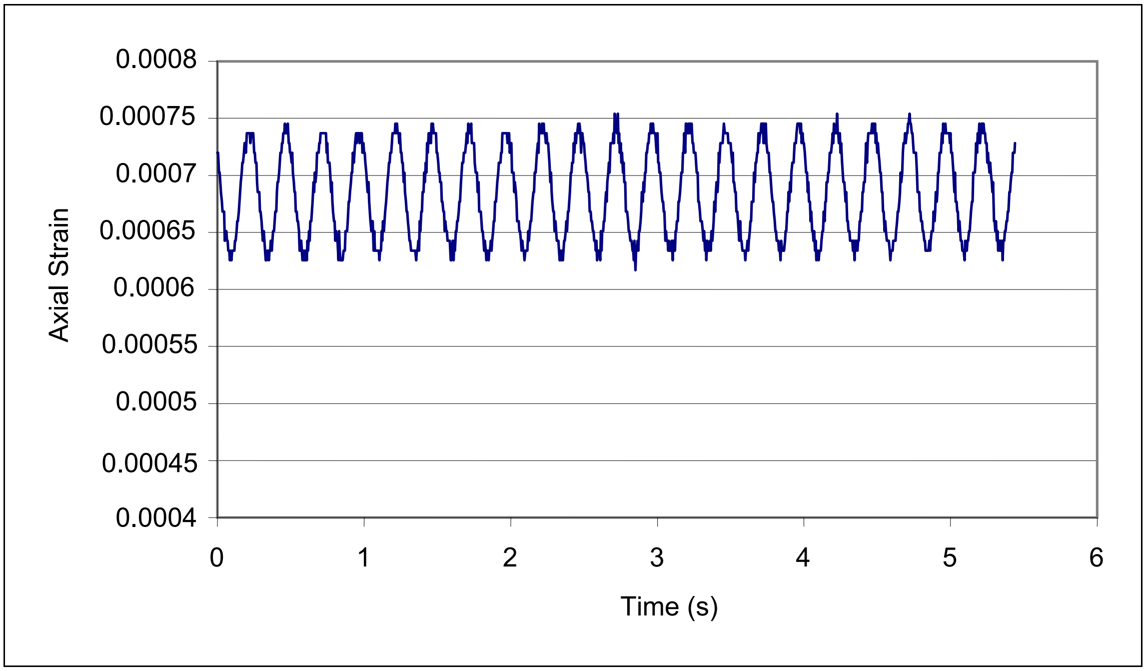

Figure 5-1. Typical axial strain signal in the time domain

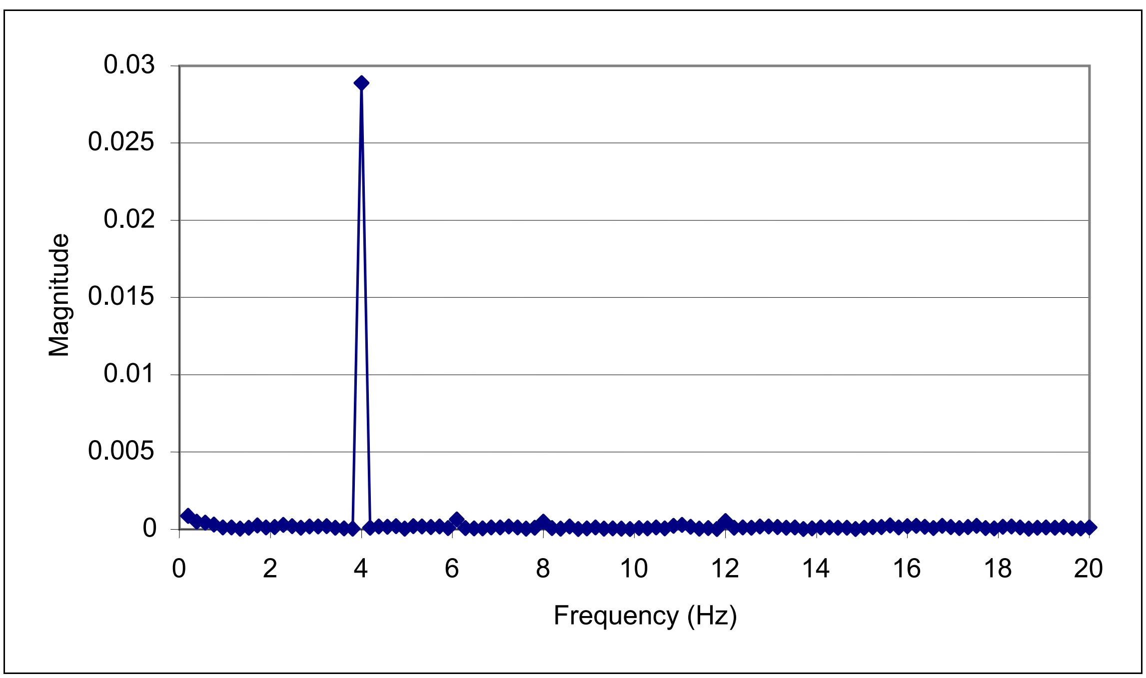

Figure 5-2. Typical axial strain signal in the frequency domain

The DFT is performed using the following equation:

$$y_p = \sum_{k=0}^{n-1} x_k \bullet \left(\cos\left(\frac{2 \bullet \pi \bullet k \bullet p}{n} \right) + i \bullet \sin\left(\frac{2 \bullet \pi \bullet k \bullet p}{n} \right) \right) \tag{5.11}$$

in which the frequency is denoted as:

$$\text{Frequency} = \frac{p \bullet (\text{Sampling Rate})}{n} \tag{5.12}$$

The value of y_p is the complex output in frequency space where p is a integer representing frequency and x_k is the time-dependent variable that is being converted. For a perfectly clean sinusoidal signal, there should be a spike at the given frequency and all other values should be zero. The amplitude of the sinusoid represented by p is given by Eq. 5.13 as:

$$\text{Amplitude} = \frac{2 \bullet |y_p|}{N} \tag{5.13}$$

where N is the number of samples recorded in the signal. The phase angle of each sinusoid can be calculated by finding the angle that is represented by the complex components of y_p.

5.5.1 Issues with the Fourier Transform

One of the problems noticed early on with the use of the Fourier Transform Technique for determining amplitude and phase angle of the complex modulus was that if the testing frequency did not occur at one of the discrete points in frequency space, then the magnitude was reduced and split between the closest frequencies on either side of the true frequency. This provided results that seemed to vary depending on the number of points tested. An example of this effect is shown in Figure 5-3. The way this was corrected was to find an integer value of p for the testing frequency using Eq. 5.12. Since the sampling rate was constant and so was the testing frequency, the only variable that was easy to manipulate

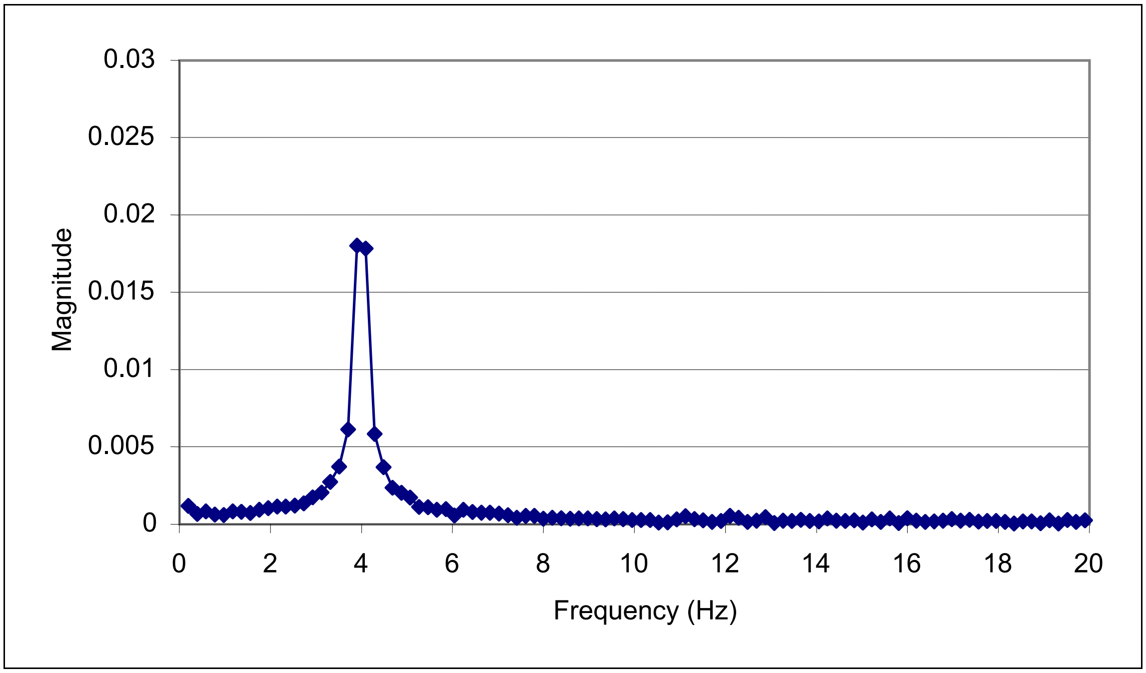

Figure 5-3. Typical axial strain with missing peak data

was the number of samples examined. To manipulate this, the mean value of the signal was added before and after the sample until the signal was the correct length. The value of p for the testing frequency can then be calculated using Eq. 5.14 where N′ is the modified number of samples in the signal:

$$p_{\text{Testing Frequency}} = \frac{f \bullet N'}{\text{Sampling Rate}} \qquad (5.14)$$

The other issue noticed with the DFT results is that if only a few cycles are used (under 20 cycles with 50 data points per cycle) then the magnitude of the signal does not accurately reflect the true value. With less data available, the peak seen in frequency space is wider and will usually include the two neighboring points. This will reduce the main peak by almost half in most cases. This led to the conclusion that more numerous data points should be used. However, an exact criteria concerning length of the sample to be used is not known.

In practice, a sufficient number of discrete data points were added until the analysis of the stress curve matched up well with the stress curve that was prescribed during the test. An example of this reduced data peak is shown in Figure 5-4.

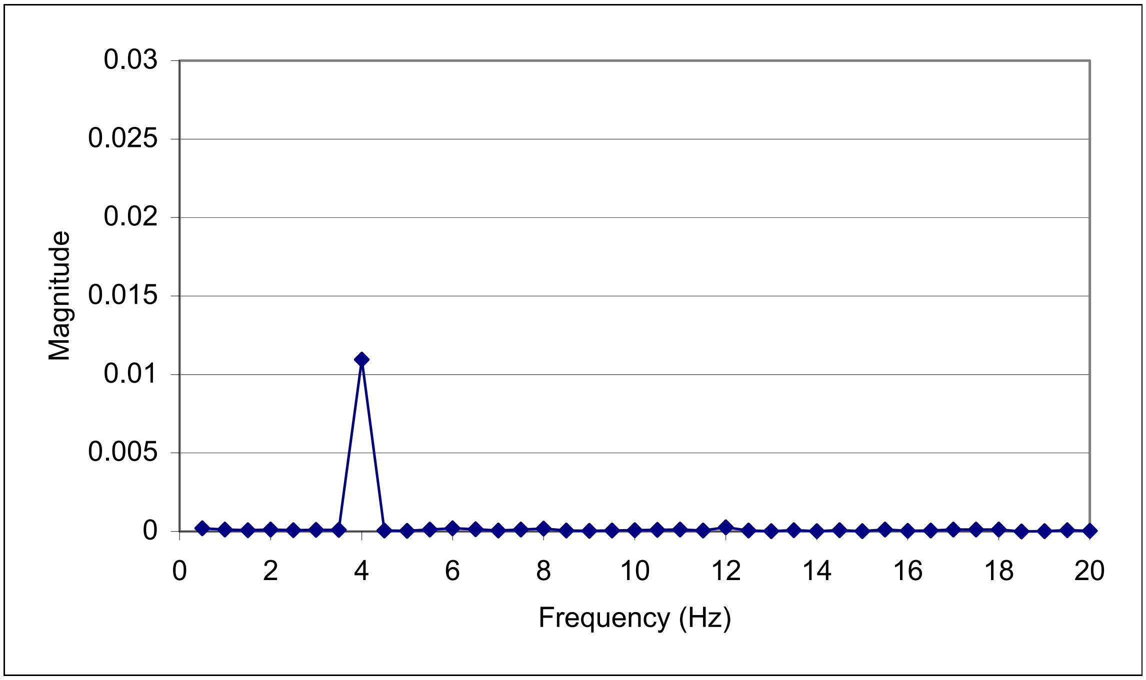

Figure 5-4. Typical axial strain signal with insufficient data

5.6 Peak and Valley Method

The peak and valley method is one of the most direct ways to calculate the amplitudes of sinusoidal signals. For any one cycle, the maximum point and the minimum point are located. The difference in the height between the peak and the valley of the signal can then be calculated as the amplitude. The phase shift can be calculated from the time lag between the strain peak and the stress peak, as described by Eq. 5.1.

There are several problems with this method that make it awkward to use consistently. For example, it is necessary to account for strain signals that are often inclined and include a trend. This can be done by either removing the trend with a curve fitting technique or by averaging the amplitude of the distance from a peak to the following valley and the distance from the valley to the following peak.

If the data are being searched for the highest point, often times in noisy signals, the highest point is a combination of the signal peak and a spike in noise. Because the strain signals tend to contain more noise then the prescribed load signals, this means that the strain amplitudes can be increased more then the load signal resulting in a lower then expected dynamic modulus value.

Another issue that complicates the development of a robust algorithm for the peak-valley method, is that the first peak in the stress signal may not be an appropriate comparison for the first peak of the strain signal. Selecting a point that occurs between either the two corresponding peaks or valleys can cause this problem. It must also be determined if the peak of the stress signal should match up with a peak or a valley of the strain signal. If the end of the selected region is not at a full cycle, it is also possible to have more peaks or valleys on one signal then the other. These things can make it difficult to correlate the correct points when calculating the phase angle.

5.7 Dissipated Energy Method

The energy density dissipated during each stress-strain cycle in a cyclic test is described as the area under the stress vs. strain curve. In a cyclic test this figure tends to most closely represent an inclined ellipse. After subtracting out the creep component of the strain measurement, it can be assumed that the shape of the time-dependent stress and strain can be represented by the following form of equations:

$$\sigma = A + \sigma_0 \cdot \cos(\omega \cdot t) \tag{5.15}$$

$$\varepsilon = B + \varepsilon \bullet_0 \bullet \cos(\omega \bullet t - \delta) \tag{5.16}$$

These parametric equations can be rearranged to eliminate time as follows:

$$\left(\frac{\sigma - A}{\sigma_0}\right)^2 + \left(\frac{\varepsilon - B}{\varepsilon_0}\right)^2 = \sin^2(\delta) + 2 \bullet \cos(\delta) \bullet \left(\frac{\sigma - A}{\sigma_0}\right) \bullet \left(\frac{\varepsilon - B}{\varepsilon_0}\right) \tag{5.17}$$

This relationship can also be seen in the testing data as well. Figure 5-5 is an example of a typical stress versus strain loop.

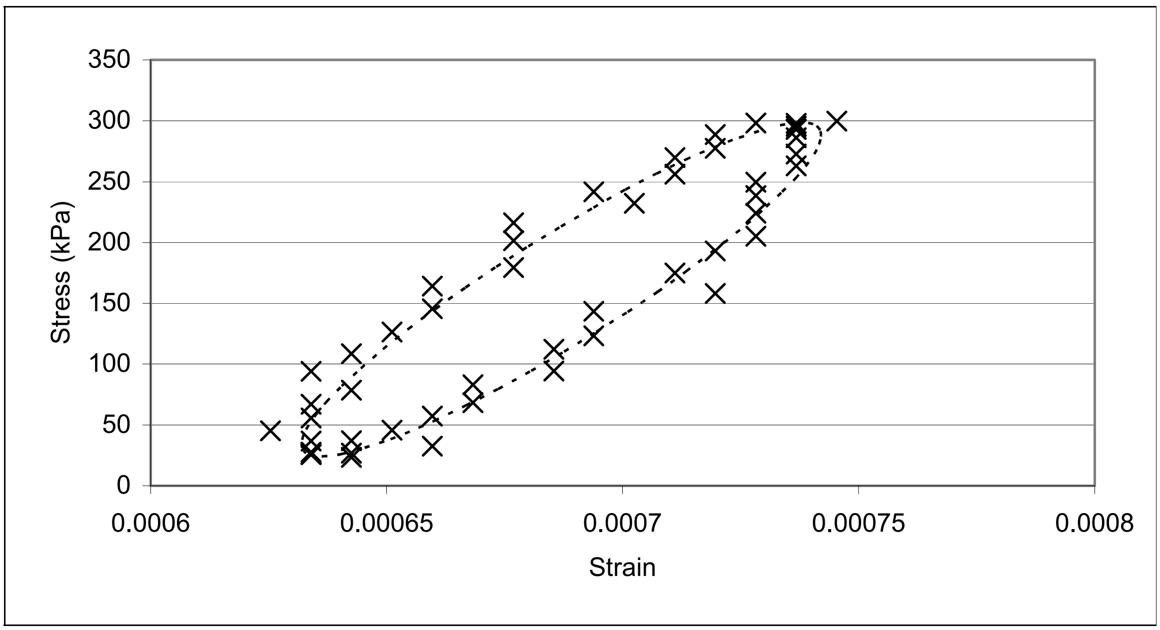

Figure 5-5. Typical stress vs. strain loop

Using Eqs. 5.15 and 5.16, the area of this ellipse can also be calculated. This area, which represents the dissipated strain energy density (ΔW), can be calculated using Eq. 5.18:

$$\Delta W = \frac{\pi}{4} \bullet \sigma_0 \bullet \varepsilon_0 \bullet \sin\delta \tag{5.18}$$

This area can also be calculated from the experimental data by assuming that the shape of the area is a polygon. The polygon is reduced to a series of trapezoids so that the areas of all trapezoids can be summed to determine the total area. Equation 5.18 can then be rearranged if the signal amplitudes and the ΔW are known so that the phase angle can be calculated.

One drawback with the dissipated energy method is that the method does not provide a way to measure the signal amplitudes easily though. Therefore another method is also required to measure the stress and strain amplitudes. However, when averaged over several cycles, this method has shown to produce phase angles very similar to the other methods.

5.8 Evaluation of Data Interpretation Methods

A typical sample frequency was selected and the following data interpretation methods were compared: 1) hand calculations, 2) the iterative curve fit method 3) the linear regression method, 4) the peak-valley method, 5) the DFT method, and 6) the dissipated energy method. The Visual Basic for Applications (Version 6.0) source code for methods 2 through 6 (where applicable) is presented in Appendices A and B.

In the following, the robustness of each method will be examined in terms of how well each method predicts known results. Various different signal effects will be evaluated, including: 1) noise, 2) type of noise, 3) signal skewness, and 4) the effects of cyclic creep. All results compared were in the steady state region of the test.

A comparison of the data analysis methods was performed using theoretical signals that were generated to compare the affects of different data interpretation methods on the complex modulus. The advantage of this is that signals can be used with known amplitude and phase angle.

5.8.1 Pure Sinusoidal Signal

A data set was generated that had a clean sinusoidal signal. This represents the ideal conditions under which the data interpretation will be used. A total of 40 cycles were analyzed in each run with 50 data points per cycle to simulate testing conditions.

Since the DFT method and the Peak/Valley method require another signal to give a comparison, all of the methods were run using a clean cosine curve with a unity magnitude and a zero phase angle as the benchmark. All the methods developed were designed to work well on a clean sinusoidal curve. As can be seen in Table 5-1, all methods provided results near the target, except the peak-valley method, which yielded a slightly lower phase angle than the theoretical signal.

Table 5-1. Analysis Results of Clean Signal Analysis

	Amplitude	Phase Angle
True Signal	1	45
Hand Calculation	0.951	45.65
DFT	0.9994	45.032
Linear Regression	1.0000	45.000
Iterative Curve Fit	1.0000	45.000
Peak Valley	0.9995	43.200
Dissipated Energy	n/a	44.881

5.8.2 Evaluation of the Effects of Signal Noise

There are two common types of noise seen in signal analysis. The first is cyclic noise, and the second one is random noise. Cyclic noise can easily be added to a generated signal by simply adding an additional higher frequency cosine signal to the test signal. As shown in Figure 5-6, if a higher frequency component is added to a base-line sinusoidal signal at a multiple of the base-line (i.e., testing) frequency, the signal can be drastically altered, potentially affecting the interpreted phase angle and amplitude.

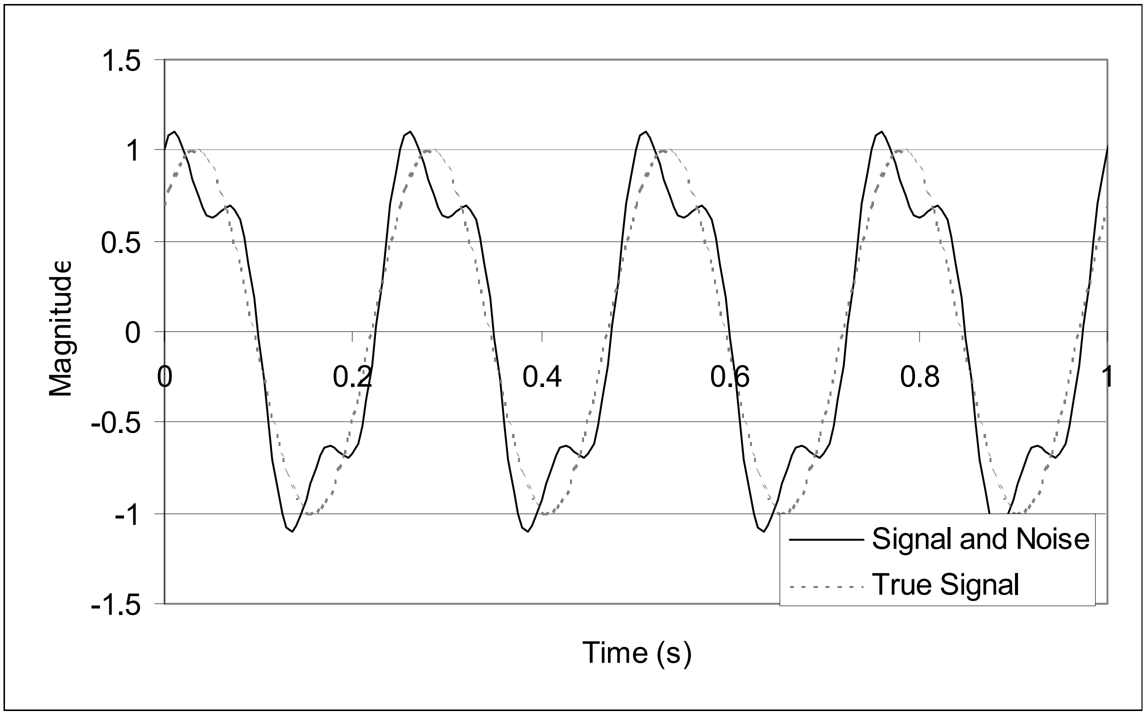

Figure 5-6. Example of cyclic noise

Table 5-2 shows the resulting interpreted amplitude and phase angle using the various calculation methods available.

Table 5-2. Analysis Results of Cyclic Noise Signal

	Amplitude	Phase Angle
True Signal	1	45
Hand Calculation	0.961	34.10
DFT	0.9991	45.054
Linear Regression	1.0000	45.000
Iterative Curve Fit	1.0000	45.000
Peak Valley	1.0997	14.400
Dissipated Energy	n/a	44.850

The DFT, the linear regression, and the iterative curve fit methods all worked well because they can take into account the higher frequency. However, these additional peaks mislead the Peak/Valley method and the hand calculations as well. It should be noted that for most practical cases, the frequency of the noise would be much higher and hence the difference in phase angle would be much smaller. The dissipated energy method also produces a phase angle that is close to the true phase angle. It slightly under estimates the phase angle however due to the polygon approximation used.

As stated previously, the other common type of noise seen in signals is random noise. Random noise was generated with approximately the same magnitude as the cyclic noise generated and it was normally distributed about the signal. An example of the effect of the random noise can be seen in Figure 5-7.

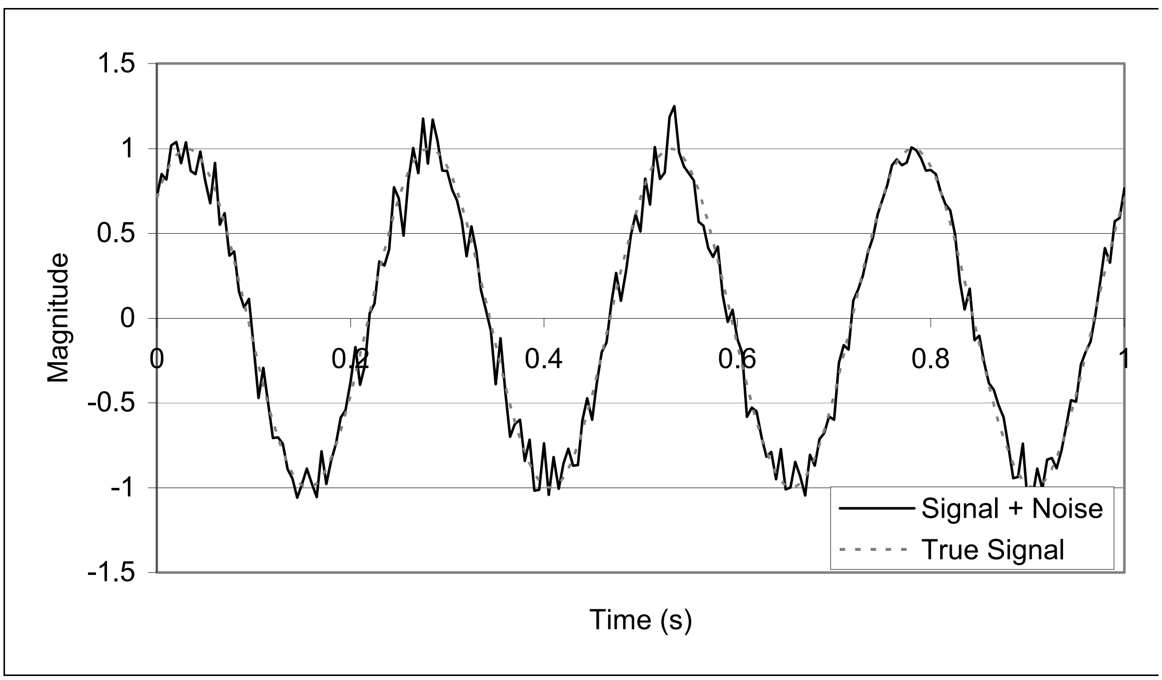

Figure 5-7. Example of random noise

All of the analysis methods were then used to evaluate the signal. The results for the analysis are displayed in Table 5-3. These results show that the least squared regression methods better characterizes the random data then the Fourier transform method. This is because the Fourier transform method tries to describe the random noise in terms of cycles, and this can often decrease the true signal amplitude. The dissipated energy method provides a phase angle that is closest to the true value. The peak/valley method produces a higher amplitude than the true amplitude, because this method measures the highest and lowest points and hence these values will include the noise as part of the amplitude.

Table 5-3. Analysis Results for Random Noise Signal

	Amplitude	Phase Angle
True Signal	1	45
Hand Calculation	0.944	48.29
DFT	0.9949	45.241
Linear Regression	0.9956	45.209
Iterative Curve Fit	0.9956	45.209
Peak Valley	1.1061	44.100
Dissipated Energy	n/a	45.053

Finally, the combined effects of cyclic and random noise were evaluated. Figure 5-8 shows the resulting combined signal. For this signal a 65 Hz frequency was used for the

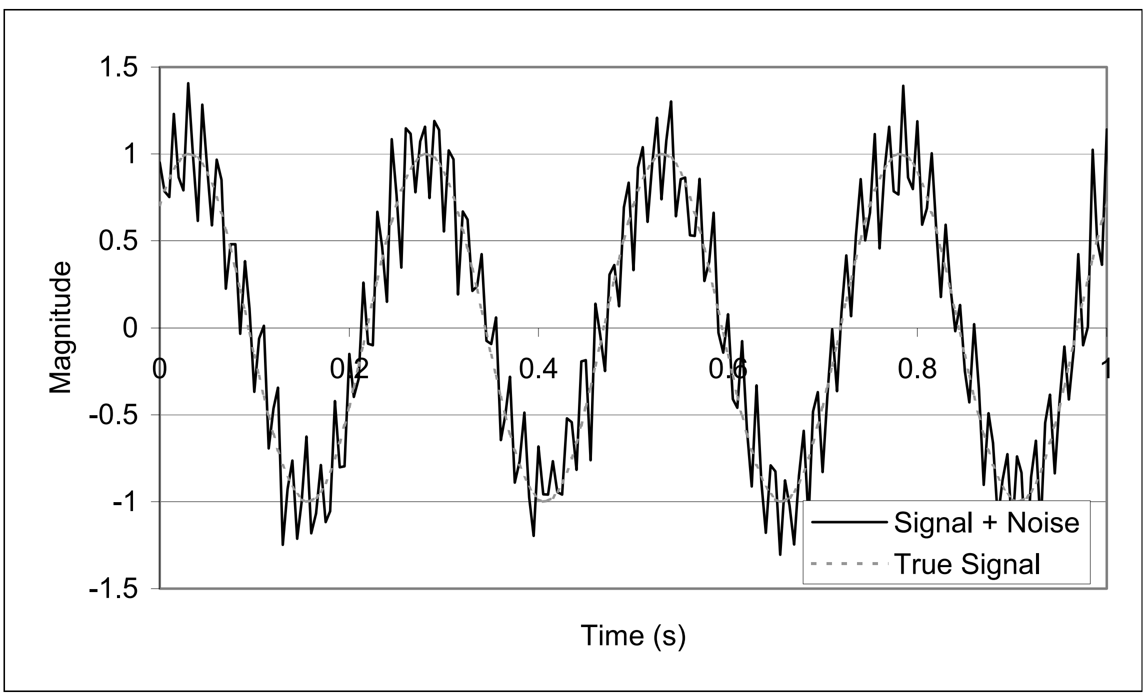

Figure 5-8. Example of random and cyclic noise

cyclic noise to closer simulate interference from an AC electrical signal. The analysis results can be seen in Table 5-4. The results show a reverse effect from the individual noise signals. In this case, the DFT results more closely represent the actual values than the least squared regression methods.

Table 5-4. Analysis Results of Signal with Random and Cyclic Noise

	Amplitude	Phase Angle
True Signal	1	45
Hand Calculation	1.012	44.91
DFT	1.0037	45.012
Linear Regression	1.0039	44.964
Iterative Curve Fit	1.0039	44.964
Peak Valley	1.3049	44.640
Dissipated Energy	n/a	44.851

Finally, a comparison of the predictions of amplitude and phase angle for the different types of noise studied is shown in Figures 5-9 and 5-10. The most consistent methods are the DFT, the linear regression, and the iterative curve fit. The dissipated energy method also performed well at predicting the phase angle. The most robust methods for theoretical signals are the DFT, the iterative curve fit, and the linear regression. However, the simplest method to use is the linear regression method. The DFT method requires a very high number of sampled data points to work well, along with some judgment from the user. Similarly, the iterative curve fit method requires judgment from the user in terms of starting input and number of iterations. However, the linear regression method is robust and requires no specific user input. Therefore, the linear regression method will be used for the remainder of this study.

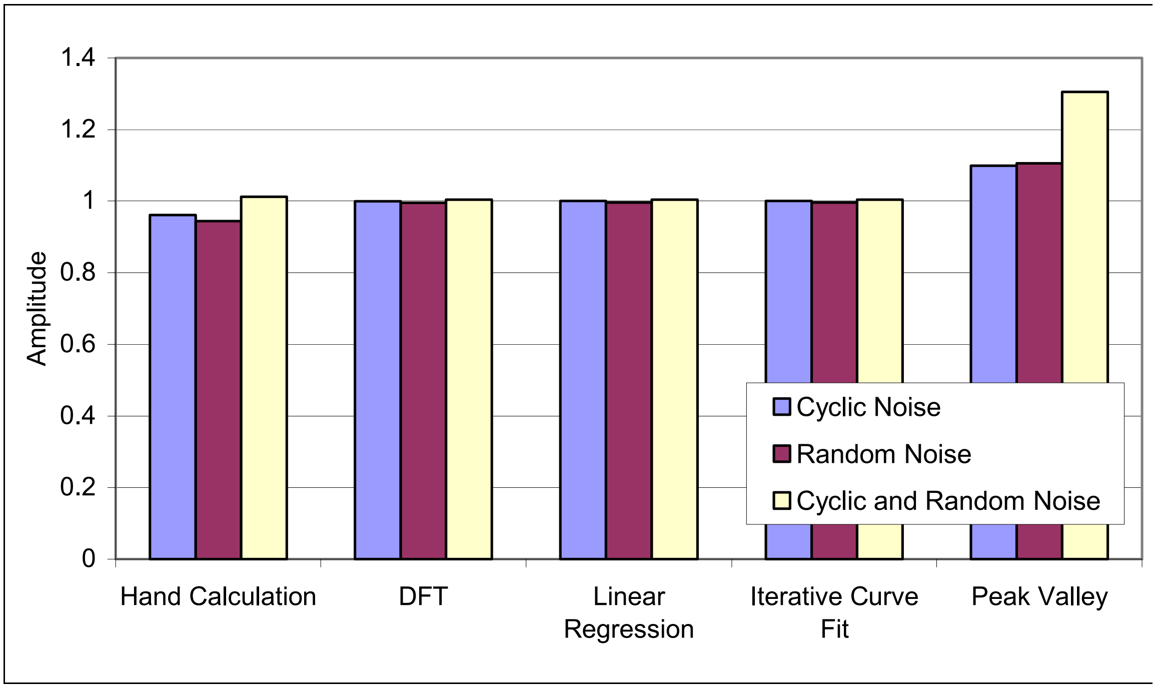

Figure 5-9. Amplitude comparison of methods for various types of noise

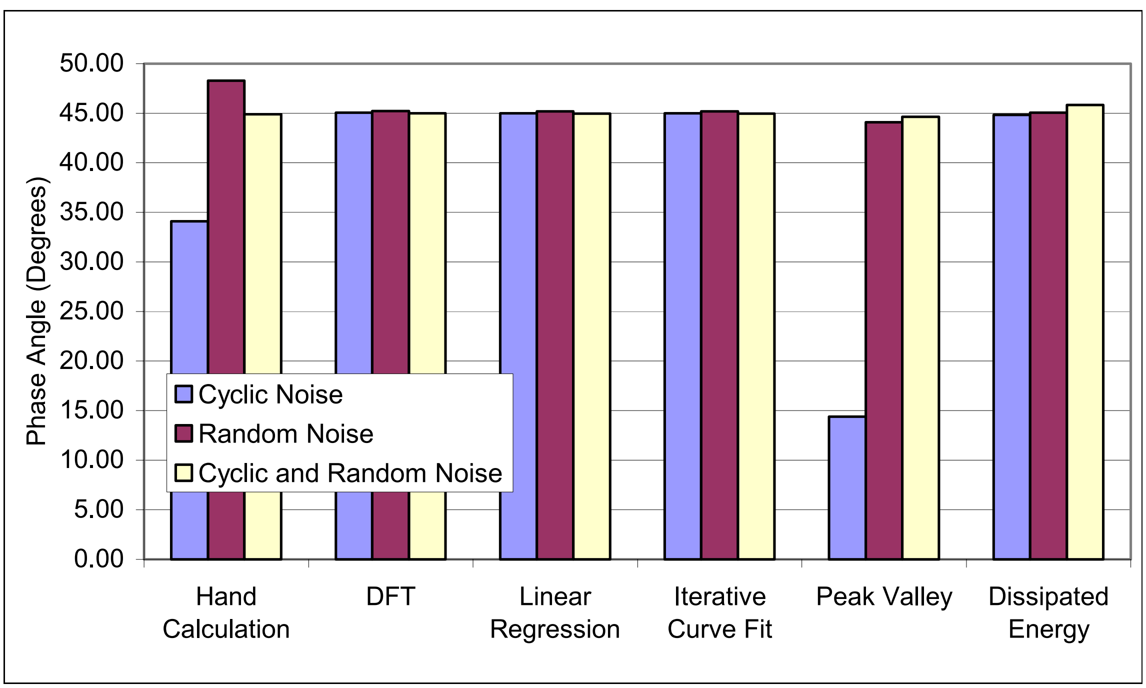

Figure 5-10. Phase angle comparison of methods for various types of noise

5.9 Computer Program for Linear Regression Method

Figure 5-11 depicts a flowchart of the data analysis program written by Swan (2001). The program was written in Visual Basic® within a Microsoft® Excel spreadsheet.

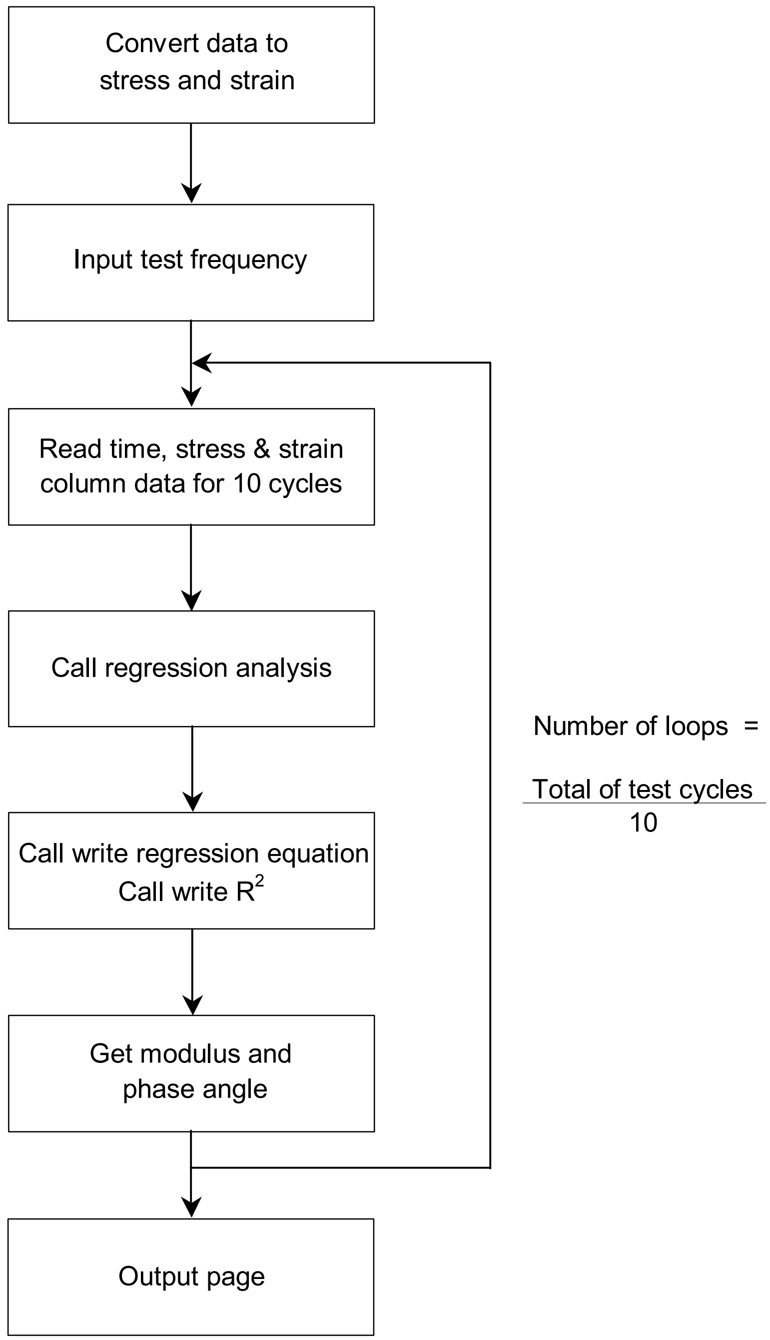

Figure 5-11. Flowchart of data analysis program

For the complex modulus program:

$$\text{axial stress column} = \frac{\text{force column}}{\text{surface area}} \tag{5.19}$$

$$\text{axial strain column} = \frac{\text{LVDT displacement column}}{\text{spacer length (50 mm)}} \tag{5.20}$$

The input data file was recorded in a standard order that the program can understand. Any change in that order will need a change in the program. At first, the load and deformation data columns are converted to stress and strain data columns. The regression analysis will work with paired columns of time and stress or time and strain. The program automatically determines the duration of the test and the number of cycles required to obtain dynamic modulus values. Besides the dynamic modulus and phase angle, the analysis program also reports the best-fit signal equation and the coefficient of determination, R^2.

Figure 5-12 shows the start page of the complex modulus program. The program automatically detects: stress and strain data columns, and start and stop times of testing. The only user defined inputs are the desired degree of polynomial in the regression analysis and testing frequency.

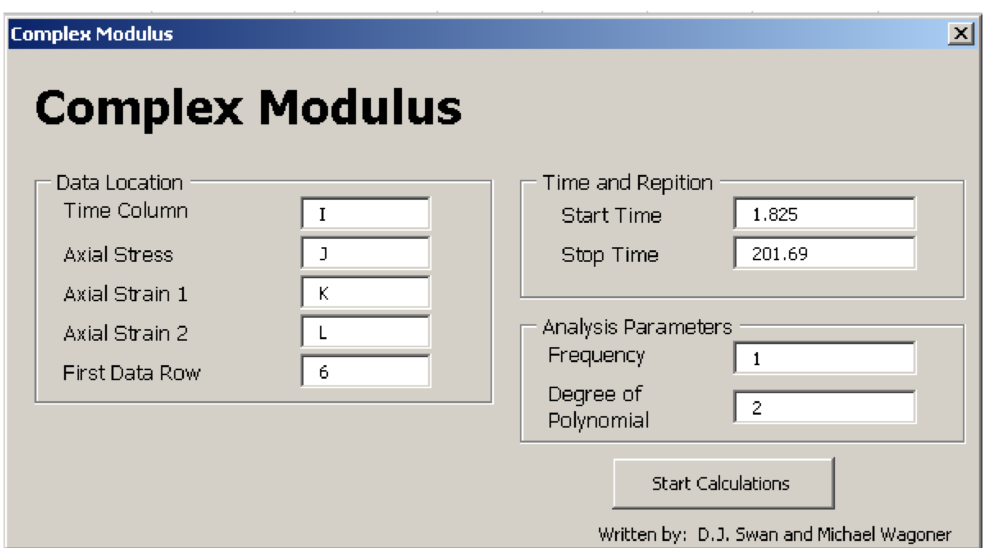

Figure 5-12. Complex modulus program

5.10 Evaluation of Optimal Degree of Polynomial

It is relatively straightforward to perform the signal analysis on the stress time history, because it is just a horizontal sinusoid. However, the strain time history contains an element of creep, which can complicate the data analysis. This effect can either be compensated for during the analysis or it can be removed prior to the analysis.

Removing the creep component out of the signal prior to analysis can prove to be very difficult. Because the shape of the creep curve is affected by both delayed elasticity and viscous creep, it cannot be simply characterized and removed a priori. Hence, it was decided to try to compensate for the creep as a part of the data analysis methods.

The linear regression method assumes that the strain time history consists of a linear or a polynomial trend, overlaid by a sinusoid. To test the effects of assuming either a linear or a higher order polynomial baseline trend in the creep strains, the complex modulus was obtained for different degrees of polynomial. The coefficient of determination, R^2 was used as a measure of the goodness-of-fit. Table 5-5 shows the effect of the degree of polynomial on the correlation, for typical 10 Hz dynamic modulus test results. It shows that a linear function will adequately describe the function. A quadratic may be used to provide a marginally better fit.

Table 5-5. The Effect of Polynomial Degree on R^2

Degree of Polynomial	R^2
0	0.8414
1	0.9788
2	0.9811
3	0.9812
4	0.9812

Figure 5-13 presents an illustration of interpreted 10 Hz complex modulus test results using a quadratic polynomial to represent the trend in the creep strain versus a linear polynomial. It was observed that there is almost no difference between two analyses.

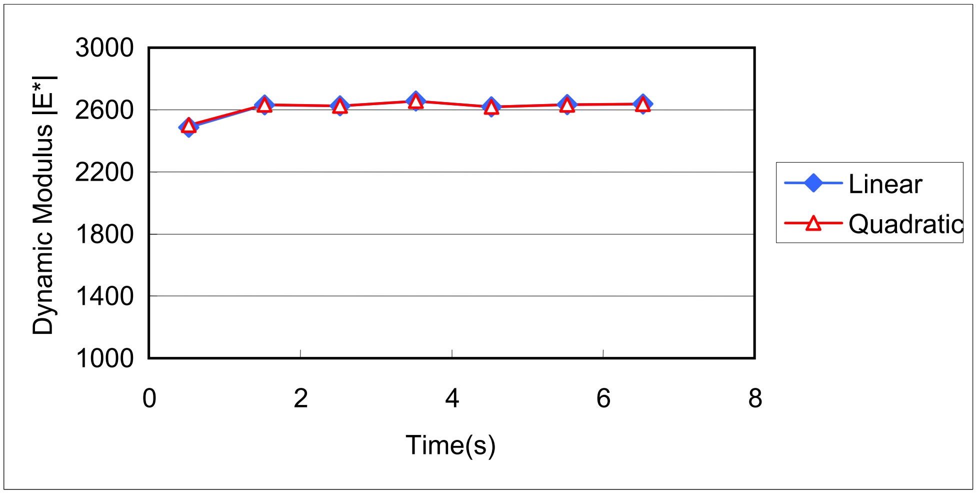

Figure 5-13. Linear regression versus quadratic regression analysis

5.11 Summary

In this chapter, various methods available for interpretation of the complex modulus were reviewed. A comparison between each of these methods was performed on an artificially generated signal. It was determined that the method based on linear regression resulted in consistently robust predictions of dynamic modulus and phase angle, and also required little or no input from the end user. All other methods evaluated were either sensitive to noise effects or required additional input and judgment from the user. Therefore, the method based on linear regression was selected for further use in this project. Finally, an evaluation of the effects of the underlying degree of polynomial in the linear regression method was performed. The results showed that for most problems, a linear representation of the underlying permanent strain time history was sufficient in terms of accuracy. Therefore, in the rest of this study, a linear representation of the underlying creep curve is used.

CHAPTER 6
AXIAL COMPRESSION DYNAMIC MODULUS: RESULTS AND DISCUSSION

6.1 Introduction

In this chapter, the results of the axial complex modulus testing are described. The triaxial compression dynamic modulus tests produced large amounts of test data. There were two to three test temperatures based on the mixtures tested (each described in Chapter 3):

- 10° C and 40° C for early tests on the FAA mixtures;
- 10° C, 25° C, and 40° C for intermediate time tests on Georgia granite mixtures and Superpave project mixtures; and
- 10° C, 30° C, and 40° C for all Whiterock aggregate mixtures and HVS mixtures.

For all temperatures tested, the following frequencies were used: 1 Hz, 4 Hz, 10 Hz, and 16 Hz. The tests were performed from the lowest temperature to the highest temperature and from the highest frequency to the lowest frequency.

6.2 Data Variables

The test variables obtained from the data acquisition system include the time, axial force, axial displacement, and the displacement from the LVDT's. The variable time is the time period from the test start to the data recording time. The axial force is the vertical load on the specimen, and the axial displacement is the vertical displacement of the load piston. Four LVDT's were used for each test, and the average displacements from the four LVDT's were calculated. The LVDT's had an axial gage length of 51 mm. Three specimens were tested for each mixture. Before the tests were performed, the height for each specimen was measured. The diameter was fixed at 102.0 mm (4 in.). To arrive at the actual stress under certain test conditions, the axial force was divided by the calculated area of the specimen.

Similarly, the LVDT displacements were divided by the axial gage length to arrive at the axial strain for the test under the same test conditions.

For any given test temperature, four data files were acquired for each specimen, namely for 16 Hz, 10 Hz, 4 Hz, and 1 Hz. At 16 Hz and 10 Hz, the test data were obtained from the 190th to the 200th cycle. For 4 Hz, the test data was obtained from the 90th to the 100th cycle. For the 1 Hz data, the data was obtained from the 10th to the 20th cycle. A rest period of at least two minutes and less than ten minutes was observed between each frequency. If at the end of any test period, the cumulative unrecovered deformation was found to be greater than 1500 micro units of strain, the test data was kept up to this last testing period and the specimen was discarded. A new specimen was used for the rest of the testing periods. For each frequency, there are about 50 sample points per cycle.

In this project, triaxial compression complex modulus tests were performed on 57 specimens, namely three specimens per mixture listed in Table 6-1. All specimens were prepared at 7 percent air voids plus or minus 0.5 percent, as listed in Table 6-1. All specimens were compacted directly to a 6.65-in. to 7.04-in. (170.0-mm to 180-mm) height in a 4-in. (102-mm) diameter mold, using the Servopac gyratory compactor. Subsequently, the ends of each specimen were trimmed with a saw, so that the target height of each specimen would be 6 inches (150 mm). The final heights are listed in Table 6-1.

Table 6-1. Sample Preparation Data

Mixture	Sample Number	Air Voids	Height, mm
Georgia Granite Mixtures			
GAC1	1	7.1	150.3
	2	6.8	150.2
	3	6.9	150.3
GAC2	1	6.9	150.1
	2	6.7	150.1
	3	7.0	150.0
GAC3	1	6.8	150.1
	2	6.7	150.0
	3	7.2	150.2

Mixture	Sample Number	Air Voids	Height, mm
GAF1	1	7.2	150.1
	2	7.3	150.3
	3	6.9	150.1
GAF2	1	6.7	150.1
	2	6.9	150.0
	3	6.7	150.2
GAF3	1	7.1	151.0
	2	6.7	150.6
	3	6.8	150.8
Whiterock Mixtures (Oolitic Limestone)			
WRC1	1	6.8	150.5
	2	6.6	150.2
	3	7.1	150.8
WRC2	1	7.4	151.2
	2	6.7	150.7
	3	6.9	150.8
WRC3	1	6.9	15.2
	2	7.4	150.8
	3	7.3	150.2
WRF1	1	7.1	150.4
	2	7.0	150.2
	3	6.6	150.9
WRF2	1	6.9	150.5
	2	6.8	151.1
	3	6.9	150.4
WRF4	1	7.1	150.9
	2	7.4	150.2
	3	6.9	151.3
WRF5	1	7.1	150.3
	2	7.3	150.7
	3	6.9	150.2
WRF6	1	7.2	150.2
	2	7.0	150.6
	3	7.1	150.3
Mixtures From Fine Aggregate Angularity Study			
RBC	1	7.0	151.2
	2	7.3	150.2
	3	6.8	150.7
RBF	1	7.2	151.2
	2	7.4	150.3
	3	6.7	151.3
CALC	1	7.1	150.5
	2	7.2	150.6
	3	6.9	151.3
CALF	1	7.1	150.5
	2	6.8	151.4
	3	6.9	150.5
CGC	1	6.9	150.3
	2	7.3	150.6
	3	6.7	151.3
CGF	1	6.7	150.6
	2	7.3	150.4
	3	6.8	150.9
CHC	1	6.8	150.5
	2	6.9	150.2
	3	6.9	150.3
CHF	1	7.2	150.8
	2	7.3	150.5
	3	7.1	151.3

Mixture	Sample Number	Air Voids	Height, mm
Superpave Project Mixtures			
P1	1	6.8	151.2
	2	7.1	151.1
	3	7.2	151.3
P2	1	7.2	150.2
	2	7.3	150.5
	3	6.8	151.7
P3	1	6.7	151.4
	2	6.7	150.5
	3	7.4	151.8
P5	1	6.7	150.5
	2	7.2	150.4
	3	6.9	151.0
P7	1	6.5	151.4
	2	6.7	151.2
	3	6.6	150.9
Heavy Vehicle Simulator Mixtures			
HVS67-22	1	6.9	150.2
	2	7.1	150.8
	3	6.8	151.1
HVS76-22	1	7.3	150.4
	2	6.8	150.7
	3	7.0	150.3

6.3 Raw Data Plots

For asphalt mixtures, the complex dynamic modulus and phase angle change with the temperature and frequency of loading. At low temperature, the modulus for asphalt mixtures is large, so it is easy to control the applied axial force to obtain small displacements. At high temperatures, such as 40° C, the modulus is lower, making it more difficult to control the axial force to get small displacements.

Figures 6-1 and 6-2 show typical force and single LVDT displacement versus time plots at 10° C and 40° C for the frequency of 4 Hz. The displacement results have very little noise in the data, even at the higher testing temperature of 40° C. Finally, Figures 6-3 and 6-4 show the calculated stress and strain versus time plots after averaging the displacements from the four LVDTs, which were used to calculate the dynamic modulus and the phase angle. The final stress and strain time histories were found to be sinusoidal for all frequencies tested.

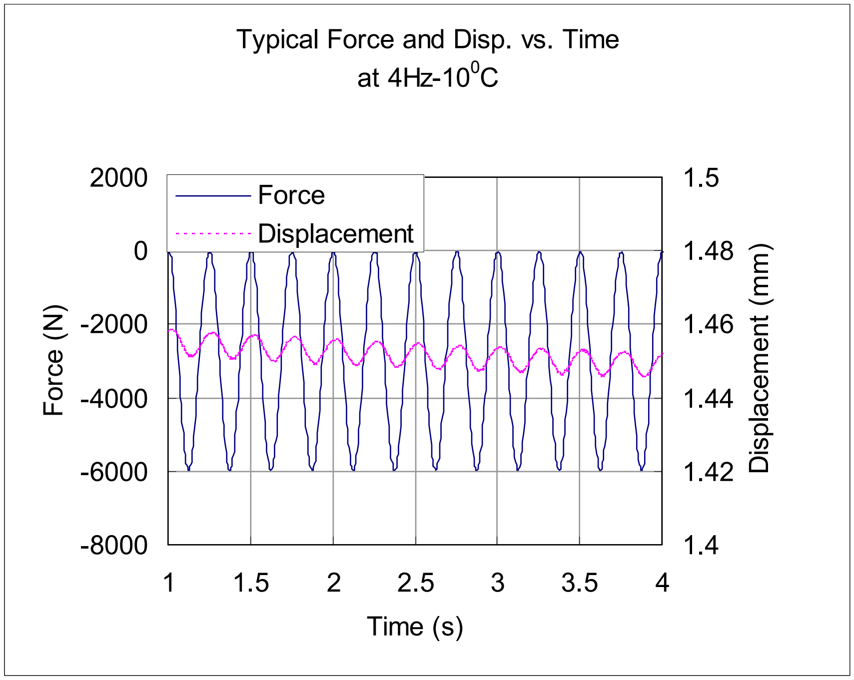

Figure 6-1. Typical plot of force and LVDT displacement versus time at low temperature (10° C and 4 Hz) for mixture WRC1

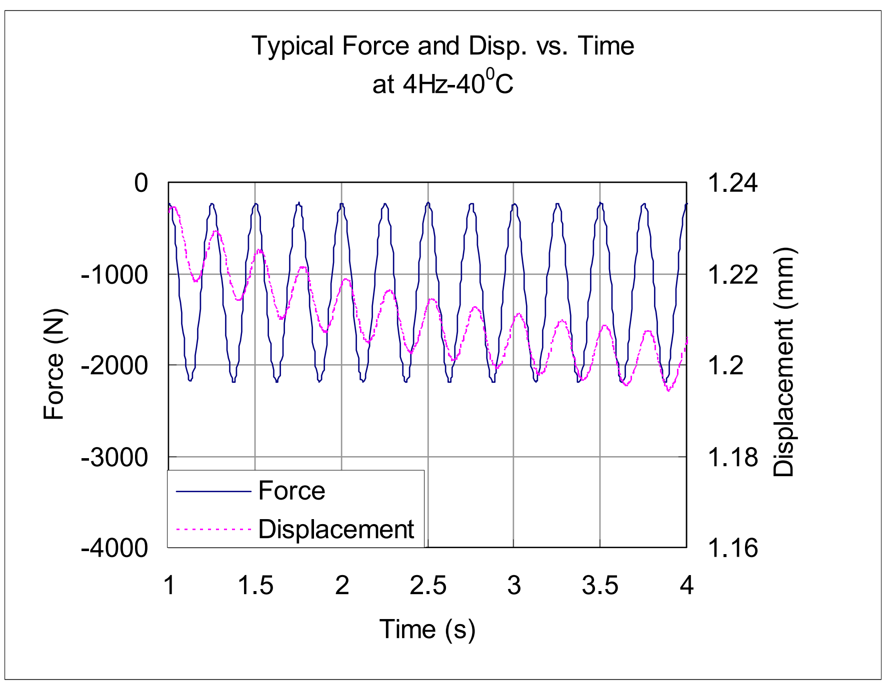

Figure 6-2. Typical plot of force and LVDT displacement versus time at high temperature (40° C and 4 Hz) for mixture WRC1

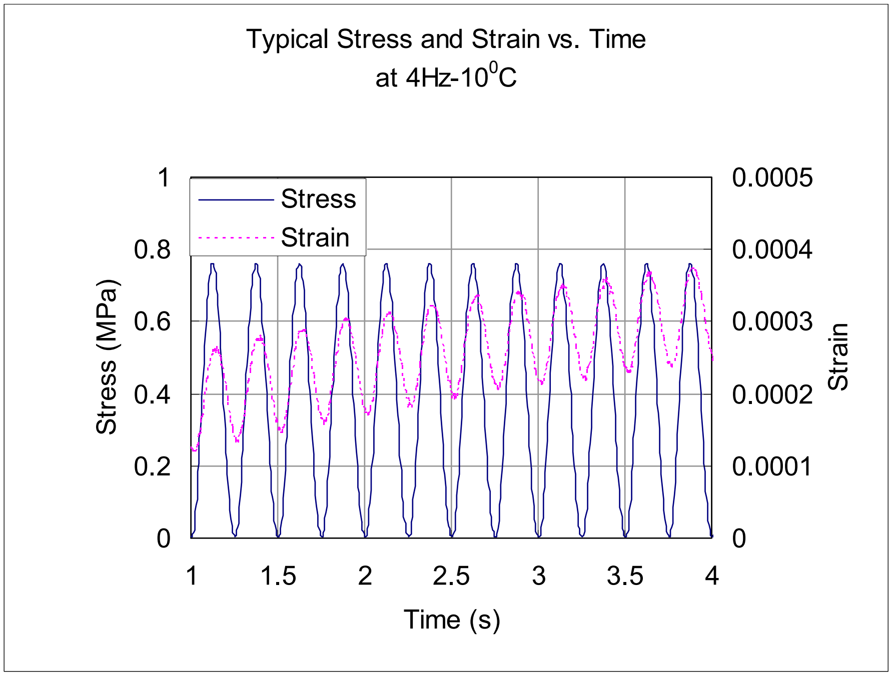

Figure 6-3. Typical plot of vertical stress versus strain at low temperature (10° C and 4 Hz) for mixture WRC1

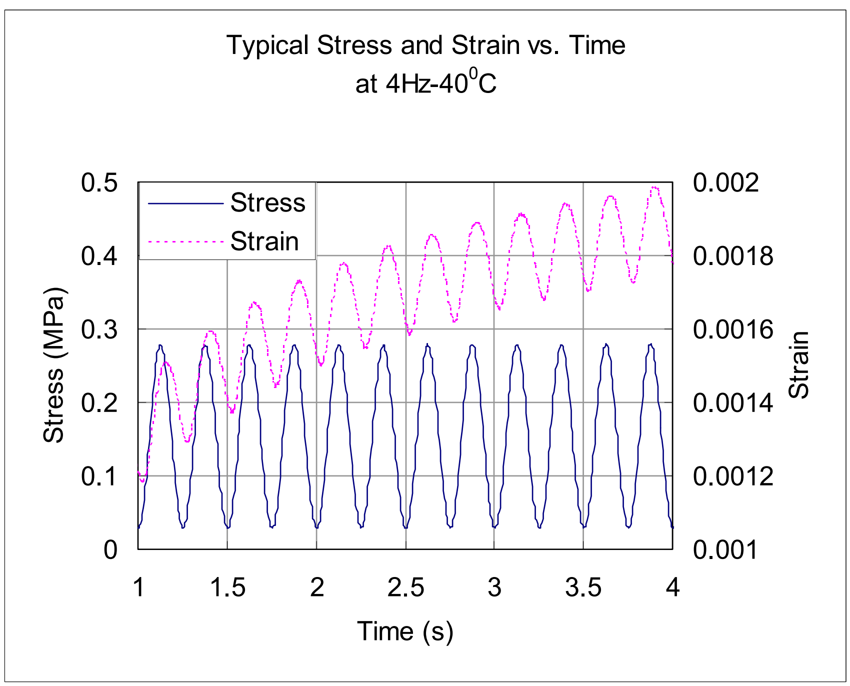

Figure 6-4. Typical plot of vertical stress versus strain at high temperature (40° C and 4 Hz) for mixture WRC1

6.4 Data Analysis Method

The data obtained for the complex modulus test is quite extensive; for one temperature, there are thousands of lines of data for one specimen. To analyze the complex modulus data, this project used the linear regression approach, presented in Chapter 5. For each sample at a given test temperature and frequency, ten cycles consisting of 1000 points were analyzed to obtain the dynamic modulus and phase angle. For interpretation purposes, within these ten cycles the axial strain history was assumed to consist of a linear trend with a sinusoidal oscillation around the trend. All calculations were performed using the SI system.

6.5 Analysis of Test Data Results

6.5.1 Test Data

One analysis file was obtained for each load frequency and testing temperature. In this analysis file, the dynamic modulus in GPa and the phase angle in degrees were obtained for the given test temperature and frequency. There were three replicate specimens tested for each asphalt mixture. After all the dynamic modulus and phase angle values were calculated for each specimen under the same test conditions, the average value for both of these parameters was calculated. Tables 6-2 and 6-3 list the average values for the three specimens for each asphalt mixture.

Table 6-2. Average Dynamic Modulus (|E*|) Testing Results

Mixture	Temperature (° C)	Frequency			
		1 Hz	4 Hz	10 Hz	16 Hz
Georgia Granite Mixtures					
GAC1	10	3457.54	4696.16	5577.41	6222.62
	25	931.93	1440.62	1788.84	1962.27
	40	317.12	475.14	656.60	742.96
GAC2	10	5289.30	7142.33	7983.76	8913.45
	25	1559.11	2308.10	2776.70	3318.24
	40	535.77	787.74	1126.96	1313.66

Mixture	Temperature (° C)	Frequency			
		1 Hz	4 Hz	10 Hz	16 Hz
GAC3	10	5096.07	6797.11	7250.03	7660.00
	25	1606.35	2523.14	3079.15	3496.77
	40	530.76	757.09	1109.68	1250.70
GAF1	10	4594.94	6228.22	7302.91	7636.35
	25	1409.17	2107.13	2672.85	2950.80
	40	401.02	635.50	867.07	1035.55
GAF2	10	7142.75	9597.93	11966.62	12883.30
	25	2277.25	3201.00	4068.22	4630.38
	40	535.97	905.80	1309.77	1574.02
GAF3	10	5184.00	6523.47	7956.86	8798.66
	25	1586.94	2400.60	3041.56	3437.54
	40	377.70	614.91	886.58	1044.15
Whiterock Mixtures (Oolitic Limestone)					
WRC1	10	3540.81	4757.85	5512.43	5953.88
	30	1026.46	1896.38	2552.73	2951.30
	40	526.05	898.81	1222.07	1464.86
WRC2	10	3499.12	5327.66	6449.00	7073.89
	30	1379.32	2256.92	3051.51	3466.68
	40	759.48	1368.38	1835.72	2073.94
WRC3	10	5405.49	6995.86	7967.39	8463.57
	30	1653.59	2852.46	3718.31	4441.98
	40	801.08	1470.36	1996.97	2375.12
WRF1	10	5122.06	6630.20	7917.74	8456.48
	30	1769.34	2662.57	3518.02	4005.78
	40	849.60	1273.70	1663.57	1960.74
WRF2	10	6301.77	7744.18	8990.34	9662.49
	30	2030.73	2931.80	3764.94	4442.58
	40	1076.16	1610.34	2169.11	2512.69
WRF4	10	7037.92	9142.90	10511.22	11141.74
	30	2211.26	3357.67	4339.52	5024.28
	40	1044.19	1584.81	2076.40	2431.11
WRF5	10	5285.91	6581.71	7583.78	8229.52
	30	1515.52	2442.77	3188.31	3688.46
	40	726.94	1146.45	1556.87	1912.52
WRF6	10	4391.76	5725.85	6722.84	7152.49
	30	1753.47	2479.71	3195.30	3643.92
	40	879.93	1374.06	1850.43	2136.52
Mixtures From Fine Aggregate Angularity Study					
RBC	10	5521.86	6877.95	7694.13	8327.94
	40	770.75	1175.36	1492.91	1962.94
RBF	10	6242.28	7994.98	9592.44	9862.88
	40	954.17	1415.66	1799.59	2027.84
CALC	10	5434.98	7143.53	8025.87	8248.25
	40	1182.66	1792.49	2357.34	2730.40
CALF	10	6651.62	8106.39	9194.52	10285.22
	40	1184.06	1779.33	2413.68	2682.04
CGC	10	4320.02	5210.02	6136.57	6307.82
	40	923.08	1363.60	1772.90	2003.03
CGF	10	6693.18	7387.65	9630.43	9827.05
	40	1217.77	1777.24	2219.22	2500.47
CHC	10	4624.45	6216.22	7417.98	7848.56
	40	744.73	1166.04	1559.65	2500.47
CHF	10	8812.68	14397.88	16405.10	18827.05
	40	756.82	1073.82	1554.89	2500.47
Superpave Project Mixtures					
P1	10	5517.08	7454.96	8422.86	
	40	523.74	807.66	1161.49	1447.81

Mixture	Temperature (° C)	Frequency			
		1 Hz	4 Hz	10 Hz	16 Hz
P2	10	4459.33	5616.50	6668.22	6728.17
	40	606.97	953.37	1349.82	1578.43
P3	10	2869.59	3797.12	4583.94	4754.91
	40	458.87	655.21	892.31	978.19
P5	10	5147.749	6263.335	7132.291	7648.227
	40	638.095	918.3859	1180.378	1354.904
P7	10	3479.68	4640.86	5562.11	6055.44
	40	549.95	796.88	1048.63	1193.51
Heavy Vehicle Simulator Mixtures					
HVS67-22	10	5559.568	6676.453	7747.892	8016.232
	30	1309.809	1900.426	2349.412	2638.219
	40	620.8512	925.0246	1179.977	1323.562
HVS76-22	10	5021.711	6411.433	7161.738	7702.334
	30	1226.468	1855.661	2401.104	2639.515
	40	646.3819	967.5163	1260.443	1439.98

Table 6-3. Average Phase Angle (δ) Testing Results

Mixture	Temperature (° C)	Frequency			
		1 Hz	4 Hz	10 Hz	16 Hz
Georgia Granite Mixtures					
GAC1	10	26.59	26.18	27.84	29.96
	25	30.61	33.25	35.01	36.92
	40	27.11	32.77	40.96	46.10
GAC2	10	25.20	23.37	24.94	26.96
	25	30.17	31.79	34.67	36.72
	40	26.67	32.14	37.23	41.91
GAC3	10	25.79	26.05	26.58	31.13
	25	29.87	31.44	33.30	35.24
	40	37.05	42.79	48.87	51.98
GAF1	10	26.84	25.68	27.65	29.81
	25	32.47	33.68	36.02	38.65
	40	27.25	32.35	38.16	45.09
GAF2	10	21.62	20.66	22.25	24.82
	25	28.84	30.89	32.67	35.46
	40	31.63	38.32	43.39	48.28
GAF3	10	22.38	21.47	23.64	25.13
	25	30.32	31.86	33.78	36.42
	40	32.91	38.87	44.30	49.53
Whiterock Mixtures (Oolitic Limestone)					
WRC1	10	22.85	22.03	22.39	23.89
	30	33.13	29.81	31.75	33.18
	40	29.02	30.42	35.05	37.62
WRC2	10	21.73	20.03	20.63	22.43
	30	33.29	29.93	31.08	32.74
	40	32.19	32.15	35.12	37.04
WRC3	10	19.08	18.02	18.81	20.72
	30	32.79	29.05	29.81	30.49
	40	32.84	32.25	34.98	37.07
WRF1	10	19.59	18.00	19.01	21.42
	30	32.00	31.07	32.14	33.91
	40	29.38	32.11	34.78	38.42
WRF2	10	18.37	17.62	18.81	20.82
	30	31.76	29.54	30.53	32.76
	40	31.21	33.67	35.68	37.73

Mixture	Temperature (° C)	Frequency			
		1 Hz	4 Hz	10 Hz	16 Hz
WRF4	10	19.83	19.11	20.57	22.76
	30	33.64	30.43	31.56	33.14
	40	31.70	34.00	35.85	37.65
WRF5	10	22.20	20.17	20.94	22.24
	30	32.65	31.28	31.67	33.20
	40	30.05	33.13	36.10	38.59
WRF6	10	22.27	20.76	22.02	23.52
	30	31.63	30.28	30.88	32.14
	40	31.92	33.59	36.09	37.62
Mixtures From Fine Aggregate Angularity Study					
RBC	10	22.75	20.91	23.20	26.69
	40	27.38	31.09	35.68	39.56
RBF	10	14.08	15.34	15.82	17.91
	40	25.90	28.66	31.85	36.08
CALC	10	17.58	17.23	19.56	20.82
	40	30.53	34.24	38.89	43.18
CALF	10	18.31	18.27	20.55	22.61
	40	26.97	33.92	39.90	44.36
CGC	10	23.02	22.81	24.74	26.58
	40	31.40	31.10	34.84	38.26
CGF	10	16.22	18.64	20.70	23.58
	40	25.70	30.95	34.18	38.65
CHC	10	21.91	20.96	22.35	25.52
	40	30.45	33.33	36.00	39.82
CHF	10	29.84	29.65	33.06	32.94
	40	35.50	35.40	41.68	49.31
Superpave Project Mixtures					
P1	10	23.62	22.99	24.18	
	40	27.71	33.57	38.46	43.02
P2	10	23.80	23.67	26.44	28.96
	40	28.33	32.46	38.35	46.19
P3	10	31.93	29.13	30.46	29.29
	40	30.63	34.67	45.24	49.35
P5	10	19.67	19.12	21.15	23.34
	40	23.83	28.44	33.38	38.13
P7	10	24.60	23.99	24.62	26.15
	40	26.99	32.15	38.96	43.28
Heavy Vehicle Simulator Mixtures					
HVS67-22	10	21.98	21.11	22.93	24.82
	40	29.01	32.96	37.97	43.17
HVS76-22	10	19.47	18.51	20.04	23.31
	40	29.24	31.81	37.52	41.59

Figures 6-5 through 6-10 show dynamic modulus and phase angle results for mixture GAF1 for 10° C, 25° C, and 40° C, which exhibited a typical response for the fine-graded mixtures. Similarly, Figures 6-11 through 6-16 display typical dynamic modulus and phase angle results at the three different testing temperatures for mixture GAC1, which also exhibited a typical response for the coarse-graded mixtures.

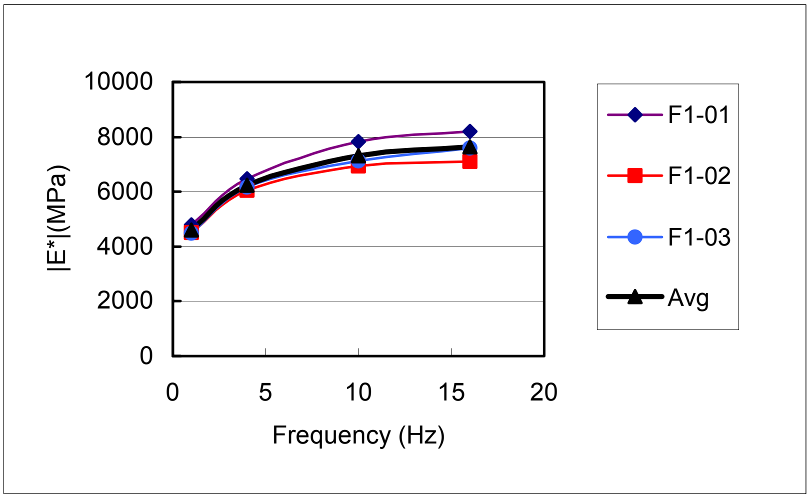

Figure 6-5. Dynamic modulus |E*| of GAF1 at 10° C

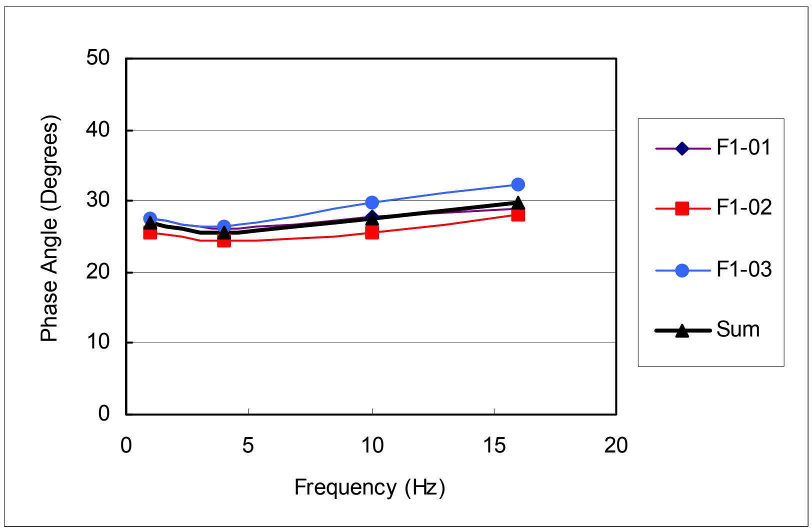

Figure 6-6. Phase angle of GAF1 mixture at 10° C

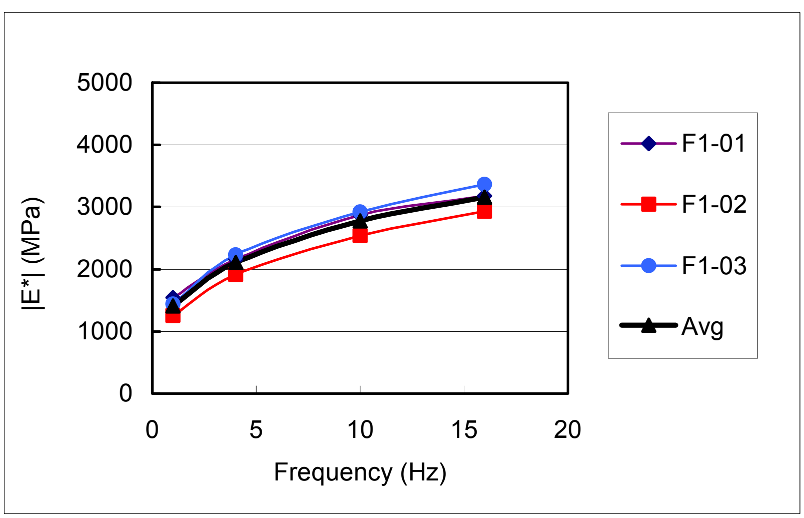

Figure 6-7. Dynamic modulus |E*| of GAF1 at 25° C

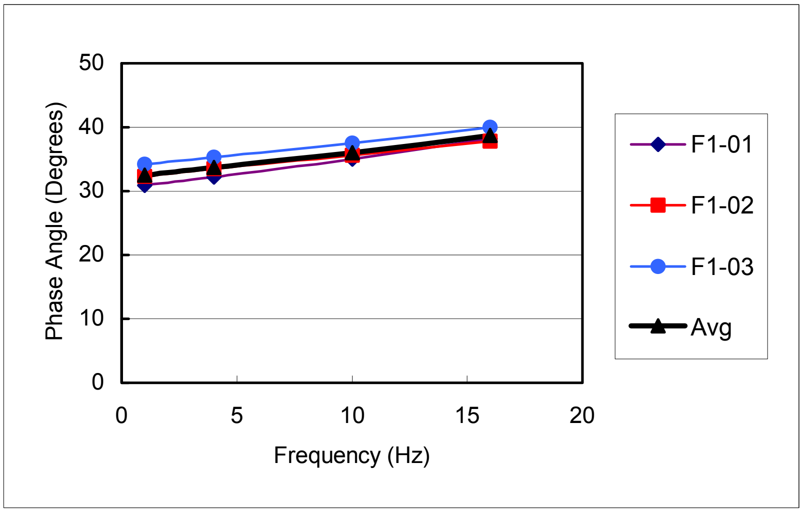

Figure 6-8. Phase angle of GAF1 mixture at 25° C

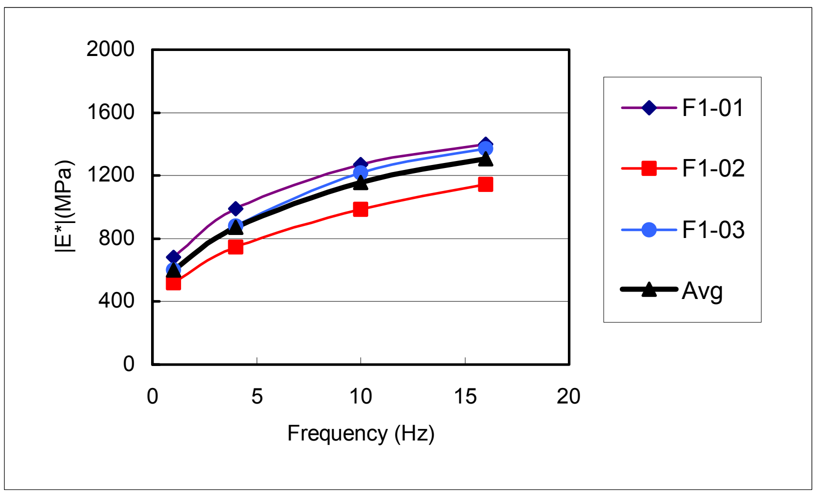

Figure 6-9. Dynamic modulus |E*| of GAF1 at 40° C

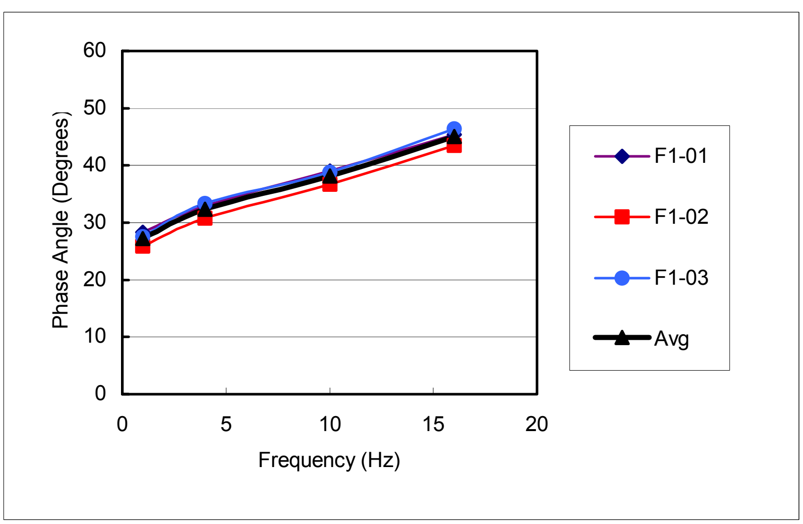

Figure 6-10. Phase angle of GAF1 mixture at 40° C

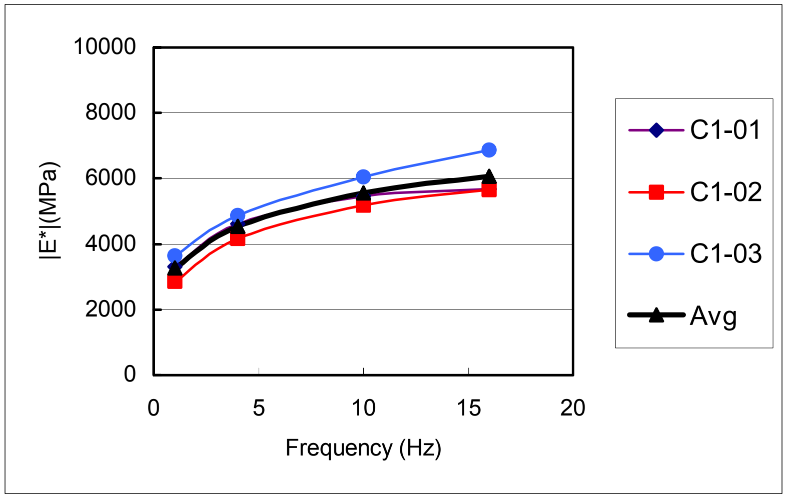

Figure 6-11. Dynamic modulus |E*| of GAC1 at 10° C

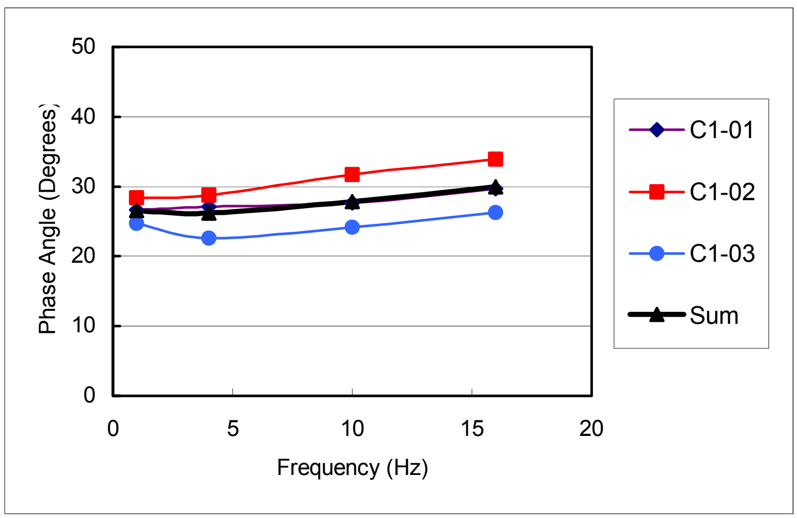

Figure 6-12. Phase angle of GAC1 mixture at 10° C

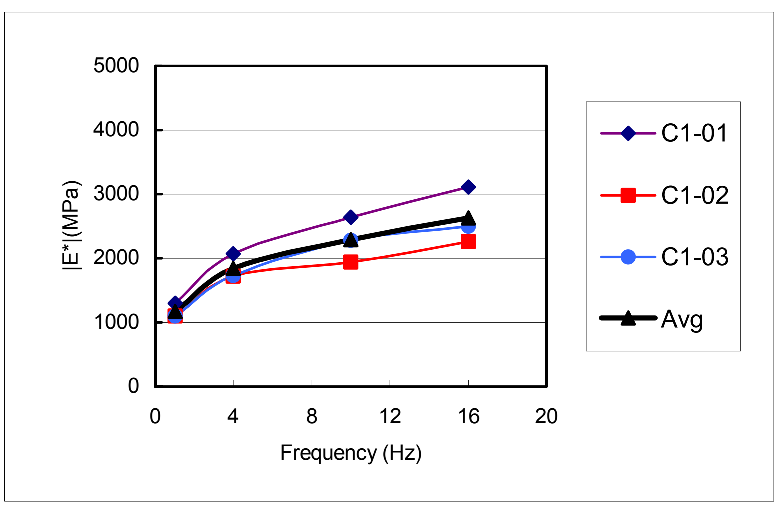

Figure 6-13. Dynamic modulus |E*| of GAC1 at 25° C

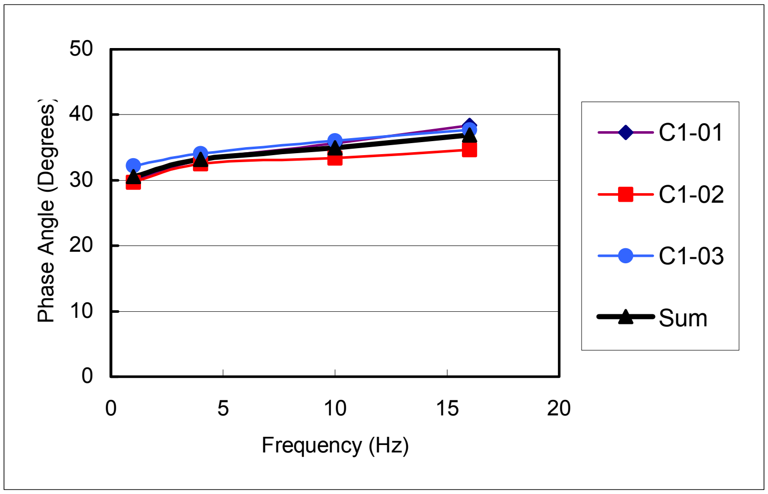

Figure 6-14. Phase angle of GAC1 mixture at 25° C

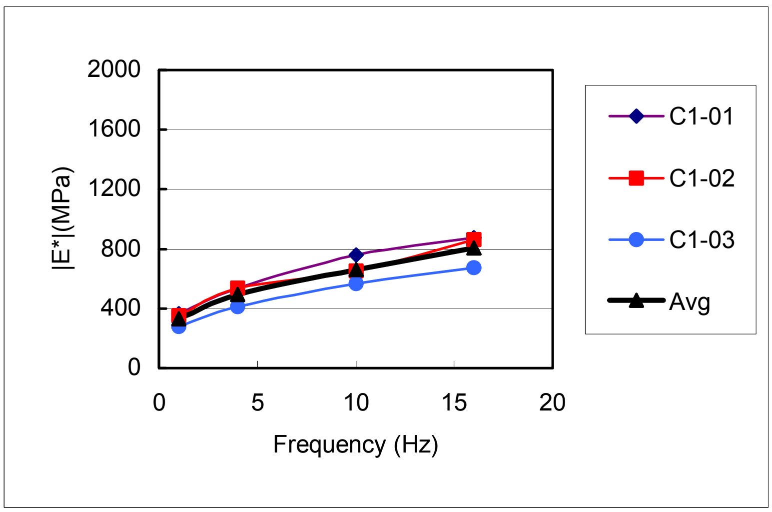

Figure 6-15. Dynamic modulus |E*| of GAC1 at 40° C

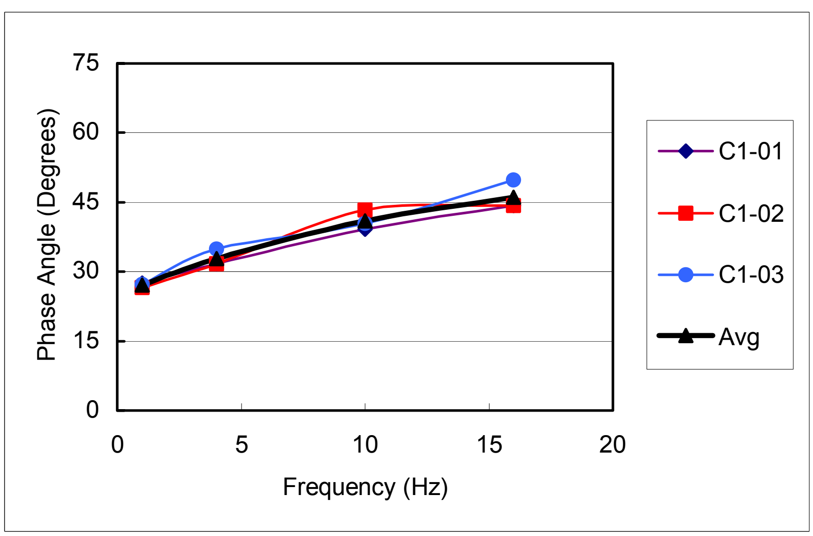

Figure 6-16. Phase angle of GAC1 mixture at 40° C

The degree of variability shown in the dynamic modulus and phase angle results for mixtures GAF1 and GAC1 in Figures 6-5 through 6-16 are typical for the other mixtures tested. The results also clearly show the expected rate dependence of the dynamic modulus for asphalt mixtures, as the dynamic modulus increases with higher frequencies (e.g., Sousa, 1986). As expected, a comparison of Figures 6-6 and 6-8 shows that the phase angle also increases with higher testing temperatures. Also interestingly, a comparison of Figures 6-6 and 6-8 shows how the phase angle decreased slightly between 1 Hz and 4Hz, but increases with frequency up to 16 Hz. At higher temperatures, the phase angle tends to increase with increased frequency, as shown for example in Figures 6-8 and 6-10.

In summary, the dynamic modulus and phase angle results show the following trends:

1. Under a constant loading frequency, the dynamic modulus decreases with an increase in test temperature for the same mixture.
2. The phase angle increases with the increase of test temperature.
3. Under a constant test temperature, the dynamic modulus increases with increased test frequencies.
4. Both the dynamic modulus and phase angle data shows relatively smooth trends, irrespective of test temperature.

The above trends are consistent with the research results reported by others.

6.6 Master Curve Construction

The dynamic modulus and phase angle of mixtures can be shifted along the frequency axis to form single characteristic master curves at a desired reference temperature or frequency. In the proposed *2002 Guide for the Design of Pavement Systems* currently under development in the NCHRP Project 1-37A, the modulus of the asphalt mixture (at all analysis levels of temperature and time rate of load) is determined from a master curve constructed at a reference temperature. The procedure assumes that the asphalt mixture is a thermo-rheologically simple material and that the time-temperature superposition principle is applicable.

Typically the shift factors, a (T), are obtained from the WLF equation (Williams et al., 1955),

$$\log a(T) = \frac{C_1\left(T - T_r\right)}{C_2 + T - T_r} \tag{6.1}$$

where C_1 and C_2 are constants; T_r is the reference temperature; and T is the temperature of each individual test.

A new method of developing the master curve for asphalt mixtures was developed by Pellinen and Witczak (2002), in which the master curves were constructed fitting a sigmoidal function to the measured complex modulus test data using non-linear least squares regression techniques. The shift can be achieved by solving the shift factors simultaneously with the coefficients of the sigmoidal function. The sigmoidal fitting function for master curve construction used by Pellinen and Witczak (2002) is defined by:

$$\log(|E^*|) = \delta + \frac{\alpha}{1 + e^{\beta - \gamma \log(f_r)}} \tag{6.2}$$

where log (|E*|) = log of dynamic modulus;

δ = minimum modulus value;

f_r = reduced frequency;

α = span of modulus value; and

β, γ = shape parameters.

The reduced frequency, f_r, is defined as:

$$f_r = \frac{f}{a(T)} \tag{6.3}$$

or alternatively,

$$\log (f_r) = \log (f) + \log [a(T)] \tag{6.4}$$

in which f = testing frequency, and a(T) is the shift factor that defines the required shift at a given temperature to get the reduced frequency, f_r. At the reference temperature, the shift factor $a(T_r) = 1$. Finally, the parameter γ influences the steepness of the function (rate of change between minimum and maximum) and β influences the horizontal position of the turning point, shown in Figure 6-17.

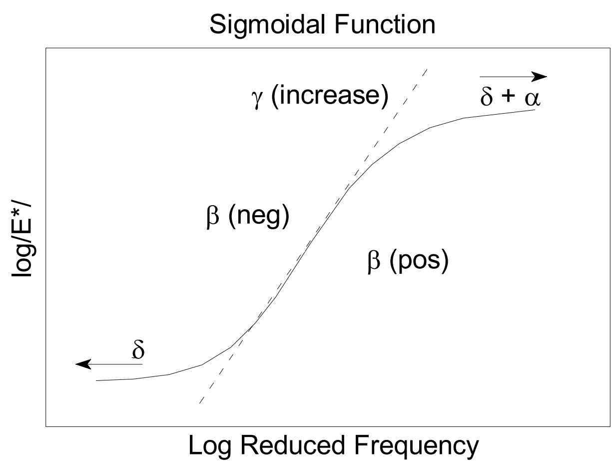

Figure 6-17. Parameters used in sigmoidal fitting function

The justification of using a sigmoidal function for fitting the compressive dynamic modulus data is based on the physical observations of the mix behavior. The upper part of the sigmoidal function approaches asymptotically the maximum stiffness of the mix, which is dependent on limiting binder stiffness at cold temperatures. At high temperatures, the compressive loading causes aggregate influence to be more dominant than the viscous binder influence. The modulus starts to approach a limiting equilibrium value, which is dependent on the aggregate gradation. Thus, the sigmoidal function captures the physical behavior of the asphalt mixture observed in the mechanical testing using compressive cyclic loading through the entire range of temperatures that are typically of interest.

6.6.1 Typical Predicted Master Curves for Florida Mixtures

In the following, the procedure developed by Pellinen and Witczak (2002) for obtaining predicted master curves for GAC3 and GAF1 is used, and the resulting master curves are presented. In all cases, the reference temperature was taken as 25° C (77° F). As stated previously, the shifting was accomplished by obtaining the shift factors simultaneously with the coefficients of the sigmoidal function through nonlinear regression, without assuming any functional form of a (T) versus temperature. The nonlinear regression was performed using the Solver Function in a Microsoft Excel® spreadsheet.

The resulting shift functions and master curves for GA-C3 and GA-F1 are presented in Figures 6-18 through Figure 6-21 below. The tails on the predicted master curves are extrapolated. In a few cases, depending on the mixture properties, the tails of the predicted mastercurve did not follow an S-shape. Rather, the mastercurve showed a slight concave-down curvature. Figures 6-22 and 6-23 show the shift function and predicted mastercurve for mixture GA-C1, respectively. The predicted mastercurve for GAC1 does not show an S-shape – rather, it shows a slight concave-down curvature indicating that, for this particular mixture, higher and lower temperature results are needed to define the tails of the mastercurve adequately. Future testing at higher and lower temperatures would help in better defining the tails.

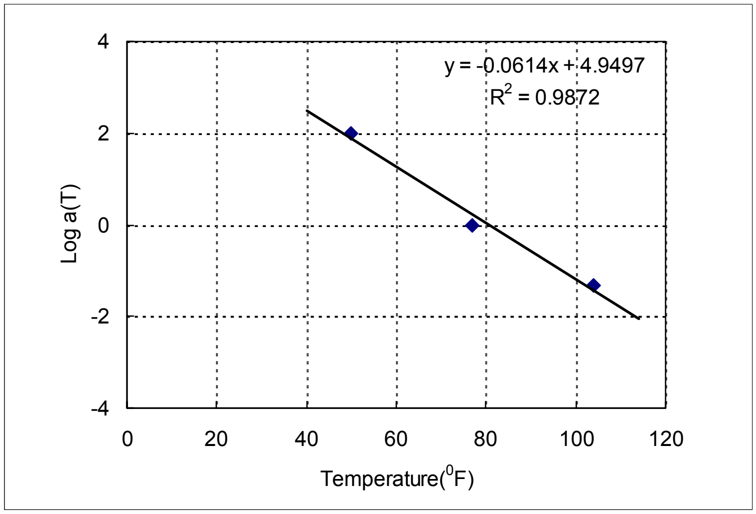

Figure 6-18. Shift function for coarse-graded GAC3 mixture

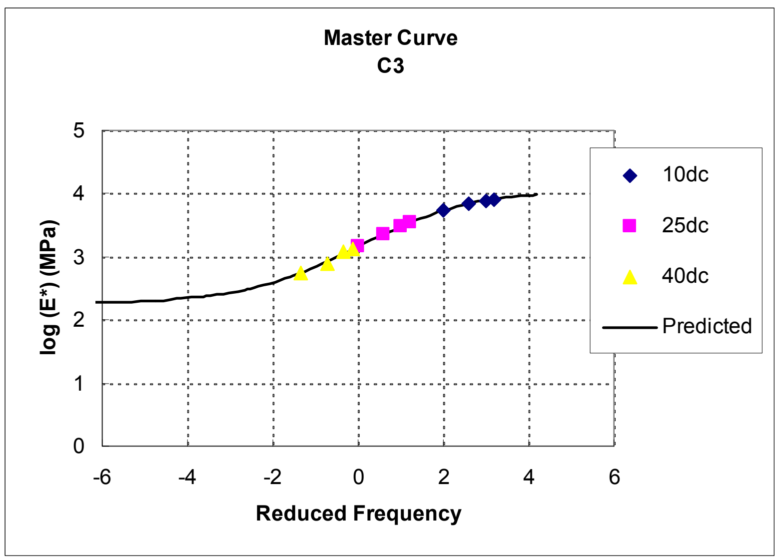

Figure 6-19. Master curve for coarse-graded GAC3 mixture

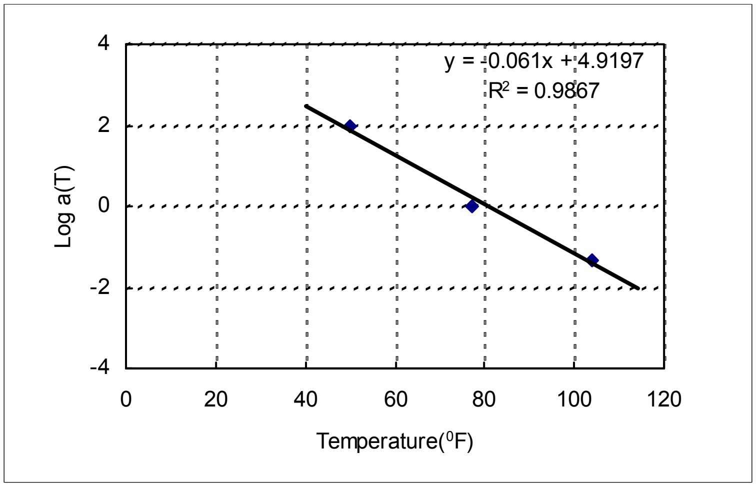

Figure 6-20. Shift function for fine-graded GAF1 mixture

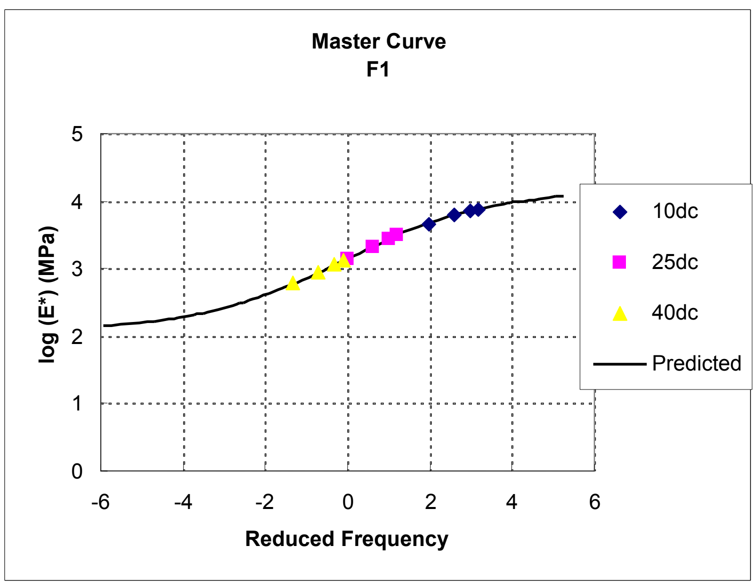

Figure 6-21. Master curve for fine-graded GAF1 mixture

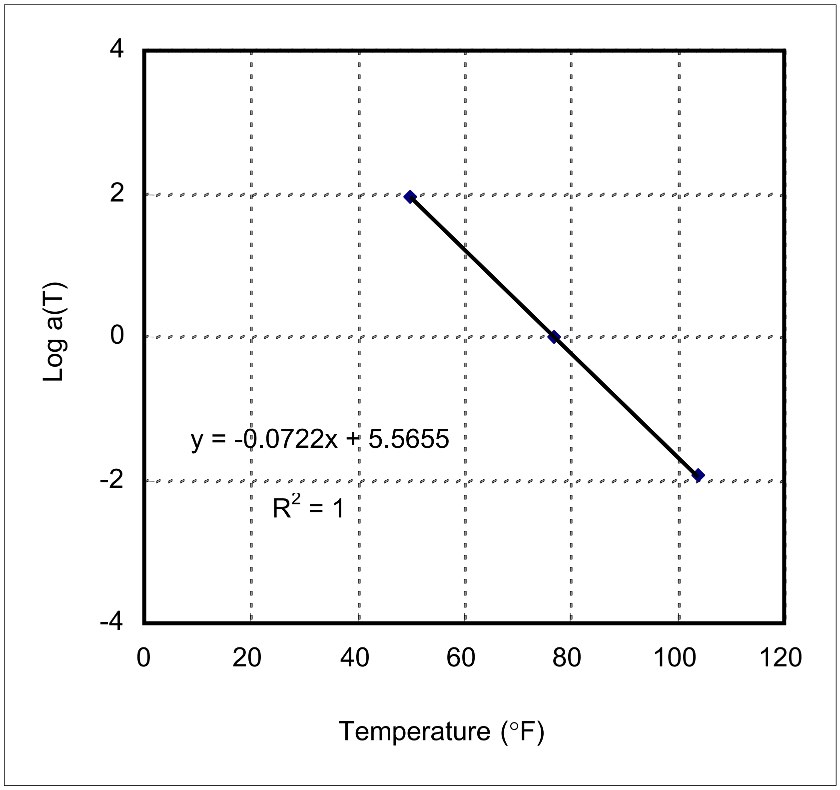

Figure 6-22. Shift function for fine-graded GAF1 mixture

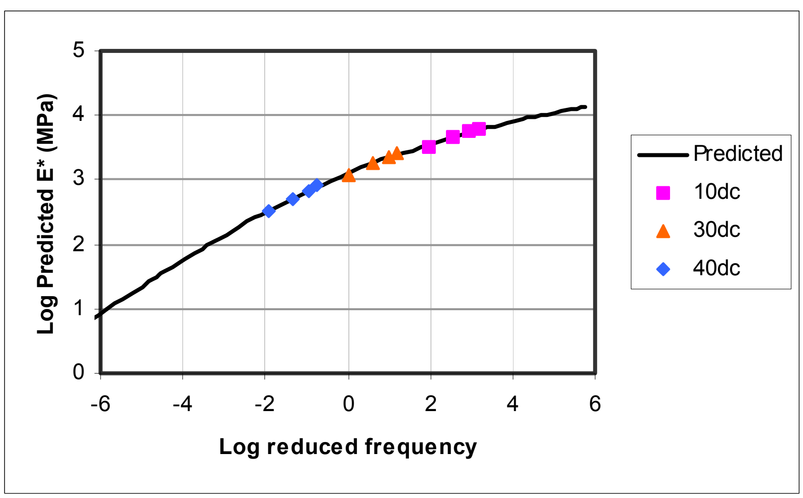

Figure 6-23. Master curve for coarse-graded GAC1 mixture

6.7 Dynamic Modulus Calculated from Predictive Regression Equations

The complex modulus test is relatively difficult and expensive to perform. Therefore, numerous attempts have been made to develop regression equations to calculate the dynamic modulus from conventional volumetric mixture properties. For example, a predictive regression equation is proposed as a part of the *2002 Design Guide* to calculate |E*| based on the volumetric properties of any given mixture. The predictive equation developed by Witczak et al. (2002) is one of the most comprehensive mixture dynamic modulus models available today (Witczak, 2002). The equation is presented below:

$$\begin{aligned} \log|E^*| = & -1.249937 + 0.029232 \times (p_{200}) - 0.001767 \times (p_{200})^2 - 0.002841 \times (p_4) \\ & - 0.058097 \times (V_a) - \frac{0.802208(V_{beff})}{V_{beff} + V_a} \\ & + \frac{3.871977 - 0.0021(p_4) + 0.003958(p_{3/8}) - 0.00017(p_{3/8})^2 + 0.005470(p_{3/4})}{1 + e^{(-0.603313 - 0.313351 \times \log(f) - 0.39353 \times \log(\eta))}} \end{aligned} \quad (6.5)$$

where $|E^*|$ = dynamic modulus, in 10^5 psi;

η = bitumen viscosity, in 0^6 poise;

f = loading frequency, in Hz;

V_a = percent air void content, by volume;

V_{beff} = effective bitumen content, percent by volume;

$p_{3/4}$ = percent weight retained on 19-mm sieve, by total aggregate weight;

$p_{3/8}$ = percent weight retained on 9.5-mm sieve, by total aggregate weight;

p_4 = percent weight retained on 4.75-mm sieve, by total aggregate weight; and

p_{200} = percent weight passing 0.75-mm sieve, by total aggregate weight.

The above dynamic modulus predictive equation has the capability to predict the dynamic modulus of dense-graded HMA mixtures over a range of temperatures, rates of loading, and aging conditions from information that is readily available from conventional binder tests and the volumetric properties of the HMA mixture. This predictive equation is based on more than 2,800 different HMA mixtures tested in the laboratories of the Asphalt Institute, the University of Maryland, and FHWA.

In this research, the dynamic modulus was calculated using the predictive equation developed by Witczak et al. (2002). Gradations data for each mixture, as well as binder content and volumetric properties, were obtained from the design mixture properties, discussed in Chapter 3. The air voids were measured using test method AASHTO T 166 on the prepared test specimens. Table 6-1 lists the air voids for each specimen tested. For each mixture listed in Table 6-1, the average air voids from the three pills tested were used. The binder viscosity was obtained at each testing temperature using,

- Brookfield rotational viscometer results on short-term RTFO aged specimens;
- Dynamic shear rheometer results on short-term RTFO aged specimens; and
- Recommended viscosity values by Witczak and Fonseca (1996) for "mixture laydown" conditions.

In the following, the binder test results will be presented, followed by a presentation of the predicted dynamic modulus results calculated from the predictive equation by Witczak et al. (2002).

6.7.1 Binder Testing Results

The asphalt binder used for all mixtures but one of the mixtures tested is graded as PG67-22 (AC-30). The HVS mixture with SBS modified binder graded as PG76-22 was not tested, due to lack of availability. The "as produced" mix was used for the complex modulus testing of the HVS mixtures, making it hard to ensure that exactly the same binder be used for the rheological testing. Table 6-4 shows the results of the Brookfield rotational viscometer testing, performed at three test temperatures (60.5° C, 70.7° C, and 80.7° C). Similarly, Table 6-5 shows the results of viscosity tests obtained from the dynamic shear rheometer. The viscosity is reported in centipoise (cP).

Table 6-4. Brookfield Rotational Viscometer Results on Unaged and RTFO Aged Binder

Testing Temperature (° C)	Unaged Binder Viscosity (cP)	RTFO Aged Binder Viscosity (cP)
60.5	328260.5	1041945.2
70.7	95682.1	236166.7
80.7	33681.6	81193.0

Table 6-5. Dynamic Shear Rheometer Results on Unaged and RTFO Aged Binder

Testing Temperature (° C)	Unaged Binder Viscosity (cP)	RTFO Aged Binder Viscosity (cP)
30	2.46E+06	5.08E+06
40	1.99E+05	1.20E+06

Based on the results shown in Tables 6-4 and 6-5, the viscosity for each complex modulus test temperature was obtained using the following equation (Witzcak and Fonseca, 1996) and *ASTM D-2493* (1985):

$$\text{Log} (\log (\eta) = A + VTS\log (T) \qquad (6.6)$$

in which η is bitumen viscosity in centipoise, T is test temperature in Rankine, and A and VTS are regression constants reflecting the specific type of asphalt cement and aging conditions of the material. Table 6-6 summarizes the calculated A and VTS values for the unaged binder, as well as the RTFO aged binder results from the Brookfield rotational viscometer test and the dynamic shear rheometer test. Similarly, Table 6-7 lists typical A and VTS values for PG 67-22 (AC- 30), recommended by Witzcak and Fonseca (1996), for two conditions: a) original; and b) short-term (mix/laydown). A comparison of Tables 6-6 and 6-7 shows that the parameters obtained from the Brookfield rotational viscometer test for

RTFO aged asphalt are close in values to the A and VTS values recommended by Witzcak and Fonseca (1996) for mix/laydown conditions. The A and VTS values obtained from the dynamic shear rheometer are slightly lower.

Table 6-6. Viscosity-Temperature Regression Coefficients (A and VTS) for Unaged and RTFO Aged PG 67-22 (AC-30) Asphalt

Regression Constants	Results based on viscosities obtained from Brookfield rotational viscometer test		Results based on viscosities obtained from dynamic shear rheometer test	
	Unaged Binder	RTFO Aged Binder	Unaged Binder	RTFO Aged Binder
A	–5.6362	–3.4655	–5.7817	–3.0165
VTS	16.207	10.407	16.63	9.0824

Table 6-7. Typical Viscosity-Temperature Regression Coefficients (A and VTS) for AC-30 (PG 67-22) at Different Hardening States

Regression Constants	Original Conditions (Unaged Binder)	Mix/Laydown Conditions
A	-3.6666	-3.56455
VTS	10.928	10.6768

Source: Witzcak and Fonseca (1996)

Based on the results presented in Tables 6-6 and 6-7, the viscosity (in poise) was finally calculated for the complex modulus testing temperatures used. The viscosities of interest are obtained from: a) Brookfield rotational viscometer testing of RTFO aged PG 67-22 (AC-30) asphalt, b) dynamic shear rheometer testing of RTFO aged PG 67-22 (AC-30) asphalt, and c) mix/laydown conditions from Witzcak and Fonseca (1996). Table 6-8 summarizes the results of the calculated viscosities for condition and test temperature.

Table 6-8. Calculated Viscosity at Four Complex Modulus Test Temperatures

Test and Aging Condition	Calculated Viscosity (in poise)			
	Complex Modulus Test Temperature			
	10° C	25° C	30° C	40° C
Brookfield test RTFO	3.89E+08	7.17E+06	2.29E+06	2.95E+05
DSR test RTFO	1.73E+06	1.12E+05	5.08E+04	1.20E+04
Mix/lay down condition (from Witzcak and Fonseca, 1996)	4.57E+08	7.39E+06	2.28E+06	2.79E+05

6.8 Comparison of Predicted and Measured Dynamic Modulus

In the following, the predictive regression equation by Witczak et al. (2002) is used to obtain predicted dynamic modulus values for all test temperature and frequencies for all mixtures tested, except the Superpave P5 mix for which a total volumetric description was not available, and the HVS PG 76-22 mix, for which binder viscosity measurements were not available. The three conditions considered are:

1. Mix/laydown condition from Witzcak and Fonseca (1996);
2. RTFO aged binder results from Brookfield rotational viscometer test; and
3. RTFO aged binder results from the DSR test.

Tables 6-9 through 6-11 list the predicted dynamic modulus values for all test temperatures and testing frequencies. Similarly, Figures 6-24 through 6-26 show the resulting comparisons between predicted and measured dynamic moduli for the three conditions studied. In order to evaluate the relative quality of the predictions, linear regressions with zero intercept were performed for the three cases. The results of the regression analysis are shown in Figures 6-24 through 6-26. The coefficient describing the slope of the regression line is a measure of the quality of fit – the closer the slope coefficient is to unity, the less of a bias is built into the prediction. A slope that is less than one indicates an unconservative prediction, in which the predicted dynamic modulus is higher than the measured dynamic modulus. Similarly, a slope that is greater than unity indicates a conservative prediction, in which the predicted dynamic modulus is lower than the measured dynamic modulus. Similarly, the R^2 value is a measure of the goodness of fit of the regression line. A high R^2 value indicates a good fit, whereas a low R^2 indicates an inadequate fit. The results from the regression analysis show that the RTFO aged binder

Table 6-9. Predicted Dynamic Modulus Using the Mix/Laydown Condition Proposed by Witzcak and Fonseca (1996)

Mixture	Temperature (° C)	Frequency			
		1 Hz	4 Hz	10 Hz	16 Hz
Georgia Granite Mixtures					
GAC1	10	6348.09	7833.00	8867.60	9409.14
	25	2233.40	3076.22	3740.45	4114.03
	40	743.46	1099.89	1409.71	1594.90
GAC2	10	7228.04	8935.16	10126.30	10750.27
	25	2519.90	3480.55	4239.32	4666.60
	40	830.82	1233.33	1584.17	1794.22
GAC3	10	7312.96	9022.68	10213.82	10837.27
	25	2519.90	3545.00	4310.05	4740.31
	40	857.33	1268.11	1625.12	1838.52
GAF1	10	7843.40	9699.73	10995.38	11674.21
	25	2729.02	3771.68	4595.62	5059.72
	40	897.89	1333.89	1714.14	1941.87
GAF2	10	8766.05	10836.87	13038.76	13038.76
	25	3055.47	4220.57	5140.85	5659.10
	40	1007.18	1495.26	1920.69	2175.41
GAF3	10	9224.27	11413.04	13742.22	13742.22
	25	3201.60	4428.16	5397.98	5944.44
	40	1050.65	1562.27	2008.80	2276.34
Whiterock Mixtures (Oolitic Limestone)					
WRC1	10	6281.57	7755.35	8782.67	9320.53
	30	1518.78	2156.30	2677.98	2978.17
	40	731.38	1083.18	1389.22	1572.26
WRC2	10	7203.20	8917.48	10114.99	10742.70
	30	1709.95	2438.73	3037.24	3382.33
	40	815.70	1214.19	1562.28	1770.95
WRC3	10	7869.28	9728.22	11025.33	11704.82
	30	1886.08	2683.56	3337.27	3713.79
	40	904.17	1342.32	1724.24	1952.90
WRF1	10	7377.84	9133.15	10359.26	11001.94
	30	1752.11	2498.61	3111.62	3465.07
	40	835.98	1244.25	1600.84	1814.59
WRF2	10	9442.18	11682.78	13247.26	14067.13
	30	2249.92	3205.85	3990.33	4442.46
	40	1075.37	1599.05	2056.11	2329.97
WRF4	10	9534.34	11792.37	13368.55	14194.41
	30	2277.65	3243.34	4035.42	4491.81
	40	1090.05	1619.74	2081.78	2358.54
WRF5	10	7756.29	9584.35	10859.48	11527.34
	30	1864.47	2650.89	3295.16	3666.12
	40	895.17	1327.87	1704.80	1930.39
WRF6	10	10642.12	13162.50	14921.81	15843.63
	30	2542.29	3620.17	4504.29	5013.71
	40	1216.70	1807.93	2323.66	2632.57
Mixtures From Fine Aggregate Angularity Study					
RBC	10	8739.16	10785.05	12210.69	12956.96
	40	745.75	1103.59	1414.71	1600.71
RBF	10	9850.64	12182.68	13810.43	14663.28
	40	868.59	1290.50	1658.48	1878.88
CALC	10		12281.01	13903.68	14753.05
	40	844.89	1250.10	1602.35	1812.93
CALF	10	11670.26	14432.67	16360.78	17370.99
	40	1029.34	1529.24	1965.23	2226.36

Mixture	Temperature (° C)	Frequency			
		1 Hz	4 Hz	10 Hz	16 Hz
CGC	10		9581.79	10852.29	11517.53
	40		1335.85	1713.68	1939.69
CGF	10	12080.89	14939.98	16935.52	17981.05
	40	1053.09	1564.43	2010.37	2277.46
CHC	10	6783.37	8377.25	9488.52	10070.40
	40	787.55	1166.97	1497.19	1694.73
CHF	10	8464.11	10483.62	11894.88	12634.78
	40	953.71	1420.92	1829.33	2074.26
Superpave Project Mixtures					
P1	10	7987.27	9213.04	10423.32	
	40	708.26	959.39	1228.08	1388.54
P2	10	7531.50	8304.65	9394.88	9965.25
	40	654.75	876.40	1121.68	1268.14
P3	10	6738.42	9866.87	11177.65	11864.09
	40	593.73	1050.05	1347.64	1525.71
P7	10	7474.52	9283.27	10502.78	11140.81
	40	649.79	966.71	1237.44	1399.13

Table 6-10. Predicted Dynamic Modulus Using RTFO Aged Binder Results from the Brookfield Rotational Viscometer Test

Mixture	Temperature (° C)	Frequency			
		1 Hz	4 Hz	10 Hz	16 Hz
Georgia Granite Mixtures					
GAC1	10	6141.71	7609.33	8636.32	9175.20
	25	2212.78	3050.25	3710.90	4082.68
	40	759.06	1121.94	1436.89	1624.97
GAC2	10	6991.03	8677.83	9859.92	10480.69
	25	2496.43	3450.91	4205.54	4630.73
	40	848.40	1258.28	1614.99	1828.34
GAC3	10	7075.32	8765.16	9947.56	10567.95
	25	2496.43	3515.08	4276.02	4704.20
	40	875.31	1293.53	1656.45	1873.16
GAF1	10	7585.74	9419.86	10705.60	11380.92
	25	2703.55	3739.50	4558.93	5020.76
	40	916.93	1360.92	1747.55	1978.87
GAF2	10	8478.56	10524.71	12711.72	12711.72
	25	3027.01	4184.62	5099.88	5615.60
	40	1028.50	1525.51	1958.07	2216.79
GAF3	10	8920.55	11082.99	13396.18	13396.18
	25	3171.66	4390.29	5354.78	5898.56
	40	1072.99	1594.01	2048.04	2319.82
Whiterock Mixtures (Oolitic Limestone)					
WRC1	10	6076.80	7533.31	8553.00	9088.18
	30	1520.14	2158.09	2680.08	2980.43
	40	746.77	1104.95	1416.09	1601.98
WRC2	10	6965.40	8658.91	9847.10	10471.47
	30	1711.50	2440.78	3039.65	3384.93
	40	833.08	1238.93	1592.88	1804.86
WRC3	10	7611.20	9448.00	10735.25	11411.25
	30	1887.78	2685.81	3339.90	3716.62
	40	923.31	1369.48	1757.79	1990.05
WRF1	10	7134.35	8868.40	10084.98	10724.24
	30	1753.69	2500.71	3114.09	3467.73
	40	853.79	1269.59	1632.19	1849.33

Mixture	Temperature (° C)	Frequency			
		1 Hz	4 Hz	10 Hz	16 Hz
WRF2	10	9131.27	11344.91	12897.32	13712.88
	30	2251.95	3208.54	3993.49	4445.87
	40	1098.22	1631.53	2096.28	2374.47
WRF4	10	9220.94	11451.92	13016.02	13837.59
	30	2279.71	3246.05	4038.61	4495.25
	40	1113.17	1652.59	2122.38	2403.51
WRF5	10	7502.42	9308.83	10574.35	11238.80
	30	1866.14	2653.10	3297.75	3668.91
	40	914.08	1354.68	1737.90	1967.03
WRF6	10	10292.30	12782.49	14528.33	15445.35
	30	2544.58	3623.20	4507.85	5017.55
	40	1242.51	1844.60	2368.98	2682.77
Mixtures From Fine Aggregate Angularity Study					
RBC	10	8454.83	10476.87	11891.99	12634.58
	40	761.40	1125.73	1442.01	1630.91
RBF	10	9526.95	11831.08	13446.37	14294.80
	40	887.02	1316.66	1690.81	1914.69
CALC	10		11930.23	13540.94	14386.14
	40	862.62	1275.17	1633.26	1847.12
CALF	10	11286.83	14016.19	15929.55	16934.52
	40	1051.17	1560.24	2003.54	2268.79
CGC	10		9307.21	10568.24	11230.14
	40		1362.73	1746.85	1976.39
CGF	10	11684.03	14508.93	16489.22	17529.32
	40	1075.42	1596.13	2049.56	2320.85
CHC	10	6561.95	8137.08	9240.06	9819.02
	40	804.14	1190.46	1526.18	1726.80
CHF	10	8184.06	10178.95	11579.14	12315.06
	40	974.08	1449.93	1865.25	2114.08
Superpave Project Mixtures					
P1	10	7232.74	8951.29	10152.84	
	40	663.35	978.53	1251.64	1414.59
P2	10	6520.58	8068.85	9151.24	9718.88
	40	606.11	893.88	1143.18	1291.91
P3	10	7726.21	9583.62	10884.56	11567.53
	40	723.20	1071.22	1373.77	1554.63
P7	10	7287.87	9019.52	10230.24	10865.22
	40	668.41	985.99	1261.18	1425.37

Table 6-11. Predicted Dynamic Modulus Using RTFO Aged Binder Results from the Dynamic Shear Rheometer Test

Mixture	Temperature (° C)	Frequency			
		1 Hz	4 Hz	10 Hz	16 Hz
Georgia Granite Mixtures					
GAC1	10	1170.78	1673.53	2088.55	2328.65
	25	441.77	662.60	859.21	978.60
	40	190.72	289.03	380.32	437.41
GAC2	10	1346.09	1936.46	2426.29	2710.49
	25	499.15	754.10	982.42	1121.53
	40	212.28	324.10	428.56	494.12
GAC3	10	1249.63	1786.03	2228.79	2484.93
	25	499.15	707.35	917.17	1044.56
	40	203.68	308.64	406.08	467.01
GAF1	10	1464.90	2104.70	2634.99	2942.50
	25	545.09	822.33	1070.31	1221.30
	40	232.51	354.47	468.26	539.63

Mixture	Temperature (° C)	Frequency			
		1 Hz	4 Hz	10 Hz	16 Hz
GAF2	10	1410.28	2025.09	2829.73	2829.73
	25	525.57	792.37	1030.90	1176.10
	40	224.48	342.00	451.60	520.31
GAF3	10	1567.56	2258.91	3166.82	3166.82
	25	578.57	875.78	1142.36	1304.93
	40	245.06	374.91	496.40	572.72
Whiterock Mixtures (Oolitic Limestone)					
WRC1	10	1331.74	1905.40	2379.31	2653.59
	30	371.92	562.39	735.10	841.28
	40	215.91	327.57	431.33	496.26
WRC2	10	1487.22	2144.65	2691.16	3008.59
	30	403.87	616.28	810.29	930.08
	40	231.68	354.72	469.91	542.31
WRC3	10	1459.92	2097.11	2625.16	2931.34
	30	401.99	610.65	800.56	917.57
	40	231.96	353.55	466.97	538.10
WRF1	10	1567.89	2256.36	2827.73	3159.30
	30	428.90	652.91	857.15	983.11
	40	246.80	376.97	498.61	574.97
WRF2	10	1593.26	2295.72	2879.29	3218.13
	30	433.91	661.49	869.22	997.42
	40	249.21	381.21	504.69	582.27
WRF4	10	1626.84	2337.06	2925.67	3266.97
	30	447.83	680.35	891.98	1022.38
	40	258.38	393.86	520.24	599.49
WRF5	10	1392.47	1997.11	2497.57	2787.54
	30	385.55	584.63	765.55	876.93
	40	223.00	339.28	447.58	515.44
WRF6	10	1813.53	2605.27	3261.44	3641.91
	30	499.22	758.41	994.34	1139.70
	40	288.03	439.05	579.93	668.28
Mixtures From Fine Aggregate Angularity Study					
RBC	10	1441.83	2062.97	2576.12	2873.12
	40	233.72	354.60	466.94	537.23
RBF	10	1777.05	2556.73	3203.69	3579.08
	40	280.06	427.66	565.55	652.10
CALC	10		2371.26	2960.94	3302.23
	40	268.78	407.75	536.90	617.70
CALF	10	2098.32	3019.18	3783.32	4226.72
	40	330.58	504.84	667.65	769.85
CGC	10		2479.73	3096.16	3452.91
	40		426.65	561.73	646.24
CGF	10	2151.50	3096.06	3879.95	4334.83
	40	338.75	517.39	684.31	789.10
CHC	10	1511.78	2162.93	2700.85	3012.18
	40	245.13	371.89	489.68	563.39
CHF	10	1873.27	2695.30	3377.41	3773.21
	40	295.16	450.74	596.09	687.32
Superpave Project Mixtures					
P1	10	881.97	1548.08	1548.08	
	40	151.15	295.65	295.65	338.70
P2	10	1308.41	1884.07	2362.05	2639.49
	40	205.33	205.33	415.30	479.02
P3	10	1547.87	1547.87	2785.58	3110.94
	40	245.30	245.30	494.31	569.72
P7	10	1646.80	1646.80	7703.09	3331.44
	40	256.53	256.53	520.32	600.49

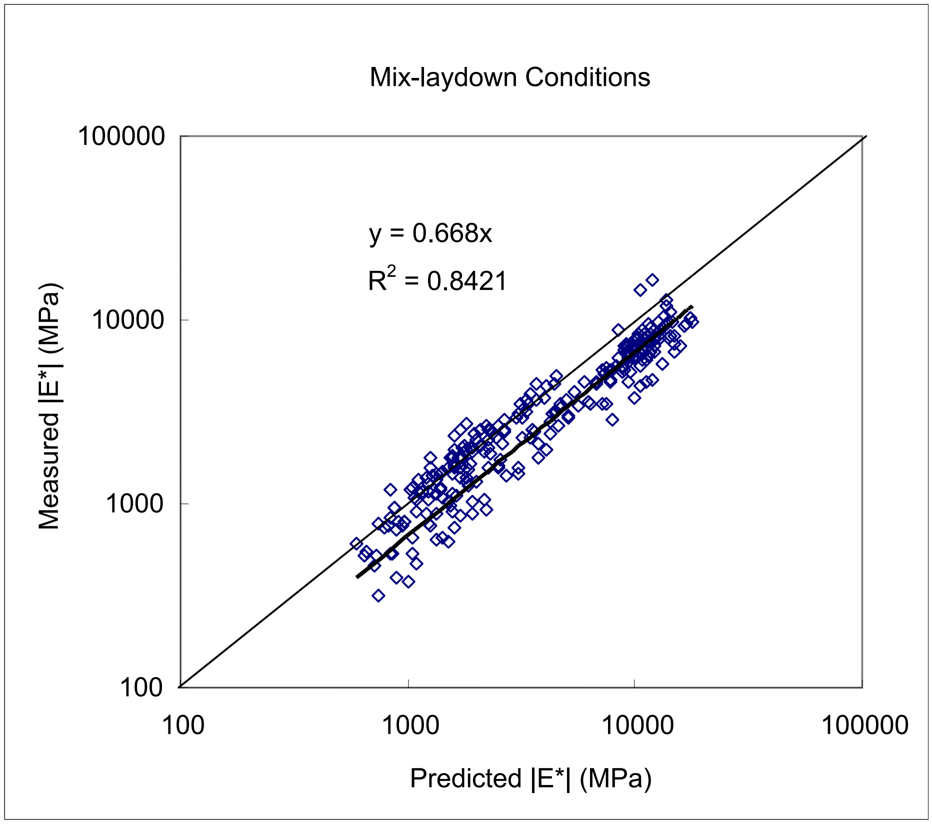

Figure 6-24. Measured values versus predicted values of |E*| on a log-log scale (Mix-laydown binder)

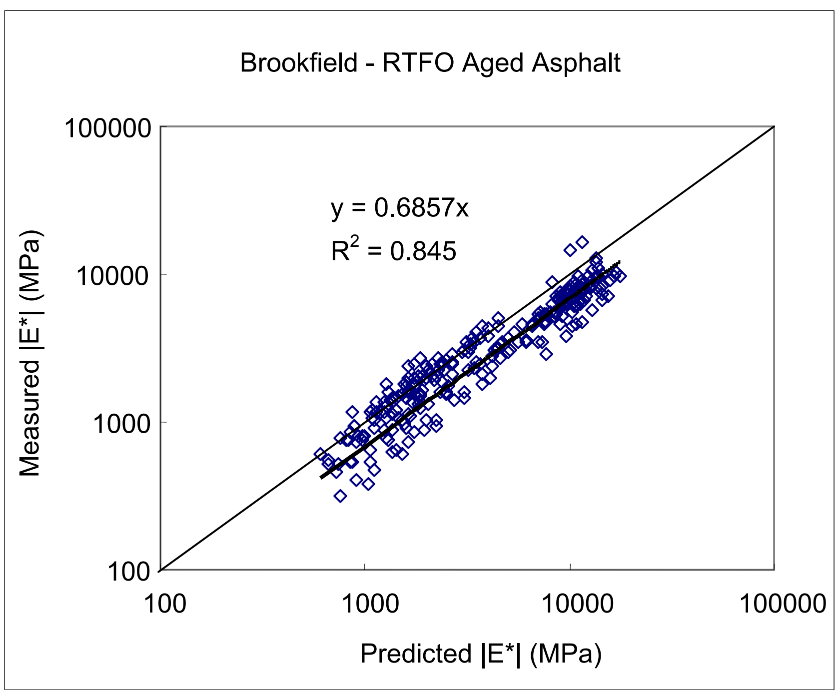

Figure 6-25. Measured values versus predicted values of |E*| on a log-log scale (RTFO-binder)

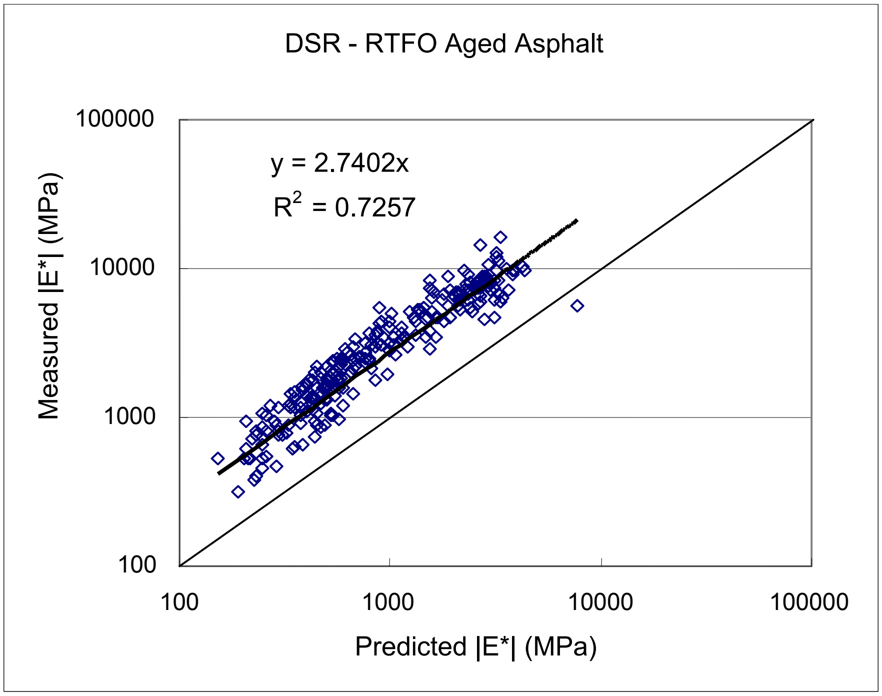

Figure 6-26. Measured values versus predicted values of |E*| on a log-log scale (DSR-RTFO binder)

results from Brookfield rotational viscometer test provide a slope that is closest to unity (0.6857), as well as the highest R^2 value (0.845). The mix/laydown binder viscosity conditions proposed by Witzcak and Fonseca (1996) provide very similar results. However, the RTFO aged binder results from the DSR test have a slope that is higher than unity (2.7402), than unity (2.7402), as well as a lower R^2 value (0.7257), which is likely the result of the higher bias in the prediction. Hence, even though the predictions based on the viscosity obtained from the Brookfield rotational viscometer test and the mix-laydown conditions proposed by Witzcak and Fonseca (1996) are statistically better than the results based on the viscosity obtained from the DSR test, the latter is the only conservative estimate of the three evaluated. This bias in the DSR-based predictions of dynamic modulus values follow similar published results (e.g., Clyne et al., 2003). Hence, consistent with the recommendations by

Witzcak et al. (2002), in order to obtain conservative predictions, it is recommended that viscocity input values for the predictive equation be obtained from the DSR test.

Interestingly, it is of interest to note that the predictions at higher temperatures (i.e., lower modulus values) generally are closer to the line of equity for all three cases than the predictions at lower temperatures. Figures 6-27 through 6-29 present a comparison of predicted and measured dynamic modulus values for the Whiterock oolitic limestone mixtures tested (F1, F2, F4, F5, F6, C1, C2, C3). As the temperature increases from 10° C to 40° C, the predicted dynamic modulus approaches the measured dynamic modulus values. This is likely the result of the much of the database used to develop the predictive equation being biased toward mixtures tested at higher temperatures.

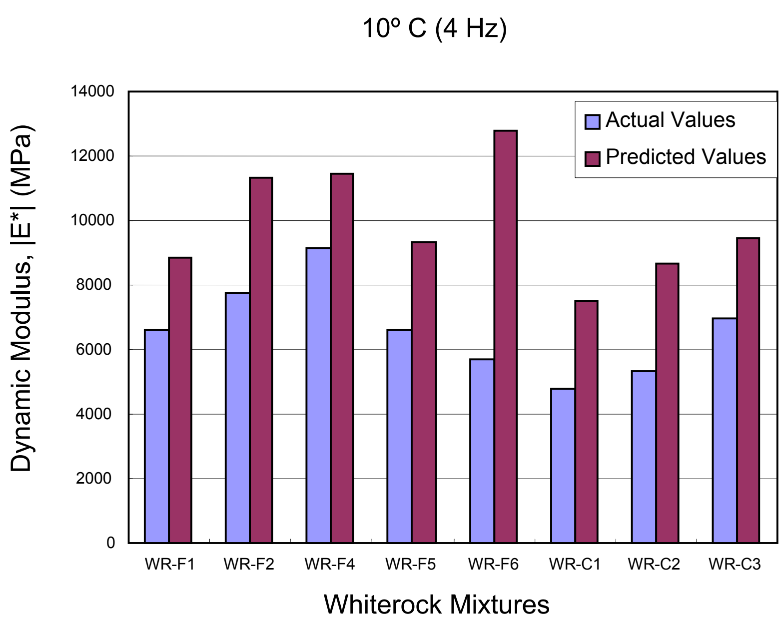

Figure 6-27. Measured vs. predicted dynamic modulus values for Whiterock limestone mixtures: Testing temperature is 10° C and testing frequency is 4 Hz

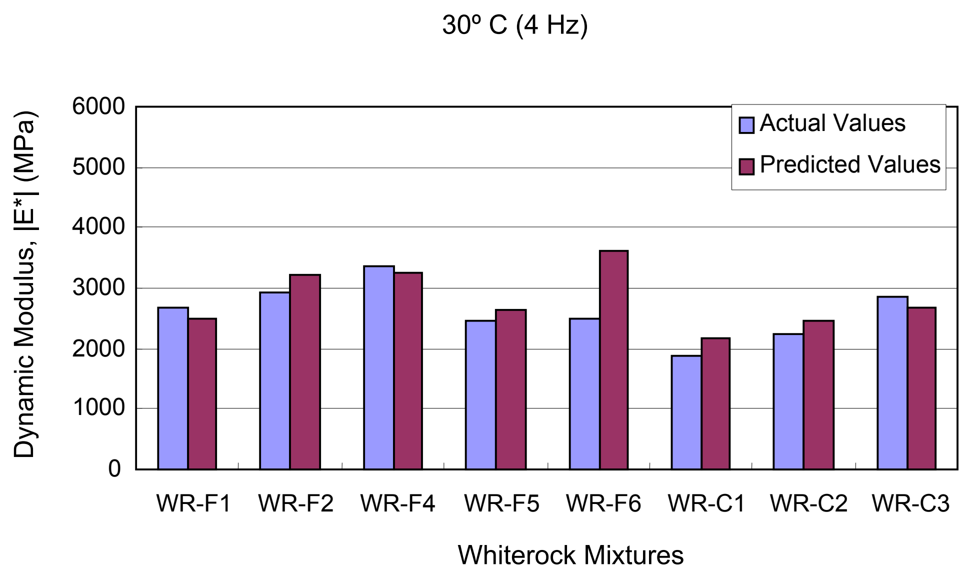

Figure 6-28. Measured vs. predicted dynamic modulus values for Whiterock limestone mixtures: Testing temperature is 30° C and testing frequency is 4 Hz

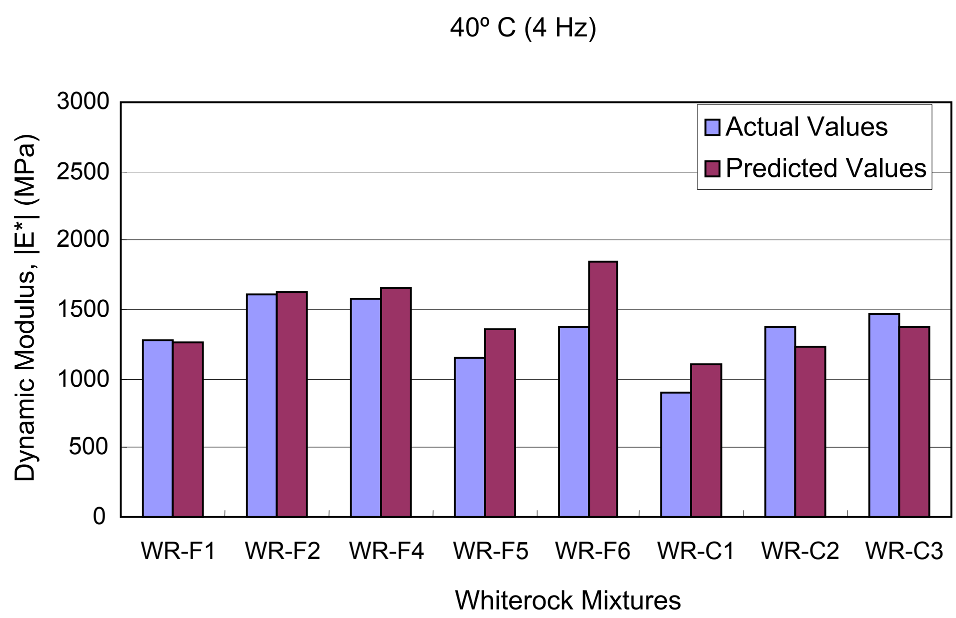

Figure 6-29. Measured vs. predicted dynamic modulus values for Whiterock limestone mixtures: Testing temperature is 40° C and testing frequency is 4 Hz

Finally, Figure 6-30 shows measured vs. predicted dynamic modulus for fine aggregate angularity mixtures (FAA), Superpave project mixtures (Project), granite mixtures (Granite), and Whiterock mixtures (WR) at a test temperature of 40° C and a testing frequency of 4 Hz. Most of the mixture groups scatter around the line of unity, with the exception of the Georgia granite mixtures (GA-C1, GA-C2, GA-C3, GA-F1, GA-F2, GA-F3), which land below the line of unity. Since the testing protocol for all mixtures was the same, the asphalt used was the same, and these mixtures were designed to be volumetrically similar to the Whiterock oolitic limestone mixtures (WR-C1, WR-C2, WR-C3, WR-F1, WR-F2, WR-F3), it is likely that this difference has to do with the aggregate type. This warrants further study through more detailed testing of mixtures of different mineral origin.

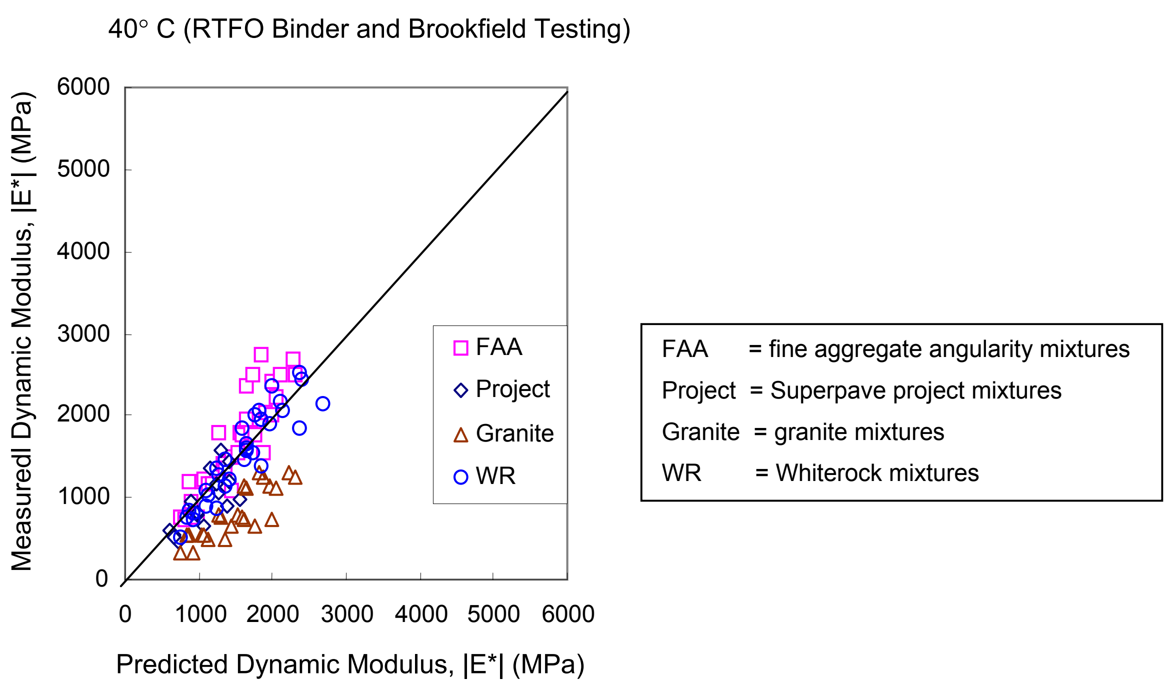

Figure 6-30. Measured vs. predicted dynamic modulus for fine aggregate angularity mixtures, Superpave project mixtures, granite mixtures, and Whiterock mixtures at a test temperature of 40° C and a testing frequency of 4 Hz

6.9 Conclusions

This chapter presented dynamic modulus testing results for 29 mixtures of different gradations and aggregate types. Mixtures were tested at two or more of the following test temperatures: 10° C, 25° C, 30° C, and 40° C. At each testing temperature, testing was conducted at four distinct frequencies, namely 16 Hz, 10 Hz, 4 Hz, and 1 Hz. The dynamic modulus and phase angle results show the following trends:

1. Under a constant loading frequency, the dynamic modulus decreases with an increase in test temperature for the same mixture.
2. The phase angle increases with the increase of test temperature.
3. Under a constant test temperature, the dynamic modulus increases with increased test frequencies.
4. Both the dynamic modulus and phase angle data shows relatively smooth trends, irrespective of test temperature.

The procedure developed by Pellinen and Witczak (2002) for obtaining predicted master curves was used for all mixtures tested at more than two temperatures. The results showed that further testing at higher and lower temperatures would help in better defining the tails of the predicted master curves.

Finally, the predictive regression equation developed by Witczak et al. (2002) was used to predict dynamic modulus values for most of the mixtures tested. The results showed that dynamic modulus predictions using DSR-based viscosity measurements, result in conservative predictions of the dynamic modulus. Therefore, it is recommended that viscosity input values for the predictive equation be obtained from the DSR test, in lieu of the Brookfield rotational viscometer test, or published mix/laydown viscosities by Witczak and

Fonseca (1996). The results also showed that dynamic modulus predictions at higher temperatures generally are closer to the line of equity for all three cases than the predictions at lower temperatures. This is likely the result of the much of the database used to develop the predictive equation being biased toward mixtures tested at higher temperatures.

Finally, a comparison was performed between measured vs. predicted dynamic modulus at 40° C for the following mixture categories:

- Fine aggregate angularity mixtures (FAA);
- Superpave project mixtures (Project);
- Granite mixtures (Granite); and
- Whiterock mixtures (WR).

Most of the mixture groups scatter around the line of unity, with the exception of the Georgia granite mixtures, which land below the line of unity. Since the testing protocol for all mixtures was the same, the asphalt used was the same, and these mixtures were designed to be volumetrically similar to the Whiterock oolitic limestone mixtures (WR-C1, WR-C2, WR-C3, WR-F1, WR-F2, WR-F3), it is likely that this difference has to do with the aggregate type. This warrants further study through more detailed testing of mixtures of different mineral origin.

CHAPTER 7
EVALUATION OF POTENTIAL CORRELATION BETWEEN COMPLEX MODULUS PARAMETERS AND RUTTING RESISTANCE OF MIXTURES

7.1 Background

In this chapter, potential relationships are evaluated between complex modulus parameters and other common measures of the rutting potential of mixtures. In particular, the complex modulus parameters are compared against asphalt pavement analyzer (APA) rut depth results and creep test results from static unconfined compressive creep testing. First, the APA test procedures and test results are discussed, followed by a description of the static creep test procedure used and presentation of creep test results. Subsequently, comparisons are made between dynamic modulus and phase angle results presented in Chapter 6 to APA rut depth measurements and static creep testing results.

7.2 Asphalt Pavement Analyzer Test Procedure and Test Results

Asphalt pavement analyzer (APA) equipment is designed to test the rutting susceptibility or rutting resistance of hot mix asphalt. With this equipment, rut performance testing is performed by means of a constant load applied repeatedly through pressurized hoses to a compacted test specimen. The test specimen for this research is a 150-mm diameter by 75-mm thick cylindrical specimen.

The procedure for sample preparation and testing is as follows:

- 4500 g samples of the aggregate are batched in accordance with the required job mix formula. The aggregate and asphalt binder are preheated separately to 300° F for about three hours, after which they are mixed until the aggregates are thoroughly coated with the binder; the amount of binder used is pre-determined to produce an optimum hot mix asphalt (HMA) using Superpave volumetric mix design procedures.

- The mixture is then subjected to two hours of short-term oven aging at 275° F in accordance with AASHTO PP2.
- The sample is compacted at the above temperature to contain 7.0 ± 0.5% air voids in the Servopac Superpave gyratory compactor. This is done by first determining the compaction height needed to obtain the required air void content from the compaction results obtained for the mixture design. The mix is then compacted to the determined height.
- The specimen is allowed to cool at room temperature (approximately 25° C) for a minimum of 24 hours. After this, the bulk specific gravity of the specimen is determined in accordance with AASHTO T 166 or ASTM D 2726. The maximum specific gravity of the mixture is determined in accordance with ASTM D2041 (AASHTO T 209). Then, the air void content of the specimen is determined in accordance with ASTM D 3203 (AASHTO T 269) to check if the target air void content has been achieved.
- The specimen is trimmed to a height of 75-mm and allowed to air dry for about 48 hours.
- The specimen is preheated in the APA chamber to a temperature of 60° C (140° F) for a minimum of six hours but not more than 24 hours before the test is run.
- The hose pressure gage reading is set to 100 ± 5 psi.
- The load cylindrical pressure reading for each wheel is set to obtain a load of 100 ± 5 lb.
- The preheated, molded specimen is secured in the APA, the chamber doors closed, and 10 minutes is allowed for the temperature to stabilize prior to starting the test.
- 25 wheel strokes are applied to seat the specimen before initial measurements are taken.
- The mold and the specimen are securely positioned in the APA, the chamber doors are closed and 10 minutes are allowed for the temperature to stabilize.
- The APA is then restarted and the rut testing continued, now for 8000 cycles.

Table 7-1 lists the resulting APA rut depth measurements, along with the dynamic modulus values obtained at 40° C at testing frequencies of 1 Hz and 4 Hz.

Table 7-1. Dynamic Modulus (|E*|), Phase Angle (δ), and Asphalt Pavement Analyzer Rut Depth Measurements from Mixture Testing at 40° C

Mixture	Phase Angle (δ) Results (degrees)		Dynamic Modulus (|E*|) Results (MPa)		Asphalt Pavement Analyzer Rut Depth (mm)
	Frequency				
	1 Hz	4 Hz	1 Hz	4 Hz	
Georgia Granite Mixtures					
GAC1	27.11	32.77	317.12	475.14	7.1
GAC2	26.67	32.14	535.77	787.74	7.1
GAC3	37.05	42.79	530.76	757.09	5.9
GAF1	27.25	32.35	401.02	635.50	5.1
GAF2	31.63	38.32	535.97	905.80	5.1
GAF3	32.91	38.87	377.70	614.91	4.4
Whiterock Mixtures (Oolitic Limestone)					
WRC1	29.02	30.42	526.05	898.81	5.4
WRC2	32.19	32.15	759.48	1368.38	4.6
WRC3	32.84	32.25	801.08	1470.36	4.6
WRF1	29.38	32.11	849.60	1273.70	5.1
WRF2	31.21	33.67	1076.16	1610.34	5.2
WRF4	31.70	34.00	1044.19	1584.81	4.3
WRF5	30.05	33.13	726.94	1146.45	7.1
WRF6	31.92	33.59	879.93	1374.06	4.8
Mixtures From Fine Aggregate Angularity Study					
RBC	27.38	31.09	770.75	1175.36	7.3
RBF	25.90	28.66	954.17	1415.66	8.5
CALC	30.53	34.24	1182.66	1792.49	6.9
CALF	26.97	33.92	1184.06	1779.33	6.2
CGC	31.40	31.10	923.08	1363.60	4.3
CGF	25.70	30.95	1217.77	1777.24	4.6
CHC	30.45	33.33	744.73	1166.04	11.9
CHF	35.50	35.40	756.82	1073.82	13.9
Superpave Project Mixtures					
P1	23.62	22.99	523.74	807.66	7.1
P2	28.33	32.46	606.97	953.37	6.6
P3	30.63	34.67	458.87	655.21	3.2
P7	26.99	32.15	549.95	796.88	4.3
Heavy Vehicle Simulator Mixtures					
HVS67-22	29.01	32.96	620.85	925.02	7.5
HVS76-22	29.24	31.81	646.38	967.52	6.5

7.3 Static Creep Test Results

Once the complex modulus test was completed, a static creep test was performed on the same samples tested in the complex modulus test. In the static creep test, a constant vertical load is applied to an unconfined (no lateral confinement pressures) HMA specimen, and the resulting time-dependent vertical deformation is measured. Figure 7-1 shows a qualitative diagram of the vertical stress and total vertical deformation during a creep test.

The same LVDT's that were used for the complex modulus test were used in the static creep test to measure vertical deformation.

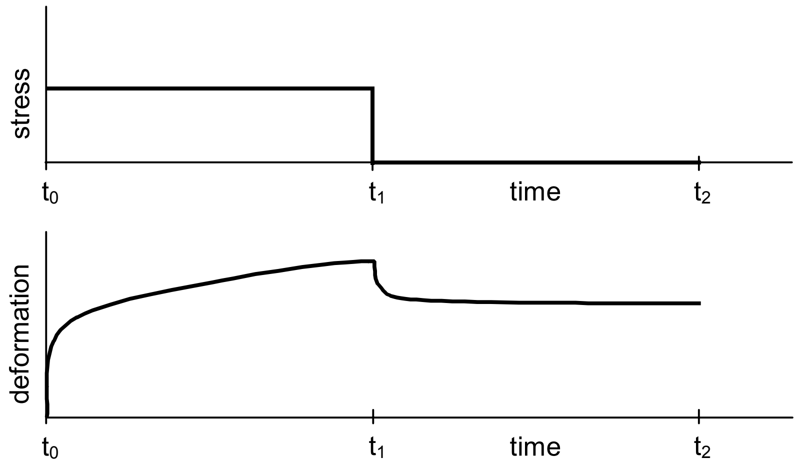

Figure 7-1. Qualitative diagram of the stress and total deformation during the creep test

The creep compliance from creep test at a higher temperature may be an indicator of the rutting potential of the mix. The compliance is calculated from this test by dividing the strain by the applied stress at a specified time in seconds.

The following equation is used to calculate the creep compliance:

$$D(t) = \frac{\varepsilon_t}{\sigma} \tag{7.1}$$

where $D(t)$ = creep compliance at the test temperature, T, and time of loading, t

ε_t = strain at time t (inch/inch); and

σ = applied stress, psi.

The static creep test was run for a total of 1000 seconds. The test load was chosen such that it produced a horizontal deformation of 150–200 micro-inches after 30 seconds of loading. The test temperature was 40° C.

Finally, the measured creep compliance D(t) can be represented using the following power function:

$$D(t) = D_0 + D_1 t^m \quad (7.2)$$

where D_0, D_1, and m are parameters obtained from creep tests. In accordance with the findings from the evaluation of creep parameters from the Superpave Indirect Tensile Test (Chapter 10) the value of D_0 is taken as 1/|E*|. The dynamic modulus |E*| is obtained from the 10 Hz frequency test, to minimize variability of the results. Table 7-2 lists the static creep test results, along with the power law parameters D_1 and m.

Table 7-2 Average Static Creep Testing Results for Test Temperature of 40° C

Mixture	Creep Compliance	Power Law Parameters	
	D (1000 seconds) (1/MPa) (× 1000)	D1 (1/MPa)	m-value
Georgia Granite Mixtures			
GAC1	19.63	8.93E-03	0.114
GAC2	17.02	5.01E-03	0.177
GAC3	15.97	6.83E-03	0.123
GAF1	17.79	5.31E-03	0.175
GAF2	9.52	3.45E-03	0.147
GAF3	11.64	3.50E-03	0.174
Whiterock Mixtures (**Oolitic** Limestone)			
WRC1	1.57	4.14E-04	0.193
WRC2	1.23	3.78E-04	0.171
WRC3	1.96	6.27E-03	0.164
WRF1	26.03	8.50E-03	0.162
WRF2	3.95	1.29E-03	0.162
WRF4	4.86	1.23E-03	0.199
WRF5	6.45	1.61E-03	0.201
WRF6	4.52	1.56E-03	0.154
Mixtures from Fine Aggregate Angularity Study			
RBC	16.49	6.40E-03	0.137
RBF	10.39	3.30E-03	0.166
CALC	3.83	5.50E-04	0.281
CALF	1.91	3.50E-03	0.128
CGF	10.76	5.00E-03	0.111
CHC	1.74	3.30E-04	0.330
CHF	15.97	4.90E-03	0.171
Superpave Project Mixtures			
P1	1.73	5.85E-04	0.157
P2	5.75	1.57E-03	0.188
P3	25.43	3.05E-03	0.307
P5	13.25	5.35E-03	0.155
P7	1.73	5.55E-03	0.126
Heavy Vehicle Simulator Mixtures			
HVS67-22	24.17	9.00E-03	0.143
HVS76-22	15.57	6.00E-03	0.138

7.4 Evaluation of Dynamic Test Results for HMA Rutting Resistance

In this section, the dynamic modulus measurements are compared to the rutting performance of the various mixtures as measured by the APA rut depths. In this research project, rutting resistance is evaluated at the high temperature of 40° C at the frequencies of 1 Hz and 4 Hz. Berthelot et al. (1996) proposed the following ranges of testing frequencies for simulating various highway speeds:

- 0.02 – 0.2 Hz to simulate parking;
- 0.2 – 2.0 Hz to simulate street and intersection speed; and
- 2.0 – 20 Hz to simulate highway speed.

However, Witczak et al. (2002) used a testing frequency of 5.0 Hz as representative of traffic speed that will trigger pavement rutting in the evaluation of the Superpave™ simple performance tests. Test results were therefore plotted for the lower frequencies of 1.0 Hz and 4 Hz. Figure 7-2 depicts the results. No discernable correlation appears to exist between the dynamic modulus and APA rut depth measurements. To check if the scatter found in Figure 7-2 might be due to gradation effects, the coarse- and fine-graded mixtures were separated into two different categories and plotted in Figure 7-3 for a testing frequency of 1 Hz. Again, the results in Figure 7-3 show no relationship between the dynamic modulus and the rut resistance for both fine- and coarse-graded mixtures at the high temperature of 40° C and low frequency of 1 Hz at which pavement rutting is most likely to occur. These results are similar to those presented by Brown et al. (2004) in an evaluation of the rutting performance on the 2000 NCAT test track sections. Figure 7-4 shows the results obtained by Brown et al. (2004), in which the relationship between the dynamic modulus at 10 Hz and test track rutting (in mm) is evaluated. No discernable relationship between dynamic modulus and test track rutting is detectable.

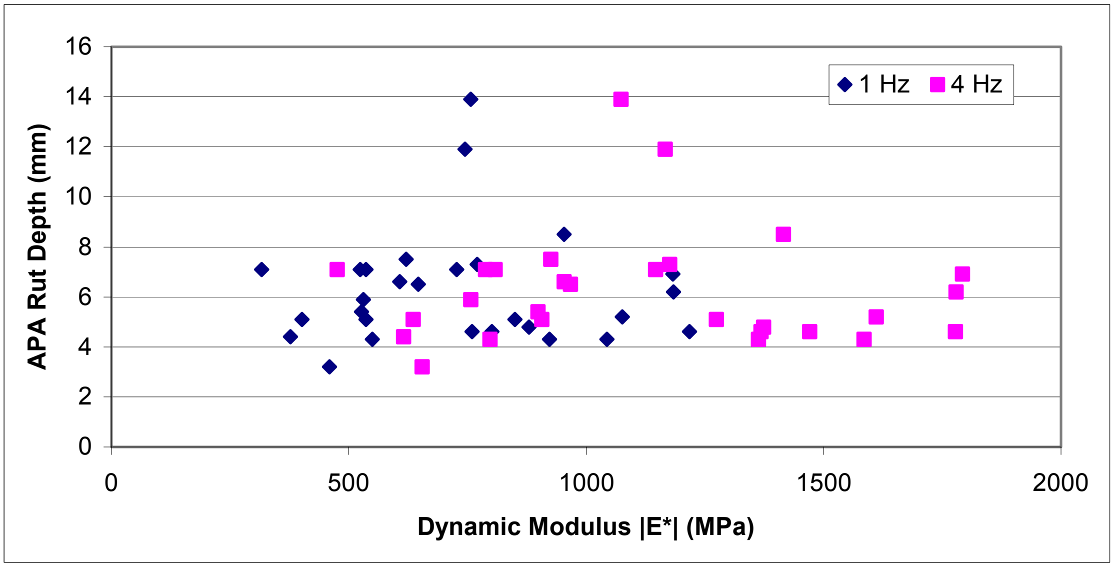

Figure 7-2. Dynamic modulus at testing frequencies of 1 Hz and 4 Hz versus APA rut depth measurements (test temperature for dynamic modulus test and APA test is 40° C)

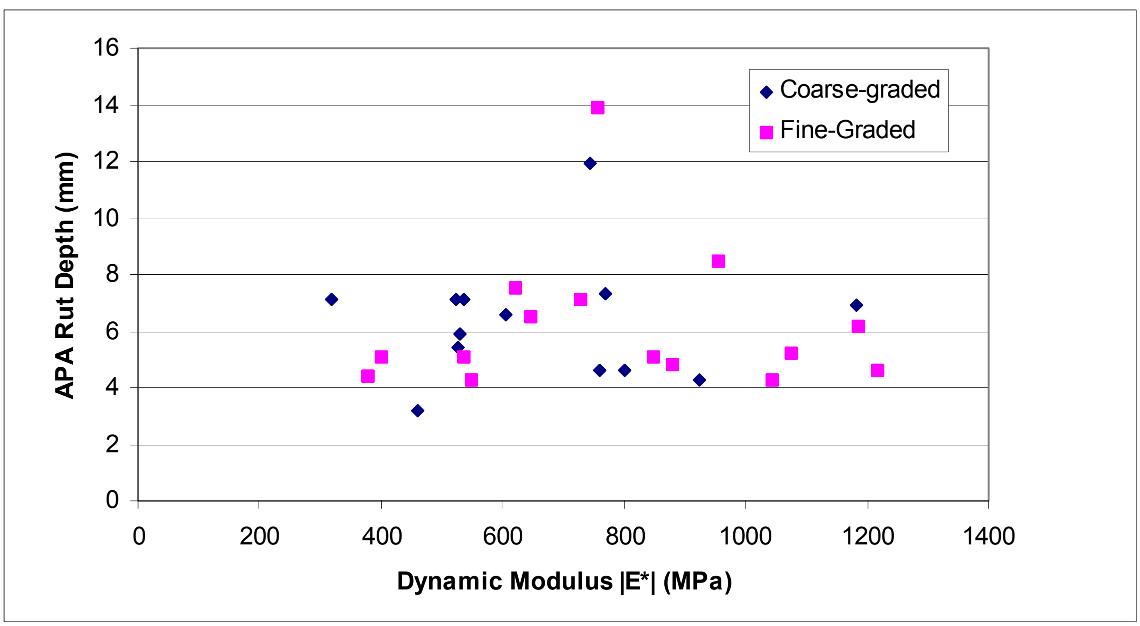

Figure 7-3. Dynamic modulus at testing frequencies of 1 Hz and 4 Hz versus APA rut depth measurements for coarse- and fine-graded mixtures (test temperature for dynamic modulus test and APA Test is 40° C)

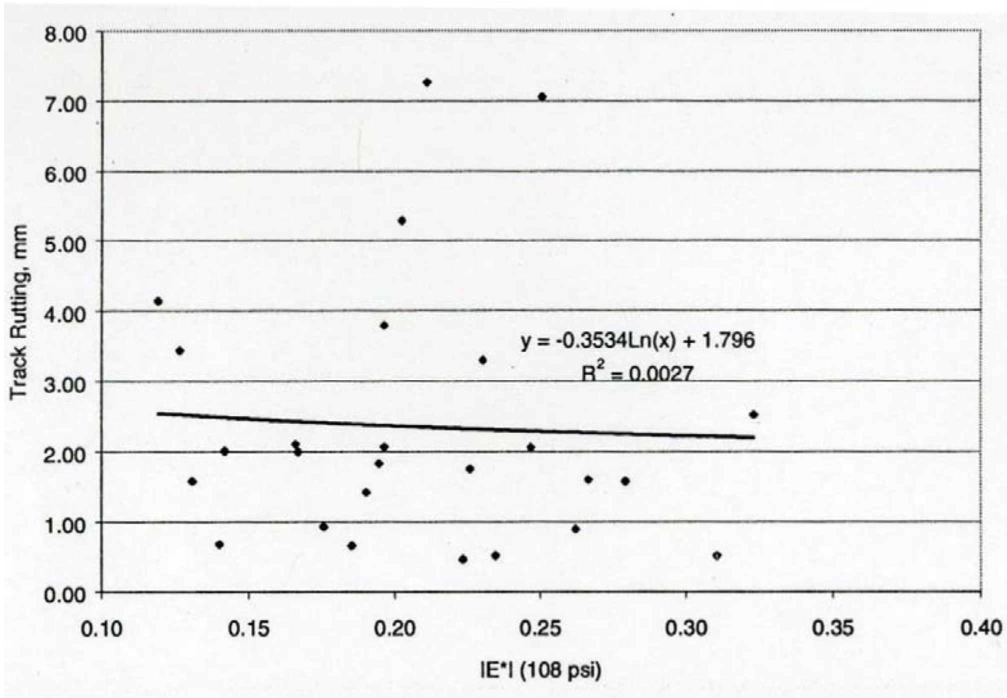

Figure 7-4. Dynamic modulus, |E*|, versus test track rutting (in mm) for the 2000 NCAT test track sections (Brown et al., 2004)

Figure 7-5 presents a plot of the phase angle at 1 Hz testing frequency and APA rut depth. The results again show no correlation.

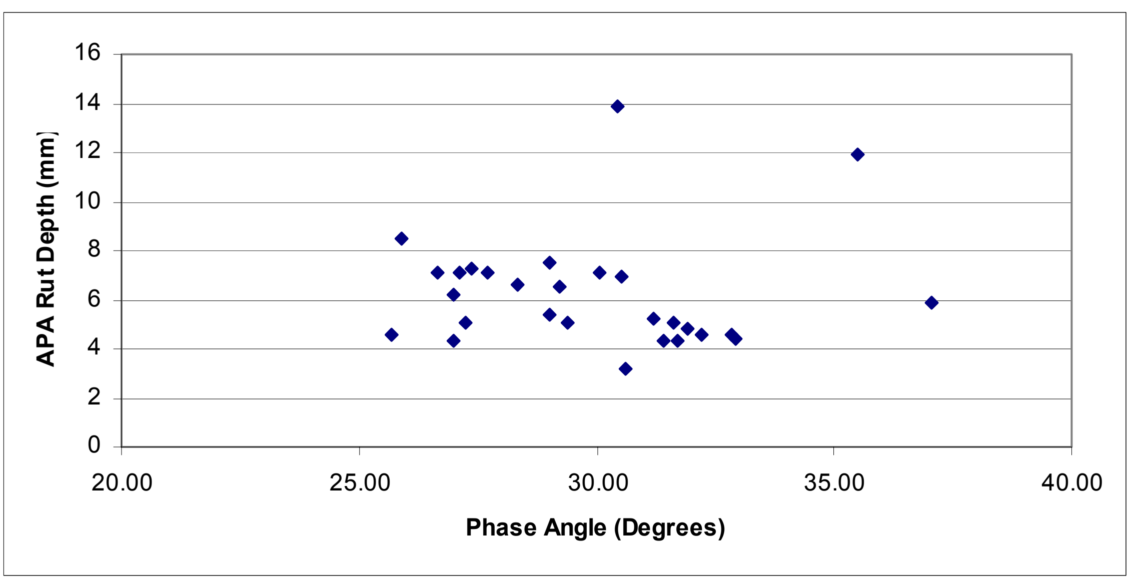

Figure 7-5. Phase angle at a testing frequency of 1 Hz versus APA rut depth measurements (test temperature for dynamic modulus test and APA test is 40° C)

The viscous stiffness based on the Maxwell model (Ullidtz, 1987), |E*|/sin δ at 40° C and 1 Hz frequency was plotted against the APA rut depth to observe any relationship of this parameter with the rutting resistance of the mixtures tested. Figure 7-6 shows the results. Again, no relationship between |E*|/sin δ and APA rut depth measurements can be detected. Figure 7-7 shows the corresponding results obtained by Brown et al. (2004), in which the relationship between the |E*|/sin δ at 10 Hz and test track rutting (in mm) is evaluated. Again, no discernable relationship between dynamic modulus and test track rutting is detectable.

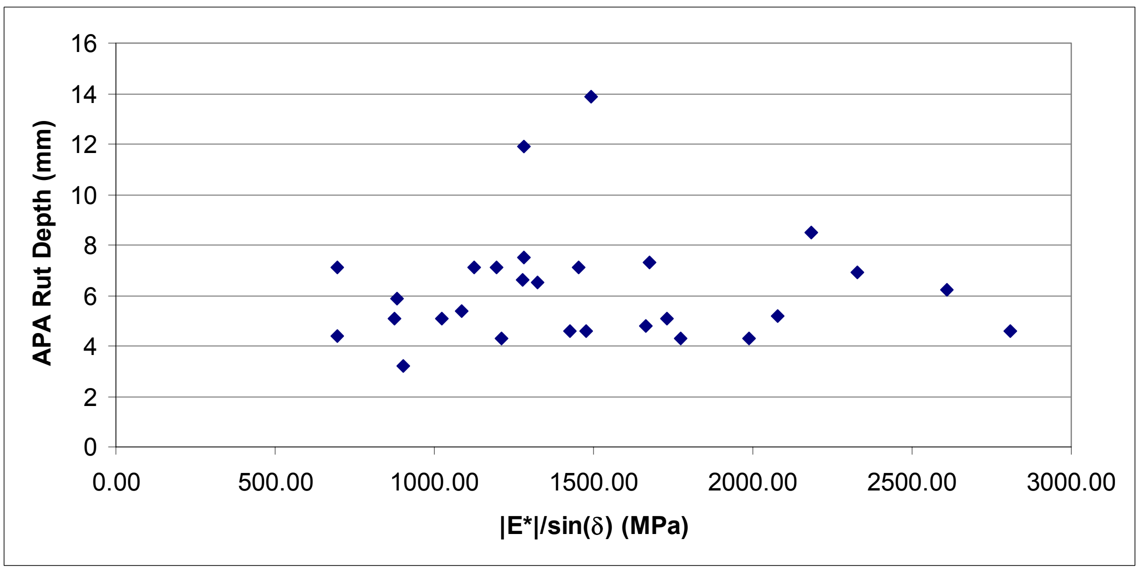

Figure 7-6. Plot of E*/sin ϕ at 40° C and 1 Hz versus the APA rut depths for all mixtures

Finally, Figure 7-8 shows a plot of the loss modulus, |E*|sin ϕ, at 40° C and 1 Hz frequency versus the APA rut depth. Again, there was no correlation between this parameter and the rutting resistance of the mixtures as measured with the APA.

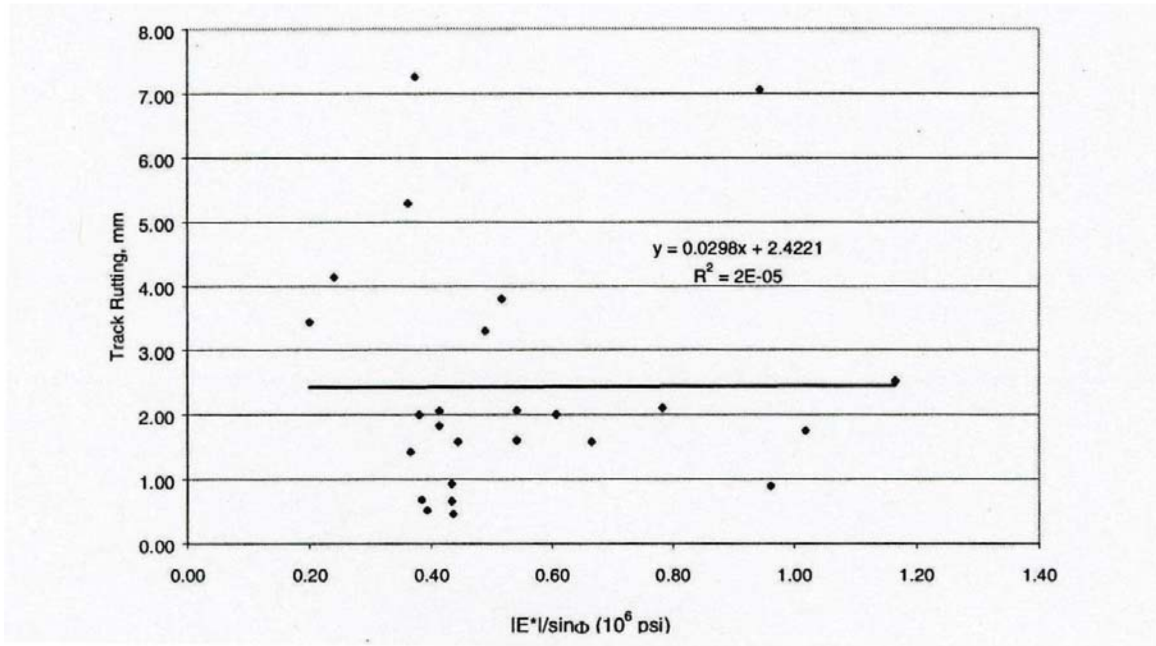

Figure 7-7. |E*|/sin δ versus test track rutting (in mm) for the 2000 NCAT test track sections (Brown et al., 2004)

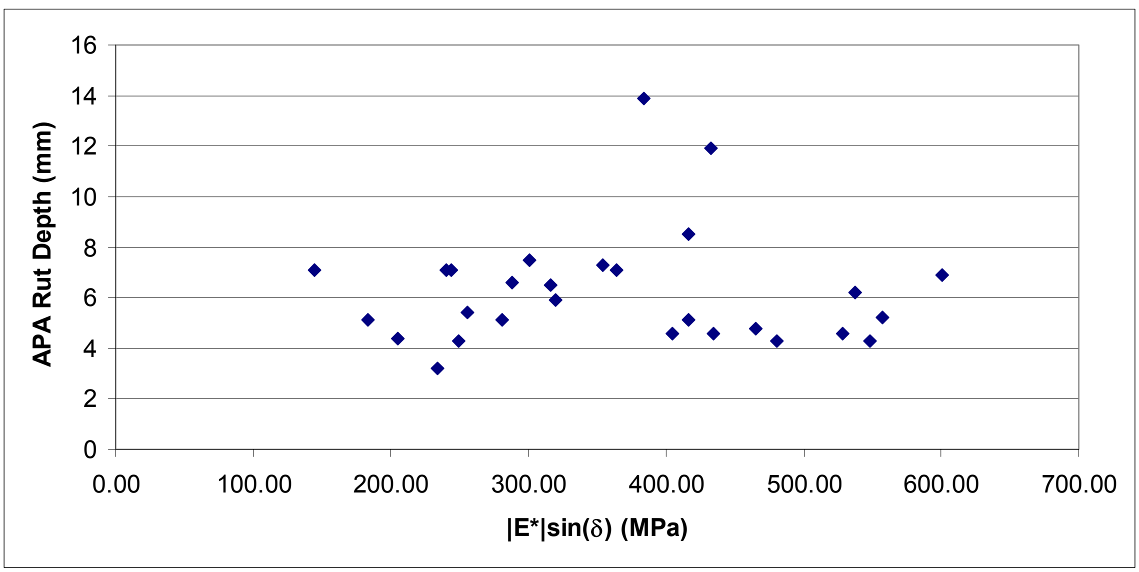

Figure 7-8. Plot of |E*|sin δ at 40° C and 1 Hz versus APA rut depth

In summary, no relationship was found between the dynamic complex modulus parameters and the APA rut depth measurements. Furthermore, research from the NCAT test track sections shows no relationship between the dynamic complex modulus parameters and track rut depths.

7.5 Evaluation of Static Creep Parameters

Figure 7-9 shows a weak relationship between the dynamic modulus at a 1 Hz testing frequency and the static creep compliance at 1000 seconds. Similarly, Figures 7-10 and 7-11 show a weak trend between the dynamic modulus and the creep compliance parameters D_1 and m. As expected, the higher the dynamic modulus, the lower the creep compliance. Interestingly, the power law parameter D_1 exhibits the same trend with higher modulus as the creep compliance, whereas the m-value increases very slightly with increasing modulus values. Unfortunately, the relationship between the dynamic modulus and static creep properties is too weak for use in any predictive type of a relationship.

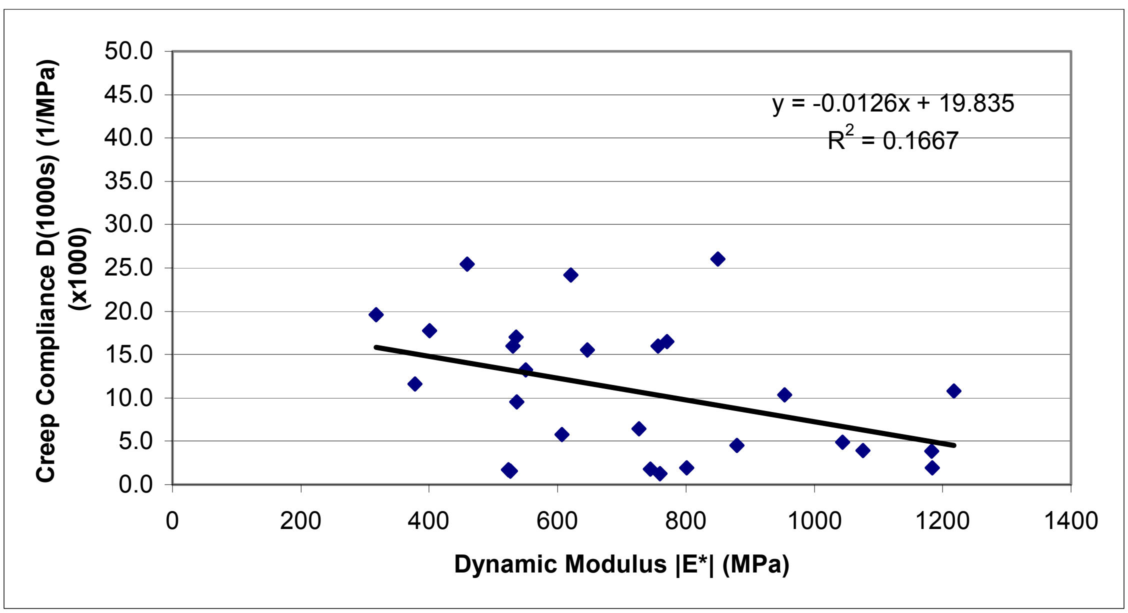

Figure 7-9. Relationship between dynamic modulus at 1 Hz frequency and static creep compliance after 1000 seconds

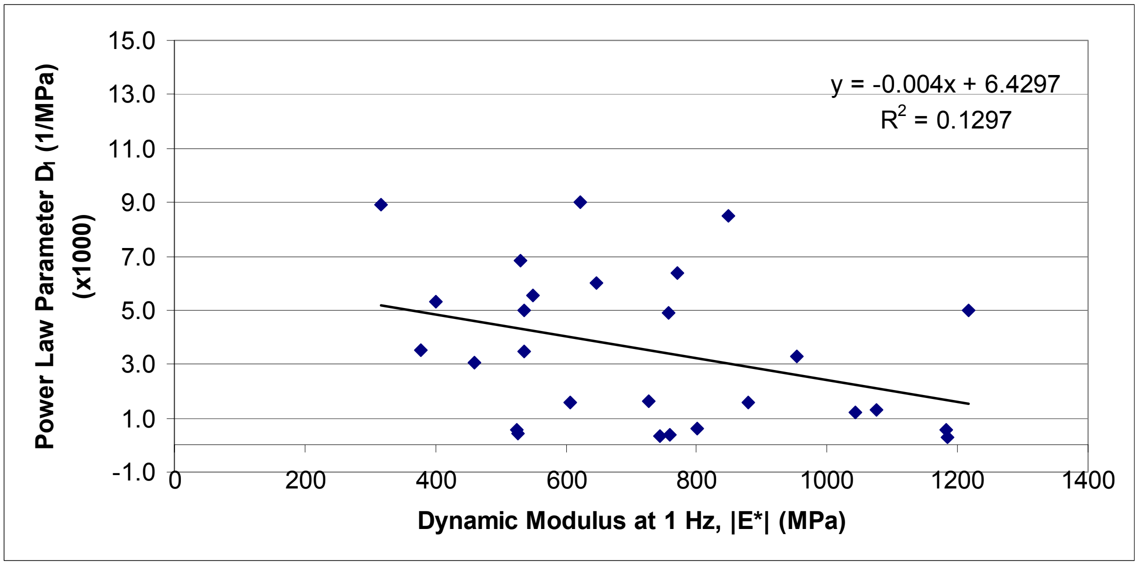

Figure 7-10. Relationship between dynamic modulus at 1 Hz frequency and the power law creep compliance parameter D_1

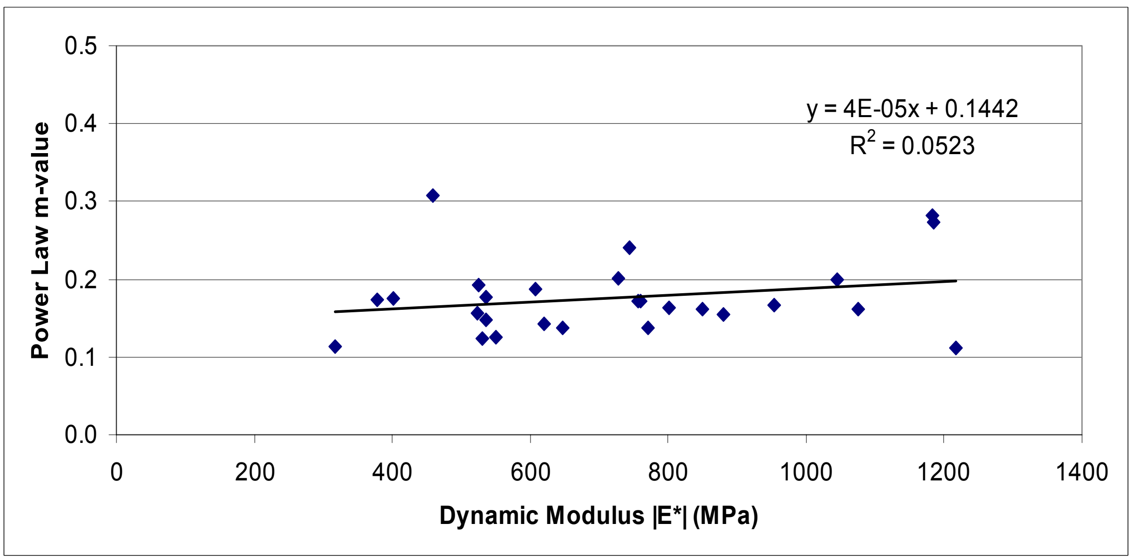

Figure 7-11. Relationship between dynamic modulus at 1 Hz frequency and power law m-value parameter

Figure 7-12 shows that there is no discernable relationship between the phase angle and the creep compliance at 1000 seconds. However, Figures 7-13 and 7-14 show a weak relationship between the phase angle and the power law parameters D_1 and m. The power law parameter D_1 shows a slight decrease with increasing phase angle, whereas the m-value shows a slight increase. Again, unfortunately, the observed trends are too weak to infer anything about the physical behavior of the mixtures.

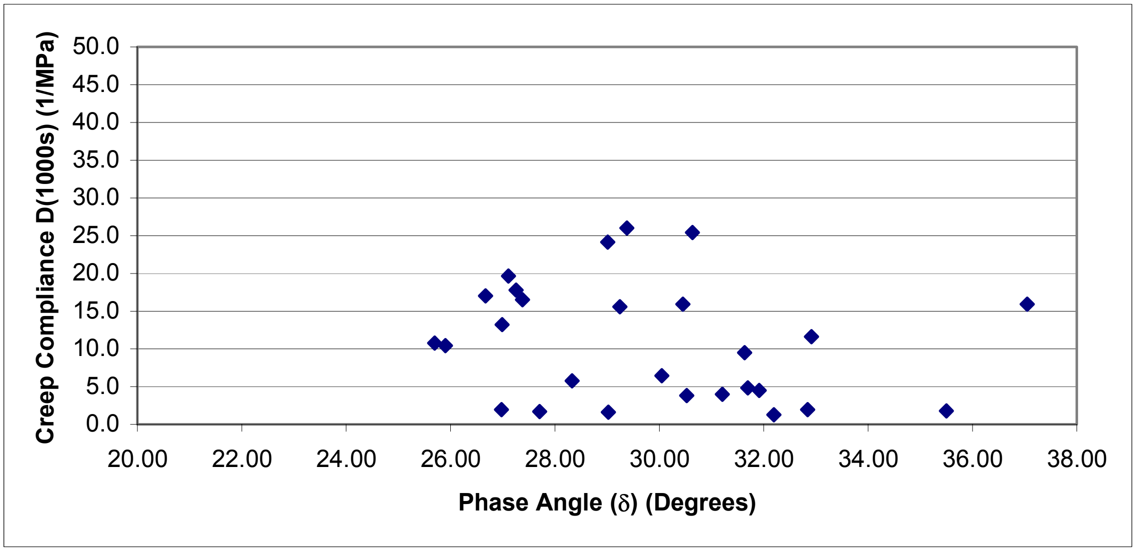

Figure 7-12. Relationship between phase angle at 1 Hz frequency and static creep compliance after 1000 seconds

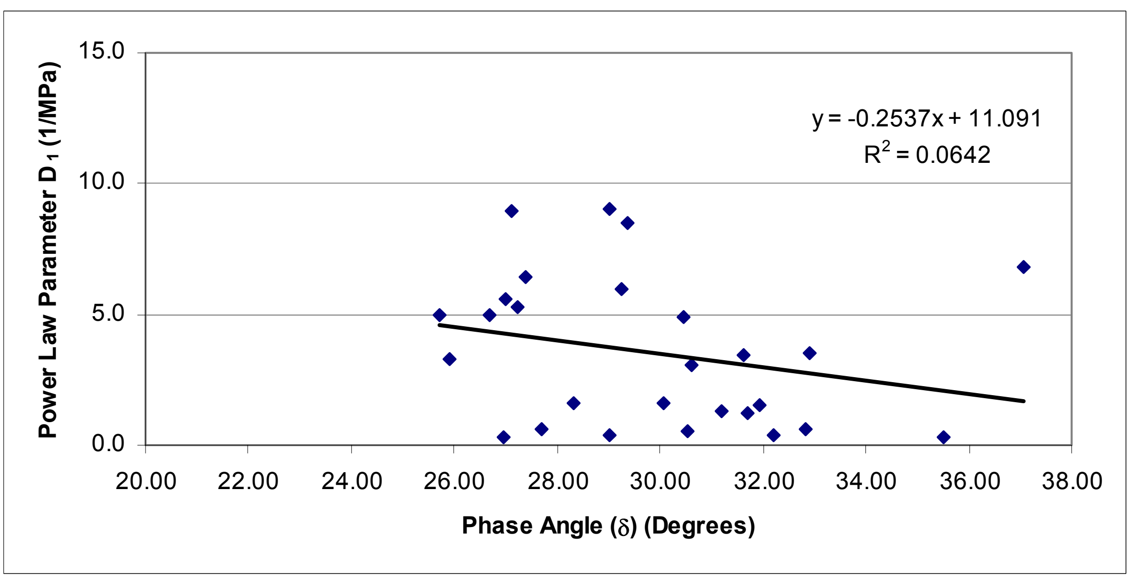

Figure 7-13. Relationship between phase angle at 1 Hz frequency and the power law creep compliance parameter D_1

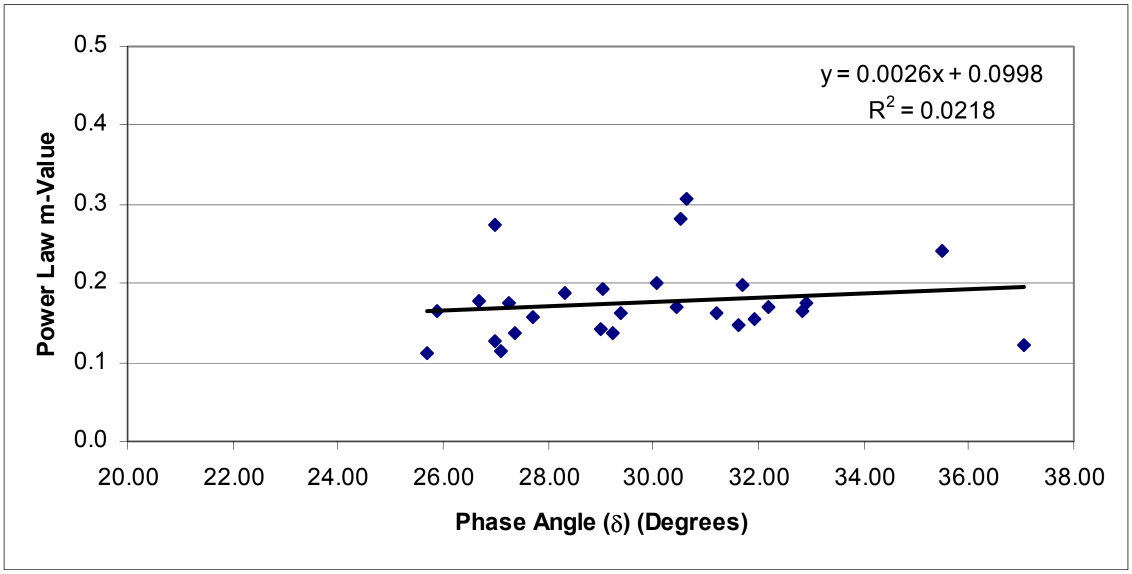

Figure 7-14. Relationship between phase angle at 1 Hz frequency and power law m-value parameter

In summary, the dynamic modulus exhibits a weak relationship with creep compliance. Unfortunately, the observed relationship is too weak for use in a predictive relationship. Similarly, no predictive relationship could be obtained from the phase angle.

7.6 Effects of Binder Type on Relationship Between Dynamic Modulus and Rutting Potential of Mixtures

Witczak et al. (2002) presented a comprehensive evaluation of any potential relationships between the dynamic modulus and the rutting performance of mixtures. The findings showed that for a given aggregate structure, but with different grades of unmodified binders, the dynamic modulus appears to relate reasonably well to the observed rutting performance of mixtures. This means that the dynamic modulus is sensitive to the binder viscosity of mixtures. Unfortunately, the work presented in this report as well as the results from the NCAT test track sections (Brown et al., 2004) show that when the aggregate structure is varied, no relationship can be found between the dynamic modulus and the rutting potential of mixtures.

7.7 Summary and Conclusions

In this chapter, the dynamic modulus and phase angle are compared against asphalt pavement analyzer (APA) rut depth results and static creep test results from unconfined axial compressive creep testing. The results showed that no predictive relationship could be identified between the dynamic modulus and phase angle on one hand and the APA rut depth on the other hand. Similarly as expected, a weak relationship was observed between the dynamic modulus and the creep compliance. Unfortunately, the quality of the regression relationship was marginal at best, precluding the development of a predictive relationship between the dynamic modulus and creep compliance. Importantly, the mixtures used in this study were of varying aggregate structure and aggregate types.

Previous work by Witczak et al. (2002) has shown that for a given aggregate structure, but with different grades of unmodified binders, the dynamic modulus appears to relate reasonably well to the observed rutting performance of mixtures. This means that the dynamic modulus is sensitive to the binder viscosity of mixtures. Unfortunately, the work presented in this report as well as the results from the NCAT test track sections (Brown et al., 2004) shows that when the aggregate structure is varied, no relationship can be found between the dynamic modulus and the rutting potential of mixtures.

The AASHTO 2002 Flexible Design Procedure uses the dynamic modulus as an input into the rutting prediction relationship used for thickness design. The relationship between dynamic modulus and the rutting resistance of the flexible pavement layer is based on traditional mechanistic-empirical pavement design considerations. The permanent deformation with the number of applied wheel loads is assumed to be inversely related to the dynamic modulus. For a given number of wheel loads, as the dynamic modulus increases, the predicted permanent strains in the pavement decrease.

Importantly, the mechanistic-empirical pavement rutting performance relationship used in the AASHTO 2002 design procedure does not account for the potential for instability rutting. Rather, the dynamic modulus in the AASHTO 2002 framework is simply used as a measurement of stiffness. The research presented in this study shows that the dynamic modulus does not relate to the mixture properties that might be controlling instability rutting, as experienced in the APA and the NCAT test track for the mixtures with observed rutting (Brown, 2004).

In summary, there appears to be no other off-the-shelf material property available right now to replace the use of the dynamic modulus as a measure of stiffness in the AASHTO 2002 Flexible Pavement Design Procedure. Based on the results from this research project and other similar efforts by NCAT (Brown, 2004), the dynamic modulus should be used with caution to predict the rutting performance of mixtures.

CHAPTER 8
EVALUATION OF GRADATION EFFECT

8.1 Introduction

The packing of particulate matter into a confined volume has long been of interest to mix designers. In the 1930's, Nijboer (1948) investigated the effects of particle size distribution using aggregate particles. He found that a gradation plotted on a log-log graph as a straight line with a slope of 0.45 produced the densest packing. Nijboer showed it to be the case for both crushed and uncrushed aggregates. In 1962, Goode and Lufsey published the results of studies they performed at the Bureau of Public Works. They performed an experiment to confirm Nijboer's findings and then investigated further to determine the packing of simulated gradations that might be actually used in road construction. As a result of their studies, they developed a specialized graph in which the vertical axis is the percent passing a sieve size and the horizontal axis is the sieve opening raised to the 0.45 power. To reduce confusion, the horizontal axis does not contain the actual calculated numbers, but instead has marks that indicate different size sieves. This specialized graph became known as the 0.45 power chart and continues to be used today. In 1992, Huber and Shuler investigated the size distribution of particles that gives the densest packing. They determined that a gradation drawn on a 0.45 power chart as a straight line from the origin to the aggregate nominal maximum size produced the densest packing. Several years later, Vavrik et al. (2001) presented the Bailey method of gradation analysis. The Bailey method takes into consideration the packing and aggregate interlock characteristics of individual aggregates and provides criteria that can be used to adjust the packing characteristics of a blend of materials.

Finally, Ruth et al. (2002) provided an experience-based methodology for the assessment of potential problems associated with aggregate gradation in the performance of asphalt pavements. The method presented introduced aggregate gradation factors based on power law regression slopes combined with either the percent passing the 4.75-mm or 2.36-mm sieves that were used to characterize ten different coarse- and fine-graded aggregate gradations. These gradation factors were used to develop relationships with surface area, tensile strength, fracture energy, and failure strain.

In the following, the gradation factors proposed by Ruth et al. (2002) will be obtained for 13 mixtures. These mixtures include the VMA mixtures described in Chapter 3 (F1, F2, F4, F5, F6, C1, C2, C3), as well as the Superpave Monitoring Project mixtures listed in Chapter 3 (P1, P2, P3, P5, P7). A relationship between the power law gradation factors and the dynamic modulus will be explored through a correlation study. Based on the findings from the correlation study, tentative gradation factor values for optimizing mixtures for high dynamic modulus values will be presented.

8.2 The Evaluation of the Effects of Aggregate Gradations on Dynamic Modulus

8.2.1 Description of Power Law Relationship

Following the procedure developed by Ruth et al. (2002), the first step in the evaluation of gradation effects was to fit a power law model to the gradation curve for each mixture. Power law constants (a_{ca}, a_{fa}) and exponents (n_{ca}, n_{fa}) for the coarse and fine aggregate portions of these mixtures were established by regression analyses. The format of the power law equations used in this investigation was:

$$P_{CA} = a_{CA} \cdot (d)^{n_{CA}} \qquad (8.1)$$

and

$$P_{FA} = a_{FA} \bullet (d)^{n_{FA}} \qquad (8.2)$$

where P_{CA} or P_{FA} = percent of material by weight passing a given sieve having opening of width d;

a_{CA} = constant (intercept) for the coarse aggregate;

a_{FA} = constant (intercept) for the fine aggregate;

d = sieve opening width, mm;

n_{CA} = slope (exponent) for the coarse aggregate; and

n_{FA} = slope (exponent) for the fine aggregate.

The method used for determining the "break" between coarse and fine aggregate is based on the Bailey method (Vavrik et al. 2001). The primary control sieve defining the break between fine and coarse aggregate in the mix is determined as follows to find the closest sieve size:

$$PCS = NMPS \times 0.22 \qquad (8.3)$$

where PCS = primary control sieve for the overall blend (i.e., division between coarse and fine aggregate); and

NMPS = nominal maximum particle size for the overall blend as defined in Superpave, which is one sieve larger than the first sieve that retains more than 10%.

The 0.22 value used in the equation was determined empirically, as discussed by Vavrik et al. (2002). For example, for a 12.5-mm nominal maximum size mix, the primary control sieve is 2.36 mm (NMPS × 0.22 = 2.750), whereas for a 19.0-mm nominal maximum size mix, the primary control sieve is 4.75 (NMPS × 0.22 = 4.180).

Table 8-1 presents the power law coefficients for the fine and the coarse aggregate portions of the mixtures studied. Generally, the R^2 values obtained indicate a fairly good power law fit to the existing gradation curves (R^2 greater than 0.88 for all cases). A preliminary observation of the results in Table 8-1 shows that:

$n_{fa} > n_{ca}$ for "Fine-Graded" mixtures, and

$n_{ca} > n_{fa}$ for "Coarse–Graded" mixtures.

Table 8-1. Power Regression Constants and Dynamic Modulus for All Mixtures

Mixture	Dynamic Modulus, |E*| at 1 Hz and 40°C	Coarse Aggregate Portion			Fine Aggregate Portion		
		a_{ca}	n_{ca}	R^2	a_{fa}	n_{fa}	R^2
F1	850	39.445	0.348	0.996	31.196	0.667	0.988
F2	1076	31.469	0.410	0.993	29.525	0.588	0.989
F4	1044	39.445	0.348	0.996	35.612	0.530	0.986
F5	727	37.017	0.366	0.972	28.719	0.612	0.978
F6	880	31.519	0.448	0.996	29.564	0.586	0.989
C1	526	17.948	0.734	0.887	19.852	0.534	0.988
C2	759	16.644	0.667	0.965	18.763	0.527	0.998
C3	801	20.964	0.644	0.883	22.984	0.498	0.998
P1	524	25.295	0.593	0.999	24.489	0.624	0.997
P2	607	13.074	0.834	0.989	19.921	0.509	0.975
P3	459	24.33	0.571	0.972	22.523	0.698	0.989
P5	638	23.739	0.625	0.992	26.238	0.591	0.963
P7	550	40.857	0.339	0.999	36.146	0.899	0.985

8.2.2 Correlation Study Between Power Law Gradation Factors and Dynamic Modulus

In order to identify a potential relationship between the power law gradation parameters in Table 8-1 and dynamic modulus, a zero-order correlation study was performed using the power law coefficients listed in Table 8-1 and the dynamic modulus at 40°C and 1 Hz frequency. The dynamic modulus at 40°C was selected in lieu of lower testing temperature results to better capture any potential relationship with the gradation characteristics of the mixtures tested. The term "zero-order" means that no controls are imposed on the correlation study.

Table 8-2 shows the results of the zero-order correlation study. Strong correlations exist between a_{ca} and n_{ca} (R = -0.98) and a_{fa} and n_{fa} (R = 0.543), respectively. Based on the strong correlation observed between the parameters studied, it was decided to focus the study on only two out of the four power law parameters, namely n_{ca} and n_{fa}. The results show a weak negative correlation between $n_{ca,}$ $n_{fa,}$ and $|E_{40}*|$. Further testing for statistical significance revealed no statistically significant correlations between $n_{ca,}$ $n_{fa,}$ and $|E_{40}*|$.

Table 8-2. Results of Correlation Study Between Power Law Parameters and Dynamic Modulus at 40°C and 1 Hz Frequency

	$\lvert E_{40}*\rvert$[1]	Power Law Regression Coefficients			
		a_{ca}	n_{ca}	a_{fa}	n_{fa}
$\lvert E_{40}*\rvert$[1]	1	0.414	-0.498	0.464	-0.348
a_{ca}	0.414	1	-0.98	0.948	0.578
n_{ca}	-0.498	-0.98	1	-0.908	-0.536
a_{fa}	0.464	0.948	-0.908	1	0.543
n_{fa}	-0.348	0.578	-0.536	0.543	1

[1]Denotes the dynamic modulus at 1 Hz frequency and 40°C.

In order to further evaluate the relationship between n_{ca}, n_{fa} and $|E_{40}*|$, a bivariate partial correlation study was performed. In here, a bivariate partial correlation denotes the correlation obtained between two variables, while controlling for a third variable. For example, $r_{12.3}$ denotes the correlation of variables 1 and 2, while controlling for variable 3. In most cases, a partial correlation of the general form $r_{12.3}$ will turn out to be smaller than the original correlation r_{12}. In the rare cases where it turns out to be larger, the third variable, 3, is considered to be a suppressor variable, based on the assumption that it is suppressing the larger correlation that would appear between 1 and 2 if the effects of variable 3 were held constant.

Table 8-3 presents the results of the bivariate partial correlation study, in which p denotes the level of significance of a potential correlation. Hence, $p < 0.01$ means that the probability of not having a significant relationship in the population is less than 1 percent. The results revealed a statistically significant negative correlation ($r = -.8654$, $\underline{p} = .0008$) between n_{ca} and $|E_{40}^*|$, when controlling for n_{fa}, implying that a high n_{ca} results in a low $|E_{40}^*|$.

Table 8-3. Partial Correlation Analysis for n_{ca} and $|E_{40}^*|$ When Controlling for n_{fa}

	n_{ca}	
	N	r (Correlation coefficient)
$\|E_{40}^*\|$	13	-.8654**

* $\underline{p} < .05$; ** $\underline{p} < .01$

8.2.3 Category Analysis of Power Law Parameters

In order to further evaluate the relationship between power law parameters (n_{ca} and n_{fa}) and the dynamic modulus, four simplified categories of power law parameters were hypothesized. The four hypothesized categories to be tested are as follows:

1. Category 1 – [Low n_{ca} (smaller than .50) and Low n_{fa} (smaller than .59)]
2. Category 2 – [Low n_{ca} (smaller than .50) and High n_{fa} (greater than .59)]
3. Category 3 – [High n_{ca} (greater than .50) and Low n_{fa} (smaller than .59)]
4. Category 4 – [High n_{ca} (greater than .50) and High n_{fa} (greater than .59)].

Table 8-4 shows the mean and standard deviation of $|E_{40}^*|$ for the four different categories studied. Since the underlying power law parameters n_{fa} and n_{ca} are slightly correlated, a discriminant category analysis is not appropriate. Rather, a one-way analysis of variance (ANOVA) is used to uncover the effects of the categorical variables (i.e., four different categories) on the interval dependent variable (i.e., $|E_{40}^*|$). According to Table 8-5, the results are statistically significant at an alpha level of 0.01 ($F(3,9) = 7.64$, $p = 0.008$). Since the results showed a significant omnibus F, a post-hoc analysis using a Tukey test was performed to evaluate whether differences between any two pairs of category means were significant.

Table 8-4. Mean and Standard Deviation of $|E_{40}^*|$ for the Four Different Categories

Category Groups	N	Mean	Std. Deviation
Low n_{ca} + Low n_{fa}	3	1000.00	105.14
Low n_{ca} + High n_{fa}	3	709.00	150.80
High n_{ca} + Low n_{fa}	4	673.25	128.76
High n_{ca} + High n_{fa}	3	540.33	90.61
Total	13	726.23	198.83

Table 8-5. One-way Analysis of Variance (ANOVA) of $|E_{40}^*|$ (Total N = 13)

	Sum of Squares	df	Mean Square		Sig.
Between Groups	340640.89	3	113546.96	7.64	0.008
	133763.41	9	14862.60		
Total	474404.30	12			

Table 8-6 displays the means for groups in homogeneous subsets. According to Table 8-6, only the dynamic modulus values for the first category (combination of Low n_{ca} and Low n_{fa}) are significantly different from the other category groups at an alpha level = .05. This means that if n_{ca} is less than 0.5 and n_{fa} is less than 0.59, a “high” dynamic modulus will likely be obtained for a given aggregate type and asphalt grade.

Table 8-6. Post-Hoc Analysis for Homogeneous Subsets of Hypothesized Categories

Group	N	Subset for alpha = .05	
		Statistically Significant	Not Statistically Significant
Low n_{ca} + Low n_{fa}	3	1000.00	–
Low n_{ca} + High n_{fa}	3	–	709.00
High n_{ca} + Low n_{fa}	4	–	673.25
High n_{ca} + High n_{fa}	3	–	540.33

8.2.4 Category Analysis of Power Law Parameters: Coarse- and Fine-Graded Mixtures Separated

The mixtures in Table 8-1 were divided into two subsets, depending on whether the mixtures were coarse-graded or fine-graded, according to the Superpave mixture design system. A mixture is considered to be coarse-graded if the gradation band passes below the restricted zone. Conversely, a gradation band for a fine-graded mixture passes above the restricted zone. Hence, the two different graded subsets to be tested are as follows:

1. Coarse-Graded Mixtures, and
2. Fine-Graded Mixtures.

Tables 8-7 and 8-8 list the coarse- and fine-graded mixtures and their categories, respectively.

Table 8-7. Mixtures in Coarse-Graded Category

Mixture	Dynamic Modulus, |E*| at 1 Hz and 40°C	Classification Category	Aggregate Portion	
			Coarse	Fine
			n_{ca}	n_{fa}
C1	526	Category 3	0.734	0.534
C2	759	Category 3	0.667	0.527
C3	801	Category 3	0.644	0.498
P1	524	Category 4	0.593	0.624
P2	607	Category 3	0.834	0.509
P3	459	Category 4	0.571	0.698
P5	638	Category 4	0.625	0.591

Table 8-8. Mixtures in Fine-Graded Category

Mixture	Dynamic Modulus, $\lvert E^* \rvert$ at 1 Hz and 40°C	Classification Category	Aggregate Portion	
			Coarse (n_{ca})	Fine (n_{fa})
F1	850	Category 2	0.348	0.667
F2	1076	Category 1	0.410	0.588
F4	1044	Category 1	0.348	0.530
F5	727	Category 2	0.366	0.612
F6	880	Category 1	0.448	0.586
P7	550	Category 2	0.339	0.899

Table 8-9 shows the correlation analysis results for the coarse-graded mixtures. Due to the few data points available (N = 6), a zero-order bivariate correlation study found no statistically significant relationship between $n_{ca,}$ $n_{fa,}$ and $\lvert E_{40}^* \rvert$. However, the results show that a strong negative correlation exists between n_{fa} and $\lvert E_{40}^* \rvert$.

Table 8-9. Zero-Order Correlation Analysis for $n_{ca,}$ $n_{fa,}$ and $\lvert E_{40}^* \rvert$ for Coarse-Graded Mixtures

	n_{ca}	n_{fa}	$\lvert E_{40}^* \rvert$
n_{ca}	1	-.7120	-.1350
n_{fa}	–	1	-.7280
$\lvert E_{40}^* \rvert$	–	–	1

* $p < .05$, ** $p < .01$

Table 8-10 shows the correlation results for fine-graded mixtures. The zero-order bivariate correlation study found a statistically significant relationship between n_{fa} and $\lvert E_{40}^* \rvert$. In addition, considering the small sample size (N = 6), Table 8-10 also shows that a strong negative relationship appears between n_{fa} and $\lvert E_{40}^* \rvert$.

Table 8-10. Zero-Order Correlation Analysis for n_{ca}, n_{fa}, and $|E_{40}^*|$ for Fine-Graded (N = 7) Mixtures

	n_{ca}	n_{fa}	$\|E_{40}^*\|$
n_{ca}	1	-.4472	-.3928
n_{fa}	–	1	-.8447*
$\|E_{40}^*\|$	–	–	1

* $p < .05$, ** $p < .01$

8.3 Summary and Conclusions

The results of the combined analysis of coarse-and fine graded mixtures together showed a low n_{fa} combined with a low n_{ca} results in a "high" dynamic modulus value. Importantly, the n_{fa} variable was identified as a suppressor variable on n_{ca}, meaning that a low n_{ca} by itself was not sufficient in guaranteeing a high dynamic modulus value.

The results of the separate analyses on coarse- and fine-graded mixtures showed that a negative correlation was observed between n_{fa} and the dynamic modulus at 40°C. Again, this means that the lower the n_{fa} value, the higher the dynamic modulus. Since n_{fa} is a measure of the rate of change in the gradation band on the fine side of the gradation, the results indicate that a gradual or a slow rate of change of the gradation band on the fine side results in a higher dynamic modulus value.

Observation of the coarse-graded mixtures in Table 8-7 shows that all the coarse-graded mixtures are either in category 3 (high n_{ca} and low n_{fa}) or in category 4 (high n_{ca} and high n_{fa}). The overall high n_{ca} values are likely due to the nature of coarse-graded Superpave mixtures, where the gradation band starts above the maximum density line, but has to cross the maximum density line in order to pass below the restricted zone. Hence, for coarse-graded mixtures the rate of change in the slope of the gradation band on the coarse side is fairly high, translating into a relatively high n_{ca} value.

Similarly, most of the fine-graded mixtures in Table 8-8 are in category 1 (low n_{ca} and low n_{fa}) or category 2 (low n_{ca} and high n_{fa}), with one mixture (Superpave Project P1 mix) in category 4 (high n_{ca} and high n_{fa}). Hence, since their gradation bands do not typically cross the maximum density line, the rate of change in the slope of the gradation bands for fine-graded mixtures on the fine and coarse sides tends to be lower than for the coarse-graded mixtures.

In summary, a relationship between a low n_{fa} and a high dynamic modulus (at 40°C) has been identified. This means that a slow rate of change in the gradation band on the fine side of the gradation is related to a high dynamic modulus value. Gap-grading the mixture on the fine side will generally increase the rate of change in the gradation band, and thus n_{fa}, and will lead to a lower dynamic modulus.

CHAPTER 9
TORSIONAL SHEAR COMPLEX MODULUS TEST

9.1 Background

The torsional shear modulus may be a useful parameter in characterizing the shear behavior of HMA mixtures. A study of simple shear test (SST) conducted by Harvey et al., (2001) suggests that a laboratory test which measures primarily shear deformation would be the most effective way to define the propensity of rutting for a mixture.

In the linear viscoelastic range (75 to 200 μstrains), the dynamic modulus of asphalt mixtures can be investigated by either an axial or torsional complex modulus test. The axial complex modulus test can provide the dynamic Young's modulus |E*| and phase angle (δ). The torsional complex modulus test can provide the dynamic shear modulus |G*| and the phase angle (δ). Previous work by Papazian (1962) has shown that the Poisson's ratio is dependent upon frequency. The complex shear modulus G* can be used in combination with E* to obtain the complex Poisson's ratio, νυ*. However, Harvey et al. (2001) concluded that G* can be related to E* using:

$$G^* = \frac{E^*}{2(1+\upsilon)} \qquad (9.1)$$

in which the Poisson's ratio can be taken as a constant.

With complex modulus |E*| now formally integrated into the *2002 AASHTO Pavement Design Guide*, there is also a need for simpler measurement of the complex modulus of a mixture. The complex shear modulus obtained from the torsional shear test has the potential to be a simple alternative to the more involved confined axial complex modulus test.

This chapter focuses on:

- The development of the testing and interpretation methodology needed to obtain the complex shear modulus from a torsional shear test.
- A comparison of the torsional shear test to the hollow cylinder torsional shear test to obtain an estimate of the error associated with the testing of solid cylinders.
- A comparison of the torsional shear complex modulus to the axial complex modulus from a triaxial test to obtain the complex Poisson's ratio.

9.2 Development of Analysis Method for Torsional Complex Modulus

The basic principle behind the torsional complex modulus test is to apply a cyclic torsional force to the top of the specimen, and measure the torsional displacement on the outside diameter, as shown in Figure 9-1. Knowing the torsional stress and strain, the shear modulus is then calculated based on the theory of elasticity. The torsional force is generated by a piston that can move laterally. The specimen is glued to the platens at the top and bottom ends. The bottom is rigidly fixed and the top is connected to a torsional load actuator. The frequencies used in the test are the same as those used in the axial complex modulus test.

The dynamic shear modulus is calculated from the following relationship:

$$G^* = \frac{\tau}{\gamma} \tag{9.2}$$

which assumes that pure torque, T, is applied to the top of a hot mix asphalt (HMA) specimen, so that the shearing stress varies linearly across the radius of the specimen. The average torsional shear stress, on a cross section of a specimen τ_{avg} is defined as:

$$\tau_{avg} = S/A \tag{9.3}$$

in which S is the total magnitude of shearing force and A is the net area of the cross section

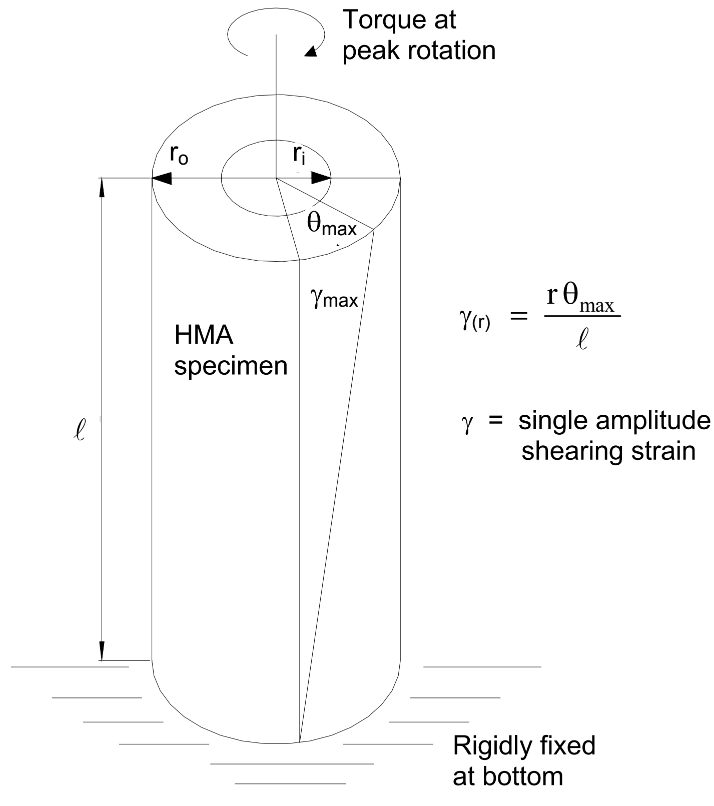

Figure 9-1. Torsional shear test for a hot mix asphalt specimen

of the specimen, i.e., $A = \pi(r_o^2 - r_i^2)$, where r_o and r_i are the outside and inside radius of a hollow specimen, respectively. For a solid specimen, $r_i = 0$. The shear force S can be calculated as:

$$S = \int_{r_i}^{r_o} \tau_r \, (2\pi r)\, dr \tag{9.4}$$

where τ_r is the shear stress at the distance r from the axis of the specimen, i.e., $\tau_r = \tau_m r/r_o$, where τ_m is the maximum shearing stress at r = 0. On the other hand, the torque, T, can be calculated from:

$$T = \int_{r_i}^{r_o} \tau_r (2\pi r)\, r dr = \frac{\tau_m}{r} J \tag{9.5}$$

where J is the area polar of inertia, $J = \pi (r_o^4 - r_i^4)/2$. From Eq. 9.5, τ_m can be expressed as:

$$\tau_m = \frac{T r_o}{J} \tag{9.6}$$

From Eqs. 9.3, 9.4, and 9.6, the equation for τ_{avg} can be written as:

$$\tau_{avg} = \frac{2}{3} \frac{r_o^3 - r_i^3}{r_o^2 - r_i^2} \frac{T}{J} \tag{9.7a}$$

or, alternatively:

$$\tau_{avg} = r_{eq} \frac{T}{J} \tag{9.7b}$$

in which r_{eq} is defined as the equivalent radius. It can be seen from Eq. 9.7a that r_{eq} = $2/3 r_o$ for a solid specimen, and $r_{eq} = 2/3 \left(r_o^3 - r_i^3 / r_o^2 - r_i^2\right)$ for a hollow specimen. In practice, r_{eq} is defined as the average of the inside and outside radii. Shear strain is calculated as follows:

$$\gamma = \frac{r_{eq}\,\theta}{\ell} \tag{9.8}$$

where ℓ is the length of specimen, and θ is the angle of twist. The angle of twist, θ, can be measured either using an LVDT or a proximitor sensor at the top of the sample.

In order to maintain the linear relationship between shear stress and shear strain, the shear strain should be below a certain range. From the study on axial complex modulus testing, shear strains smaller than 200 microstrain were found reasonable.

Complicating the analysis of solid specimens in torsion is the fact that the shear stress is not uniform across the specimen. An obvious way to minimize the shear stress non-uniformity across the test specimen is to make the specimen hollow, and thus reduce the wall thickness. However, for complex modulus testing, the use of hollow specimens over solid specimens or torsional complex modulus testing provides no advantage. This is because complex modulus testing occurs solely in the linear range across the specimen, regardless if the specimen is hollow or solid. The equations presented above ensure this is true as long as testing is at low strain levels across the specimen. The fact that there is more stress uniformity in a hollow specimen only means that the same material tested as a hollow specimen needs less torque to achieve the same average strain and shear stress across it. Figure 9-2 depicts the decrease in torque needed to maintain the same strain level between a hollow and solid specimen. If testing were to result in large strains (non-linear range), large creep strains, or if failure were to occur, the equations would no longer be valid, and solid and hollow specimen testing could not be equated.

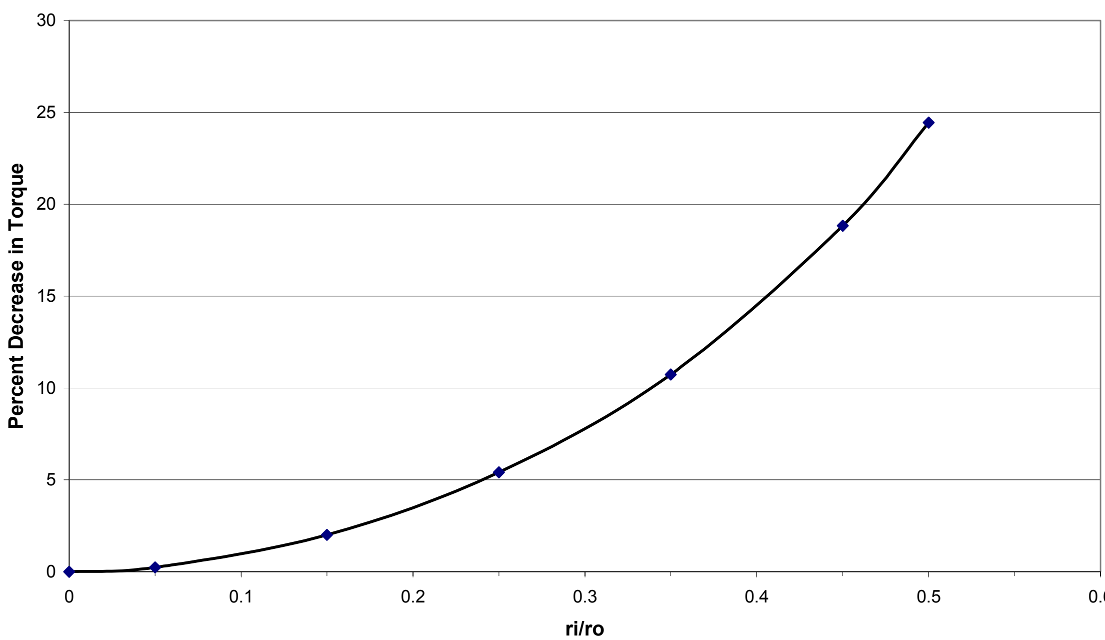

Figure 9-2. Difference in torque between hollow and solid specimens to achieve the same average strain

9.3 Testing Environment

All data acquisition and test control protocols that were used for the axial complex modulus were also used for the torsional complex modulus test, except for the loading frame used and the sample preparation. The torsional shear test was conducted on a Geotechnical Consulting and Testing Services (GCTS) load frame, rather than the MTS load frame, described previously. The GCTS hydraulic system has the capacity of applying both vertical and torsional load. The vertical load capacity is 100 kN (22 kip) and the torsional load capacity is ±225 N-m (2000 in-lbf).

In the torsional complex modulus test, the specimen is prepared in exactly the same fashion as for the axial complex modulus test. However, due to the torsional load applied to the specimen during testing, it is necessary to glue the specimen to the end platens. The end platens used also have a textured surface, for better grip, as shown in Figure 9-3.

Figure 9-3. Texture end plate for torsional shear test

The glue used in the test was an epoxy glue, which required 8 hours for the development of full strength. A few different epoxy glue types were tried, with no noticeable change in the measured complex modulus.

9.3.1 Closed-loop Servo-control Testing Issues

A closed-loop servo-controller works by transmitting a command signal to the hydraulic servo valve, and subsequently collecting a feed back signal to determine how the command was realized. In theory, the feed back signal is supposed to coincide with the control command. For low frequency testing (4 Hz, 1 Hz or lower), this can be achieved easily. But for higher frequencies, i.e., 10 Hz, 16 Hz, the feed back signal may be either higher or lower than the command signal, which means the actual applied load is higher or lower than specified. In addition, the feed back signal is subject to noise as compared to the specified command signal. A key testing variable that needs to be accounted for includes the effect of the sample stiffness on the system stiffness. The stiffness of the specimen is both frequency and temperature dependent. Thus, the stiffness of the system can change during the testing of a single specimen that is tested at varying temperatures and frequencies. This means that when performing testing at a high frequency, a shaking of the system may be observed occasionally. This may cause both a distortion and noise in the feed back load signal and the LVDT deformation measurements.

The system response can be adjusted by modifying the gain in the control program. It is worthwhile to know that there are four gain options provided to adjust a feed back signal to match the command signal, namely proportional gain (P gain), integral gain (I gain), derivative gain (D gain) and feed forward gain (F gain):

- The “P gain” increases system response.

- The “I gain” increases system accuracy during static or low-frequency operations and maintains the mean level at high frequency operation.
- The “D gain” improves the dynamic stability when high proportional gain is applied.
- The “F gain” increases system accuracy during high-frequency operations.

The “P gain” is used most of the time to adjust for the effects on the system stiffness on varying specimen stiffness. It introduces a control factor that is proportional to the error between the command and the feedback signal. As proportional gain increases, the error decreases and the feedback signal tracks the command signal more closely. Higher gain setting increase the speed of the system response, but too much proportional gain can cause the system to become unstable. Too little proportional gain can cause the system to become sluggish. Figure 9-4 illustrates the effects of various possible “P gain” settings.

The P gain setting for different control modes may vary greatly. For example, the gain for force may be as low as one, while the gain for strain may be as high as 10000. A useful “rule of thumb” is to adjust the gain as high as possible, without making the system unstable.

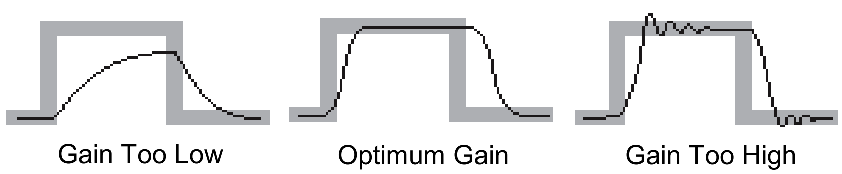

Figure 9-4. Effect of using P gain

Due to the torsional testing mode, using appropriate P gains at each frequency and temperature was found to be important. This may also be partly due to the relatively light weight of the GCTS testing frame, which makes it more susceptible to vibration problems during testing. Secondly, because the specimen is glued to the bottom and top end platens, which are rigidly fixed to the triaxial chamber and torsional head, the effects of the specimen stiffness on the system stability may be more pronounced. The optimal ranges for the P gain are listed in Table 9-1.

Table 9-1. Suggested Values for Proportional (P) Gain Settings for the GCTS Testing System

Frequency	Test Temperature		
	10° C	25° C	40° C
1 Hz	0.6	0.5	0.3 – 0.5
4 Hz	0.6	0.5	0.3 – 0.5
10 Hz	0.45 – 0. 55	0.4	0.2 – 0.3
16 Hz	0.65 – 0.75	0.5	0.2 – 0.5

9.4 Test Setup for the Torsional Complex Modulus Test

The sample specimen was glued to a fixed base platen and a top stainless steel platen in the triaxial cell. The displacement on top of the sample was determined by measuring the torsional movement between a small arm rigidly connected to the top platen and two LVDTs attached to the support struts of the cell. The sample was protected from water by a thin membrane of the same type used for the axial complex modulus test. The test set up used is shown in Figure 9-5.

The overall testing protocol was kept exactly the same as for the axial complex modulus test, discussed previously. The testing frequencies were 16 Hz, 10 Hz, 4 Hz and 1 Hz. The test was carried out at 10° C, room temperature (25° C), and 40° C.

The procedure of the test is described in chronicle order as below:

- Apply the axial seating load, and the torsional seating load, not to exceed 5 percent of the applied cyclic load amplitude.
- Start applying the cyclic torsional load. The magnitude of the load was selected in order to obtain cyclic resilient strain amplitudes in range of 75 to 200 microstrain.

The torsional force may vary depend on the stiffness of the mixture, as well as testing frequency and temperature. For Florida mixtures, it is suggested that the first trial for torsional load amplitude be: 12000N-mm, 20000N-mm and 30000N-mm for 40° C, 25° C and 10° C, respectively.

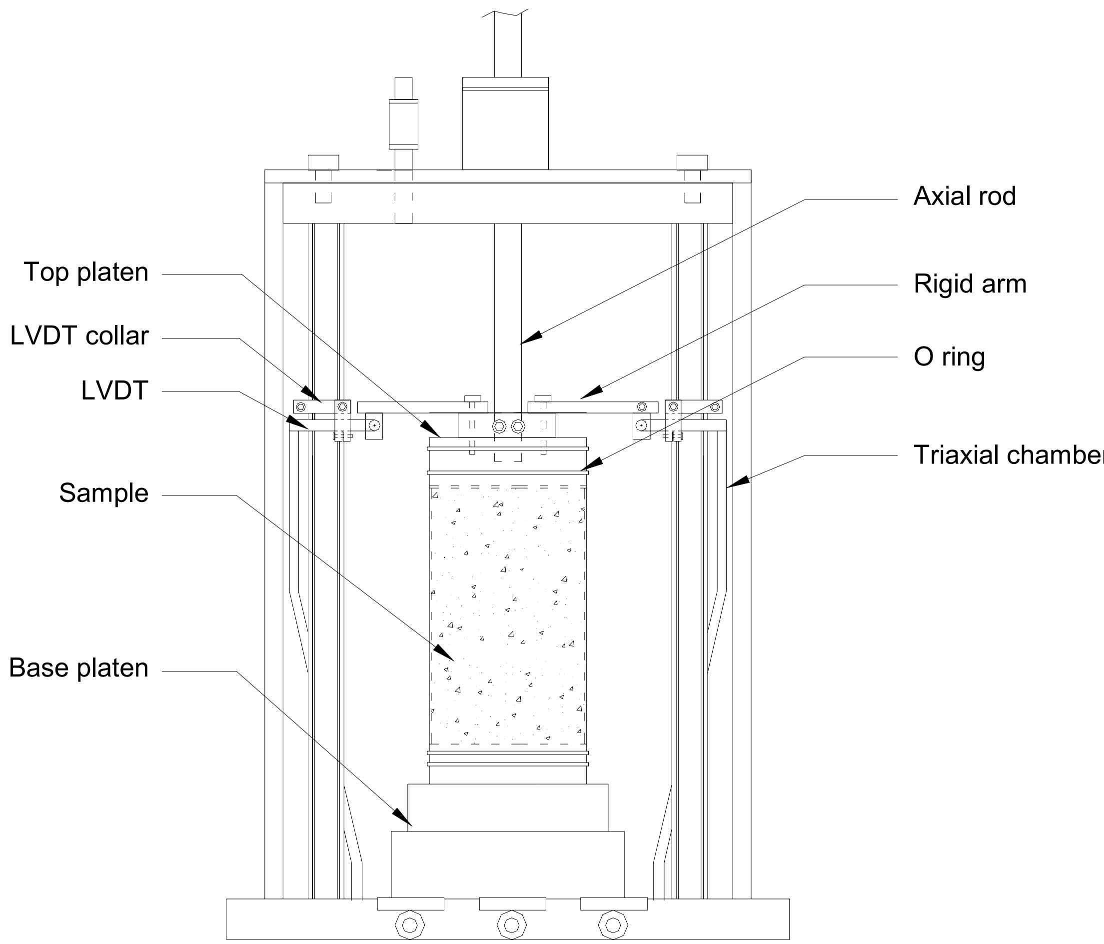

Figure 9-5. Torsional shear testing set up

Figure 9-6 shows a photograph of the GCTS torsional shear testing system used for the torsional complex modulus testing.

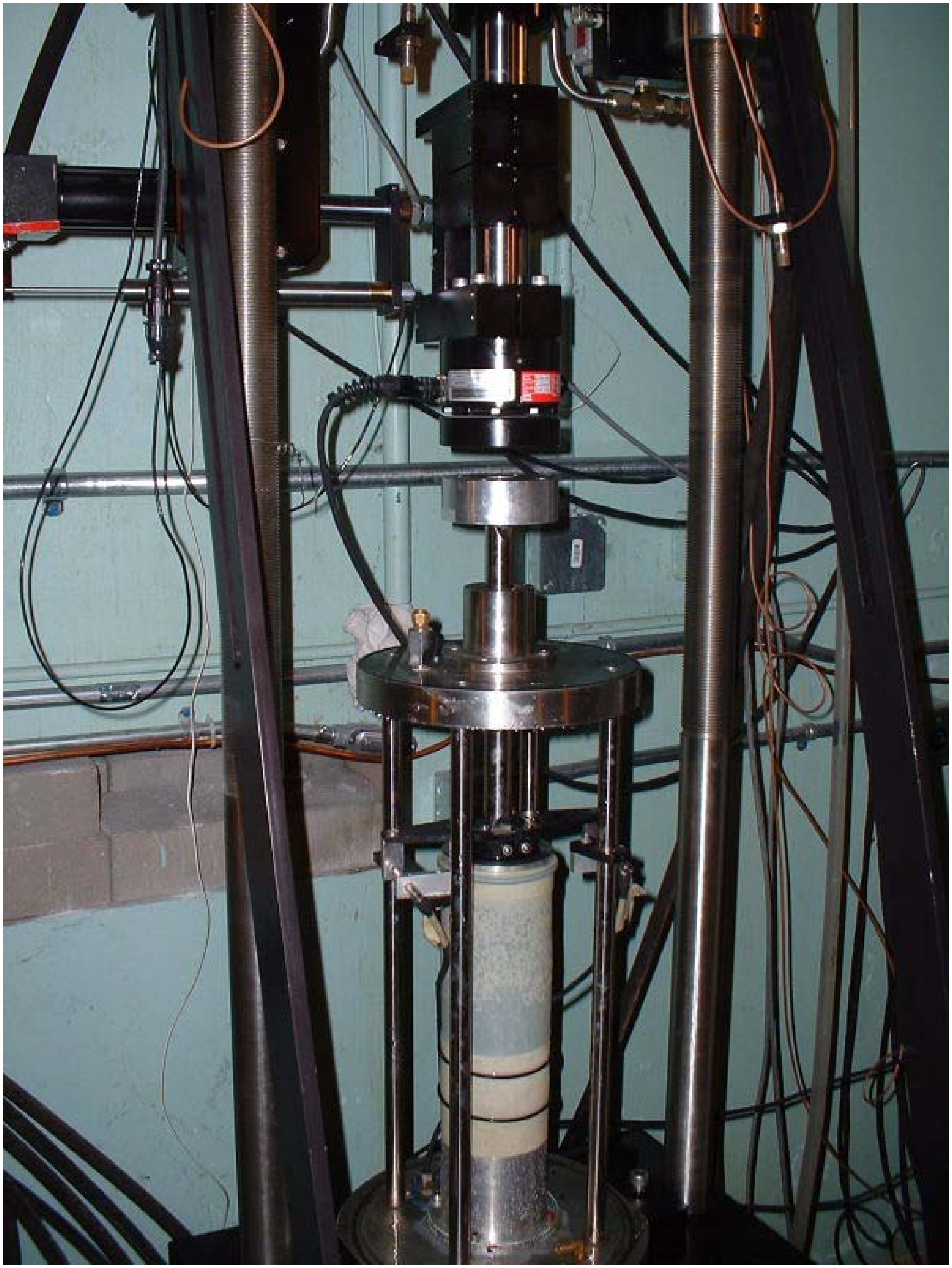

Figure 9-6. Photograph of torsional shear testing set up

9.5 Computer Program for Calculating Complex Shear Modulus

As discussed previously, the analysis program for the axial complex modulus test was written in Visual Basic within Excel. The modified version for calculating the torsional shear modulus follows the same approach, with the only change being in the calculation of torsional shear stress and shear strains.

The shear stress is determined as follows:

$$\text{Shear stress} = \frac{\text{Torque} \times r_0}{J} \tag{9.9}$$

and the corresponding shear strain is:

$$\text{Shear strain} = \frac{\text{Torsional displacement} \times r_0}{\ell \times L} \tag{9.10}$$

where r_0 is the radius of sample, r_0 = 50 mm;

J is the area polar of inertia, $J = \pi * r_o^4 / 2$;

ℓ is the length from center of sample to the LVDT measurement point, ℓ = 107.7 mm;

L is the height of sample, L = 150 mm.

The input data file was recorded in the same standard order as for the axial complex modulus program. At first, the load and deformation data columns are converted to stress and strain data columns. The program automatically determines the duration of the test and the number of calculation windows required. This means that the program has provides the option of calculating the complex shear modulus and the phase angle in user specified windows from the beginning to the end of each test. The number of cycles in each analysis window was set to 10 cycles for the complex torsional shear modulus interpretation.

Besides the dynamic shear modulus and phase angle, the analysis program was also designed to report the best-fit equation for stress and strain, as well as the corresponding coefficient of determination, R^2. Figure 9-7 shows the data input page for the torsional shear program. The columns for the test time, stress, and strain are predetermined, along with the start and stop times of the test. Since each raw data file includes a header, the first row of data is noted. The only user-defined inputs are the degree of polynomial used in the regression analysis and the test frequency.

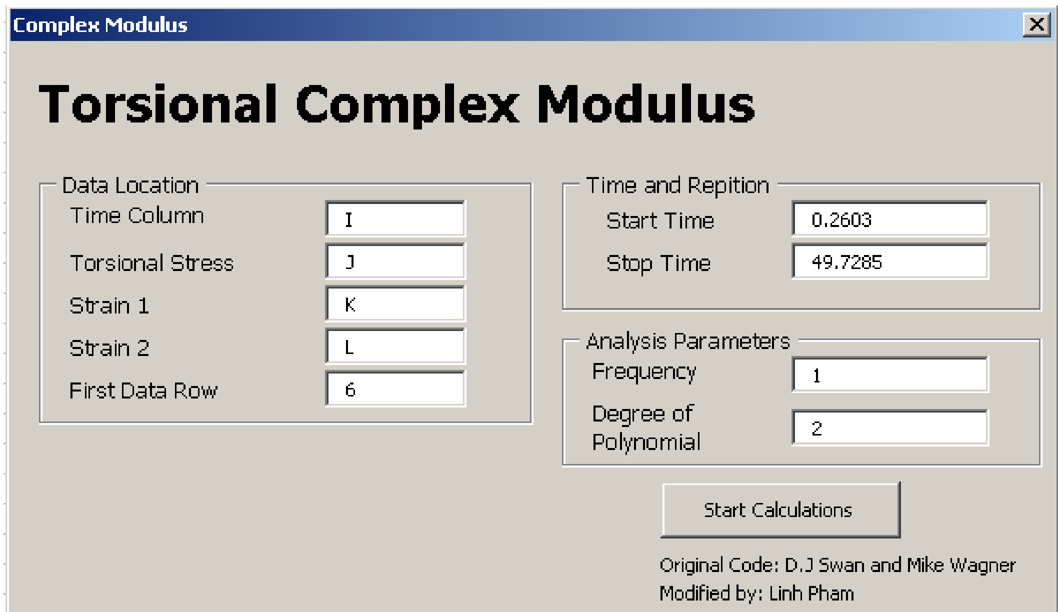

Figure 9-7. Torsional shear modulus program

Figure 9-8 shows a typical output file for the torsional shear modulus data reduction program. The output contains all the information necessary, such as shear stress, shear strain amplitude, and phase angle. The default format only presents the best-fit regression equations for the last 10 cycles.

Complex Shear Modulus Test Results

Sample:		**Shear Stress Ampli$\tau_u$de (t0)**	0.10169
Test Frequency:	10	**Shear Strain Ampli$\tau_u$de (d0)**	0.00012
Number of Cycles:	100	**Dynamic Shear Modulus (|G*|) (MPa)**	883.945
Calculation Date:	March 31, 2003	**Phase Angle (d) (Degrees)**	47.211
		Elastic Shear Modulus (G') (MPa)	600.459
		Loss Shear Modulus (G") (MPa)	648.697

Signal Equations:

$\sigma_0(t) = 7.481E-02 - 5.718E-03*t^1 + 2.930E-04*t^2 + 5.084E-02*Cos(10*t*360° - -175.64°)$ $[R^2=0.994]$

LVDT 1: $\varepsilon_0(t) = 7.091E-04 + 1.387E-04*t^1 - 2.213E-06*t^2 + 5.711E-05*Cos(10*t*360° - -128.08°)$ $[R^2=0.997]$

LVDT 2: $\varepsilon_0(t) = 6.881E-04 + 1.271E-04*t^1 - 1.877E-06*t^2 + 5.792E-05*Cos(10*t*360° - -128.78°)$ $[R^2=0.998]$

Dynamic Shear Modulus Chart

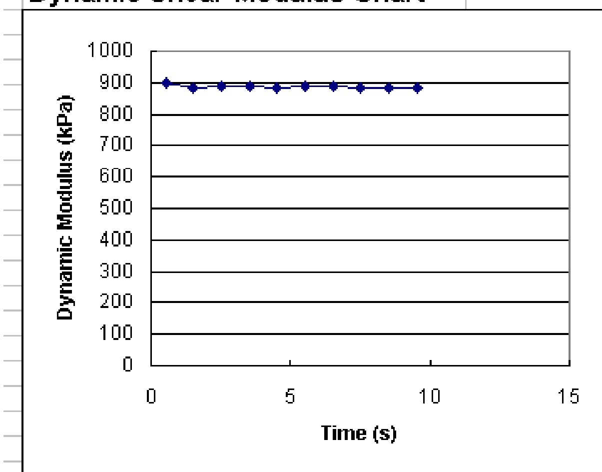

Phase Angle Chart

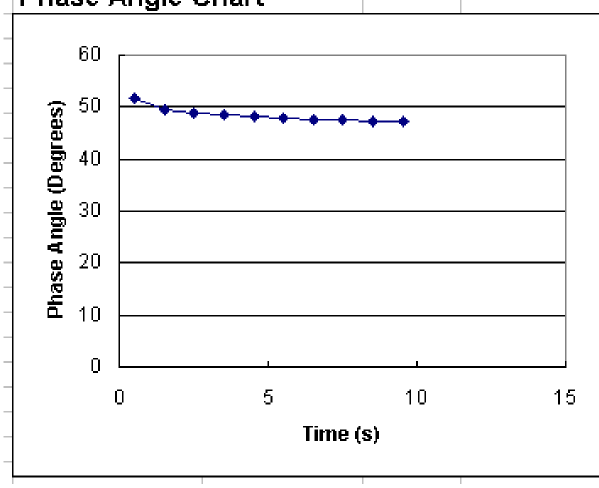

Figure 9-8. Output page of complex shear modulus program

9.6 Results from Shear Complex Modulus Testing

In order to investigate the relationship between the torsional shear complex modulus test and the axial complex modulus test, the torsional shear complex modulus test was performed under the same temperature and frequency conditions as used for the axial testing, previously discussed in Chapter 6. The mixtures studied included: GA-C1, GA-C2, GA-C3, GA-F1, GA-F2, and GA-F3. The specimens listed in Table 6.1 for axial testing were subsequently used for the torsional shear testing. The test temperatures were 10° C, 25° C, and 40° C, and the order of testing was from a lower test temperature to a higher test temperature. At each test temperature, each specimen was tested at the following four frequencies: 16 Hz, 10 Hz, 4 Hz and 1 Hz.

It was noted that at 10° C, because of control problems associated with the torsional shear closed-loop servo-hydraulic testing system discussed previously, the applied force for 16 Hz test was much higher than the specified command force. These results were therefore not reported. Thus, for the 10° C testing temperature, the results are only reported for 1 Hz, 4 Hz and 10 Hz tests.

9.7 Complex Shear Modulus Test Results

9.7.1 Test Data

One analysis file was obtained for each load frequency and testing temperature. In this analysis file, the dynamic shear modulus in GPa and the phase angle in degrees were obtained for the given test temperature and frequency. There were three replicate specimens tested for each asphalt mixture. After all the dynamic shear modulus and phase angle values were calculated for each specimen under the same test conditions, the average value for both of these parameters was calculated. Tables 9-2 and 9-3 list the average values of dynamic shear modulus and phase angle for the three specimens for each asphalt mixture.

Table 9-2. Average Dynamic Shear Modulus (|G*|) Testing Results (in MPa)

Mixture	Temperature (° C)	Frequency			
		1 Hz	4 Hz	10 Hz	16 Hz
Georgia Granite Mixtures					
GAC1	10	1308.56	1814.28	2090.14	
	25	440.92	711.21	901.42	953.94
	40	156.08	234.28	296.67	315.40
GAC2	10	2245.361	2846.74	3020.726	3223.7
	25	683.3389	1079.207	1341.745	1366.187
	40	188.4197	330.7724	456.6326	479.4994
GAC3	10	2238.739	2902.047	3172.981	
	25	721.1127	1116.788	1387.407	1406.922
	40	234.623	371.8126	483.7309	495.3849
GAF1	10	2045.95	2649.30	2904.12	
	25	541.30	863.11	1095.80	1130.92
	40	207.04	339.75	433.40	440.7339
GAF2	10	2795.103	3384.34	3606.631	
	25	1002.046	1469.33	1690.811	1764.619
	40	295.0541	466.6922	589.4631	636.1276
GAF3	10	2340.951	3032.854	3269.732	
	25	736.9684	1151.382	1388.299	1410.627
	40	213.7811	354.582	455.6341	475.8043

Table 9-3. Average Phase Angle (δ) Testing Results (in degrees)

Mixture	Temperature (° C)	Frequency			
		1 Hz	4 Hz	10 Hz	16 Hz
Georgia Granite Mixtures					
GAC1	10	34.15	31.02	33.37	
	25	44.44	44.47	44.54	46.19
	40	47.70	50.03	48.31	53.11
GAC2	10	38.22572	37.82	41.70033	46.70682
	25	44.77739	44.37781	44.07127	44.52188
	40	50.14491	52.89108	53.20399	59.64771
GAC3	10	40.48389	39.66756	41.82911	
	25	45.97733	45.56398	45.10795	46.82108
	40	46.8103	50.57471	53.35022	59.59761
GAF1	10	38.18	37.13	39.37	
	25	45.78	45.33	45.49	46.27
	40	45.88	48.47	52.01	58.67768
GAF2	10	43.91086	46.86466	50.68351	
	25	44.24114	43.28644	42.3709	43.96889
	40	45.97328	48.68716	50.18734	54.26639
GAF3	10	40.44169	40.63288	45.66202	
	25	46.07858	45.95873	46.44175	48.36404
	40	50.89461	53.59587	54.15951	59.69552

Figures 9-9 through 9-11 present the results of the dynamic shear modulus measurements for the GAF1 mixture, which was found to be representative for fine-graded mixtures. Similarly, Figures 9-12 through 9-14 show the results for the dynamic shear modulus for the GAC1 mixture, which was also representative for the coarse-graded mixtures.

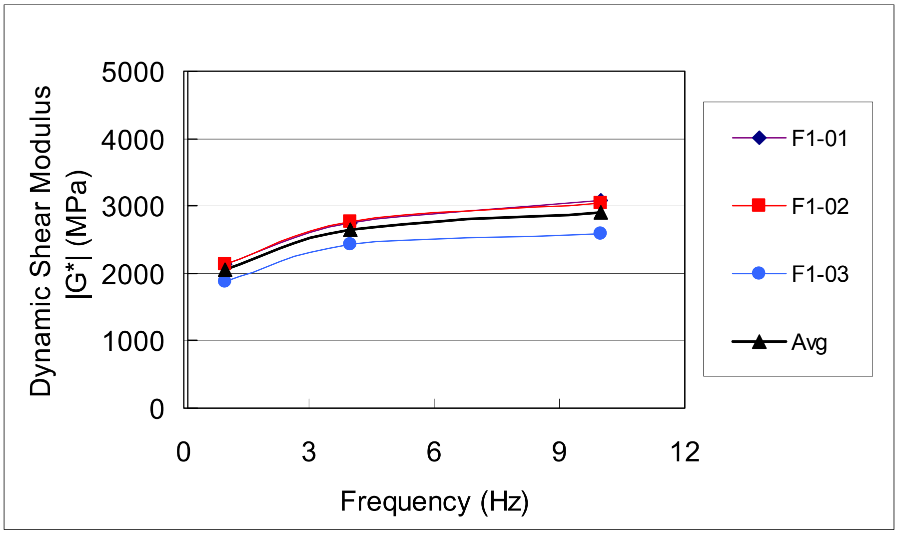

Figure 9-9. Dynamic shear modulus |G*| of GAF1 at 10° C

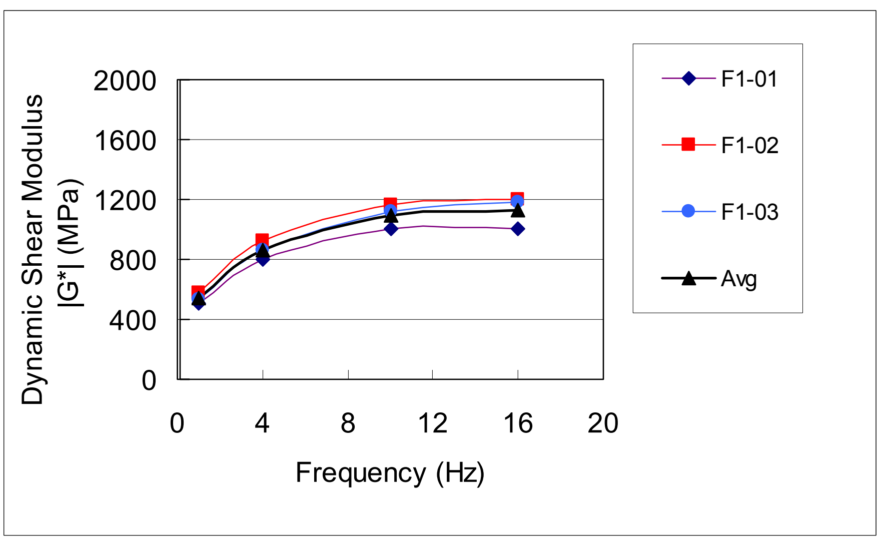

Figure 9-10. Dynamic shear modulus |G*| of GAF1 at 25° C

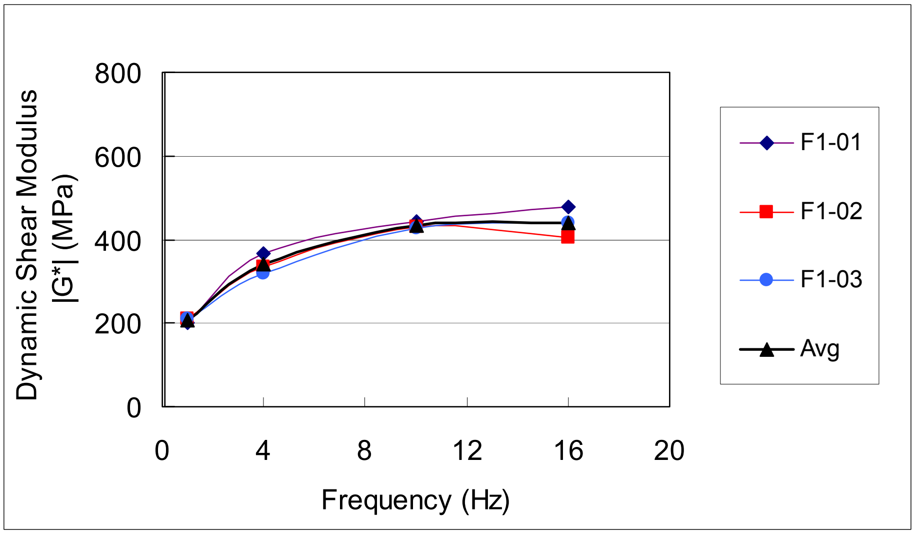

Figure 9-11. Dynamic shear modulus |G*| of GAF1 at 40° C

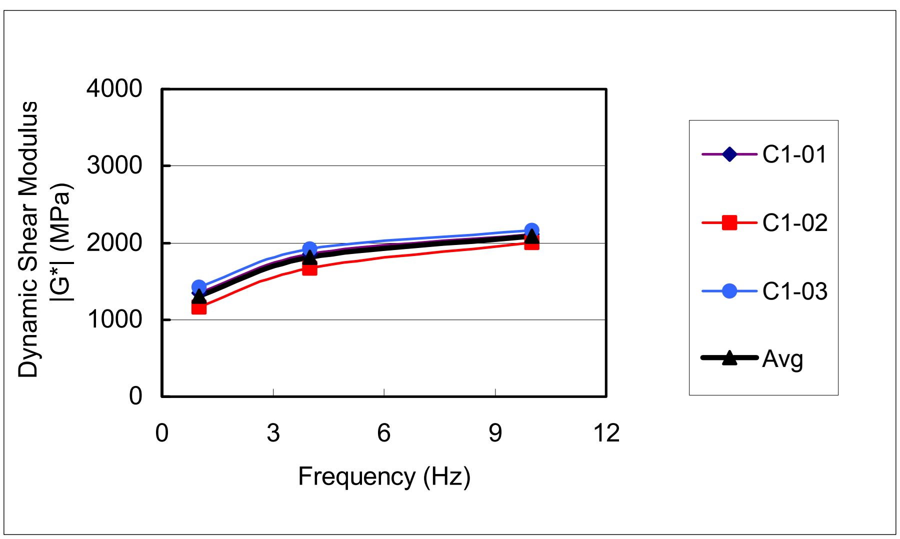

Figure 9-12. Dynamic shear modulus |G*| of C1 at 10° C

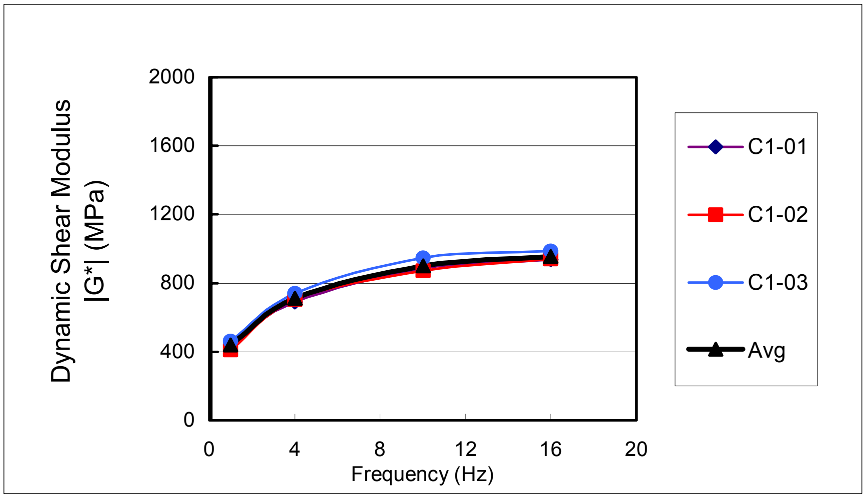

Figure 9-13. Dynamic torsional shear modulus |G*| of C1 at 25° C

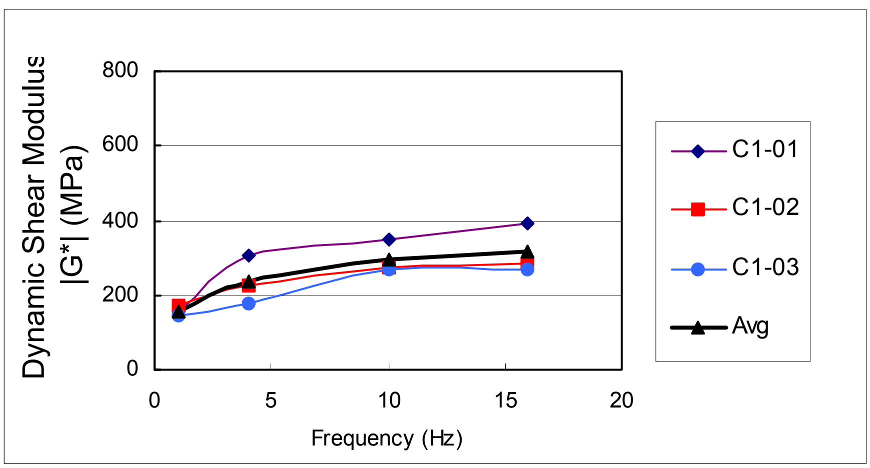

Figure 9-14. Dynamic torsional shear modulus |G*| of C1 at 40° C

For both the GAF1 and the GAC1 mixtures, the test results from each individual specimen display a high degree of consistency at the different temperatures tested. As expected, the dynamic shear modulus increases with increasing frequency. At 10° C, the dynamic shear modulus, |G*|, increased from 1100 MPa at 1 Hz to 2100 MPa at 16 Hz for the GAC1 mixture and from 2000 MPa (1 Hz) to 3000 MPa (16 Hz) for the GAF1 mixture. At 25° C, the dynamic shear modulus, |G*|, increased from about 400 MPa at 1 Hz test to 900 MPa at 16 Hz test for the GAC1 mixture and from 500 MPa at 1 Hz test to 1200 MPa at 16 Hz test for the GAF1 mixture. At 40° C, |G*| increases from 140 MPa at 1 Hz to 390 MPa at 16 Hz for the GAC1 mixture and from 200 MPa at 1 Hz to 480 MPa at 16 Hz for the GAF1 mixture.

Figures 9-15 through 9-20 display the measured phase angles for the GAF1 and GAC1 mixtures. It was observed that phase angle for the torsional shear test is higher than the axial complex modulus test. One possible explanation for this difference is the anisotropic nature of hot mix asphalt samples.

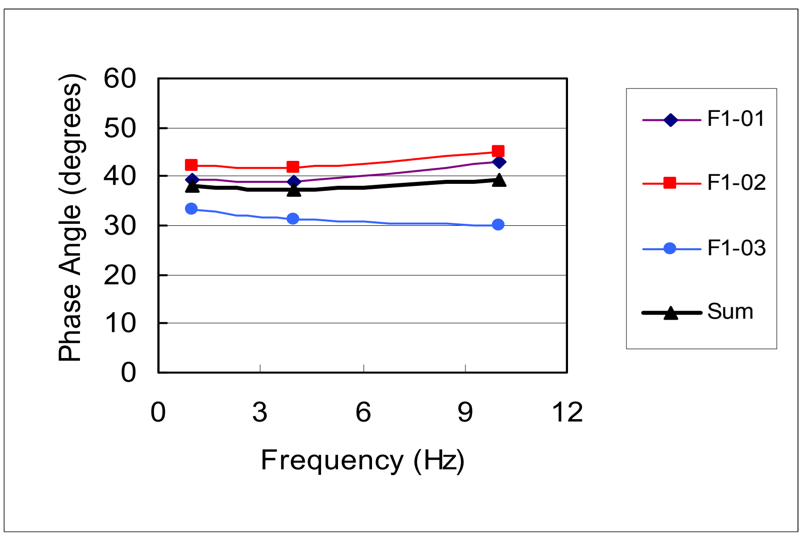

Figure 9-15. Phase angle for GAF1 mixture at 10° C

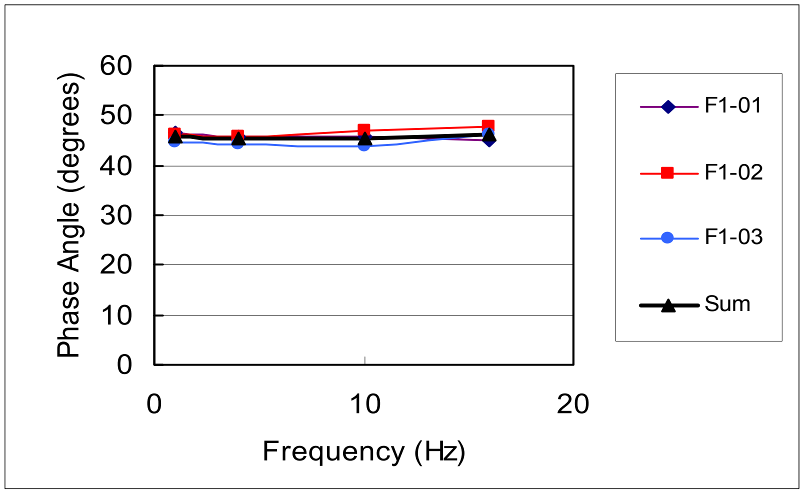

Figure 9-16. Phase angle for GAF1 mixture at 25° C

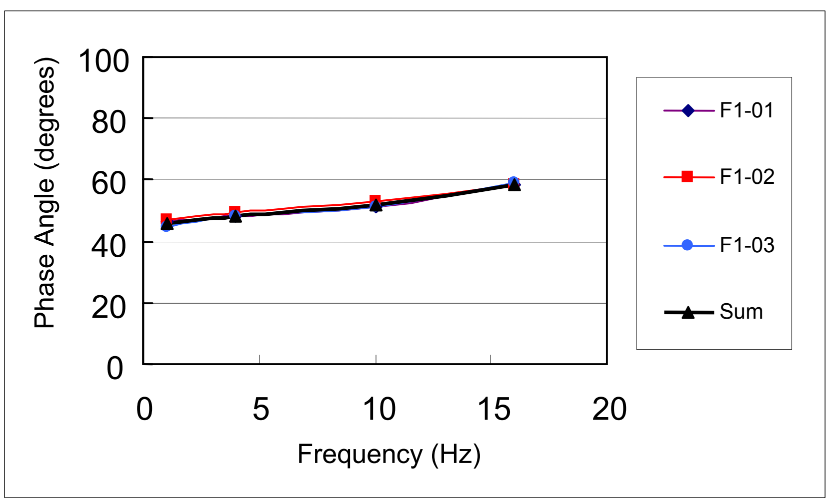

Figure 9-17. Phase angle for GAF1 mixture at 40° C

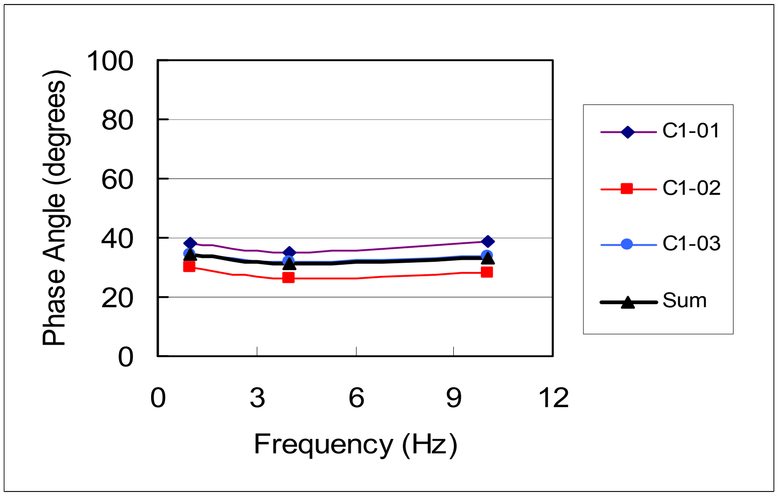

Figure 9-18. Phase angle for GAC1 mixture at 10° C

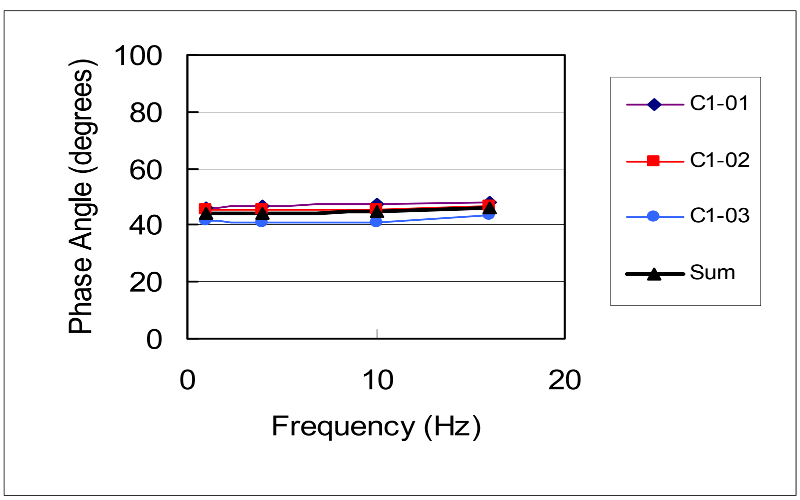

Figure 9-19. Phase angle for GAC1 mixture at 25° C

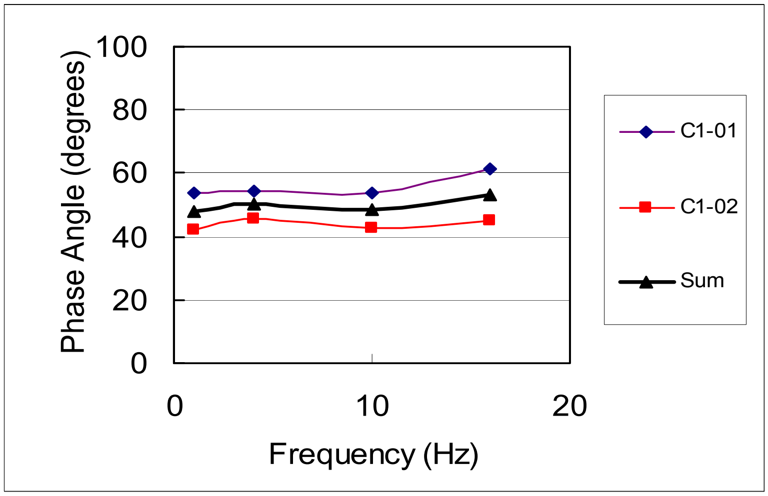

Figure 9-20. Phase angle for GAC1 mixture at 40° C

9.8 Comparison to Axial Dynamic Modulus

9.8.1 Poisson's Ratios

The complex shear modulus can be related to axial complex modulus through the Poisson's ratio. Harvey et al. (2001) concluded that the Poisson's ratio could be taken to be constant, resulting in the following relationship between G* and E*:

$$G^* = \frac{E^*}{2(1+\nu)} \qquad (9\text{-}11a)$$

or

$$\nu = \frac{E^*}{2G^*} - 1 \qquad (9\text{-}11b)$$

Figures 9-21 and 9-22 show typical results for the Poisson's ratio at different temperatures for the coarse-graded GAC2 mixture and the fine-graded GAF2 mixture, which were found to show typical trends in the Poisson's ratios for the mixtures tested. It can be observed that Poisson ratio is not constant, but varies with frequency. It can also be observed that for the most part, the Poisson's ratios fall below 0.5, which implies that the mixtures tested are within the linear range. In comparison, results from the Superpave Simple Shear Tester often show Poisson's ratios that are higher than 0.5 (e.g., Saadeh et al., 2003). For the GAC2 mixture at a testing temperature of 10° C, the Poisson's ratio varies from about 0.28 at the 1 Hz frequency to 0.52 at the 16 Hz.

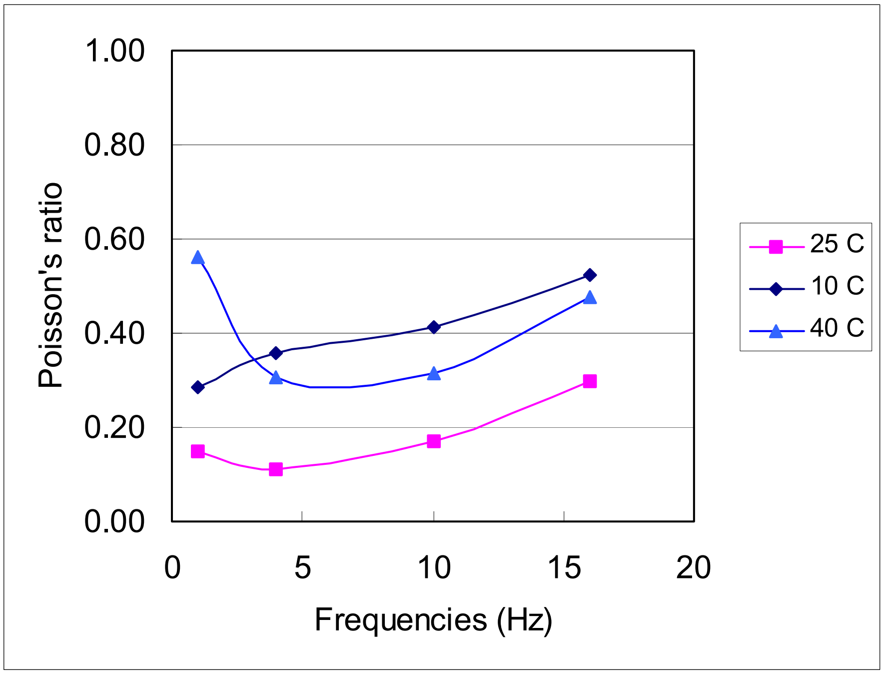

Figure 9-21. Poisson ratio of coarse mixture GAC2

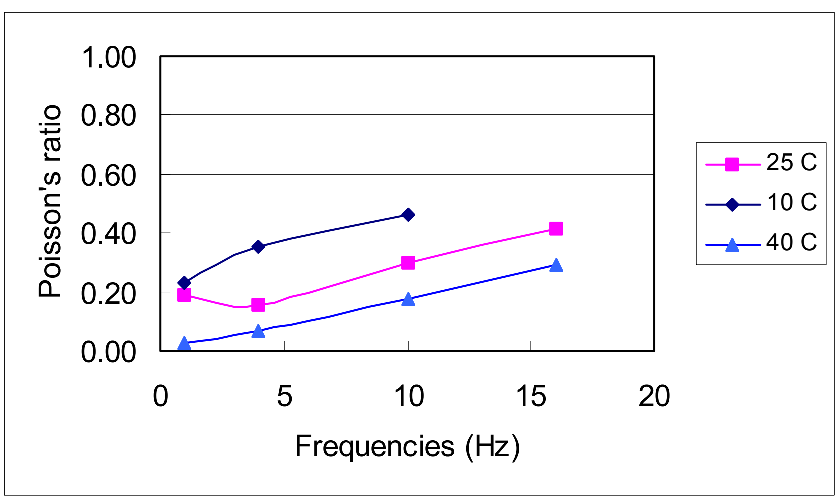

Figure 9-22. Poisson ratio of fine mixture GAF2

Similarly, at a testing temperature of 10° C, the Poisson's ratio varies from 0.23 to 0.47 as the testing frequency is increased from 1 Hz to 10 Hz for the GAF2 mixture. As the temperature increases to 25° C, the Poisson's ratio tends to decrease slightly at each frequency, as compared to 10° C test temperature results. At 25° C, the Poisson's ratio ranged from 0.15 at 1 Hz to 0.3 at 16 Hz for the GAC2 mixture and from 0.19 at 1 Hz to 0.42 at 16 Hz for the GAF2 mixture. The Poisson's ratios at testing temperature of 40° C for both the mixtures tended to be more variable, ranging from 0.3 to 0.56 for the GAC2 mixture, and from 0.03 to 0.29 for the GAF2 mixture. A Poisson's ratio greater than 0.50 indicates that the mixture has entered a nonlinear range and may be dilating. It is possible that for the GAC2 mixture, enough damage was induced in previous testing to cause the mixture to dilate at very last test at the 1 Hz frequency and highest temperature. Similarly, the very low value of 0.03 at the 1 Hz frequency may imply an inadequate load level. The load level at that point was found to induce only 50 $\mu\varepsilon$, which may be insufficient for mobilizing the mixture for modulus testing with the solid cylindrical specimen, thus resulting in an artificially high dynamic shear modulus.

9.8.2 Comparison Between Dynamic Shear Modulus and Axial Dynamic Modulus

Figure 9-23 shows a comparison of dynamic shear modulus and axial dynamic modulus for the mixtures tested. In general, the dynamic moduli follow a similar trend – the GAC1 mixture has the lowest modulus values and the GAF2 mixture has the highest modulus values. However, there are slight overall differences in the rankings for the other mixtures, with the dynamic shear modulus falling off slightly for the GAC3 and GAC2 mixtures, as compared to the axial dynamic modulus.

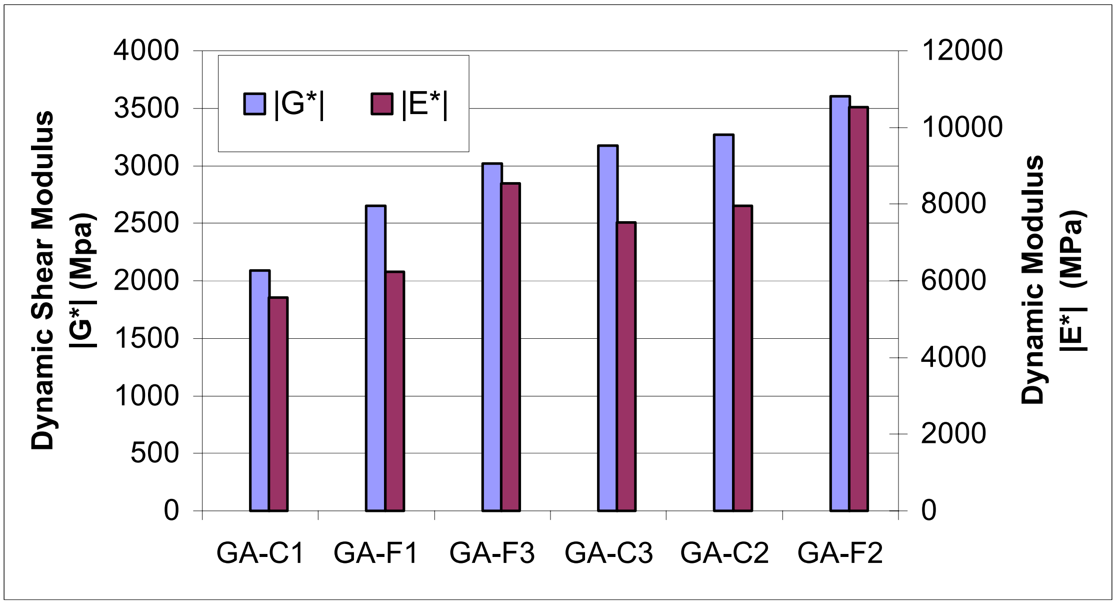

Figure 9-23. Comparison of dynamic shear modulus and axial dynamic modulus (test temperature: 10° C; test frequency: 10 Hz)

9.8.3 Comparison Between Dynamic Shear Modulus and Resilient Modulus Obtained from the Superpave Indirect Tension Test

Once the dynamic complex modulus testing and the dynamic shear testing was completed, resilient modulus testing was performed using the Superpave indirect tension test at a test temperature of 10° C. The testing methodology used for the resilient modulus testing was described previously by Roque et al. (1997). Figures 9-24 and 9-25 show a comparison between the dynamic shear modulus and the resilient modulus obtained from the Superpave IDT test at testing frequencies of 4 Hz and 10 Hz, respectively. In both cases, the dynamic shear modulus follows the same trend as the Superpave IDT resilient modulus.

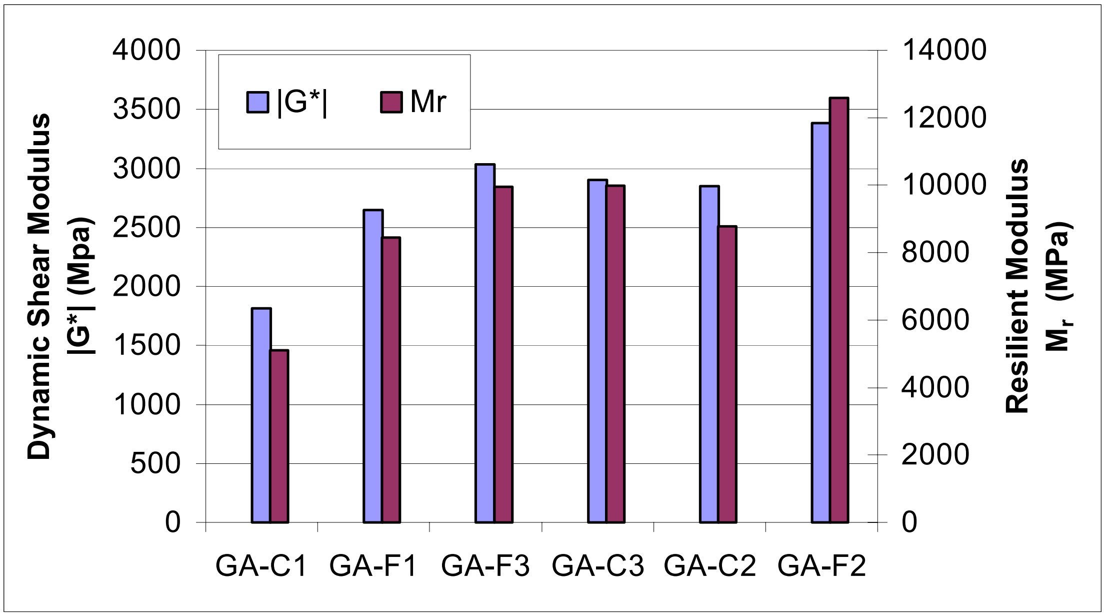

Figure 9-24. Comparison of dynamic shear modulus and resilient modulus from the Superpave IDT test (test temperature: 10° C; test frequency: 4 Hz)

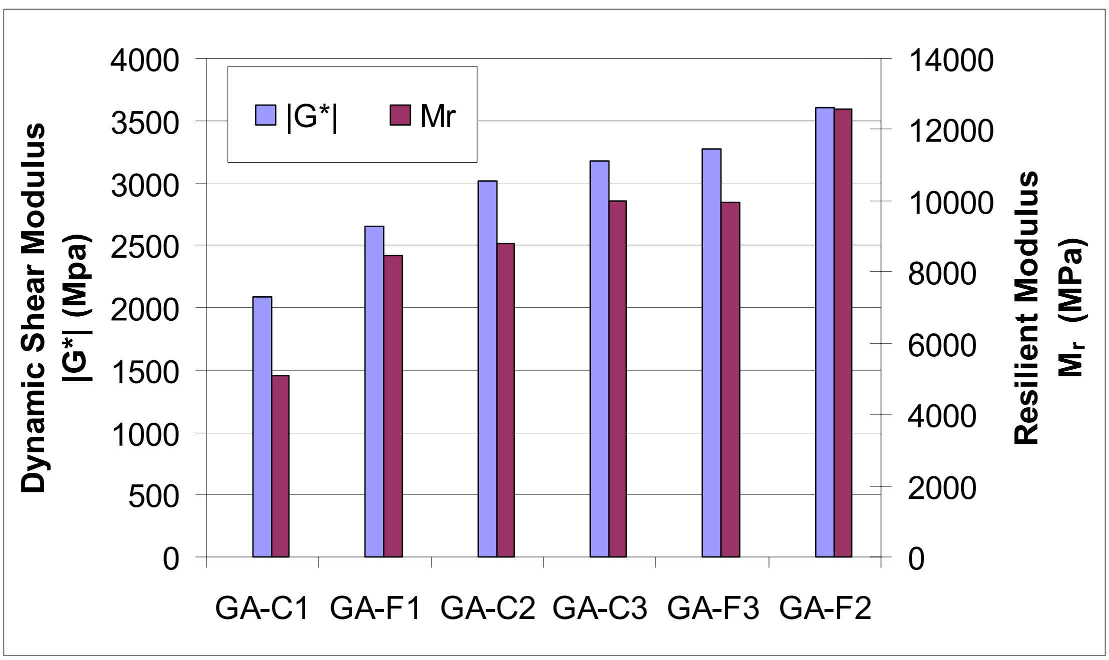

Figure 9-25. Comparison of dynamic shear modulus and resilient modulus from the Superpave IDT test (test temperature: 10° C; test frequency: 10 Hz)

9.8.4 Comparison of Dynamic Shear Modulus to Film Thickness

Following the procedure proposed by Nukunya et al. (2001), the effective film thickness for the coarse-graded mixtures was calculated. Similarly, the theoretical film thickness was calculated for the fine-graded mixtures. Figures 9-26 and 9-27 show the plots of the dynamic shear modulus versus effective film thickness for the coarse-graded mixtures and the theoretical film thickness for the fine-graded mixtures. Interestingly, for the coarse-graded mixtures, the dynamic shear modulus varies inversely with the effective film thickness, such that as the film thickness increases, the dynamic shear modulus decreases. Similarly, for the fine-graded mixtures, the dynamic shear modulus varies inversely with the theoretical film thickness. Since the aggregate type for all mixtures was the same, the film thickness can be view as an indirect measure of aggregate structural effects. Hence, as the amount of fines increases from the coarse-graded GAC1 mixture to the more dense-graded GAC3 mixture, the effective film thickness decreases and the dynamic shear modulus increases. Similarly, as the amount of fines increases from the GAF1 mixture to the GAF2 mixture, the theoretical film thickness decreases and the dynamic shear modulus increases. Finally, the results presented in Figures 9-26 and 9-27 also show that the dynamic shear modulus is sensitive to binder content and volumetric effects.

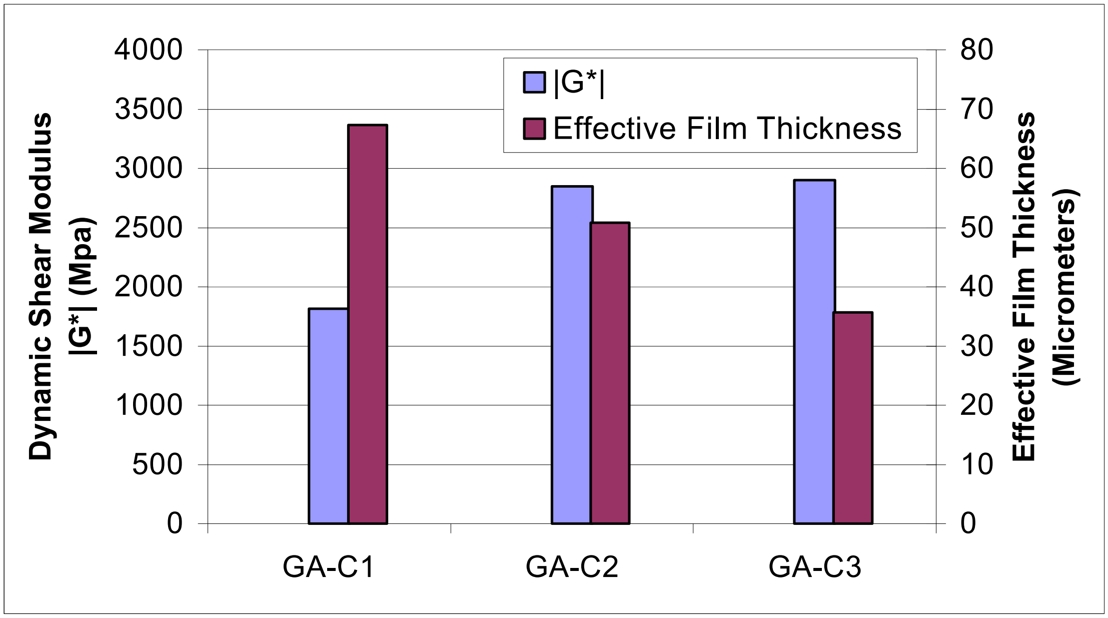

Figure 9-26. Comparison of dynamic shear modulus and effective film thickness for the coarse-graded mixtures tested (test temperature: 10° C; test frequency: 4 Hz)

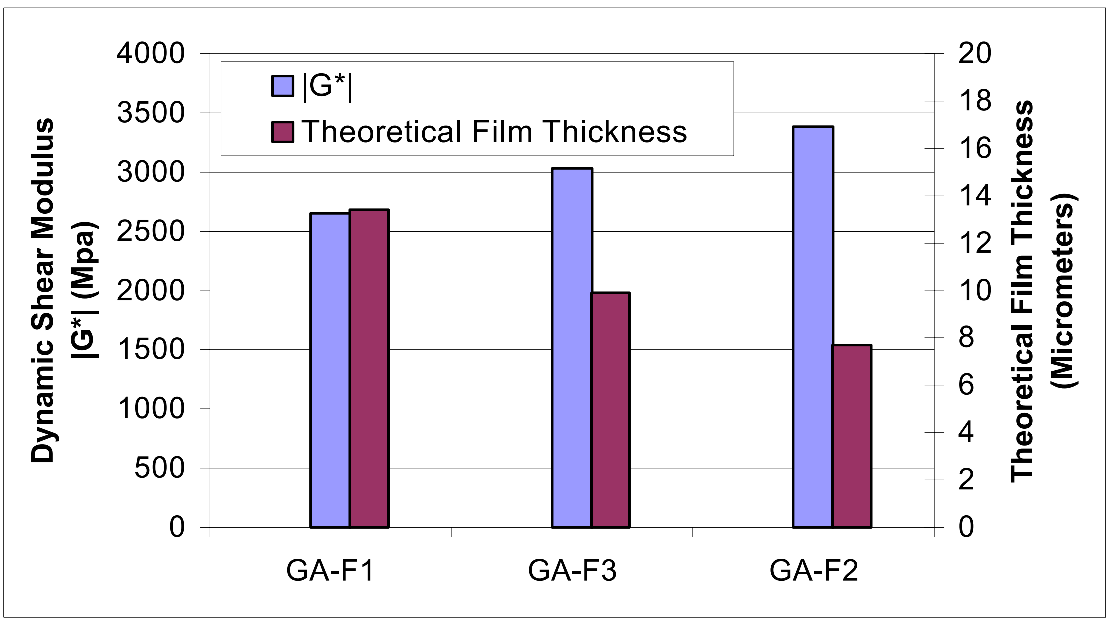

Figure 9-27. Comparison of dynamic shear modulus and effective film thickness for the fine-graded mixtures tested (test temperature: 10° C; test frequency: 4 Hz)

9.9 Summary and Conclusions

This chapter presented a new complex modulus testing procedure, based on torsional shear modulus testing of solid specimens. The theory behind the torsional shear modulus test is presented, followed by a discussion of the interpretation method and the testing protocols that were developed for dynamic shear modulus testing. Six mixtures were tested with the proposed testing protocol.

The results generally showed similar trends to those observed form the axial dynamic modulus test. Calculated Poisson's ratios generally ranged from about 0.2 to 0.5, depending on test temperature and test frequency. Importantly, the results also showed similar trends to those obtained from Superpave IDT resilient modulus testing. Finally, an inverse relationship between the dynamic shear modulus and the asphalt film thickness was observed – as the film thickness decreases, the dynamic shear modulus increases.

The main benefit of the dynamic shear modulus test over the axial dynamic modulus test is that no on-specimen instrumentation is needed. Rather, the deformation measurements are performed at the top loading platens. However, a drawback with this test is that the specimens need to be glued to the end platens during testing. Generally, the test results showed a fairly high degree of consistency from one specimen to another. However, the results may possibly also be affected by eccentricity due to the specimen ends not being completely parallel.

In summary, the results of this study show that the dynamic torsional shear modulus test may be promising in the dynamic characterization of mixtures. Therefore, it is recommended that more mixtures be tested in the torsional complex shear modulus test.

CHAPTER 10
COMPLEX MODULUS OF ASPHALT MIXTURES IN TENSION

10.1 Introduction

10.1.1 Background

Complex modulus of asphalt mixtures (i.e., dynamic modulus and phase angle) has been studied since the 1960s (Papazian, 1962). In recent years, the complex modulus, which is based on the theory of viscoelasticity, has become more widely accepted for use as a fundamental parameter to characterize asphalt mixture for design of flexible pavement. Complex modulus test results provide more information about the mixture's rheology than resilient modulus, which is primarily a measure of the mixture's elastic stiffness. However most, if not all, dynamic testing on mixtures to date has been performed in compression or shear. Given that cracking is primarily a tensile mode of failure, it can be argued that the determination of complex modulus in tension is more relevant for the evaluation of mixture cracking performance. Therefore, it would potentially be of great value to have a practical testing system to determine the rheological characteristics of mixtures in tension using dynamic methods.

The indirect tension test is the most practical, and probably the most reliable way to measure the tensile properties of asphalt mixtures, and it is the only possibility for testing field cores from thin layers in tension. Specifically, the Superpave indirect tension test (IDT), which was developed by Roque and Buttlar (1992) as part of the strategic highway research program (SHRP), has been shown to result in accurate determination of tensile properties of asphalt mixtures at intermediate and low in-service temperatures. Buttlar and Roque (1994) and Roque et al. (1997) have developed testing procedures and data reduction methods to obtain the following properties from the Superpave IDT: resilient modulus, creep compliance and m-value, tensile strength, failure strain, and fracture energy. The test has not been used for determination of complex modulus. However, it seems reasonable to assume that the basic procedures used in the Superpave IDT can be extended so that complex modulus can be determined from the test.

Consequently, this research program was undertaken to develop and evaluate a testing and analysis system to obtain complex modulus (dynamic modulus and phase angle) accurately using the Superpave IDT.

10.1.2 Objectives

As indicated above, the primary objective of this study was to develop and evaluate a testing and analysis system to obtain tensile complex modulus accurately from Superpave IDT tests. Since tensile complex modulus has not been widely reported for asphalt mixtures, the system developed was evaluated by comparing trends and magnitudes for the complex modulus parameters measured to those reported in the literature, which have been determined primarily in compression and shear. In addition, complex modulus values determined at higher frequency should approach the elastic or resilient modulus of the mixture. Therefore, these values should compare favorably to resilient modulus measured in tension. More specific objectives of this study may be summarized as follows:

- To identify or establish suitable testing methods, as well as data acquisition and data reduction procedures to obtain complex modulus parameters using the Superpave IDT.
- To develop computer software to determine complex modulus parameters accurately and consistently from the data obtained.
- To evaluate the reasonableness of tensile complex modulus parameters by comparing results to available data and trends.

- To identify relationships between the dynamic modulus and resilient modulus that may be of practical use.

10.1.3 Scope

The study involved six dense-graded mixtures obtained from pavements in Florida. Nine 6-in. diameter cores were obtained from each of the six pavement sections that were part of a larger study to investigate top-down cracking performance of pavements in Florida.

Two-in. thick slices were taken from each core for Superpave IDT testing. Three specimens were tested at each of three test temperatures: 0°, 10°, and 20° C. Complex modulus test for performed at five testing frequencies: 0.33, 0.5, 1.0, 2.0, and 8.0 Hz. In addition, resilient modulus tests were performed on all test specimens.

10.2 Review of Complex Modulus Test

Complex modulus tests have mainly been performed using unconfined uniaxial compression tests. The standard test procedure is described in ASTM D 3497 which recommends three test temperatures (41° F, 77° F, and 104° F) and three loading frequencies (1, 4, and 16 Hz). Sinusoidal loading without rest periods for a period of 30 to 45 seconds starting at the lowest temperature and highest frequency, and proceeding to the highest temperature and the lowest frequency.

10.2.1 Complex Modulus Testing Issues

The complex modulus test is based on principles of linear viscoelasticity. Therefore, the test should be performed at small strain levels where principles of stress and strain superposition are thought to apply for asphalt mixtures. Witczak et al. (2000) recommended a cyclic strain amplitude of between 75 and 200, depending on temperature, for complex modulus tests performed in uniaxial compression. Damage accumulated during cyclic testing can also have a negative effect on complex modulus test results. Kim et al. (2002) conducted tests at multiple frequencies, temperatures, and test durations to evaluate the effect of accumulated strain on complex modulus. Their goal was to identify a limiting strain beyond which then made to render to the complex modulus test results as uninterpretable. They recommended a maximum of 70 micro-strain cyclic strain amplitude and the minimum rest period of five minutes between testing at different frequencies to relieve the effects of accumulated strain.

Buttlar and Roque (1994) and Roque et al. (1997) developed testing procedures and data reduction methods to obtain the following properties from the Superpave IDT: resilient modulus, creep compliance and m-value, tensile strength, failure strain, and fracture energy. The test has not been used for determination of complex modulus. Kim (2002) used the Superpave IDT to perform tensile complex modulus tests on asphalt mixtures at the University of Florida. He extended the test methods and data reduction procedures developed by Buttlar and Roque (1994) and Roque et al. (1997) to obtain dynamic modulus and phase angle from Superpave IDT tests. The tests were performed at room temperature for 1000 loading cycles on one mixture at four frequencies: 0.33, 1.0, 4.0, and 8.0 Hz. The limited results were encouraging as they compared favorably with trends reported in the literature. Significant changes in complex modulus were observed in the first 10 to 20 cycles of loading, after which the results stabilized. For all frequencies evaluated, the dynamic modulus remained constant between 100 and 1000 cycles of loading.

<u>10.2.2 Materials</u>

Six dense-graded mixtures were tested. Nine test specimens were obtained for each mixture from field cores taken from test sections associated with the evaluation of top-down cracking in Florida. The six sections were all extracted from locations in southwest Florida. Sections 1U and 1C were taken from I75 in Charlotte County. Sections 2U and 3C were taken from I75 in Lee County. The SR 80 sections were also taken from Lee County. Table 10-1 summarizes the locations of the sections and Figure 10-1 shows the gradations for the six pavement sections tested.

Table 10-1. Location of the Sections

Section Number	Section Name	Condition	Code	County	Section Limits	State Mile Posts
1	Interstate 75 Section 1	U	I75-1U	Charlotte	MP 149.3 - MP 161.1	0 - 11.8
2	Interstate 75 Section 1	C	I75-1C	Charlotte	MP 161.1 - MP 171.3	11.8 - 22.0
3	Interstate 75 Section 2	U	I75-2U	Lee	MP 115.1 - MP 131.5	0 - 16.4
4	Interstate 75 Section 3	C	I75-3C	Lee	MP 131.5 - MP 149.3	16.4 - 34.1
5	State Road 80 Section 1	C	SR 80-2C	Lee	From East of CR 80A to west of Hickey Creek Bridge	10.8 - 13.6
6	State Road 80 Section 2	U	SR 80-1U	Lee	From Hickey Creek Bridge to east of Joel Blvd.	13.6 - 18.3

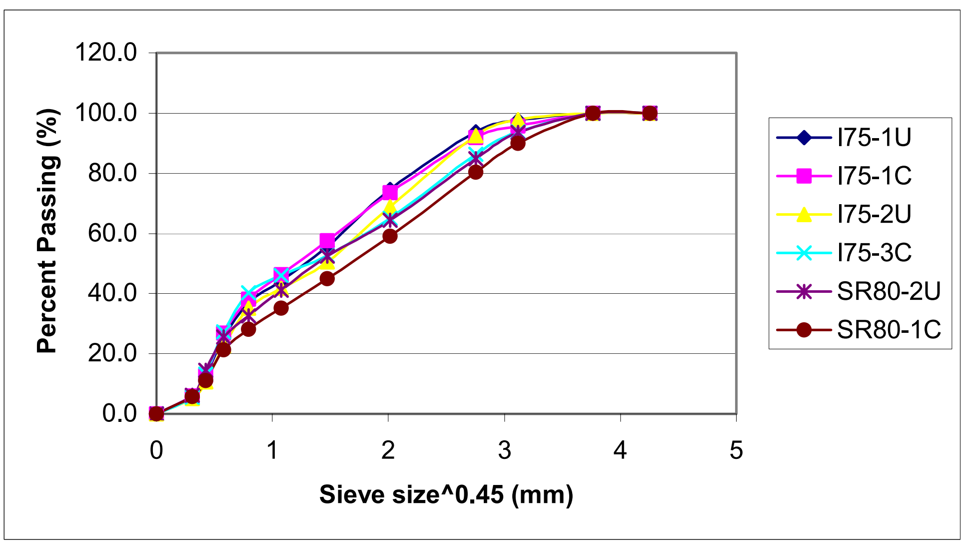

Figure 10-1. Gradations for the six pavement sections tested

The age of the sections is defined as the time from the most recent resurfacing. The age of each section is summarized in Table 10-2.

Table 10-2. Age of the Sections

Section	Year Let	Age as of 2003
I75-1U	1989	14
I75-1C	1988	15
I75-2U	1989	14
I75-3C	1988	15
SR 80-2U	1984	19
SR 80-1C	1987	16

10.2.3 Asphalt Extractions and Binder Testing

Two samples from each section were broken down to determine the theoretical maximum specific gravity (G_{mm}) or Rice Gravity according to AASHTO T 209-94. The G_{mm} value for each section made it possible to calculate the air void content for each sample. These samples were then placed in an asphalt extraction device that uses trichloroethylene (TCE) to separate the binder from the aggregate. The binder-TCE mixture was then placed in an extraction device, which evaporated the TCE. Viscosity tests were performed on the binder at 60C using the Brookfield Thermosel Apparatus. These tests were performed according to ASTM D 4402-87. Table 10-3 summarizes the material properties for the field cores used in the complex modulus test. These material properties include viscosity and effective asphalt content of the extracted binder, along with the air void levels, bulk specific gravity, and maximum theoretical specific gravity.

Table 10-3. Material Properties of Field Cores

Name	Air Void (%)	G_{mb}	G_{mm}	Effective AC (%)	Viscosity (Poise)
I75-1U	2.53	2.242	2.242	4.92	7773
I75-1C	4.13	2.274	2.274	4.83	10844
I75-2U	5.32	2.241	2.241	3.90	12001
I75-3C	5.81	2.190	2.190	4.41	13812
SR 80-2U	6.13	2.213	2.213	3.84	64408
SR 80-1C	4.24	2.197	2.197	4.32	34635

10.2.4 Testing Equipment

The basics of the Superpave IDT test equipment and data acquisition system have been specified by Buttlar and Roque (1994), Roque et al., (1997), and AASHTO TP-9. Figure 10-2 shows a picture of the Superpave IDT testing setup used. Additional information on the specific testing system used in this study is as follows:

- An environmental chamber was used to control specimen temperature. The chamber is capable of maintaining temperatures between -30° C and 30° C with an accuracy of ±0.1° C. Figure 10-3 shows a picture of the environmental chamber used.
- Loads were controlled using a MTS Model 418.91 MicroProfiler.
- The data acquisition system used was Labtech Notebook Pro software. A data acquisition program written specially for complex modulus tests. Approximately 50 data points per loading cycle were obtained.
- Vertical and horizontal deformation measurements were obtained using extensometers designed by MTS specifically for use with the Superpave IDT. A gage length of 1.5 inches was used for all specimens. Figure 10-4 shows a picture of the extensometers used.

Figure 10-2. IDT testing device

Figure 10-3. Temperature controlled chamber

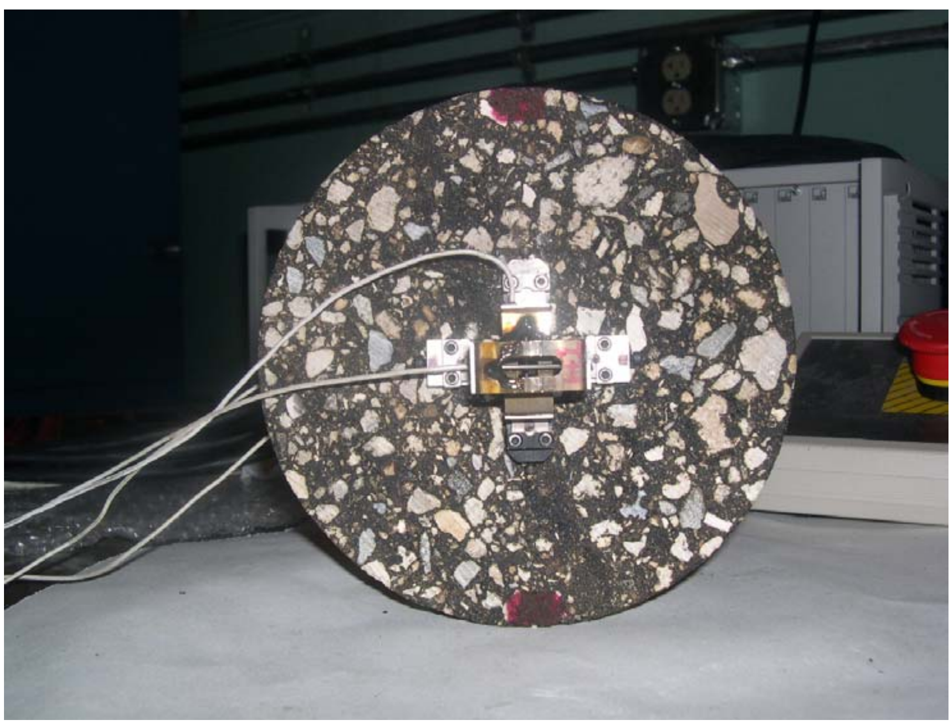

Figure 10-4. Testing sample with extensometers attached

10.2.5 Testing Procedure

A continuous sinusoidal load was applied to the specimen. The load was selected to maintain a horizontal strain amplitude of between 35 and 65 micro strain. It was determined that lower strain amplitudes resulted in problems with data interpretation because of the relatively high noise to signal ratios. Since prior work by Kim (2002) showed the dynamic modulus values did not change between 100 and 1000 load cycles, testing was limited to 100 load cycles. This reduced the potential for micro damage to affect the test results due to accumulated creep strain. In fact, the accumulated creep strain at the end of testing for tests performed at all temperatures and loading frequencies was between 65 and 130 micro strain. This is well below the maximum recommended strain to stay within the linear visco elastic limit of asphalt mixtures, which was conservatively determined to be in the order of 500 micro strain in earlier work performed with the Superpave IDT (Buttlar and Roque, 1994). In addition, a 10-minute rest period was allowed between tests to further minimize the potential effect of accumulated creep strain.

Test specimens were obtained from 6-in. diameter field cores from which 1-in. thick slices were taken using a water-cooled masonry saw that produces smooth and parallel faces. Three specimens were tested at each of three test temperatures for each mixture. Each specimen was tested at the following five frequencies: 0.33, 0.5, 1.0, 4.0, and 8.0 Hz. In all cases, the highest frequency test was performed first as recommended by ASTM D 3497. Additional details on the testing procedure used are as follows:

- After cutting, all specimens were allowed to dry in a constant humidity chamber for a period of two days. Figure 10-5 shows a picture of the dehumidifying chamber used.
- Four brass gage points (5/16-in. diameter by 1/8-in. thick) were affixed with epoxy to each specimen face.

- The extensometers were mounted on the specimen. Horizontal and vertical deformations were measured on each side of the specimen.
- The test specimen was placed into the load frame. A seating load of 8 to 15 pounds was applied to the test specimen to ensure proper contact of the loading heads.
- The specimen was loaded by applying a repeated and continuous sinusoidal load, where strain level by one cyclic load was adjusted between 35 and 65 micro-strain.
- When the applied load was determined, a total of 100 cycles were applied to the specimen, and the computer software began recording the test data.
- As mentioned earlier, a 10-minute rest period was allowed between tests at different frequencies.

Figure 10-5. Dehumidifying chamber

10.3 Development of Data Analysis Procedure

A data analysis system was developed for determination of complex modulus from the Superpave IDT. The following equations, previously used for the axial and torsional complex modulus testing interpretation, were used to obtain the deformation amplitude and phase angle from measured sinusoidal load and deformation response:

$$x = X \bullet \sin(\omega \bullet t + \phi) + a \bullet t + b \tag{10.1}$$

$$x = X \bullet \cos(\phi) \bullet \sin(\omega \bullet t) + X \bullet \sin(\phi) \bullet \cos(\omega \bullet t) + a \bullet t + b \tag{10.2}$$

$$x = A \bullet \sin(\omega \bullet t) + B \bullet \cos(\omega \bullet t) + a \bullet t + b \tag{10.3}$$

$$\phi = \tan^{-1}\left(\frac{B}{A}\right) \tag{10.4}$$

$$X = \sqrt{A^2 + B^2} \tag{10.5}$$

where x = deformation;

X = amplitude of deformation;

ϕ = phase angle;

t = time;

ω = frequency; and

a, b, A, B = regression coefficients.

The deformation resulting from the sinusoidal load can be represented as a sinusoidal curve with a linear slope (see Eq. 10.1). Equation 10.2 is obtained by expanding Eq. 10.1 using trigonometric identities. Since the terms Xcos (ϕ) and Xsin (ϕ) are constant at each test temperature and frequency, they can be simplified by denoting them as A and B (Eq. 10.3), respectively, in order to simplify the relationship for regression analysis. Finally, the coefficients, a, b, A and B were obtained using linear least-squares regression analysis.

The complex modulus deformation test data include a noise component in the signals, so accurate values of phase angle and magnitude cannot be expected from one or two loading cycles. On the other hand, the use of too many cycles may introduce error from nonlinearity in the deformation curve. In the case of the Superpave IDT, it was determined that five loading cycles, recorded immediately before the 100th loading cycle, resulted in consistent and accurate determination of phase angle and strain amplitude.

10.3.1 Mechanical and Electrical Phase Lag Effects

Zhao and Kim (2003) observed that a phase lag existed in dynamic measurements purely due to electronic effects and/or mechanical vibration effects on strain gages. This observed phase lag (phase angle) was observed to vary with testing frequencies. In view of these findings, an aluminum specimen (linear elastic material) was used to test the current Superpave IDT test setup. The aluminum specimen used was approximately the same size as the asphalt mixture specimens tested (6-in. diameter × 1.25-in. thickness). The results of the testing with the aluminum specimen showed that a phase lag was observed with the aluminum specimen. It is known that the phase angle from the linear elastic materials, such as the aluminum specimen must be zero. Consequently, the phase angle resulting from Superpave IDT complex modulus tests on an aluminum specimen must be due to testing equipment error. Thus, these phase angles obtained from the aluminum specimen were subtracted from the phase angle obtained from complex modulus tests on asphalt mixtures.

Phase angles and dynamic modulus values determined from complex modulus tests performed on the aluminum specimen are presented in Table 10-4 and Figure 10-6, respectively. The modulus values of aluminum determined from Superpave IDT tests were between 10,536 ksi and 10,982 ksi, which is clearly within the known range of values for the Young's modulus of aluminum (10,000 ksi to 11,400 ksi). Additional details regarding the testing and data reduction procedures are presented below.

Table 10-4. Phase Angles and |E*| from Aluminum Specimen

Frequency (hz)	Phase Angle (degree)	|E*| (ksi)
0.333	2.15	10822
0.5	1.37	10857
1	1.34	10982
4	5.46	10633
8	11.59	10536

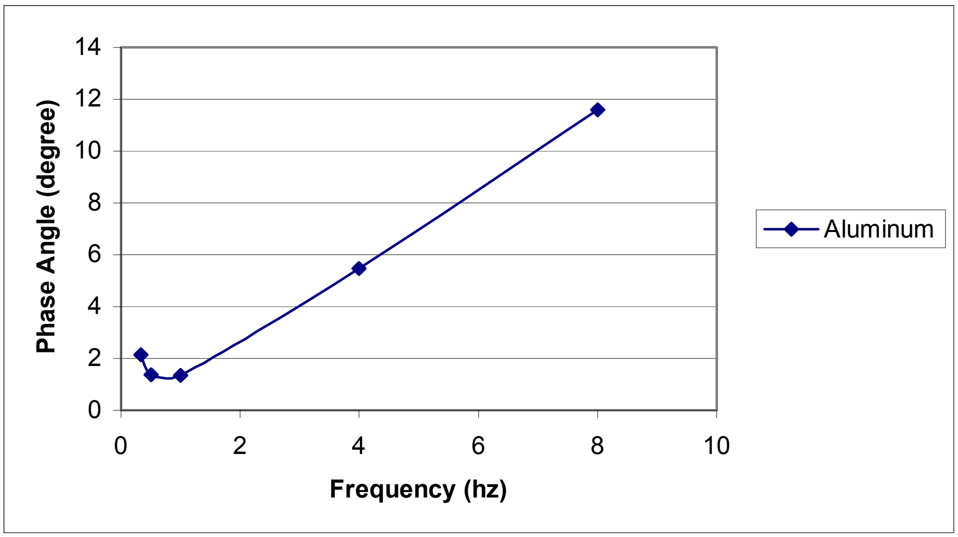

Figure 10-6. Measured phase angle versus frequency from aluminum specimen

The data analysis procedures developed by Roque and Buttlar (1992) and Roque et al. (1997), were modified and adopted for use with the complex modulus test. The procedure requires three data sets obtained from three specimens for proper interpretation. The horizontal deformation carries the symbol, ΔH, while the vertical deformation carries the symbol, ΔV. The horizontal phase angle carries the symbol, ΔPA. Herein, the deformations and phase angle were computed using Eq. 10.4 and 10.5. In addition, the following equations are required for proper data interpretation using the Superpave IDT:

1. Normalization factors

Since different specimens may have different thickness, diameter, or load, the deformations need to be normalized.

$$C_{NORM\ i} = \frac{t_i}{t_{AVG}} \bullet \frac{D_i}{D_{AVG}} \bullet \frac{P_{AVG}}{P_i} \tag{10.6}$$

$$H_{NORM\ j} = \Delta H_j \bullet C_{NORM\ i} \tag{10.7}$$

$$V_{NORM\ j} = \Delta V_j \bullet C_{NORM\ i} \tag{10.8}$$

where t_i = thickness of each specimen (i = 1 ~ 3);

D_i = diameter of each specimen (i = 1 ~ 3);

P_i = loading amplitude of each specimen (i = 1 ~ 3);

t_{AVG} = average thickness of three specimens;

D_{AVG} = average diameter of three specimens;

P_{AVG} = average loading amplitude of three specimens;

ΔH_j = horizontal deformations for three specimens (j = 1 ~ 6);

ΔVj = vertical deformations for three specimens (j = 1 ~ 6);

$H_{NORM\ j}$ = normalized horizontal deformations (j = 1 ~ 6); and

$V_{NORM\ j}$ = normalized vertical deformations (j = 1 ~ 6).

2. Trimmed mean deformation and trimmed mean phase angle

The six normalized horizontal and vertical deformations, and the six horizontal phase angles from three replicate specimens are ranked. To get the trimmed mean deformation and the trimmed mean phase angle, the highest and lowest deformation and the highest and lowest phase angle are deleted and then the remaining four deformations and four phase angles are averaged.

$$\Delta H_{TRIM} = \frac{\sum \Delta H_{NORM\ j}}{2n-2} \tag{10.9}$$

$$\Delta V_{TRIM} = \frac{\sum \Delta V_{NORM\ j}}{2n-2} \tag{10.10}$$

$$\Delta PA_{TRIM} = \frac{\sum \Delta PA_j}{2n-2} \tag{10.11}$$

where n = the number of specimens for each temperature (n = 3);

ΔH_{TRIM} = trimmed mean horizontal deformation;

ΔV_{TRIM} = trimmed mean vertical deformation; and

ΔPA_{TRIM} = trimmed mean horizontal phase angle.

3. Poisson's ratio

$$\nu = -0.100 + 1.480\left(\frac{\Delta H_{TRIM}}{\Delta V_{TRIM}}\right)^2 - 0.778\left(\frac{t_{AVG}}{D_{AVG}}\right)^2 \bullet \left(\frac{\Delta H_{TRIM}}{\Delta V_{TRIM}}\right)^2 \tag{10.12}$$

where ν = Poisson's ratio.

4. Correction factors

Buttlar and Roque (1994) developed the following equations, to account for three-dimensional stress states in diametrically loaded specimen of finite thickness. Also, the phase angles from the aluminum specimen test were included as one of the correction factors to obtain true phase angles at specific test frequencies.

$$C_{BX} = 1.030 - 0.189 \cdot \left(\frac{t_{AVG}}{D_{AVG}} \right) - 0.081 \cdot \nu + 0.089 \cdot \left(\frac{t_{AVG}}{D_{AVG}} \right)^2 \qquad (10.13)$$

$$C_{BY} = 0.994 - 0.128 \cdot \nu \qquad (10.14)$$

$$C_{EX} = 1.07 \qquad (10.15)$$

$$C_{EY} = 0.98 \qquad (10.16)$$

$$C_{SX} = 0.9480 - 0.01114 \cdot \left(\frac{t_{AVG}}{D_{AVG}} \right) - 0.2693 \cdot \nu + 1.4360 \left(\frac{t_{AVG}}{D_{AVG}} \right) \cdot \nu \qquad (10.17)$$

$$C_{SY} = 0.901 + 0.138 \cdot \nu + 0.287 \cdot \left(\frac{t_{AVG}}{D_{AVG}} \right) - 0.251 \cdot \nu \cdot \left(\frac{t_{AVG}}{D_{AVG}} \right)^2 - 0.264 \cdot \left(\frac{t_{AVG}}{D_{AVG}} \right)^2 \qquad (10.18)$$

$$PA_{COR} = \text{Phase angles from aluminum (elastic material) specimen test} \qquad (10.19)$$

5. Horizontal moduli of E*, E′ and E″

The following equations were developed to obtain horizontal moduli of |E*|, E′ and E″:

$$\left| E^* \right| = \left(\frac{1}{\frac{\Delta H_{TRIM}}{GL} \cdot C_{BX} \cdot C_{EX}} \right) \cdot \left(\frac{2P_{AVG}}{\pi D_{AVG} \, t_{AVG}} \cdot C_{SX} - \nu \cdot \frac{6P_{AVG}}{\pi D_{AVG} \, t_{AVG}} \cdot C_{SY} \right) \qquad (10.20)$$

$$\Delta PA = \Delta PA_{TRIM} - PA_{COR} \qquad (10.21)$$

$$E' = \left| E^* \right| \cdot \cos(\Delta PA) \qquad (10.22)$$

$$E'' = \left| E^* \right| \cdot \sin(\Delta PA) \qquad (10.23)$$

where $|E^*|$ = dynamic modulus;

E' = storage modulus;

E'' = loss modulus; and

GL = gage length.

The overall process to calculate the complex modulus using the Superpave IDT is shown in Figure 10-7. The basic concepts used in the data analysis program (ITLT_dynamic) are explained, which was specially developed for the complex modulus test using the process described above. The program was thoroughly evaluated using hundreds of trial data sets, and it was found to be accurate, fast and reliable. All complex modulus test results presented in this study were obtained using this data analysis program.

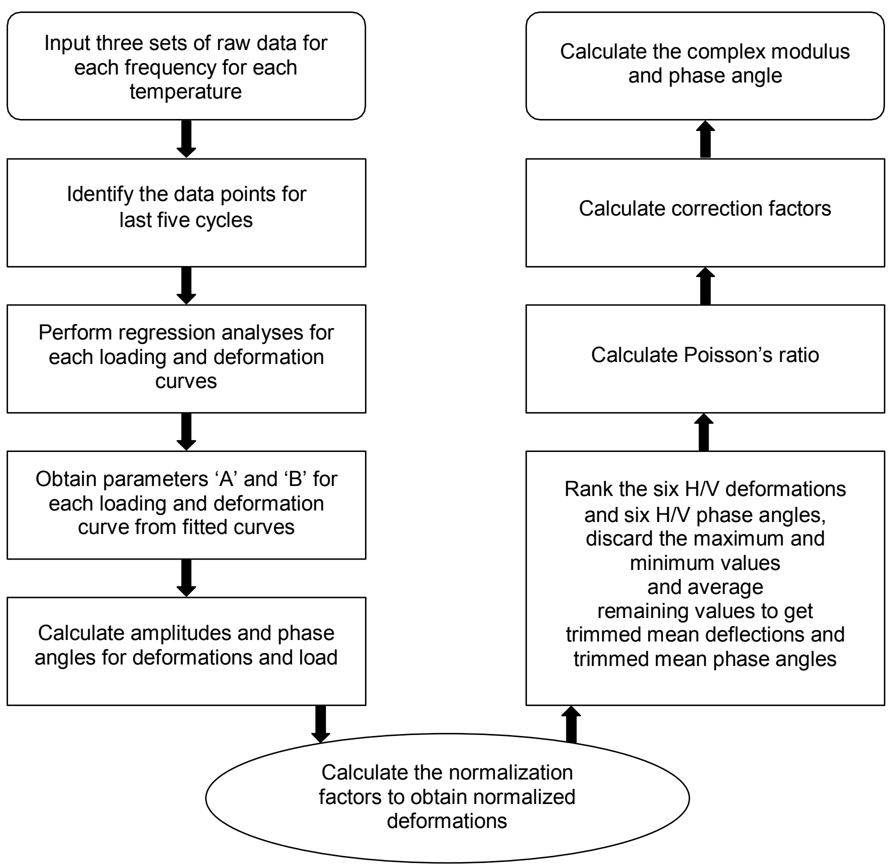

Figure 10-7. Complex modulus data analysis procedure

10.4 Evaluation of Complex Modulus Test

10.4.1 Complex Modulus Test Results

The complex modulus test was performed with the Superpave IDT on a total of 54 field specimens from six state road sections to evaluate the testing and analysis system developed and described above. Dynamic properties such as |E*|, phase angle, E′ and E″ were successfully calculated with data analysis program developed (ITLT_dynamic).

Figure 10-8 shows the relationship between dynamic modulus and phase angle for all mixtures, test temperatures, and frequencies involved this study. In general, the dynamic modulus showed an increasing trend as temperature decreased or frequency increased. Conversely, the phase angles showed a decreasing trend as temperature decreased, or frequency increased. These are obviously reasonable and expected trends, since asphalt mixture becomes stiffer and more elastic as test temperature decreases or frequency increases. Conversely, asphalt stiffness decreases and viscous response increases as temperature or frequency increase. Furthermore, the trends obtained agree closely with

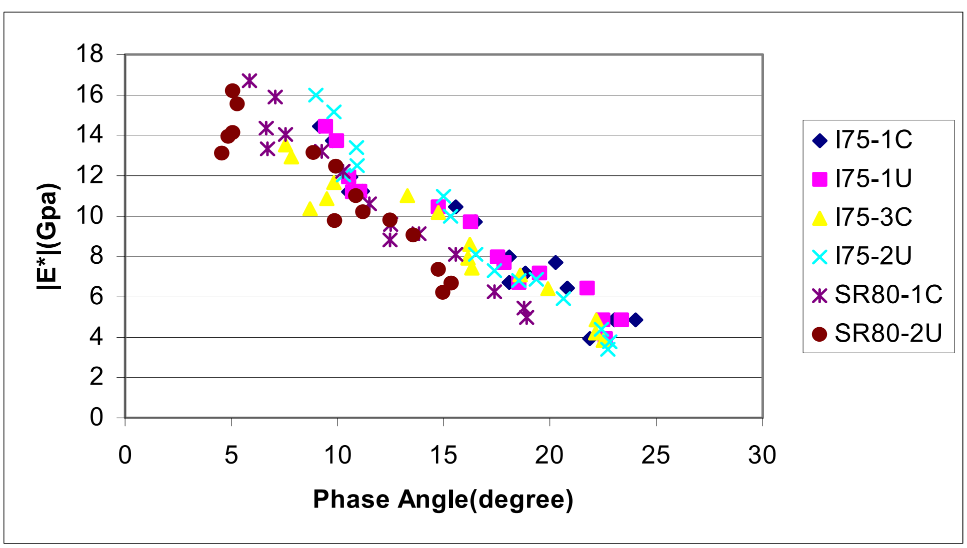

Figure 10-8. Dynamic modulus and phase angle

trends reported in the literature for complex modulus test results using other modes of testing including uniaxial compression (Kim et al., 2002), triaxial compression (Pellinen and Witczak, 2002), and bending beam (Francken, 1998) tests.

10.4.2 Comparison of Dynamic Modulus and Resilient Modulus from IDT

Since tensile complex modulus has not been widely reported for asphalt mixtures, the Superpave IDT complex modulus test was evaluated by comparing trends for the complex modulus parameters measured, to those reported in the literature, which have been determined primarily in compression and shear. However, it is noted that complex modulus values determined at higher frequency should approach the elastic or resilient modulus of the mixture. Therefore, dynamic modulus values determined at higher frequency should compare favorably to resilient modulus measured in tension.

Figures 10-9 and 10-10 clearly show this to be the case. Dynamic and storage modulus values measured at a frequency of 8 Hz compared closely with resilient modulus values measured on the same materials. The resilient modulus tests were performed using a haversine load of 0.1 seconds, which can be said to roughly correspond to a frequency of 10 Hz. As expected, the resilient modulus values were slightly higher than dynamic and storage modulus at 8 Hz. The values reported in figures five and six correspond to all 54 specimens tested, including the three test temperatures and five frequencies used.

It was interesting to note that the relationship between dynamic and resilient modulus had almost exactly the same slope for all testing frequencies, and that the relationships were equally strong at all frequencies ($R^2 > 0.94$ in all cases). This implies that the frequency dependence of dynamic modulus is constant for mixtures at a given level of elastic stiffness.

Consequently, it also follows that the dynamic modulus at a given frequency is a function of the elastic modulus of the mixture and the frequency.

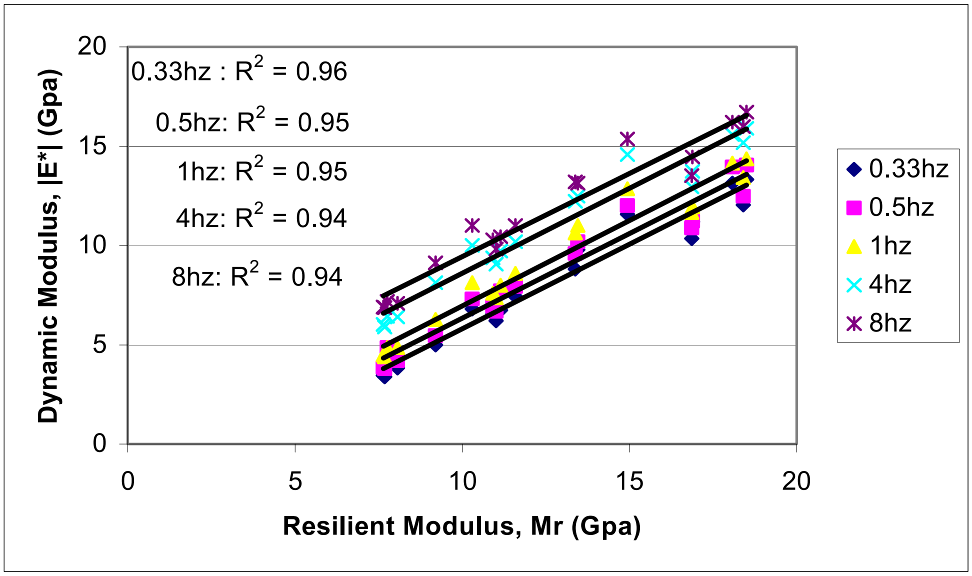

Figure 10-9. Comparison of resilient modulus versus dynamic modulus from the Superpave IDT test

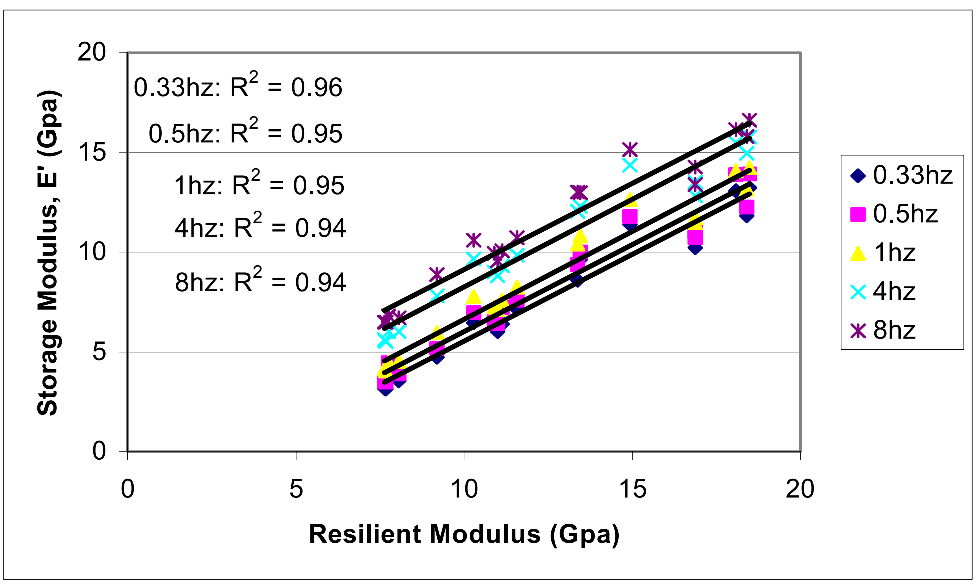

Figure 10-10. Comparison of resilient modulus versus storage modulus for the Superpave IDT test

The relationship shown in Figure 10-11 and presented as Eq. 10.24 below, verifies this observation. The dynamic modulus values for the range of mixtures, temperatures, and frequencies tested in this study are strongly correlated with resilient modulus and frequency of the mixtures tested.

$$\text{Dynamic Modulus (GPa)} = 0.85188 \times \text{Mr (GPa)} + 0.4937 \bullet \log_{10}\left(\text{Frequency (hz)}\right)^2$$

$$+ 2.4711 \bullet \log_{10}\left(\text{Frequency (hz)}\right) - 1.5985 \qquad (10.24)$$

where Frequency = seeking frequency;

Mr = resilient modulus tested in a certain temperature; and

Dynamic Modulus = predicted dynamic modulus.

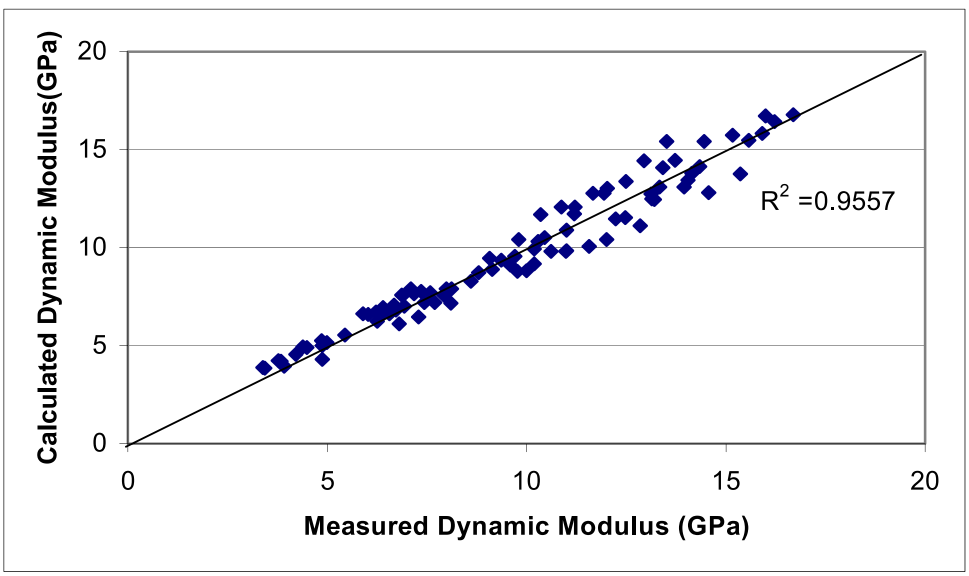

Figure 10-11. Comparison of predicted and measured dynamic moduli

Although empirical in nature, the strength of the correlation presented above (R^2 = 0.9557) appears to indicate that more fundamental relationships may exist between these parameters. In any case, a relationship that allows prediction of dynamic modulus as a function of frequency from mixture properties that are much easier to measure (e.g., resilient modulus and/or creep compliance) would be of great value to the practicing engineer.

10.5 Summary and Conclusions

A testing and analysis system was developed and evaluated in this study to obtain tensile complex modulus accurately from Superpave IDT tests. Since tensile complex modulus properties have not been widely reported in the literature, the system was evaluated by comparing trends for the complex modulus parameters measured to those reported in the literature, which have been determined primarily in compression and shear. In addition, complex modulus values determined at higher frequency were compared to resilient modulus values measured on the same mixtures. The following conclusions were drawn on the basis of tensile complex modulus tests performed on six mixtures at three test temperatures and five loading frequencies using the Superpave IDT along with a testing and data analysis procedures developed in this study:

- The system developed appears to provide reasonable and accurate complex modulus parameters for asphalt mixtures in tension. The parameters exhibited well appropriate trends, and dynamic modulus values measured at higher testing frequency compared closely with resilient modulus measured on the same mixtures.
- It appears that it may be possible to identify more fundamental relationships between dynamic modulus as a function of frequency and other mixture properties that are easier to measure, such as resilient modulus and creep compliance. For the range of mixtures temperatures and testing frequencies investigated, dynamic modulus was found to be strongly correlated with resilient modulus and testing frequency.

- It is very important to evaluate, and if necessary correct for, the potential effects of testing equipment error on complex modulus test results. The use of an aluminum specimen was determined to be an effective way to identify and measure this type of error.

CHAPTER 11
OBTAINING CREEP COMPLIANCE PARAMETERS ACCURATELY FROM STATIC OR CYCLIC CREEP TESTS

11.1 Introduction

Creep compliance is a fundamental property that describes the relationship between the time dependent strain and applied stress in viscoelastic materials. Accurate determination and representation of the creep compliance of asphalt mixture is essential to evaluate both the thermal and load induced cracking performance of pavements. It is well known that creep compliance directly controls the magnitude of thermal stress development in pavements subjected to given environmental conditions. More recently, it has been determined that the rate of load induced micro damage development in asphalt mixture is directly related to the amount of dissipated creep strain energy induced by applied load stresses. Although creep compliance includes elastic and delayed elastic as well as dissipated creep (viscous) response, it is possible to theoretically isolate these responses by using a function that accurately describes the creep compliance and whose parameters meaningfully represent the different types of responses. A power law function, which uses three parameters to describe the creep compliance curve, has been used successfully in this regard. However, the specific values of the parameters obtained can depend on both the testing and the data interpretation methods used to determine the function parameters. This may lead to errors in predicting the relative amount of elastic, delayed elastic, and dissipated creep response of mixtures subjected to load or temperature changes, which in turn leads to erroneous evaluation of cracking performance.

Consequently, there is a need to evaluate the effects of testing and data interpretation methods on the determination of creep compliance power law parameters. More specifically, it would be useful to identify and standardize testing and data interpretation methods to determine creep compliance parameters consistently and accurately from mechanical tests typically performed on asphalt mixture. Determination of parameters associated with the tensile response of asphalt mixtures at intermediate temperatures (0° C to 20° C) are of particular interest since load induced micro damage and fracture are generally considered to be tensile failure mechanisms that predominantly occur in the intermediate temperature range.

11.2 Objectives

The overall objective of this study was to identify, evaluate, and standardize testing and data interpretation methods to determine tensile creep compliance power law parameters consistently and accurately from mechanical tests typically performed on asphalt mixture at intermediate temperatures (0° C to 20° C). Creep compliance can be determined either from static creep tests or from cyclic tests performed at multiple loading frequencies. Static creep tests using the Superpave indirect tensile test (IDT) have been used successfully to determine tensile creep compliance master curves at low temperatures (< 0° C) to predict thermal cracking performance of asphalt pavement using models developed during the SHRP program. These models are currently being incorporated into the latest version of the AASHTO design guide for asphalt pavement structures. More recent work by Roque et al. (1997) has shown that the Superpave IDT can also be used to accurately determine tensile properties of asphalt mixtures, including creep compliance, at intermediate temperatures. However, the greater degree of time dependent response exhibited by asphalt mixture at intermediate temperatures poses some new challenges in terms of accurately isolating elastic, delayed elastic, and viscous response.

Complex modulus and phase angle values determined from cyclic tests performed at multiple frequencies can be related theoretically to the creep compliance of the mixture. Determination of creep compliance from complex modulus tests offer several potential advantages over static creep tests including better definition of creep compliance at shorter load times, as well as the potential of being able to define the creep compliance function from tests requiring significantly less time. The complex modulus test method described in Chapter 10 will be used in this study.

The specific objectives of the study were as follows:

- To develop the appropriate analytical procedures to convert complex modulus and phase angle values at multiple frequencies to creep compliance power law parameters.
- To perform static creep tests and cyclic tests at multiple loading frequencies on several asphalt mixtures in the intermediate temperature range using the Superpave IDT.
- To evaluate the effects of testing and data interpretation methods on the determination of creep compliance power law parameters from both static and cyclic tests.
- Based on the evaluation, identify appropriate testing and data interpretation methods to determine tensile creep compliance power law parameters consistently and accurately from mechanical tests typically performed on asphalt mixture.

11.3 Scope

The study involved the same six dense-graded mixtures obtained from pavements in Florida and discussed in Chapter 10. Nine 6-in. diameter cores were obtained from each of the six pavement sections that were part of a larger study to investigate top-down cracking performance of pavements in Florida.

Two-in. thick slices were taken from each core for Superpave IDT testing. A total 54 specimens from the 6 sections were tested at each of three test temperatures: 0°, 10°, and

20° C. Complex modulus test were performed at five testing frequencies: 0.33, 0.5, 1.0, 4.0, and 8.0 Hz, and also static creep compliance tests were performed on the same specimens.

11.4 Overview of Tests for Viscoelastic Response

11.4.1 Creep Compliance Test

A typical creep compliance test on asphalt mixture is commonly performed using a static constant load. Creep compliance is simply obtained as the time-dependent strain divided by the constant stress. The creep compliance test using the Superpave IDT (AASHTO TP-9; Buttlar and Roque, 1994; and Roque et al., 1997) was used as the reference test for comparison to the creep compliance from complex modulus tests using the Superpave IDT.

11.4.2 Complex Modulus Test

Complex modulus tests have mainly been performed using unconfined uniaxial compression tests. The standard test procedure is described in ASTM D 3497, which recommends three test temperatures (41°, 77°, and 104° F) and three loading frequencies (1, 4, and 16 Hz). Sinusoidal loads are applied without rest periods for a period of 30 to 45 seconds starting at the lowest temperature and highest frequency, and proceeding to the highest temperature and the lowest frequency. The complex modulus test is based on the principles of linear viscoelasticity. Therefore, the test should be performed at small strain levels where principles of stress and strain superposition are thought to apply for asphalt mixtures. Witczak et al. (2000) recommended a cyclic strain amplitude of between 75 and 200 micro strain, depending on temperature, for complex modulus tests performed in uniaxial compression. Damage accumulated during cyclic testing can also have a negative effect on complex modulus test results. Kim et al. (2002) conducted tests at multiple frequencies, temperatures, and test durations to evaluate the effect of accumulated strain on complex modulus. They recommended a maximum of 70 micro strain to relieve the effects of accumulated strain in compression test.

The following equations, which are based on the theory of linear visco-elasticity, can be used to obtain creep compliance from complex modulus tests performed at multiple frequencies:

$$D(t) = \frac{2}{\pi}\int_0^{\infty} \frac{D'(\omega)}{\omega} \bullet \sin(\omega t) \bullet \, d\omega \tag{11.1}$$

$$D(t) = \frac{2}{\pi}\int_0^{\infty} \frac{D''(\omega)}{\omega} \bullet \cos(\omega t) \bullet d\omega \tag{11.2}$$

$$D'(\omega) = \frac{1}{|E^*|} \bullet \cos(\phi) \tag{11.3}$$

$$D''(\omega) = \frac{1}{|E^*|} \bullet \sin(\phi) \tag{11.4}$$

where $D(t)$ = static creep compliance;

$|E^*|$ = dynamic modulus;

ϕ = phase angle;

ϖ = frequency; and

t = time.

Meanwhile, general viscoelastic books had introduced a way to convert the complex modulus to creep compliance (Eq. 11.1 to 11.4). These equations, which were theoretically derived using the appropriate Laplace and Fourier transformations, indicate that creep compliances from static and cyclic load tests will be the same if the frequency and time domains are matched for the different modes of testing. Direct comparisons between creep compliance from static and dynamic tests have not been widely reported, especially for asphalt mixture. Zhang et al. (1997b) showed a generally good correlation between creep compliance of asphalt mixture from static and cyclic loading using the indirect tension test (IDT). The tests were performed over wide frequency ranges: 0.03, 0.1, 0.5, 1, 5, 10, 20, 30, 40, 50, and 60 Hz at room temperature.

11.4.3 Indirect Tension Test (IDT) for Complex Modulus

Complex modulus tests using IDT have also been very limited. Buttlar and Roque (1994) and Roque et al. (1997) developed testing procedures and data reduction methods to obtain the following properties from the Superpave IDT: resilient modulus, creep compliance, tensile strength, and strain and fracture energy to failure. Kim (2002) used the Superpave IDT to perform tensile complex modulus tests on asphalt mixtures at the University of Florida. He extended the test methods and data reduction procedures developed by Buttlar and Roque (1994) and Roque et al. (1997) to obtain dynamic modulus and phase angle from Superpave IDT tests. The tests were performed at room temperature for 1000 loading cycles on one mixture at four frequencies: 0.33, 1.0, 4.0, and 8.0 Hz. Kim observed significant changes in complex modulus during the first 20 to 30 cycles of loading, after which the results stabilized. For all frequencies evaluated, the dynamic modulus remained constant between 100 and 1000 cycles of loading, which indicates that a certain number of cycles must be applied before steady state conditions are reached. The resulting testing and interpretation methodology for Superpave IDT complex modulus testing, described in Chapter 10, will be used in this study.

11.5 Material and Methods

11.5.1 Materials

The same six dense-graded mixtures were tested that were previously discussed in Chapter 10. Nine test specimens were obtained for each mixture from field cores taken from test sections associated with the evaluation of top-down cracking in Florida. Four test sections were from I-75: two in Charlotte County and two in Lee County. The other two sections were from SR 80 located in Lee County in southwest Florida. A total of 54 field specimens were prepared for the Superpave IDT. In addition, extraction and binder recovery was performed to determine binder and mixture properties. Extracted binder and mixture properties are presented in Table 11-1 and mixture gradations are shown in Figure 11-1.

Table 11-1. Material Properties

Name	Air Void (%)	Gmb	Gmm	Effective AC (%)	Viscosity (Poise)
I75-1U	2.53	2.242	2.242	4.92	7773
I75-1C	4.13	2.274	2.274	4.83	10844
I75-2U	5.32	2.241	2.241	3.90	12001
I75-3C	5.81	2.190	2.190	4.41	13812
SR 80-2U	6.13	2.213	2.213	3.84	64408
SR 80-1C	4.24	2.197	2.197	4.32	34635

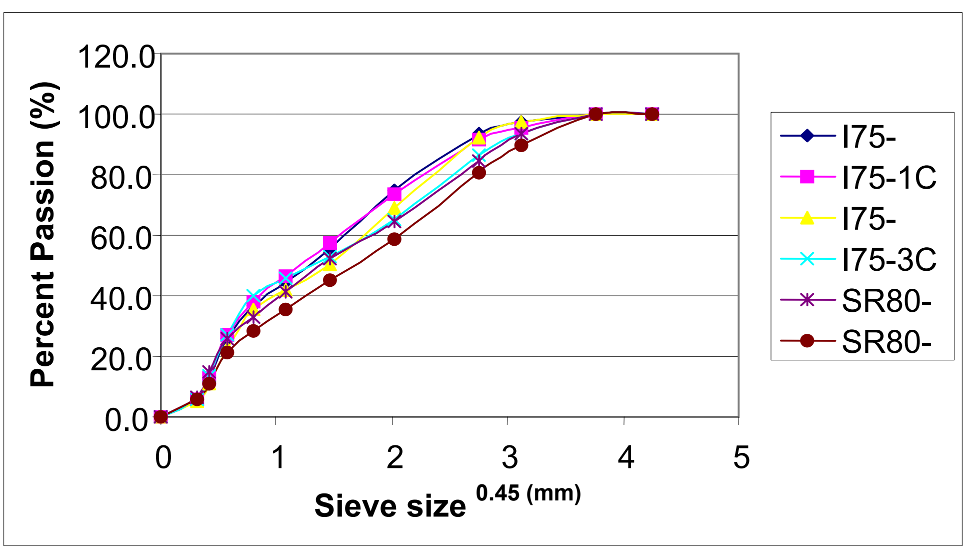

Figure 11-1. Gradation

11.5.2 Testing Equipment

The basics of the test equipment and data acquisition system has been specified by Buttlar and Roque (1994), Roque et al. (1997), and AASHTO TP-9. Additional information on the specific testing system used in this study is as follows:

- An environmental chamber was used to control specimen temperature. The chamber is capable of maintaining temperatures between –30° C and 30° C with an accuracy of +0.1° C.
- Loads control and data acquisition system used was accomplished with the MTS Teststar IIm system. A data acquisition program was written specifically for complex modulus tests.
- Vertical and horizontal deformation measurements were obtained using extensom-eters designed by MTS specifically for use with the Superpave IDT. A gage length of 1.5 in was used for all specimens.

11.6 Testing Procedure

11.6.1 Static Tests

Resilient modulus, complex modulus, creep compliance, and strength tests were performed on the same specimens using the Superpave IDT. A total 54 specimens from 6 mixtures were tested at three temperatures: 0°, 10°, and 20° C. Specific testing procedures for the resilient modulus, creep compliance, and strength tests were specified by Roque and Buttlar (1992), Buttlar and Roque (1994), and Roque et al. (1997).

11.6.2 Dynamic Tests Using Superpave IDT

A continuous sinusoidal load was applied to the specimen. The load was selected to maintain a horizontal strain amplitude of between 35 and 65 micro-strain. It was determined that the relative ratios between noise and true signal measured by the extensometers resulted in insignificant errors related to data interpretation within this strain range. Since prior work by Kim (2002) showed the dynamic modulus values did not change between 100 and 1000 load cycles, testing was limited to 100 load cycles. This reduced the potential for micro-damage to affect the test results due to accumulated creep strain. In fact, the accumulated creep strain at the end of testing, for tests performed at all temperatures and loading frequencies, was limited to between 65 and 130 micro strain. This is well below the maximum recommended strain to stay within the linear viscoelastic limit of asphalt mixtures, which was conservatively determined to be in the order of 500 micro strain in earlier work performed with the Superpave IDT (Buttlar and Roque, 1994). In addition, a 10-minute rest period was allowed between tests to further minimize the potential effect of accumulated creep strain.

Test specimens were obtained from 6 in. diameter field cores from which 1-in. thick slices were taken using a water-cooled masonry saw that produces smooth and parallel faces. Three specimens were tested at each of three test temperatures for each mixture. Each specimen was tested at the following five frequencies: 0.33, 0.5, 1.0, 4.0, and 8.0 Hz. In all cases, the highest frequency test was performed first as recommended by ASTM D 3497. Additional details on the testing procedures used are as follows:

- After cutting, all specimens were allowed to dry in a constant humidity chamber for a period of two days.
- Four brass gage points (5/16-inch diameter by 1/8-inch thick) were affixed with epoxy to each specimen face.
- Extensometers were mounted on the specimen. Horizontal and vertical deformations were measured on each side of the specimen.

- The test specimen was placed into the load frame. A seating load of 8 to 15 pounds was applied to the test specimen to ensure proper contact of the loading heads.
- The specimen was loaded by applying a repeated and continuous sinusoidal load, where strain amplitude was adjusted between 35 and 65 micro strain.
- When the applied load was determined, a total of 100 cycles were applied to the specimen, and the computer software recorded the test data.
- As mentioned earlier, a 10-minute rest period was allowed between tests at different frequencies.

11.7 Development of Data Analysis Procedure

11.7.1 Creep Compliance Test

The aim of this study was to compare creep compliance obtained from static and cyclic load tests. An additional goal was to compare the power law parameters resulting from compliances obtained from each mode of loading. The following power law relationship was used to represent the time dependent creep compliance:

$$D(t) = D_0 + D_1 t^m \quad (11.5)$$

Since tests were performed at three temperatures, a single set of power law parameters were determined by fitting a master compliance curve obtained by shifting compliance data obtained at multiple temperatures to a single reference temperature. The procedure described by Buttlar et al. (1998) was used to generate the power model for the master curve. Consequently, master curves were developed for each of the six mixtures tested.

11.7.2 Complex Modulus Test

Data Fitting Algorithm. A data analysis system was developed for determination of complex modulus from the Superpave IDT. The new data analysis system was previously discussed in Chapter 10.

Analysis of Superpave IDT Data. The Superpave IDT, which was developed by Roque and Buttlar (1992) as part of the strategic highway research program (SHRP), uses two main data analysis principles: true strains must be determined by eliminating the bulging effect that occurs due to the three-dimensional geometry of specimens; and Poisson's ratio must be accurately determined from vertical and horizontal measurements. This basic analysis concept was modified and adopted for use with the complex modulus test. The details of the new Superpave IDT analysis procedure are discussed in Chapter 10.

11.7.3 Creep Compliance from Complex Modulus Test

Conversion Process. Creep compliance data is generally expressed using a well-known power function (Eq. 11.6). Equation 11.7 presents the Fourier transform version of the power law (Finley et al., 1976). This function was used by Zhang et al. (1997b) to directly obtain the power model parameters (D_0, D_1, and 'm') from the real part of complex compliance. Zhang et al. (1997b) used the following two-step regression algorithm to find the power model parameters (D_0, D_1, and 'm') was used: (a) guess initial unknown 'm' value (i.e., it should be between 0 and 1); and (b) find D_0 and D_1using linear regression (i.e., once the m-value was determined, Eq. 11.7) becomes a linear function having two unknown values). Repeat this process until the guessed 'm' value has least square errors, where x-axis data are time and y-axis data are $D'(\varpi)$ from the complex modulus test.

$$D(t) = D_0 + D_1 \bullet t^m \tag{11.6}$$

$$D'(\omega) = D_1 \bullet \frac{\Gamma(m+1)}{\omega^m} \bullet \cos\left(\frac{m \bullet \pi}{2}\right) + D_0 \tag{11.7}$$

$$D'(\omega) = \frac{1}{|E^*|} \bullet \cos(\phi) \tag{11.8}$$

where D_0, D_1, m = power model parameters;

t = time;

ϖ = frequency;

Γ = gamma function;

$D'(\varpi)$ = the real part of complex compliance;

$|E^*|$ = dynamic modulus; and

ϕ = phase angle.

Master Curve. The master curve describes the viscoelastic response of asphaltic materials as a function of time, or frequency, and temperature. Once determined, the master curve allows for the determination of compliance at any temperature and loading time or frequency. This is particularly useful for determination of creep compliance at longer loading times at lower temperatures, which can be determined through the master curve concept by using data obtained from short loading time tests at higher temperatures.

In order to generate a reasonable master curve, the shifting of the master curve needs to be carefully considered to fit the test data properly. One of the most well-known methods to generate the mater curve employs the WLF (Williams et al., 1955) equation, which has been used successfully to represent the compliance of asphalt binder (Christensen and Anderson, 1992). The sigmoidal function, which involves a non-linear regression (Pellinen and Witczak, 2002; Kim et al., 2002), has been used successfully to generate master curves for complex modulus from uniaxial or triaxial tests performed over a wide range of temperatures. These researchers recommended the use of the real component of the complex modulus to determine master curves. The IDT is usually performed at relatively low in-service temperatures (below 30° C) so it may be possible to use a simpler and more practical function to generate the master curve for $D'(\varpi)$ (the real part of complex compliance) from complex modulus data. Buttlar et al. (1998) developed an approach to construct the creep compliance master curve from Superpave IDT data. The approach involved fitting a second-degree polynomial function to the log compliance-log time data at each temperature in order to minimize the effects of irregular creep compliance data and to obtain sufficient overlap in data between different temperatures to allow for accurate shifting (i.e., if the creep compliance data do not have a sufficient overlap, then it can be extended using the polynomial function obtained). The authors have found that a second-degree polynomial function accurately fits measured compliance data obtained at a single temperature, which is the only time the function is used in the process. The data represented by the polynomial functions are then shifted to obtain shift factors and a regression analysis is performed to determine the creep compliance power law parameters resulting in the best fit. Buttlar et al. (1998) developed a computer program (MASTER) that automatically performs this analysis and generates a master curve. The general approach is presented in Figures 11-2 to 11-4. The program was used to generate one master curve for $D'(\varpi)$ using the following shifting and fitting regression algorism: (a) define the region 1 and region 2 (Figure 11-2); (b) shift curve 2 by using a initial shift factor selected from region 1; (c) shift curve 3 over the region 2 for the shift factor selected from region 1; (d) fit the combined data from curve 1, the shifted curve 2, and the shifted curve 3 as a second-degree polynomial function; and (e) store regression coefficients and least square errors. Go back to the regression process (b) and select another shift factor from region 1 and repeat the overall regression process steps (c) through (e) until minimum least square errors are achieved. Figure 11-3 shows a master curve using the shifting and fitting regression algorithm, and Figure 11-4 shows shift factors where reference temperature was 0° C.

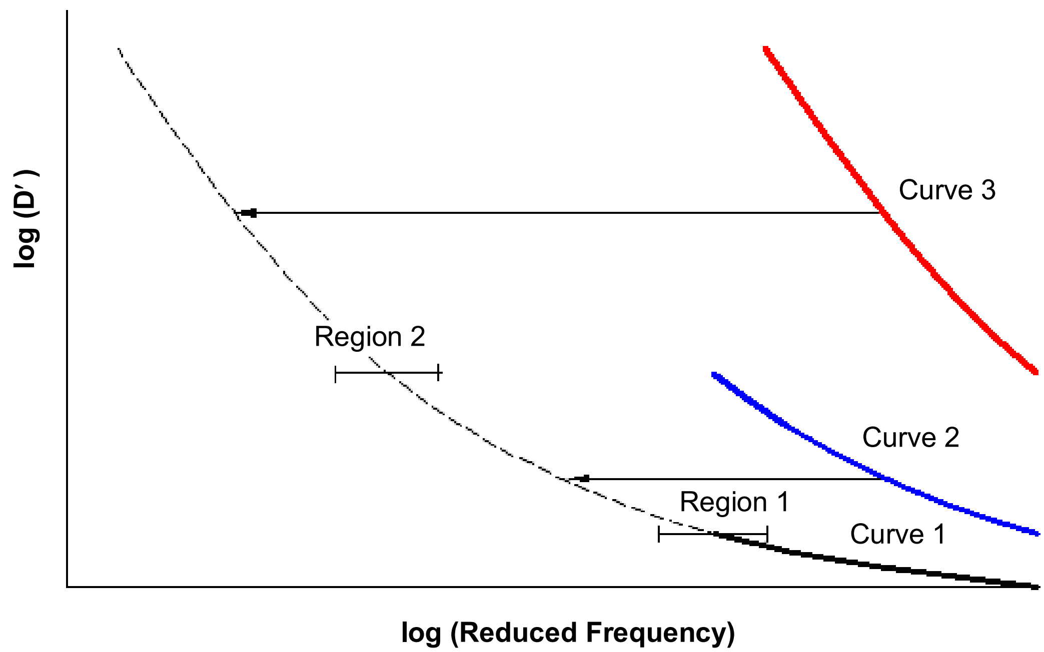

Figure 11-2. Shifting procedure

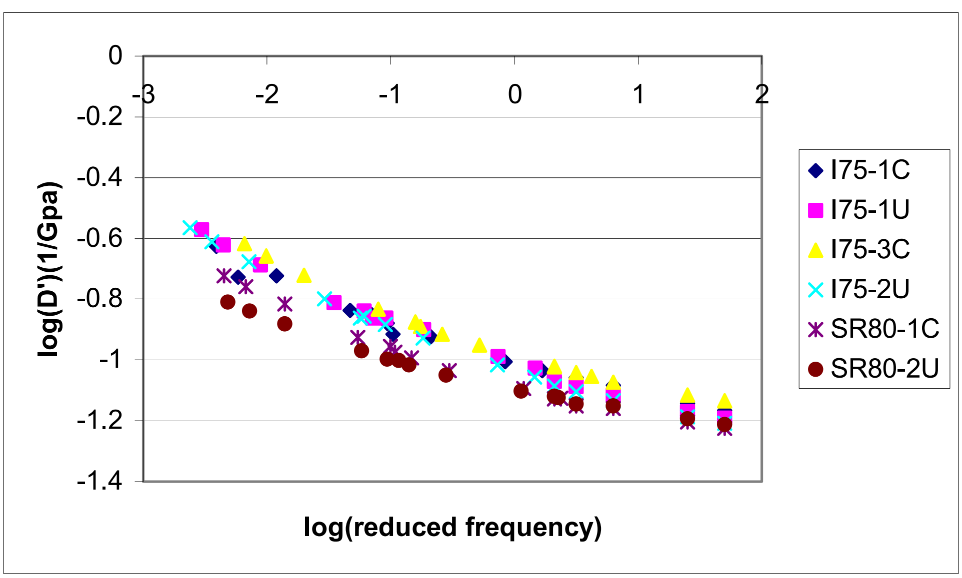

Figure 11-3. Master curve of D′ (ϖ)

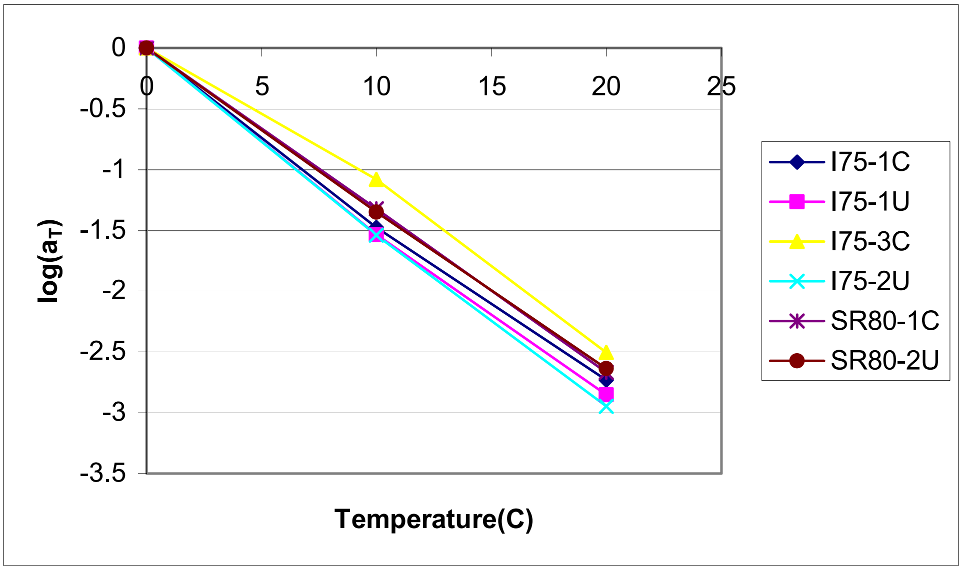

Figure 11-4. Shifting factors

Overall Procedure to Obtain Creep Compliance from Complex Modulus. The total of 54 field samples from 6 mixtures was tested using the Superpave IDT at three temperatures: 0°, 10°, and 20° C. The complex modulus test was performed right before the creep compliance test for five frequencies, 0.33, 0.5, 1, 4, 8 Hz. Six master curves were generated from the complex modulus data obtained, and then each master curve was converted to the creep compliance using the conversion procedure described above.

11.8 Results

11.8.1 Complex Modulus Test

The complex modulus test was performed with the Superpave IDT on a total of 54 field specimens from 6 state road sections to evaluate the testing and analysis system developed and described above. Dynamic properties such as |E*|, phase angle, E′ and E″ were successfully calculated with data analysis program developed (ITLT_dynamic).

Figure 11-5 shows the relationship between dynamic modulus and phase angle for all mixtures, test temperatures, and frequencies involved this study. In general, the dynamic modulus showed an increasing trend as temperature decreased or frequency increased. Conversely, the phase angles showed a decreasing trend as temperature decreased, or frequency increased. These are obviously reasonable and expected trends, since asphalt mixture becomes stiffer and more elastic as test temperature decreases or frequency increases. Conversely, asphalt stiffness decreases and viscous response increases as temperature increases or frequency decreases.

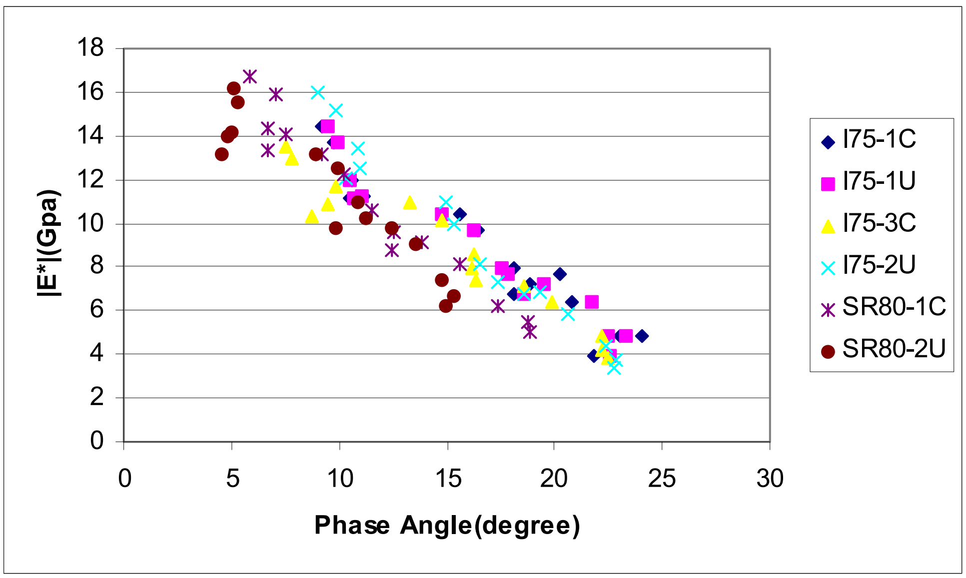

Figure 11-5. Dynamic modulus and phase angle

As shown in Table 11-2, Poisson's ratios determined from complex modulus tests for the range of mixtures, frequencies, and temperatures involved in this study were within the range generally accepted as being reasonable for asphalt mixture. The authors' extensive experience with the Superpave IDT has indicated that obtaining reasonable values of Poisson's ratio is an excellent indicator of the quality of the test data obtained. This indicates that the complex modulus values obtained from the Superpave IDT are probably also reasonable. However, it should be noted that as in all dynamic testing, the proper application of a sinusoidal loading waveform is also critical.

Table 11-2. Poisson's Ratios

Temperature (° C)	Frequencies (hz)	Sections (Poisson's ratio)					
		I75-1C	I75-1U	I75-3C	I75-2U	SR80-1C	SR80-2U
0	0.333	0.33	0.35	0.30	0.32	0.36	0.22
	0.5	0.29	0.34	0.30	0.31	0.33	0.23
	1	0.29	0.34	0.30	0.30	0.33	0.23
	4	0.30	0.31	0.33	0.30	0.34	0.25
	8	0.29	0.31	0.30	0.29	0.33	0.25
10	0.333	0.38	0.37	0.42	0.38	0.38	0.31
	0.5	0.40	0.35	0.41	0.37	0.41	0.31
	1	0.37	0.32	0.40	0.35	0.40	0.31
	4	0.37	0.32	0.37	0.35	0.39	0.31
	8	0.34	0.32	0.36	0.35	0.40	0.29
20	0.333	0.44	0.42	0.38	0.38	0.33	0.40
	0.5	0.49	0.41	0.36	0.39	0.33	0.41
	1	0.41	0.41	0.35	0.36	0.33	0.38
	4	0.43	0.39	0.35	0.36	0.35	0.39
	8	0.40	0.39	0.32	0.38	0.35	0.37
Average		0.37	0.37	0.36	0.35	0.35	0.36

11.8.2 Comparison Between Creep Compliances From Static and Cyclic Tests

Based on the regression algorithm using conversion Eq. 11.7 discussed earlier, the master curves of D′ (ϖ)s from each data set (six sections) were converted to power model parameters (D_0, D_1, and 'm') for comparison with conventional creep compliance parameters from static tests using the Superpave IDT. The creep compliance test was performed based on procedures described by Buttlar and Roque (1994), and AASHTO TP-9 for 100 sec duration. The same conditions (testing equipment, specimens, and temperatures) were used to limit the potential differences between static and dynamic results.

Table 11-3 shows that power model parameters from static and dynamic tests were different. Figure 11-6 illustrates the key differences between the creep compliance relationships as determined from the two different testing modes. In general, the dynamic test data underestimates the long-term creep response, which is reflected in the lower m-value for the dynamic test. Conversely, the static test data appears to overestimate the short-term response, which is reflected in the higher D_0 value for the static test.

Table 11-3. Power Model Parameters From Two Tests

Name	Static Creep Test			Cyclic Creep Test		
	D_0 (1/Gpa)	D_1 (1/Gpa)	m	D_0 (1/Gpa)	D_1 (1/Gpa)	m
I75-1C	6.57E-02	2.25E-02	0.454	5.09E-02	5.43E-02	0.237
I75-1U	8.75E-02	2.31E-02	0.49	4.67E-02	5.80E-02	0.256
I75-3C	9.04E-02	1.34E-02	0.531	5.96E-02	5.31E-02	0.285
I75-2U	7.29E-02	1.58E-02	0.479	4.67E-02	5.33E-02	0.268
SR80-1C	6.31E-02	7.30E-03	0.488	4.94E-02	3.84E-02	0.276
SR80-2U	6.57E-02	9.14E-03	0.402	5.05E-02	3.45E-02	0.238

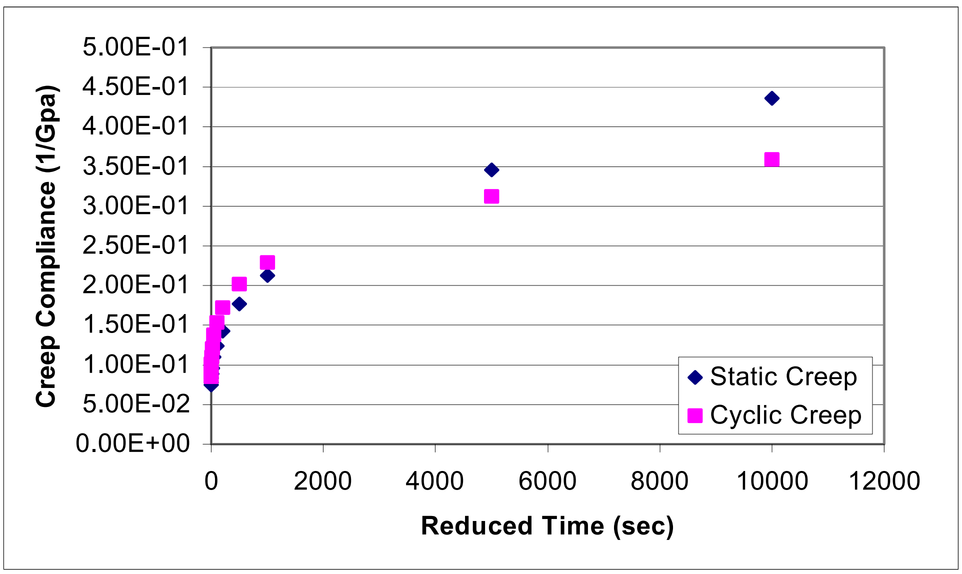

Figure 11-6. General trend of creep compliances

Upon further reflection, these results are reasonable and consistent with the sensitivity of each type of test to different response times. Static or constant stress creep tests are generally run for longer time periods, and their static nature makes the determination of the long-term creep response more accurate and reliable. However, it is difficult to accurately apply the load quickly enough in static creep tests to obtain reliable response measurements for definition of short-term response. The reverse is true for dynamic tests, which allow for very accurate application of short-term loads and measurement of associated response, but for which it is very difficult to apply low enough frequencies to obtain reliable response at longer loading times. One would lose the advantage of performing cyclic tests if one were to use frequencies that are low enough to obtain long-term response accurately (i.e., one may as well run a static test, which is simpler and generally more reliable).

Based on the observations presented above, it appears that the power model parameter D_0, which is primarily dependent on the mixture's short-term response, can be more accurately determined from dynamic tests. Conversely, the parameters D_1 and m-value, which are primarily dependent on the mixture's long-term response, can be more accurately determined from static creep tests.

11.8.3 Comparison Between Power Model Parameters From Static and Cyclic Tests

Figures 11-7 to 11-9 compare power model parameters from static and dynamic tests. The parameters D_1 and m-value are important to predict thermal stress or load-induced fatigue cracking in asphalt mixture (Zhang et al., 2001; Hiltunen and Roque, 1994). The comparisons indicate that although the values are quite different, the general trend of the parameters is very similar between the two test methods. In other words, the parameters from one test method are well correlated with those of the other. This implies that either test method would result in similar comparisons between any one of the parameters obtained from two different mixtures. However, prior work by Roque et al. (AAPT 2004) has shown that mixture performance cannot be properly evaluated on the basis of any single parameter. Instead, the effects of the parameters must be considered together in the context of a fracture model that appropriately accounts for their relative effects. Consequently, the magnitude of

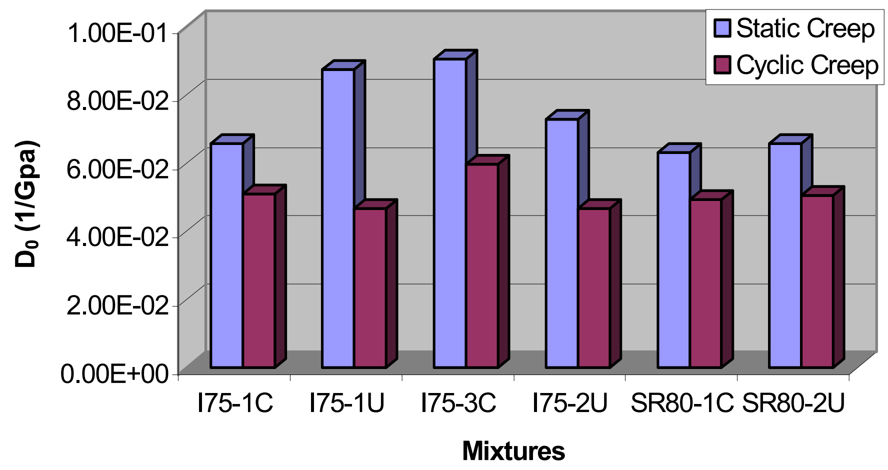

Figure 11-7. Power model parameter, D_0

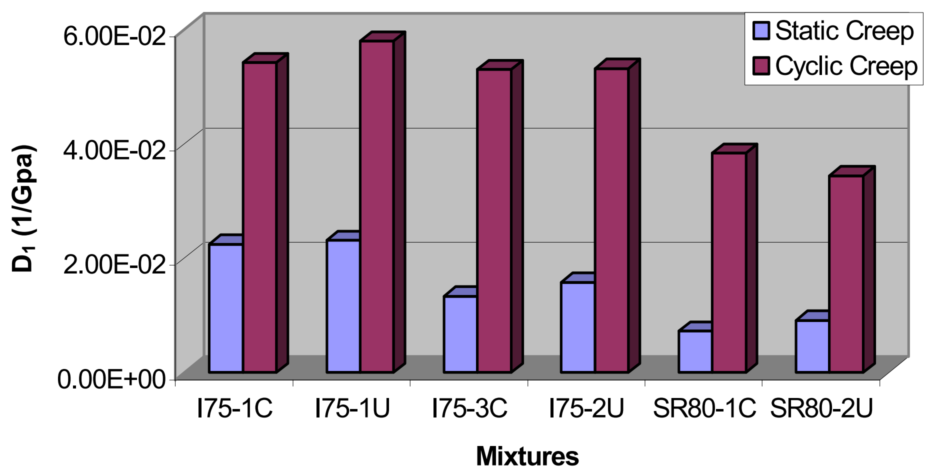

Figure 11-8. Power model parameter, D_1

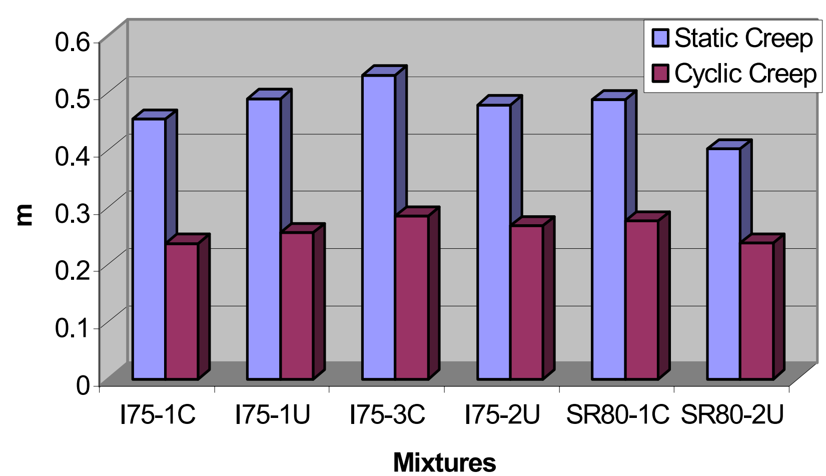

Figure 11-9. Power model parameter, m

the parameters, and not just their relative ranking, is also important for proper evaluation. The challenge is to identify an approach to accurately determine the power law parameters using static creep tests, dynamic creep tests, or a combination of both.

11.8.4 Obtaining Creep Compliance Accurately and Efficiently

The discussion above indicates that it may be difficult, if not impossible, to obtain long-term creep response accurately from dynamic tests performed in the typical range of frequencies (0.1 Hz or higher), and that it may be difficult or impossible to obtain short-term response accurately from static creep test data. In other words, static creep tests are better suited for determination of power law parameters D_1 and m-value, whereas D_0 can be obtained more reliably from dynamic tests. The effects can be observed in the simple rheological model presented in Figure 11-10, which indicates that D_0 represents the purely elastic or time-independent behavior of the mixture. Consequently, one can isolate this response by performing tests at higher frequencies, such that the time-dependent components do not contribute much to the response of the material. In fact, if one could test at a high enough frequency, approaching the point where the load is applied in zero time (obviously impossible), then one could approach the true D_0 of the material. In practice, an estimate of this value can be obtained by extrapolating dynamic modulus data obtained at different frequencies to predict the dynamic modulus of the material at zero phase angle, which corresponds to the purely elastic behavior of the material. Thus, an accurate estimate of D_0 can be obtained by taking the inverse of the dynamic modulus at zero phase angle (E_0) through extrapolation of the data shown in Figure 11-5.

One would expect that the D_0-values obtained in this manner should be very similar to those obtained from interpretation of complex compliance data. Figure 11-11 shows that for all mixtures tested, the values were almost identical, indicating that D_0-values obtained from dynamic modulus tests appear to be accurate.

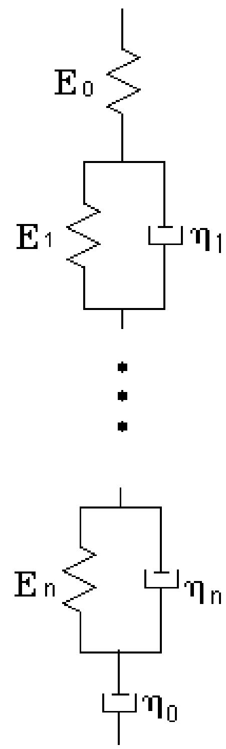

Figure 11-10. Rheological viscoelastic model

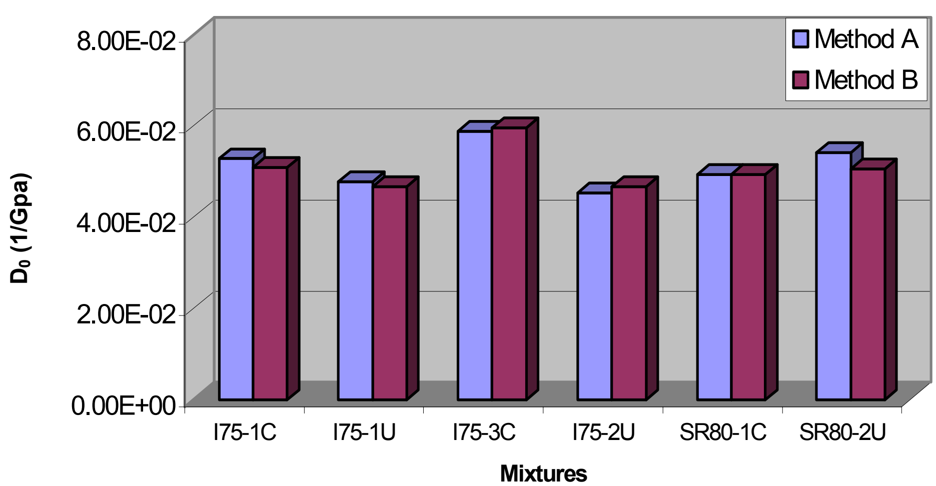

Figure 11-11. Comparison between D_0-values

Note that the power model parameters, D_0, D_1, and m-value determined from creep compliance data are interrelated. Once any of the parameters is changed, the values of the other parameters are inevitably affected. Consequently, the values of D_1 and m-value obtained from static creep tests should be corrected to account for the fact that D_0 determined from the static data alone is inaccurate. A more accurate approach would be to obtain D_0 from dynamic test data, then use the static creep data to determine D_1 and m-value only.

Figures 11-12 and 11-13 show a comparison of D_1 and m-values determined by these two different approaches (method A is based on static creep data only; method B is based D_0 from dynamic tests and D_1 and m-value from static creep data). As shown in the figures, method B results in a lower D_1 and slightly higher m-value for all mixtures evaluated.

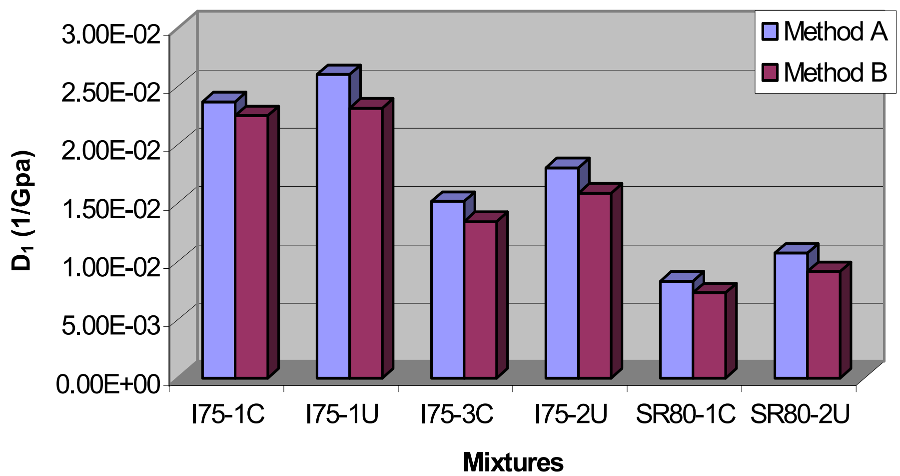

Figure 11-12. Corrected power model parameter, D_1

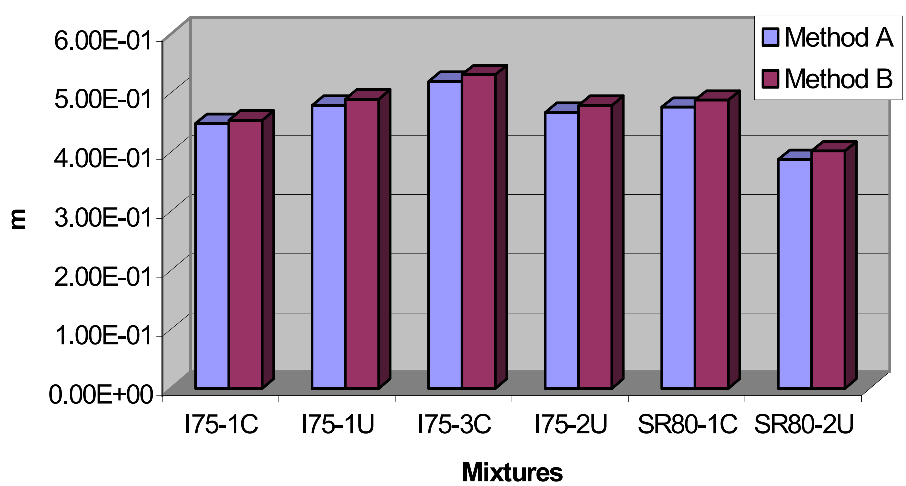

Figure 11-13. Corrected power model parameter, m

11.9 Summary and Conclusions

The test methods, data acquisition and data reduction procedures established in Chapter 10 were used for the determination of complex modulus and phase angle from cyclic load tests with the Superpave IDT. Tests performed at multiple frequencies on six different asphalt mixtures obtained from field test sections indicated that dynamic modulus and phase angle values were within reasonable and expected ranges, and exhibited appropriate trends. Analytical procedures were developed to convert complex modulus and phase angle values at multiple frequencies to creep compliance as a function of time.

Static creep tests were performed on the same mixtures using the Superpave IDT to compare creep compliance and creep compliance power law parameters to those derived from the cyclic test data. Significantly different power law parameters were obtained, and it was determined that static tests resulted in more accurate determination of the parameters that describe the longer-term creep response (D_1 and m-value), while dynamic tests resulted in more accurate determination of D_0, which describes the short-term elastic response.

An approach was developed and proposed to determine creep compliance parameters accurately by combining the results of dynamic and static tests. Cyclic tests performed at a minimum of two loading frequencies are first used to define D_0 as the inverse of the extrapolated dynamic modulus at zero phase angle (E_0). D_1 and m-value are then obtained from the static creep data, using this pre-determined value of D_0.

This work implies that for the normal range of testing frequencies used in laboratory dynamic testing of asphalt mixture, it may not be possible to accurately define the long-term creep response of the mixture. Use of creep data obtained in this fashion may result in serious errors in prediction of dissipated creep strain and damage in asphalt mixture.

CHAPTER 12
THE PHASE ANGLE IN THE DYNAMIC COMPLEX MODULUS TEST

An often-stated advantage of the complex modulus is that the dynamic modulus is that the phase angle, δ, is an indicator of the viscous properties of the material being evaluated. For a pure elastic material, δ = 0, and for pure viscous material, δ = 90 degrees (e.g., Witczak et al., 2002). In particular, for the complex modulus test, the assumption is made that the phase lag is due to viscous effects in the material. Many researchers have proposed ways to extract creep compliance properties from the dynamic modulus and the phase angle (e.g., Witzcak et al., 2002; Zhang et al., 1997).

The recently developed Hot Mix Asphalt Fracture Mechanics framework (Zhang et al., 2000; Roque and Birgisson, 2002) assumes that microdamage in asphalt mixtures is directly related to the creep rate of the mixture, as described by the dissipated creep strain energy (DCSE) per cycle. The higher the creep rate, the greater the microdamage, after a given number of loading cycles. In this chapter, the HMA fracture mechanics framework will be reviewed briefly, followed by an evaluation of the use of short term dynamic measurements for obtaining creep rate properties for mixtures as an input for the HMA fracture mechanics model. A comparison between creep rates obtained from dynamic and static tests will be performed. The results show that the phase angle in the complex modulus test includes other effects, besides viscous effects, thus resulting in differences between the rate of creep obtained from static and dynamic tests. The results illustrate that short-term dynamic measurements cannot generally be used to obtain input properties for the HMA fracture mechanics framework. However, first the materials and methods used will be reviewed briefly.

12.1 Material and Methods

12.1.1 Materials

The same six dense-graded field pavement sections described in Chapter 10 were used in this part of the study. Four test sections were from I-75 where two in Charlotte County and two in Lee County and two test sections were from SR 80 in Lee County Florida. Six-inch diameter mixtures taken from each section were cut by an electric saw, which allows mixtures to be sliced into a predefined thickness, approximately 1.5 inches. Three test specimens were obtained for each mixture from field cores taken from test sections associated with the evaluation of top-down cracking in Florida. A total of fifty-four specimens were prepared for indirect tensile test (Superpave IDT) and three temperatures, 0°, 10°, and 20° C were selected to evaluate the performance of predefined cracked or uncracked asphalt pavement sections. In addition to the dynamic modulus testing, discussed in Chapter 10, additional testing included resilient modulus testing, static creep testing, and strength testing.

12.1.2 Pavement Structure

The layer moduli for each of the pavement test sections described in Chapter 10 were determined with the Falling Weight Deflectometer (FWD). The values were then back calculated using elastic layer analysis. The FWD procedure used the standard SHRP configuration for the sensors (i.e., 8″, 12″, 18″, 24″, 36″, and 60″). For each section, ten tests were conducted in the travel lane in the wheel path at relatively undamaged locations, on both sides of the coring area. A half-inch hole was drilled in the pavement and filled with mineral oil or glycol for heat transfer and the pavement temperatures were recorded. The pavement surface and ambient temperatures were also recorded. A 9-kip seating load was applied, followed by 7-, 9-, and 11-kip loads. Deflection measurements at each of the sensors were recorded. The layer thickness and back-calculated moduli appear in Tables 12-1 and 12-2, respectively. The base and sub-base thickness were not available so a typical thickness of 12 inches was assumed for the back calculation analysis.

Table 12-1. Thickness of the Layers (in.)

Section	Friction Course	AC	Base	Sub-base
I75-1U	0.44	6.23	12	12
I75-1C	0.51	6.54	12	12
I75-2U	0.46	7.42	12	12
I75-3C	0.62	6.47	12	12
SR 80-2U	0.80	6.29	12	12
SR 80-1C	0.37	3.38	12	12

Table 12-2. Layer Moduli for Each Section (ksi)

Section	AC	Base	Sub-base	Sub-grade
I75-1U	1000	64	51	36
I75-1C	800	55	50	30
I75-2U	1000	107	90	31
I75-3C	900	60	35	36
SR80-2U	500	57	46	19
SR80-1C	800	44	61	28

12.1.3 Testing Procedures

The standard test procedure for complex modulus is described in ASTM D 3497 which recommends three test temperatures (41° F, 77° F, and 104° F) and three loading frequencies (1, 4, and 16 Hz). The testing protocol calls for sinusoidal loading starting at the lowest temperature and highest frequency, and proceeding to the highest temperature and the lowest frequency. The dynamic modulus test performed at University of Florida was conducted at the typical low temperature ranges, 0, 10, and 20° C, in Florida, and three frequencies, 0.333, 0.5, and 1 Hz during 100 sec loading time, which allowed obtaining both of the dynamic and static strain response at steady state. Also, as discussed in Chapter 10, the continuous sinusoidal load applied to the specimen was selected to maintain the horizontal strain amplitude of between 35 and 65 micro strain. Additional details on the dynamic modulus testing procedure used are discussed in Chapter 10.

Similarly, the basics of the Superpave IDT test equipment and test protocols for resilient modulus testing, static creep testing, and strength testing have been specified by Buttlar and Roque (1994), Roque et al., (1997), and AASHTO TP-9.

12.2 Dynamic Modulus Data Interpretation

In the dynamic modulus test, a continuous sinusoidal load with a constant stress amplitude σ_{avg} is applied to the specimen. The resulting strain time history, shown in Figure 12-1, can be divided into a permanent creep strain component and a short-term sinusoidal strain component with a phase lag due to damping that is quantified through the phase angle δ. In the small strain range, the linear viscoelastic superposition principle is valid, so each component of the strain or stress can be fitted with one of the following functions:

$$\sigma_{sta}(t) = \sigma_{avg} \tag{12.1}$$

$$\sigma_{dyn}(t) = \sigma_0 \bullet \sin(\omega t) \tag{12.2}$$

$$\varepsilon_{sta}(t) = \varepsilon_1 + \varepsilon_2 \bullet t^m \tag{12.3}$$

$$\varepsilon_{dyn}(t) = \varepsilon_0 \bullet \sin(\omega t - \delta) + \varepsilon_{sta}(t) \tag{12.4}$$

in which the sinusoidal stress, average stress, sinusoidal strain including the phase angle δ, and creep strain are noted as σ_{dyn}, σ_{sta}, ε_{dyn}, and ε_{sta} respectively, and ω is the angular frequency. In Eq. 12.3, the creep strain was determined at the last five loading cycles, recorded immediately before the 100-sec loading cycle. Figure 12-2 shows the resulting creep strain ε (t).

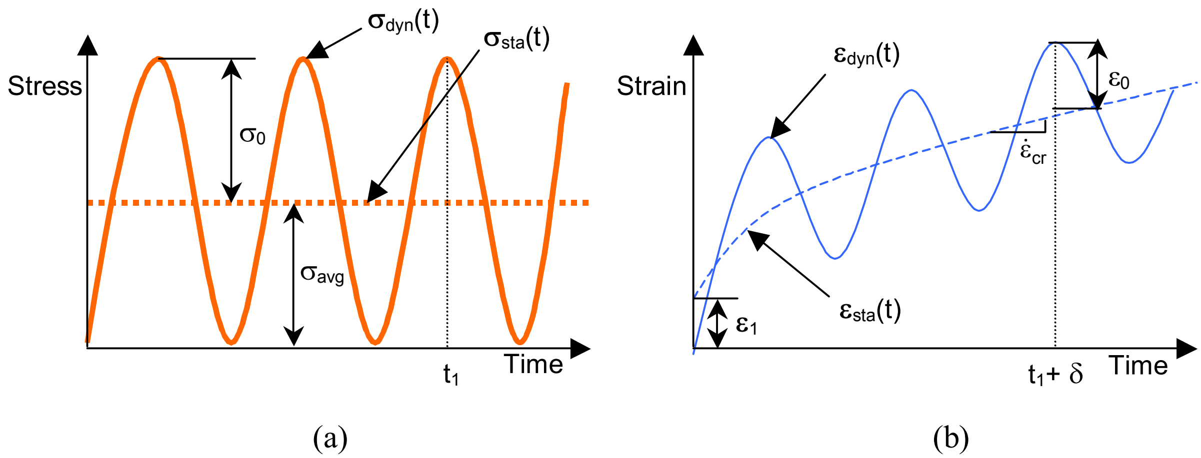

Figure 12-1. Applied cyclic stress and resulting strain in a dynamic test

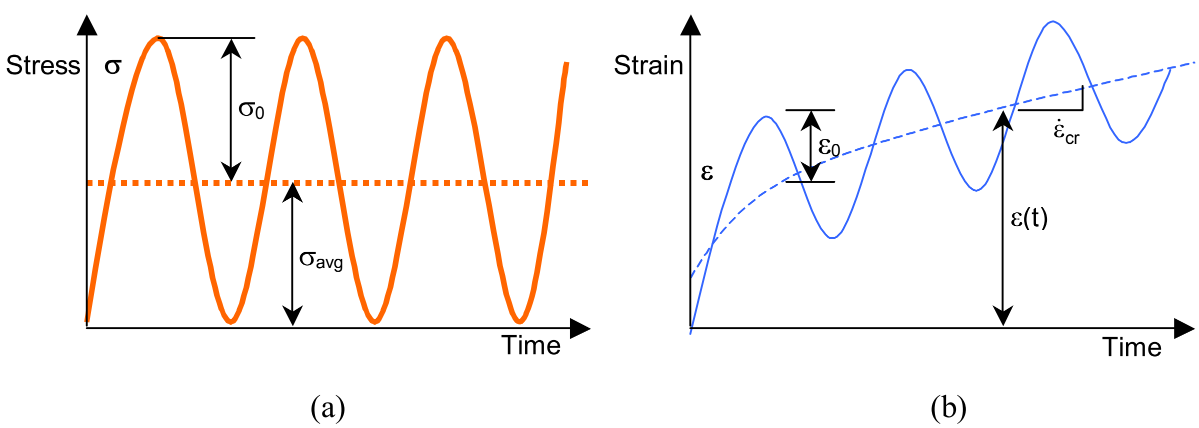

Figure 12-2. The superposition of short-term response and creep response during dynamic testing

12.3 HMA Fracture Mechanics

12.3.1 The Threshold Concept

The concept of the existence of a fundamental crack growth threshold is central to the HMA fracture mechanics framework presented by Zhang et al. (2001). The concept is based on the observation that micro-damage (i.e., damage not associated with crack initiation or crack growth) appears to be fully healable, while macro-damage (i.e., damage associated with crack initiation or growth) does not appear to be healable. This indicates that a damage threshold exists below which damage is fully healable. Therefore, the threshold defines the development of macro-cracks, at any time during either crack initiation or propagation, at any point in the mixture. As shown in Figure 12-3, if loading and healing conditions are such that the induced energy does not exceed the mixture threshold, then the mixture may never crack, regardless of the number of loads applied.

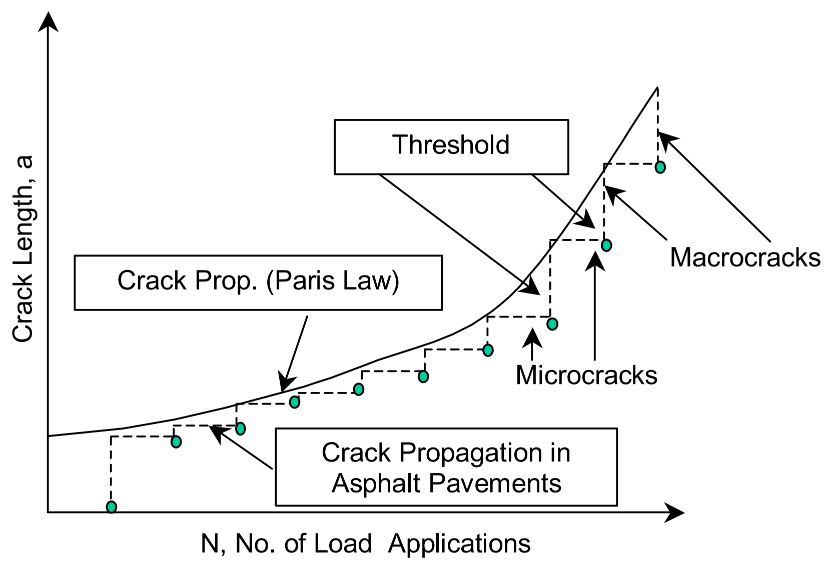

Figure 12-3. Illustration of crack propagation in asphalt mixtures

As discussed by Roque et al. (2002b), fracture (crack initiation or crack growth) can develop in asphalt mixtures in two distinct ways, defined by two distinct thresholds (Figure 12-4). First (case 1), continuous repeated loading using stresses significantly below the tensile strength would lead to cracking if the rate of damage accumulation exceeds the rate of healing during the loading period. The energy threshold associated with this case is lower than the threshold required to fracture the mixture with a single load application. Second (case 2), fracture would occur if any single load applied during the loading cycle exceeds the threshold required to fracture the mixture with a single load application. Finally, case 3 shows that fracture would not occur during a single load application unless the upper threshold is exceeded, even when the lower threshold is exceeded.

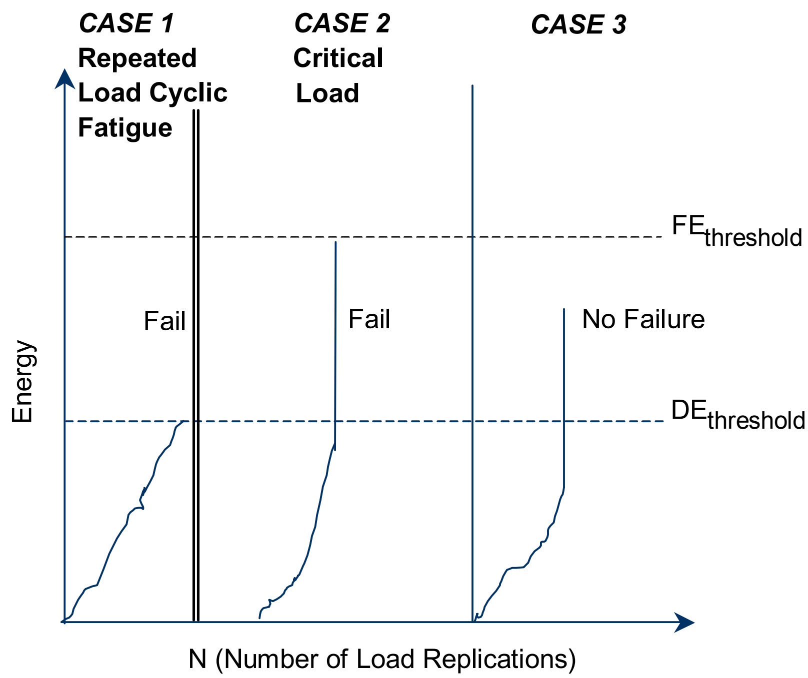

Figure 12-4. Illustration of potential loading condition (continuous loading)

It has been determined that the dissipated creep strain energy (DCSE) limit and the fracture energy limit (FE) of asphalt mixtures suitably define the lower and upper threshold values for cases 1 and 2, respectively. These parameters can be easily determined from the stress-strain response of a tensile strength test, as shown in Figure 12-5, and discussed by Roque et al. (2002b). It is necessary to know the elastic modulus of the mixture to determine the elastic energy at fracture. Thus, the FE limit and the DCSE limit account indirectly for the effects of strength, stiffness, strain to failure, as well as the viscoelastic response of mixtures.

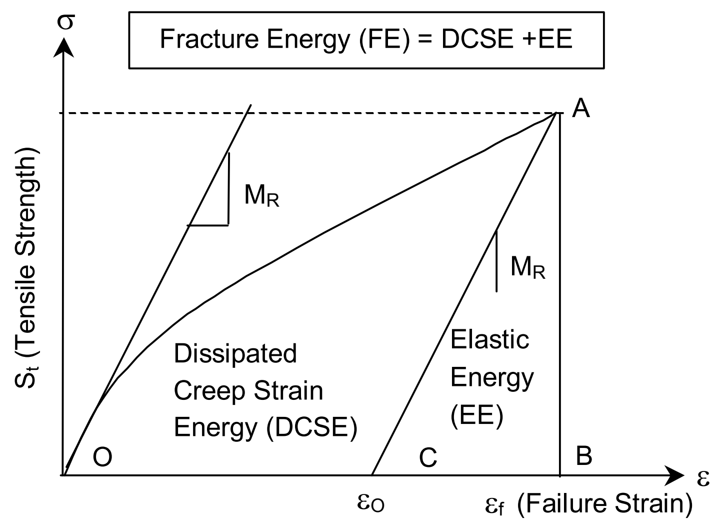

Figure 12-5. Determination of dissipated creep strain energy

12.3.2 Key HMA Fracture Mechanics Mixture Parameters

Based on the HMA fracture mechanics framework, there are four key parameters that govern the cracking performance of asphalt mixtures:

- FE limit: fracture energy at the initiation of fracture
- DCSE limit: dissipated creep strain energy to failure
- D_1 and m-value: parameters governing the creep strain rate.

In addition, mixture stiffness, as described by modulus, will affect stress distribution in the pavement system. Figure 12-6 shows the effects of the rate of creep, governed by D_1 and the m-value, on the rate of damage accumulation. The higher the rate of creep based on the D_1 and the m-value, the faster is the rate of accumulation of DCSE per cycle, and thus the faster the DCSE limit is reached. These parameters can be used not only to predict damage and crack growth in mixtures subjected to generalized loading conditions, but they are also suitable for use in the evaluation of changes in mixture performance due to water damage. For example, it is clear that cracking performance deteriorates as the DCSE limit decreases. Similarly, a lower creep rate will result in a lower rate of damage accumulation. However, a lower creep rate does not necessarily assure improved cracking performance, since mixtures with lower creep rates may also have lower DCSE limits and lower rates of healing.

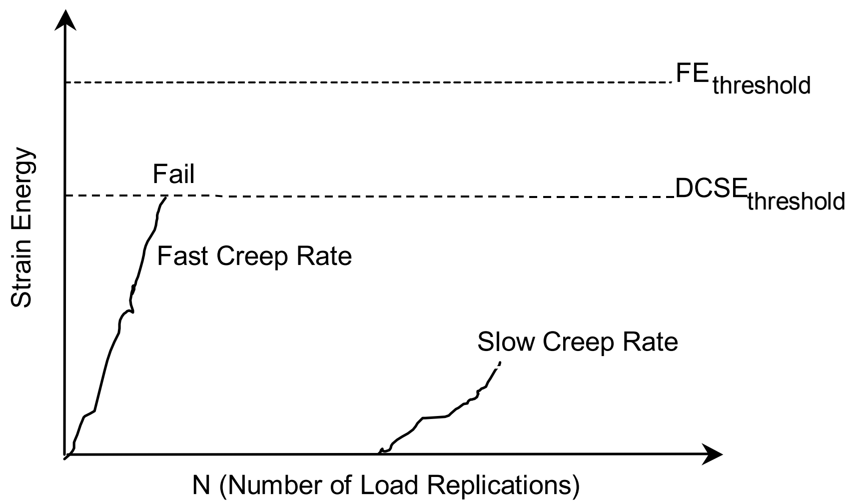

Figure 12-6. Effects of rate of creep and rate of creep on the rate of damage

12.4 Correspondence Between Creep and Dissipated Creep Strain Energy Limit

In a static creep test, a constant stress is applied at time zero, and the strain as a function of time is measured. Figure 12-7 shows the results of a static creep test, in which $\dot{\varepsilon}_{cr}$ is the rate of creep strain, and ε_{cr} is the amount of creep strain. In a viscoelastic material, three regions of creep are generally present – namely, primary creep, secondary creep, and tertiary creep. At the onset of tertiary creep, a macrocrack will form, and then propagate through the specimen. Kim (2003) reported that the dissipated creep strain energy up to the crack initiation during the creep test is approximately the same as the DCSE limit, shown in

Figure 12-5 in a strength test. Hence, for a static creep test, the accumulated DCSE as the start of tertiary creep can be denoted as:

$$DCSE_{LIMIT} = \int_0^{t_c} \sigma_0 \bullet \dot{\varepsilon}_{cr} dt \qquad (12.5)$$

in which t_c is the time of crack initiation (onset of tertiary creep), and σ_0 is the magnitude of static stress. Subsequently, the crack growth can be predicted using the crack growth law in the HMA fracture mechanics framework (Zhang et al., 2001).

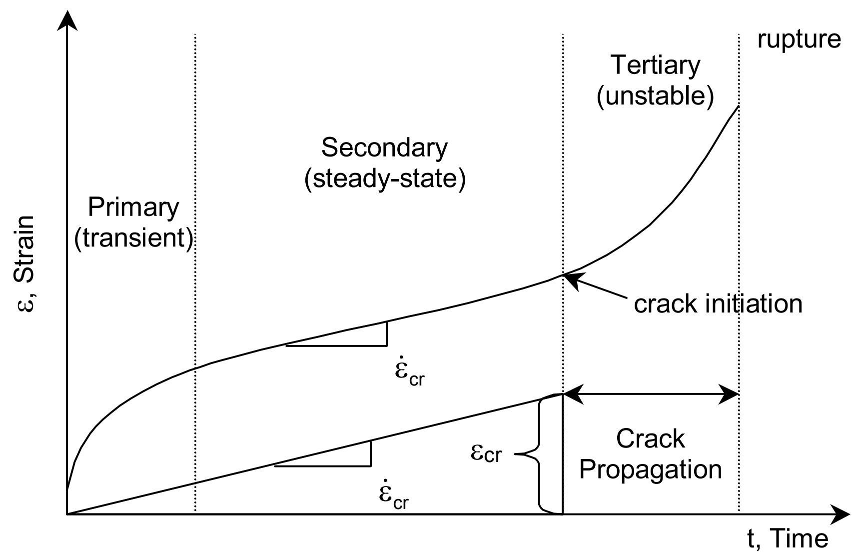

Figure 12-7. Typical strain vs. time behavior during creep

12.5 HMA Fracture Mechanics Crack Growth Law

The HMA crack growth law developed by Zhang et al. (2001) makes use of fracture mechanics theory along with the threshold concept and limits presented above. The basic elements of the law are illustrated in Figure 12-8, which shows a generalized stress distribution in the vicinity of a crack subjected to uniform tension. The specific stress distribution for a given loading condition will depend on several factors, including crack geometry and the failure limits of the specific mixture. The HMA fracture mechanics framework defined the area in front of crack tip where stress reaches a maximum limit as a "process zone." The crack will propagate by the length of the process zone when strain energy representing damage in that zone exceeds the appropriate energy threshold. The details of the development of the crack growth law are discussed by Zhang et al. (2001).

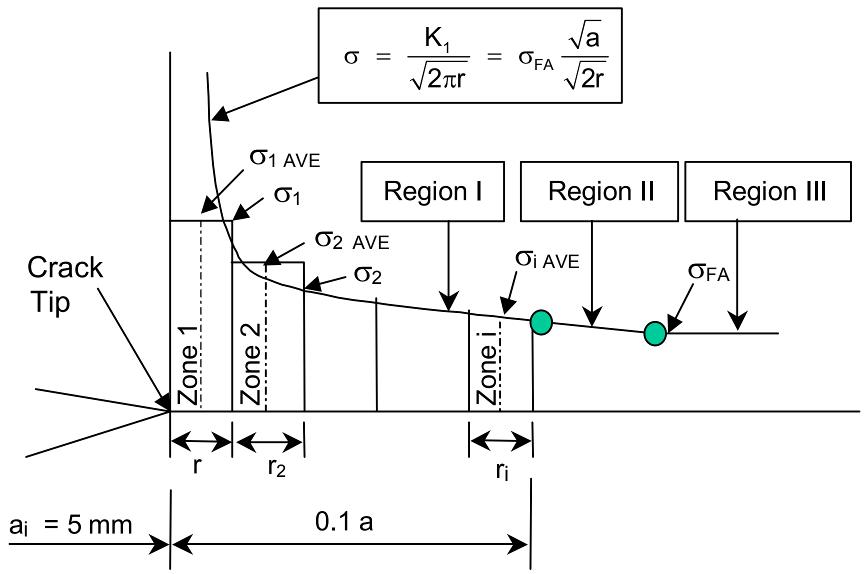

Figure 12-8. Stress distribution near the crack tip

Once a crack initiates, the length of the zone of maximum stress is predicted using fracture mechanics. The HMA fracture model describes discontinuous crack growth by increasing the crack length in increments equal to the length of each crack zone, shown in Figure 12-8. The crack will advance if the accumulated dissipated creep strain energy limit in the zone exceeds the dissipated creep strain energy limit of the mixture. The details of the development of the crack growth law presented are discussed by Zhang et al. (2001).

12.6 Testing Requirements and Fracture Parameters

As stated previously, the HMA fracture mechanics framework simply needs three types of tests, resilient modulus, creep compliance, and tensile strength obtained from the Superpave IDT. In case of creep compliance, the well-known power law is used to represent creep compliance D(t):

$$D(t) = D_0 + D_1 t^m \tag{12.6}$$

The power law parameters D_0, D_1, and m are determined through a linear regression of the measured creep compliance curve versus time. The parameters D_1 and m can also be also used to predict the rate of dissipated creep strain during secondary (or steady-state) creep (i.e., at t_{steady}) as follows:

$$\dot{\varepsilon}_{cr} = \sigma_0 \bullet D_1 \bullet m \bullet t_{steady}^{\,m-1} \tag{12.7}$$

Subsequently, the DCSE limit can be obtained, by denoting the onset of tertiary creep, followed by the integration of the creep rate, represented in Eq. 12.7.

12.7 Dissipated Creep Strain Energy Per Cycle

Energy released per each periodic cyclic loading may be expressed as dissipated creep strain energy per cycle (DCSE per cycle) in asphalt mixtures. Ordinarily, a pavement undergoes cyclic loading, which can be represented by either a haversine or sinusoidal signal. Sangpetngam (2003) mathematically derived the equivalency between DCSE per cycle during haversine loading and that obtained from a static creep test as shown below:

$$\text{DCSE per cycle} = \frac{\sigma_{max}^{\;2} \bullet D_1 \bullet m \bullet t^{m-1} \bullet T}{2} \quad \text{(haversine)} \tag{12.8}$$

in which t is the time determined under steady state loading conditions, shown in Figure 12-2, T is the period of cyclic loading, and σ_{max} is the maximum amplitude of cyclic loading. Subsequently, Sangpetgnam (2003) extended the equivalency to sinusoidal loading at any given frequency as follows:

$$\text{DCSE per cycle} = \frac{\sigma_{max}{}^2 \bullet D_1 \bullet m \bullet t^{m-1} \bullet T}{8} \quad \text{(sinusoidal)} \tag{12.9}$$

In the HMA fracture mechanics framework, both DCSE and DCSE per cycle are truly important fracture parameters, in terms of energy-based analysis. Nevertheless, the DCSE per cycle obtained from a cyclic test has not been validated for either haversine or sinusoidal cyclic loading tests.

In order to measure the DCSE per cycle experimentally during a dynamic test, two types of analytical methods were considered. The first one is based on the measurement of the area under the stress-strain hysteresis loop during dynamic testing, which is related to the phase angle. The second one is based on a determination of the rate of creep strain during a cyclic test. The rate of creep strain during the dynamic test is determined through an application of the linear viscoelastic superposition principle.

12.8 Dissipated Energy from the Area of the Stress-Strain Hysteresis Loop

Within the small strain range, the behavior of viscoelastic material may be explained through the theory of linear viscoelasticity (e.g., Findley et al., 1976). If an external loading source σ applies a constant cyclic amplitude of stress σ_0 to a viscoelastic to a specimen made of viscoelastic material, then the strain response ε will be an oscillation at the same frequency as the stress but lagging behind by a phase angle δ, shown in Figure 12-9(a), where ε_0 is the amplitude of the strain, ϖ is the angular frequency ($f = \varpi/2\pi$ is the cyclic frequency) and $T=2\pi/\varpi$ is the period of the oscillation. In this case, dissipated energy is denoted as ΔW, in which ΔW is the energy loss per cycle, shown in Figure 12-9(b). There is no energy loss per cycle if the stress and the stain are in phase, and hence $\delta = 0$. The amount of energy loss during one complete cycle can be calculated by integrating the increment of work done $\sigma d\varepsilon$ over complete cycle of period T, as follows:

$$\Delta W = \int_0^T \sigma \frac{d\varepsilon}{dt} dt \tag{12.10}$$

Inserting $\sigma = \sigma_0 \sin\varpi t$ and $d\varepsilon/dt = \varpi\varepsilon_0 \cos(\varpi t - \delta)$ into Eq. 12.8, results in:

$$\Delta W = \int_0^T \varepsilon_0 \sigma_0 \omega \sin \omega t \bullet \cos(\omega t - \delta)\, dt \tag{12.11}$$

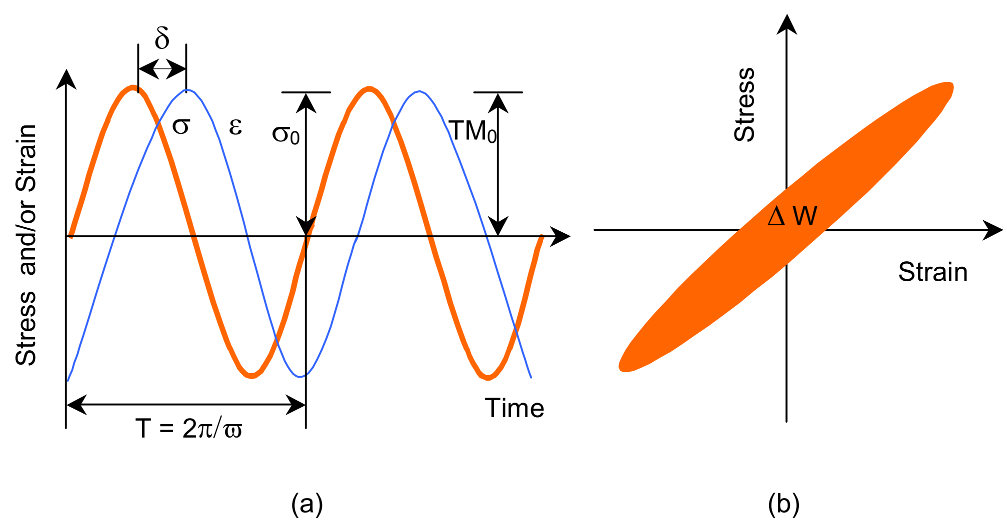

Figure 12-9. Oscillating stress, strain and phase lag during a dynamic test

Analytical integration of Eq. 12.10 yields the following expression for energy loss per cycle:

$$\Delta W = \pi \sigma_0 \varepsilon_0 \sin\delta \tag{12.12}$$

in which ΔW represents the internal stress-strain loop area, shown in Figure 12-9(b). For linear viscoelastic materials that are undergoing secondary creep, the internal loop area ΔW corresponds to the dissipated creep strain energy per cycle.

12.9 Energy Dissipation Using the Linear Viscoelastic Superposition Principle

A material is said to be linearly viscoelastic if stress is proportional to strain at any given time, and the linear viscoelastic superposition principle is applicable. An actual dynamic test is typically performed using vertically continuous compression or horizontally continuous tension loading. Within a small strain range, the linear viscoelastic superposition principle also allows for the combination of static and cyclic loading, as shown e.g., in Figures 12-2(a) and 12-2(b), in which σ_{avg} is the average magnitude of cyclic loading, $\varepsilon(t)$ is the strain given by the average stress, and $\dot{\varepsilon}_{cr}$ is the rate of creep strain induced by the average stress. A stress-independent compliance η, defined as $\dot{\varepsilon}_{cr}$ divided by σ_{avg} can therefore be obtained, and using the power function, it can be simplified as follows:

$$\eta = \frac{\dot{\varepsilon}_{cr}}{\sigma_{avg}} = D_1 \bullet m \bullet t_{steady}^{\;m-1} \tag{12.13}$$

where the constant time t_{steady} is the time in steady state (secondary) creep. During any given cycle T, the dissipated creep strain energy per cycle representing energy loss during one cycle at the steady state can be computed by integrating the increment of work $\sigma(t)\,\dot{\varepsilon}_{cyc}$ as follows:

$$\text{DCSE per cycle} = \int_0^T \sigma(t) \bullet \dot{\varepsilon}_{cyc}\, dt = \int_0^T \sigma(t)^2 \bullet \eta dt \tag{12.14}$$

where $\dot{\varepsilon}_{cyc}$ is the rate of cyclic creep strain, obtaining from σ (t) η, T is the period of the oscillation, and ω (= 2π*f*) is the angular frequency given by frequency *f*. Replacing σ (t) with a sinusoidal loading function $\sigma_0 \sin \omega t$ at the given frequency ω, results in:

$$\text{DCSE per cycle} = \int_0^T \sigma_0 \sin \omega t \bullet \dot{\varepsilon}_{cyc}\, dt = \int_0^T (\sigma_0 \sin \omega t)^2 \bullet \eta dt \tag{12.15}$$

Similarly, inserting $\eta = D_1 m\, (t_{steady})^{m-1}$ into Eq. 12.13, results in:

$$\text{DCSE per cycle} = \int_0^T (\sigma_0 \sin \omega t)^2 \bullet D_1 \bullet m \bullet (t_{steady})^{m-1}\, dt \tag{12.16}$$

Finally, integration of Eq. 12.14 yields the following expression for energy loss per cycle:

$$\text{DCSE per cycle} = \frac{{\sigma_0}^2 \bullet D_1 m \bullet {t_{steady}}^{m-1} \bullet T}{2} \tag{12.17}$$

Importantly, as compared to Eq. 12.12, Eq. 12.17 does not include the phase angle. Thus, the DCSE per cycle is only a function of stress and strain. Equation 12.17 is also the same as Eq. 12.9, as long as $\sigma_{max} = 2\sigma_0$, and the rate of creep strain $\dot{\varepsilon}_{cr}$ from the cyclic loading test is the same as the rate of creep strain $\dot{\varepsilon}_{cr}$ in the static loading test. As a result, all three equations (Eq. 12.9, 12.12, and 12.17) finally will provide the same dissipated creep strain energy per cycle.

12.10 Analysis and Findings

In the following, the three methods for calculating the DCSE per cycle, described by Eqs. 12.9, 12.12, and 12.17, are used and compared. These include the equivalent DSCE per cycle from a static creep test (Eq. 12.9), as well as the two methods for obtaining the DCSE per cycle from dynamic testing–namely, conventional energy dissipation theory (Eq. 12.12) and energy dissipation using the linear viscoelastic superposition principle (Eq. 12.17). Effectively, the same amount of energy should be dissipated per cycle from all three methods. The average stress magnitude σ_0 used in the analysis was determined from a structural analysis of each of the pavement sections as one half of the tensile stress at the bottom of each pavement section due to a 9000-lb axle load at the pavement surface. In the structural analysis, the layer thicknesses and backcalculated modulus values, shown in Tables 12-1 and 12-2, were used to determine the tensile stress at the bottom of each pavement section.

12.11 Energy Dissipation Using the Linear Viscoelastic Superposition Principle–Results

The rate of dissipated creep strain energy per cycle obtained from cyclic response based on Eq. 12.17 was calculated and compared to the calculated DCSE per cycle from a static creep test using Eq. 12.9. It was assumed that the DCSE per cycle from the cyclic response (Eq. 12.17) was induced by the average stress σ_{avg} during cyclic loading (Figure 12-2(a)).

Table 12-3 lists the results of the comparison for the six pavement sections, three temperatures, and three frequencies. Similarly, Figure 12-10 shows a comparison between the predicted DCSE per cycle using Eq. 12.17) and that obtained from Eq. 12.9. The results clearly show that there is a good agreement between predicted DCSE per cycle from Eqs. 12.9 and 12.17 for all six sections, temperatures, and frequencies. Figure 12-10 also shows that the trends in the predictions are similar, meaning that the rate of creep strain from Eq. 12.17 is the same as the rate of creep strain from Eq. 12.9. The results effectively show that reliable creep compliance parameters can be obtained from dynamic test results, based on the rate of permanent deformation.

Table 12-3. Measured and Calculated DCSE Per Cycle from Equations 12.9 and 12.17

Frequencies (hz)		DCSE per cycle					
Name	Temp (° C)	Measured from dynamic creep test (KJ/m^3)			Calculated from static creep test (KJ/m^3)		
		0.333	0.5	1	0.333	0.5	1
I75-1C	0	4.815E-04	3.132E-04	1.407E-04	5.429E-04	3.620E-04	1.810E-04
I75-1U	0	4.138E-04	2.457E-04	1.539E-04	6.104E-04	4.070E-04	2.035E-04
I75-3C	0	4.801E-04	2.845E-04	1.521E-04	5.274E-04	3.516E-04	1.758E-04
I75-2U	0	2.336E-04	1.636E-04	7.432E-05	2.413E-04	1.608E-04	8.042E-05
SR-1C	0	1.147E-03	6.613E-04	3.492E-04	8.552E-04	5.701E-04	2.851E-04
SR-2U	0	2.719E-04	1.759E-04	5.791E-05	1.312E-04	8.746E-05	4.373E-05
I75-1C	10	1.950E-03	1.332E-03	6.333E-04	1.892E-03	1.261E-03	6.307E-04
I75-1U	10	1.327E-03	1.117E-03	5.631E-04	1.736E-03	1.158E-03	5.788E-04
I75-3C	10	1.461E-03	9.842E-04	5.562E-04	1.550E-03	1.034E-03	5.168E-04
I75-2U	10	8.079E-04	5.493E-04	2.675E-04	9.269E-04	6.179E-04	3.090E-04
SR-1C	10	3.279E-03	2.401E-03	1.156E-03	4.063E-03	2.708E-03	1.354E-03
SR-2U	10	5.771E-04	3.551E-04	1.666E-04	6.039E-04	4.026E-04	2.013E-04
I75-1C	20	4.311E-03	2.733E-03	1.522E-03	3.567E-03	2.378E-03	1.189E-03
I75-1U	20	3.664E-03	2.612E-03	1.430E-03	4.435E-03	2.957E-03	1.478E-03
I75-3C	20	5.420E-03	3.798E-03	1.917E-03	5.141E-03	3.427E-03	1.714E-03
I75-2U	20	2.199E-03	1.431E-03	6.936E-04	1.937E-03	1.291E-03	6.457E-04
SR-1C	20	9.222E-03	6.454E-03	2.986E-03	8.756E-03	5.838E-03	2.919E-03
SR-2U	20	1.310E-03	9.157E-04	4.778E-04	1.450E-03	9.669E-04	4.835E-04
Equations		$\text{DCSE per cycle} = \frac{\sigma_0^2 \bullet D_1 m \bullet t^{m-1} \bullet T}{2}$			$\text{DCSE per cycle} = \frac{\sigma_0^2 \bullet D_1 m \bullet t^{m-1} \bullet T}{2}$		

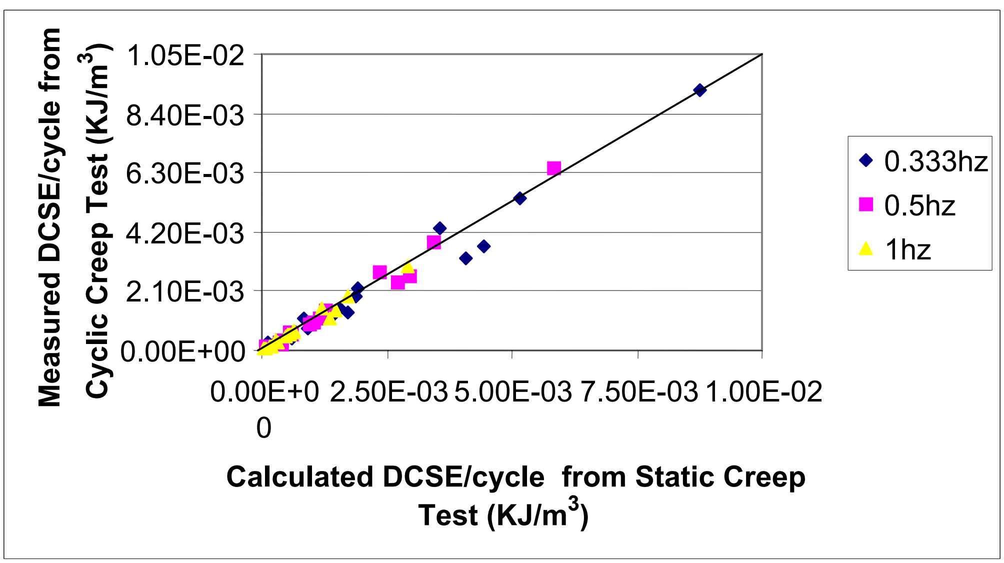

Figure 12-10. Measured DCSE per cycle versus calculated DCSE per cycle using Equations 12.9 and 12.17

12.12 Application of Conventional Energy Dissipation Theory–Results

As discussed previously, in conventional energy dissipation theory, dissipated energy per cycle is defined as the hysteresis area, as shown in Figure 12-9(b), and calculated by Eq. 12.12. Assuming that during secondary creep, the hysteresis area is only dominated by dissipated creep strain energy, the measured DCSE per cycle from a dynamic test should match closely the calculated DCSE per cycle from a creep test, as defined by Eq. 12.9.

Table 12-4 compares the measured DCSE per cycle from dynamic test results obtained from Eq. 12.12 to the calculated DCSE per cycle from static creep tests obtained from Eq. 12.9. The results listed in Table 12-4 include test results from all six pavement sections, three temperatures, and three frequencies. The measured DCSE per cycle from the dynamic tests was much higher than the calculated DCSE per cycle from the static creep tests, regardless of pavement section, temperature, or frequency. As shown in Figure 12-11, the ratios of between the measured DCSE per cycle from Eq. 12.12 and the calculated DCSE per cycle from static creep testing (Eq. 12.9) show an increasing trend as the frequency increases. As a result, the measured DCSE per cycle using the conventional energy approach does not appear to correspond well with the DCSE per cycle obtained from the static creep test (Eq. 12.9). This means that the hysteresis loop area and therefore the measured phase angle in dynamic modulus tests contain another component besides that caused by creep strain energy.

It is well known that asphalt mixtures exhibit delayed elastic behavior. During steady state sinusoidal loading of mixtures, delayed elasticity is still present in the mixture response, but does not change from one cycle to another. However, within each cycle, a part of the strain response is due to delayed elasticity. Hence, based on the results presented, it appears that delayed elasticity may play a significant role in the phase angle and the DCSE per cycle, in addition to the proportion of the DCSE per cycle caused by creep strain energy.

Table 12-4. Measured and Calculated DCSE Per Cycle from Equations 12.9 and 12.12

Frequencies (hz)		DCSE per cycle					
Name	Temp (°C)	Measured from dynamic test (KJ/m^3)			Calculated from static creep test (KJ/m^3)		
		0.333	0.5	1	0.333	0.5	1
I75-1C	0	1.961E-02	1.960E-02	1.805E-02	4.815E-04	3.132E-04	1.407E-04
I75-1U	0	1.789E-02	1.876E-02	1.569E-02	4.138E-04	2.457E-04	1.539E-04
I75-3C	0	1.691E-02	1.829E-02	1.730E-02	4.801E-04	2.845E-04	1.521E-04
I75-2U	0	1.551E-02	1.170E-02	8.619E-03	2.336E-04	1.636E-04	7.432E-05
SR-1C	0	4.284E-02	4.720E-02	4.100E-02	1.147E-03	6.613E-04	3.492E-04
SR-2U	0	8.646E-03	9.592E-03	8.484E-03	2.719E-04	1.759E-04	5.791E-05
I75-1C	10	4.166E-02	4.118E-02	3.352E-02	1.950E-03	1.332E-03	6.333E-04
I75-1U	10	4.218E-02	4.160E-02	3.472E-02	1.327E-03	1.117E-03	5.631E-04
I75-3C	10	3.728E-02	3.298E-02	2.992E-02	1.461E-03	9.842E-04	5.562E-04
I75-2U	10	1.075E-02	1.585E-02	1.304E-02	8.079E-04	5.493E-04	2.675E-04
SR-1C	10	9.385E-02	8.457E-02	7.077E-02	3.279E-03	2.401E-03	1.156E-03
SR-2U	10	2.357E-02	2.085E-02	1.954E-02	5.771E-04	3.551E-04	1.666E-04
I75-1C	20	7.261E-02	5.720E-02	5.226E-02	4.311E-03	2.733E-03	1.522E-03
I75-1U	20	8.105E-02	7.066E-02	5.450E-02	3.664E-03	2.612E-03	1.430E-03
I75-3C	20	7.903E-02	6.895E-02	5.430E-02	5.420E-03	3.798E-03	1.917E-03
I75-2U	20	3.528E-02	2.987E-02	2.354E-02	2.199E-03	1.431E-03	6.936E-04
SR-1C	20	1.812E-01	1.720E-01	1.241E-01	9.222E-03	6.454E-03	2.986E-03
SR-2U	20	4.053E-02	4.189E-02	3.154E-02	1.310E-03	9.157E-04	4.778E-04
Equations		$\text{DCSE per cycle} = \pi \frac{\sigma_0}{\lvert E^* \rvert} \cdot \sin(\delta)$			$\text{DCSE per cycle} = \frac{\sigma_0^2 D_1 m (100)^{m-1} T}{2}$		

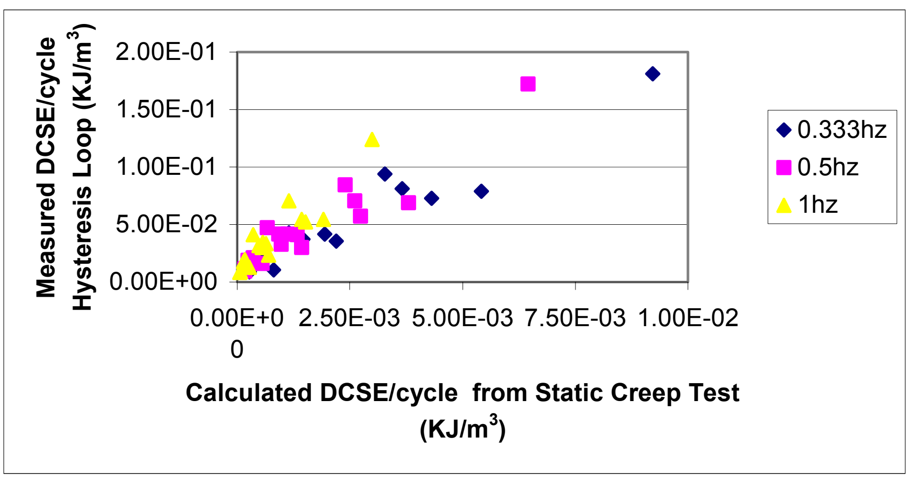

Figure 12-11. Measured DCSE per cycle versus calculated DCSE per cycle Equations 12.9 and 12.12

In summary, the results of the comparison between DCSE per cycle from Eqs. 12.9, 12.12, and 12.17 show that in order to measure the DCSE per cycle from a dynamic test, the energy dissipation using the linear viscoelastic superposition principle (Eq. 12.17), can be used to obtain DCSE per cycle. However, the phase angle in dynamic test measurements includes a component due to delayed elasticity, and therefore cannot be used to obtain the DCSE per cycle. Based on these results, it is recommended that the DCSE per cycle should be obtained based on the creep strains generated in either a static or a cyclic creep test.

12.13 Summary and Conclusions

The recently developed Hot Mix Asphalt Fracture Mechanics framework (Zhang et al., 2000; Roque and Birgisson, 2002) assumes that microdamage in asphalt mixtures is directly related to the creep rate of the mixture, as described by the DCSE per cycle. The higher the DCSE per cycle, the greater the microdamage, after a given number of loading cycles. In this chapter, the HMA fracture mechanics framework was reviewed briefly, followed by an evaluation of the use of short-term dynamic measurements for obtaining the DCSE per cycle for mixtures as an input for the HMA fracture mechanics model. A comparison between the DCSE per cycle obtained from cyclic and static creep tests was also performed. The results show that the phase angle in the complex modulus test includes delayed elasticity effects, besides viscous effects, thus resulting in differences between the rate of creep obtained from static and dynamic tests. This means that short-term dynamic measurements cannot be used to obtain input properties for the HMA fracture mechanics framework. The results also show that in order to measure the DCSE per cycle from a dynamic test, the energy dissipation from either a cyclic creep test using the linear viscoelastic superposition principle (Eq. 12.17), or a static creep test (Eq. 12.9) can be used to obtain DCSE per cycle.

Based on these results, it is recommended that the DCSE per cycle should be obtained based on the creep strains generated in either a static or a cyclic creep test.

REFERENCES

AASHTO (American Association of State Highway and Transportation Officials). 1993. *AASHTO Design Guide*. AASHTO: Washington, D.C.

AASHTO. 1996. *AASHTO Provisional Standard*s: *TP-9*. AASHTO: Washington, D.C.

AASHTO. 1998. *AASHTO Provisional Standards: TP-5*. AASHTO: Washington, D.C.

Asiamah, S. 2002. Relationship between laboratory mix properties and rutting resistance for Superpave mixtures. *Master's Thesis*. University of Florida: Gainesville.

ASTM (American Society for Testing and Materials). 1985. *Annual Book of ASTM Standard*s: *D 2493*. ASTM: Philadelphia, PA.

ASTM. 1997. *Annual Book of ASTM Standard*s: *D 3497*. ASTM: Philadelphia, PA. Vol. 4.20.

Azari, H., R. McCuen, and K. Stuart. 2004. The effect of vertical inhomogeneity on compressive properties of asphalt mixtures. *Journal of the Association of Asphalt Paving Technologists*. Vol. 73.

Berthelot, C., B. Crackford, S. White, and G. Sparks. 1996. Mechanistic quality control/quality assurance evaluation of Saskatchewan specific pavement studies – 9A asphalt mixes. *Proceedings of the 42nd Annual Conference of Canadian Technical Asphalt Association*.

Bonneaure, F., G. Gest, A. Gravois, and P. Uge. 1977. A new method of predicting the stiffness of asphalt paving mixtures. *Proceedings of the Association of Asphalt Paving Technologists*. Vol. 46, pp. 64-100.

Brown, E.R., B. Prowell, A. Cooley, J. Zhang, R. Powell. 2004. Evaluation of rutting performance on the 2000 NCAT test track. *Journal of the Association of Asphalt Paving Technologists*. Vol. 73.

Buttlar, W. G., and R. Roque. 1994. Development and evaluation of the strategic highway research program measurement and analysis system for indirect tensile testing at low temperatures. *Transportation Research Record. No. 1454*. Transportation Research Board: Washington, D.C. pp. 163-171.

Buttlar, W. G., R. Roque, and B. Reid. 1998. Automated procedure for generation of creep compliance master curve for asphalt mixtures. *Transportation Research Record No. 1630*. Transportation Research Board: Washington, D.C. pp. 28-36.

Çengal, Y.A. 1997. *Thermodynamics and Heat Transfer*. Irwin/McGraw-Hill: Boston.

Chehab, G.R., E. O'Quinn, and Y.R. Kim. 2000. Specimen geometry study for direct tension test based on mechanical tests and air void variation in SGC-compacted asphalt concrete specimens. *Transportation Research Record 1723*. Transportation Research Board: Washington, D.C. pp. 125-132.

Clyne, T., X. Li, M.O. Marasteanu, and E.L. Skok. 2003. Dynamic and resilient modulus of Mn/DOT asphalt mixtures. *Minnesota Department of Transportation Report MN/RC-2004-09.* 78 p.

Christensen, D. W., and D. A. Anderson. 1992. Interpretation of dynamic mechanical test data for paving grade asphalt cements. *Journal of the Association of Asphalt Paving Technologists*. Vol. 61, pp. 67-116.

Daniel, J.S., Y.R. Kim, and H.J. Lee. 1998. Effects of aging on viscoelastic properties of asphalt-aggregate mixtures. *Transportation Research Record 1630*. Transportation Research Board: Washington, D.C. pp. 21-27.

Drescher, A., D.E. Newcomb, and W. Zhang. 1997. Interpretation of indirect tension test based on viscoelasticity. *Transportation Research Record 1590*. Transportation Research Board: Washington, D.C. pp. 45-52.

Findley, W. N., J. S. Lai, and K. Onaran. 1976. *Creep and Relaxation of Nonlinear Viscoelastic Materials*. Dover Publications, Inc.: New York.

Francken, L. 1998. *RILEM Report 17: Bituminous Binders and Mixe*s. E & FN Spon.: New York.

Francken, L., M. Partl, and the Technical Committee on Bitumen and Asphalt Testing. 1996. Complex modulus testing of asphaltic concrete: RILEM Interlaboratory Test Program. *Transportation Research Record 1545*. Transportation Research Board: Washington, D.C. pp. 133-142.

Goode, J. F., and L. A. Lufsey. 1962. A new graphical chart for evaluating aggregate gradations. *Proceedings of the Association of Asphalt Paving Technologists*, Vol. 31.

Haifing, W., and Y.R. Kim. 2002. Simple performance test for fatigue cracking of asphalt concrete based on viscoelastic analysis of indirect tensile testing and its validation using WestTrack asphalt mixtures. *Transportation Research Record Preprint*. Transportation Research Board: Washington, D.C.

Harvey, J., S. Weissman, F. Long, and C. Monismith. 2001. Test to evaluate the stiffness and permanent deformation characteristics of asphalt/binder–aggregates mixes, and their use in mix design and analysis. *Journal of the Association of Asphalt Paving Technologists*. Vol. 70.

Hiltunen, D. R., and R. Roque. 1994. A mechanics-based prediction model for thermal cracking of asphaltic concrete pavements. *Journal of the Association of Asphalt Paving Technologists*. Vol. 63, pp. 81-117.

Huber, G. A., and T. S. Shuler. 1992. Providing sufficient void space for asphalt cement: Relationship of mineral aggregate void and aggregate gradation. *Effects of Aggregates and Mineral Fillers on Asphalt Mixture Performance*. ASTM.

Kaloush, K.E., and M.W. Witczak. 2002. Tertiary flow characteristics of asphalt mixtures. *Journal of the Association of Asphalt Paving Technologists*. Vol. 71, pp. 248-280.

Khanal, P.P., and M.S. Mamlouk. 1995. Tensile versus compressive moduli of asphalt concrete. *Transportation Research Record 1492*. Transportation Research Board: Washington, D.C. pp. 144-150.

Kim, B. 2003. Evaluation of the effect of SBS polymer modifier on cracking resistance of Superpave. *Ph.D. Dissertation*. University of Florida: Gainesville.

Kim, J. S. 2002. Complex modulus from indirect tension testing. *Master's Thesis.* University of Florida: Gainesville.

Kim, Y. R., G. Chehab, R. A. Schapery, M. Witczak, and R. Bonaquist. 2002. Time-temperature superposition principle for asphalt concrete mixtures with growing damage in tension state. *Preprint for Journal of the Association of Asphalt Paving Technologists*.

Lee, H.J., and Y.R. Kim. 1998. Viscoelastic constitutive model for asphalt concrete under cyclic loading. *ASCE Journal of Engineering Mechanics*. Vol. 124, No. 1, pp. 32-40.

Mehta, Y.A. and D.W. Christensen. 2000. Determination of the linear viscoelastic limits of asphalt concrete at low and intermediate temperatures. *Journal of the Association of Asphalt Paving Technologists*. Vol. 69, pp. 281-312.

NCHRP (National Cooperative Highway Research Program). 2004. *1-37A-2002 Design Guide* (Draft). NCHRP: Washington, D.C.

Nijboer, L. W. 1948. *Plasticity as a Factor in the Design of Dense Bituminous Road Carpets*. Elsevier.

Nukunya, B. 2001. Evaluation of aggregate type and gradation and other volumetric properties as criteria for the design and acceptance of durable Superpave mixtures. *Ph.D. Dissertation*. University of Florida: Gainesville.

Nukunya, B., R. Roque, M. Tia, and B. Birgisson. 2001. Evaluation of VMA and other volumetric properties as criteria for the design and acceptance of Superpave mixtures. *Journal of the Association of Asphalt Paving Technologists*. Vol. 70.

Papazian, H. S. 1962. The response of linear viscoelastic materials in the frequency domain with emphasis on asphalt concrete. *Proceedings of First International Conference on the Structural Design of Asphalt Pavements*. Ann Arbor, Michigan. pp. 454-463.

Pellinen, T. K., and M. W. Witczak. 2002. Stress dependent master curve construction for dynamic (complex) modulus. *Preprint for Journal of the Association of Asphalt Paving Technologists*.

Roque, R., and W. G. Buttlar. 1992. The development of a measurement and analysis system to accurately determine asphalt concrete properties using the indirect tensile mode. *Journal of the Association of Asphalt Paving Technologists*. Vol. 61, pp. 304-332.

Roque, R., B. Birgisson, M. Tia, and B. Nukunya. 2002a. Evaluation of Superpave criteria for VMA and fine aggregate angularity. *Final Report, UF Project No. 4910-4504-619-12*. University of Florida: Gainesville. March, 388 p.

Roque, R., B. Birgisson, B. Sangpetgnam, Z. Zhang. 2002b. *Crack Growth Behavior of Asphalt Mixtures and its Relation to Laboratory and Field Performance. Proceedings, 9th International Conference on Asphalt Pavements*. Copenhagen, Denmark. pp. 3:3-9.

Roque, R., W. G. Buttlar, B. E. Ruth, M. Tia, S. W. Dickison, and B. Reid. 1997. Evaluation of SHRP indirect tension tester to mitigate cracking in asphalt concrete pavements and overlays. *FL-DOT-MO-0510755*. University of Florida: Gainesville.

Ruth, B. E., R. Roque, and B. Nukunya. 2002. Aggregate gradation characterization factors and their relationships to fracture energy and failure strain of asphalt mixtures. *Journal of Association of Asphalt Paving Technologists*.

Saada, A.S. 1989. *Elasticity: Theory and Applications*. Robert E. Krieger Publishing Company.

Saadeh, S., E. Masad, K. Stuart, A. Abbas, T. Papagainnakis, and G. Al-Khateeb. 2003. Comparative analysis of axial and shear viscoelastic properties of asphalt mixes. *Journal of the Association of Asphalt Paving Technologists*. Vol. 72, pp. 122-153.

Sangpetngam, B. 2003. Development and evaluation of a viscoelastic boundary element method to predict asphalt pavement cracking. *Ph.D. Dissertation*. University of Florida: Gainesville.

Shook, J.F., and B.F. Kallas. 1969. Factors influencing the dynamic modulus of asphalt concrete. *Proceedings of the Association of Asphalt Paving Technologists*. AAPT: Los Angeles, CA.

Sousa, J.M.B. 1986. *Dynamic Properties of Pavement Materials*. University of California, Berkley.

Sousa, J.M.B. and C.L. Monismith. 1987. Dynamic response of paving materials. *Transportation Research Record 1136*. Transportation Research Board, Washington, D.C. pp. 57-68.

Sousa, J., J. Deacon, S. Weissman, R. Leahy, J. Harvey, G. Paulsen, J. Coplanz, and C. Monismith. 1994. Permanent deformation response of asphalt aggregate mixes. *Strategic Highway Research Program Report No.SHRP-A-415*. National Research Council: Washington, D.C.

Stroup-Gardiner, M., and D.E. Newcomb. 1997. Investigation of hot mix asphalt mixtures at MnROAD. *Minnesota Department of Transportation Final Report 97-06*.

Swan, D.J. 2001. Evaluation of the testing procedure and data analysis for the uniaxial complex modulus test on hot mix asphalt. *Master's Thesis*. University of Florida: Gainesville.

Ullidtz, P. 1987. *Pavement Analysis*. Elsevier Science Publishers B.V.: Amsterdam, The Netherlands.

Vavrik, W. R., W. J. Pine, G. Huber, and S. H. Carpenter. 2001. The Bailey method of gradation evaluation: The influence of aggregate gradation and packing characteristics on voids in the mineral aggregate. *Journal of the Association of Asphalt Paving Technologists*. Vol. 70.

Williams, M. L., R. F. Landel, and J. D. Ferry. 1955. The temperature dependence of relaxation mechanisms in amorphous polymers and other glass-forming liquids. *The Journal of the American Chemical Society*. Vol. 77, pp. 3701-3706.

Witczak, M.W., and O.A. Fonseca. 1996. Revised predictive model for dynamic (complex) modulus of asphalt mixtures. *Transportation Research Record 1540*. Transportation Research Board: Washington, D.C. pp. 15-23.

Witczak, M.W., and R.E. Root. 1974. Summary of complex modulus laboratory test procedures and results. *ASTM STP 561*. American Society of Testing and Materials. pp. 67-94.

Witczak, M.W., R. Bonaquist, H. Von Quintus, and K. Kaloush. 2000. Specimen geometry and aggregate size effects in uniaxial compression and constant height shear tests. *Proceedings of the Association of Asphalt Paving Technologists*. Vol. 69, pp. 733-793.

Witczak, M.W., T.K. Pellinen, and M.M. El-Basyouny. 2002. Pursuit of the simple performance test for asphalt concrete fracture/cracking. *Journal of the Association of Asphalt Paving Technologists*. Vol. 71, pp. 767-778.

Yoder, E.J. and M.W. Witczak. 1975. *Principles of Pavement Design*. John Wiley & Sons, Inc.

Zhang, W., A. Drescher, and D.E. Newcomb. 1997a. Determination of Viscoelastic Properties from Indirect Tension Test. *Proceedings, 8th International Conference on Asphalt Pavements*. Seattle, WA. pp. 1569-1577.

Zhang, W., A. Drescher, and D. E. Newcomb. 1997b. Viscoelastic behavior of asphalt concrete in diametral compression. *Journal of Transportation Engineering*. Vol. 123, pp. 495-502.

Zhang, Z., R. Roque, B. Birgisson, and B. Sangpetngam. 2001. Identification and verification of a suitable crack growth law. *Journal of the Association of Asphalt Paving Technologists*. Vol. 70, pp. 206-241.

Zhao, Y., and Y. R. Kim. 2003. The time-temperature superposition for asphalt mixtures with growing damage and permanent deformation in compression. *Preprint for the 2003 Annual Meeting of Transportation Research Board*.

APPENDIX A
AXIAL COMPLEX MODULUS PROGRAM AND TORSIONAL SHEAR COMPLEX MODULUS PROGRAM

A.1 Axial Complex Modulus Program

I. *Description of Input File:*

In order to use the Excel spreadsheet, a standard format of input data is needed. The input file is a text file. The input data needs to be in the following order:

Column1: Testing time,

Column2: Axial Displacement. This is the measurement of LVDT on the load frame itself. Normally, it doesn't have high a high enough resolution for consistent interpretation, but is included for completeness.

Column3: Applied Axial Force.

Column4,5, 6, 7: Displacement measurements from two to four on-specimen external LVDT's.

II. *Description of Axial Complex Modulus Program File:*

The axial complex modulus interpretation algorithm is programmed in Visual Basic, as an Excel Macro. The Program name is: Complex Modulus Macros.xls. Once this macro is selected, a Windows-based application within Excel is started. The program is simple and user friendly:

1. Once the Complex Modulus Macro is started, click the "Select File and Start" button to select the input file.
2. After selecting Input File, the following Window appears:

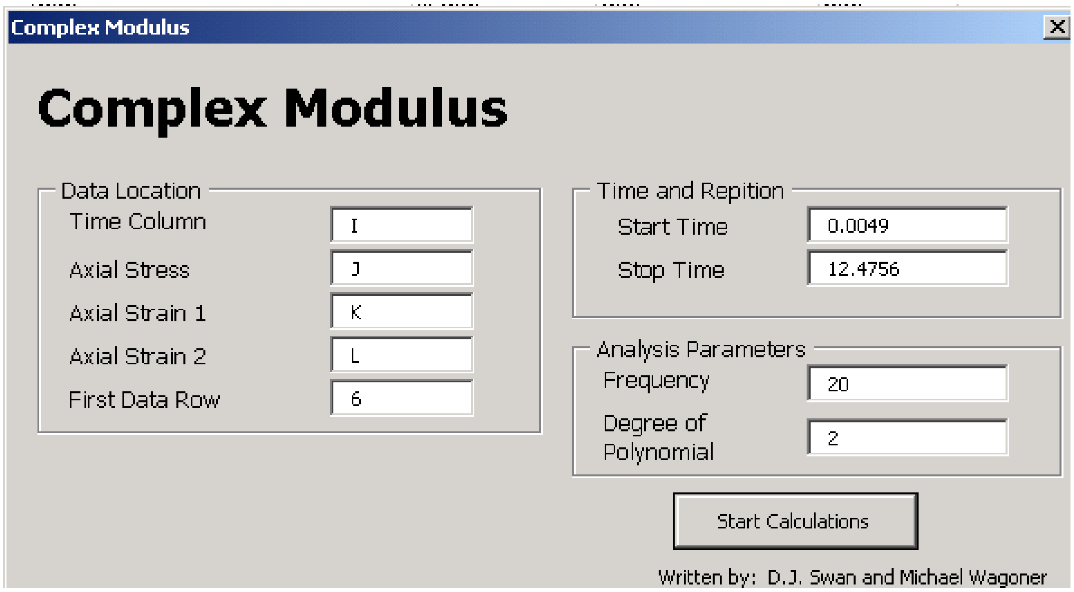

First, it requires data location of: time column, axial stresses, strain of external LVDT's, and location of first data row. These are detected automatically, but should be double-checked by the user. If there are two LVDT's, the file only shows input for two LVDT columns. Second, it requires start time and stop test times for calculation. Normally, the program detects the start and stop times automatically, but the numbers should be checked by the user. Third, the program requires testing frequency and degree of polynomial of regression equation. A second order polynomial is the default input.

III. Output

The output data is assigned to a new worksheet name entitled "Output" in the same Excel file.

IV. Source code

The source code, which is Visual Basic, is printed below. The code can be read directly from within Excel by pressing Alt+F11.

A.2 Torsional Complex Modulus Program

I. Description of Input File:

In order to use the Excel spreadsheet, a standard format of input data is needed. The input file is a text file. The input data needs to be in the following order:

Column1: Testing time.

Column2: Torsional Displacement. This is the measurement of LVDT on the load frame itself. Normally, it doesn't have high a high enough resolution for consistent interpretation, but is included for completeness.

Column3: Applied Torque.

Column4,5: Measurement of external LVDT's. Two LVDT's are used to measure torsional displacement.

II. Description of Torsional Complex Modulus Program File:

The torsional complex modulus interpretation algorithm is programmed in Visual Basic, as an Excel Macro. The Program name is: Torsional Complex Macros.xls

Once this macro is selected, a Windows-based application within Excel is started. The program is simple and user friendly:

1. Click into program. Then click to "Select File and Start" button to select input File.
2. After selecting input file, following Window appears:

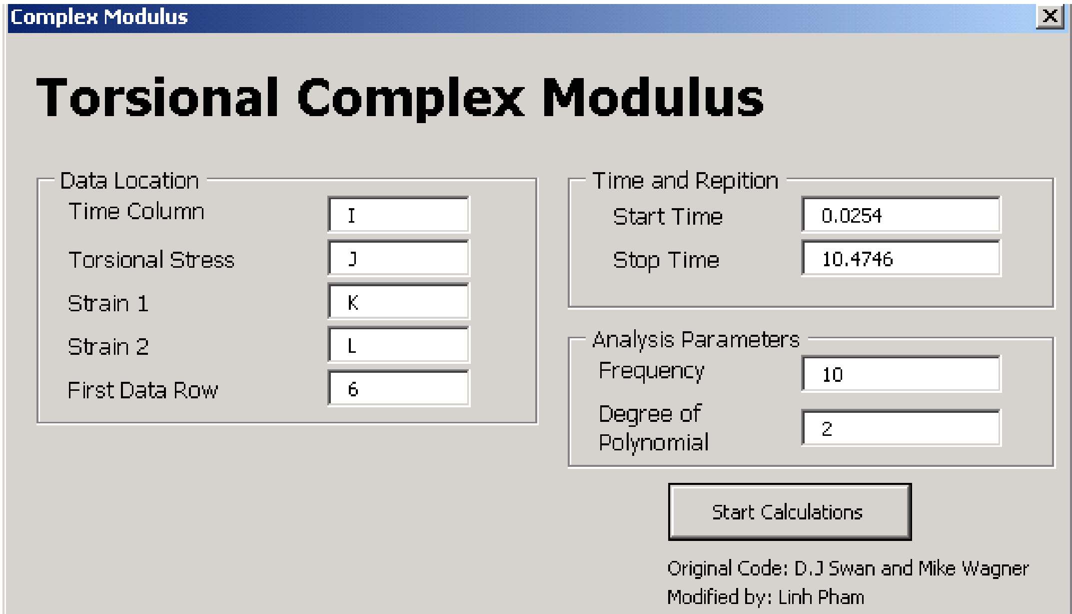

First, it requires data location of: time column, torsional stresses, strain of external LVDT's, and location of first data row. These are detected automatically, but should be double-checked by the user. If there are two LVDT's, the file only shows input for two LVDT columns. Second, it requires start time and stop test times for calculation. Normally, the program detects the start and stop times automatically, but the numbers should be checked by the user. Third, the program requires testing frequency and degree of polynomial of regression equation. A second order polynomial is the default input.

III. Output

Output data is assigned to a new worksheet name "Output" in the same Excel file.

IV. Source code

The source code, which is Visual Basic, is printed below. The code can be read directly from within Excel by pressing Alt+F11.

A.3 Axial Complex Modulus Program Source Code

1. User Form

```
Public Time_column As String
Public Stress_Column As String
Public AStrain1_Column As String
Public RStrain1_Column As String
Public AStrain2_Column As String
Public RStrain2_Column As String
Public Load_Column As String
Public H1_Column As String
Public V1_Column As String
Public H2_Column As String
Public V2_Column As String
Public Start_Row As Long
Public Which_Test As String
Public PA_Method As String
Public Start_Time As Double
Public Stop_Time As Double
Public RepeatNo As Long
Public DelayTime As Double

Public Sub Interface()
   'this display the userform to begin the test.
   UserForm1.Show
End Sub

Private Sub Triaxial_Click()
   'This confirms the columns and starts the next section...
   '
   'D.J. Swan
   Dim Flag1 As Boolean
   Dim AscNum As Integer       'Check if letter...
   Flag1 = True

   'Check to confirm that the values are the correct type.
   If IsNumeric(StartRow.Value) Then
      Start_Row = CLng(StartRow.Value)
   Else
      Flag1 = False
   End If
   If IsNumeric(StartTime.Value) Then
      Start_Time = CDbl(StartTime.Value)
   Else
      Flag1 = False
```

```
End If
If IsNumeric(StopTime.Value) Then
   Stop_Time = CDbl(StopTime.Value)
Else
   Flag1 = False
End If
If IsNumeric(Frequency) Then
   Module2.Frequency = Frequency
Else
   Flag1 = False
End If
If IsNumeric(PolyNum.Value) Then
   Module2.PolyNum = WorksheetFunction.RoundDown(PolyNum.Value, 0)
Else
   Flag1 = False
End If

'Check to see if Time is a valid column letter...
If Len(Time.Value) > 2 Then
   Flag1 = False
ElseIf Len(Time.Value) < 1 Then
   Flag1 = False
ElseIf Len(Time.Value) = 1 Then
   AscNum = Asc(UCase$(Time.Value))
   If AscNum < 65 Then
      Flag1 = False
   ElseIf AscNum > 90 Then
      Flag1 = False
   End If
Else
   AscNum = Asc(Left$(UCase$(Time.Value), 1))
   If AscNum < 65 Then
      Flag1 = False
   ElseIf AscNum > 73 Then
      Flag1 = False
   End If
   AscNum = Asc(Right$(UCase$(Time.Value), 1))
   If AscNum < 65 Then
      Flag1 = False
   ElseIf AscNum > 90 Then
      Flag1 = False
   End If
End If
```

```
'Check to see if Sensor 1 is a valid column letter...
If Len(Stress.Value) > 2 Then
   Flag1 = False
ElseIf Len(Stress.Value) < 1 Then
   Flag1 = False
ElseIf Len(Stress.Value) = 1 Then
   AscNum = Asc(UCase$(Stress.Value))
   If AscNum < 65 Then
      Flag1 = False
   ElseIf AscNum > 90 Then
      Flag1 = False
   End If
Else
   AscNum = Asc(Left$(UCase$(Stress.Value), 1))
   If AscNum < 65 Then
      Flag1 = False
   ElseIf AscNum > 73 Then
      Flag1 = False
   End If
   AscNum = Asc(Right$(UCase$(Stress.Value), 1))
   If AscNum < 65 Then
      Flag1 = False
   ElseIf AscNum > 90 Then
      Flag1 = False
   End If
End If

'Check to see if Sensor 2 is a valid column number...
If Len(AStrain1.Value) > 2 Then
   Flag1 = False
ElseIf Len(AStrain1.Value) < 1 Then
   Flag1 = False
ElseIf Len(AStrain1.Value) = 1 Then
   AscNum = Asc(UCase$(AStrain1.Value))
   If AscNum < 65 Then
      Flag1 = False
   ElseIf AscNum > 90 Then
      Flag1 = False
   End If
Else
   AscNum = Asc(Left$(UCase$(AStrain1.Value), 1))
   If AscNum < 65 Then
      Flag1 = False
   ElseIf AscNum > 73 Then
      Flag1 = False
   End If
```

```
        AscNum = Asc(Right$(UCase$(AStrain1.Value), 1))
        If AscNum < 65 Then
            Flag1 = False
        ElseIf AscNum > 90 Then
            Flag1 = False
        End If
    End If

    'Check to see if Sensor 3 is a valid column number...
    If Len(AStrain2.Value) > 2 Then
        Flag1 = False
    ElseIf Len(AStrain2.Value) < 1 Then
        Flag1 = False
    ElseIf Len(AStrain2.Value) = 1 Then
        AscNum = Asc(UCase$(AStrain2.Value))
        If AscNum < 65 Then
            Flag1 = False
        ElseIf AscNum > 90 Then
            Flag1 = False
        End If
    Else
        AscNum = Asc(Left$(UCase$(AStrain2.Value), 1))
        If AscNum < 65 Then
            Flag1 = False
        ElseIf AscNum > 73 Then
            Flag1 = False
        End If
        AscNum = Asc(Right$(UCase$(AStrain2.Value), 1))
        If AscNum < 65 Then
            Flag1 = False
        ElseIf AscNum > 90 Then
            Flag1 = False
        End If
    End If

    If Flag1 Then
        Module3.Time_C = UCase$(Time.Value)
        Module3.Sensor1_C = UCase$(Stress.Value)
        Module3.Sensor2_C = UCase$(AStrain1.Value)
        Module3.Sensor3_C = UCase$(AStrain2.Value)
        Call Module3.Complex_Modulus
        UserForm1.Hide
    Else
        MsgBox ("One or more of the entries is not valid")
    End If
End Sub
```

```
Private Sub UserForm_Initialize()

    Call Module1.FindFirstCylce

    'Starting Values...
    Time.Value = "I"
    Stress.Value = "J"
    AStrain1.Value = "K"
    AStrain2.Value = "L"
    StartTime = Module1.StartTime
    StopTime = Module1.StopTime
    StartRow = "6"

    PolyNum.Value = 2
    Frequency.Value = 20
    PolyNum.Enabled = True

    Sensor1.Caption = "Axial Stress"
    Sensor2.Caption = "Axial Strain 1"
    Sensor3.Caption = "Axial Strain 2"
    Status.Caption = ""
End Sub
```

2. Module 1

```
Public ColumnLetter(1 To 4) As String
Public StartTime As Double
Public StopTime As Double

Sub FindFirstCylce()

Dim Maxstress As Double
Dim CellCount As Double
Dim EndRow As String

Dim i As Integer
    ActiveSheet.Select
    'Find the first cycle
    CellCount = Range("J6", Range("J6").End(xlDown)).Count
    EndRow = "J" & CellCount
    Maxstress = WorksheetFunction.Max(Range("J6" & ":" & EndRow))
    i = 7
        Do While Range("J" & i).Value < Maxstress / 2
         i = i + 1
        Loop
```

```
    StartTime = Range("I" & i).Value
    StartTime = Round(StartTime, 4)
    'Find the last cycle

        Do While Range("J" & CellCount).Value < Maxstress / 2
            CellCount = CellCount - 1
        Loop
    StopTime = Range("I" & CellCount).Value
    StopTime = Round(StopTime, 4)

End Sub


Sub Setup()
    'This procedure will arrange the laboratory data output
    'into a format that is readable by the analysis software.
    'It also will add the required "Output" worksheet.
    '
    'D.J. Swan
    'August 10, 2001
    Dim OrigName As String
    Dim RowCount As Integer
    Dim EndRow As String
    Dim StartRow As String
    Application.ScreenUpdating = False
    Range("I4").Value = "Time (sec)"
    Range("I6").Formula = "=(A6-$A$6)/1000"
    Range("J4").Value = "Stress (MPa)"
    Range("J6").Formula = "=ABS(B6)/(PI()*0.05^2)/1000000"
    Range("K4").Value = "Axial Strain 1"
    Range("K6").Formula = "=ABS(D6-$D$6)/50"
    Range("L4").Value = "Axial Strain 2"
    Range("L6").Formula = "=ABS(E6-$E$6)/50"

    Selection.Copy
    RowCount = 6
    StartRow = "A6"

    Do While Range(StartRow) <> ""
        RowCount = RowCount + 1
        StartRow = "A" & RowCount

    Loop
    RowCount = RowCount - 1
    EndRow = "L" & RowCount
    Range("I6:L6").Select
```

```
    Selection.AutoFill Destination:=Range("I6" & ":" & EndRow)

    Range("4:4").Font.Bold = True
    Columns("A:L").EntireColumn.AutoFit
    Range("B6").Activate
    ActiveWindow.FreezePanes = True

    OrigName = ActiveSheet.Name
    Worksheets.Add
    ActiveSheet.Name = "Output"
    Worksheets(OrigName).Activate
    Application.ScreenUpdating = True
End Sub

Public Sub OutputPage()
    'This subroutine creates an easily printable page that displays
    'the results of the complex modulus test.
    '
    'D.J. Swan
    'March 26, 2002

    Range("Q1").Value = "Complex Modulus Test Results"
    Range("Q3").Value = "Sample:"
    Range("Q4").Value = "Test Frequency:"
    Range("Q5").Value = "Number of Cycles:"
    Range("Q6").Value = "Calculation Date:"
    Range("T3").Select
    ActiveCell.FormulaR1C1 = "Stress Amplitude (s0)"
    With ActiveCell.Characters(Start:=1, Length:=18).Font
        .Name = "Arial"
        .FontStyle = "Regular"
        .Size = 10
        .Strikethrough = False
        .Superscript = False
        .Subscript = False
        .OutlineFont = False
        .Shadow = False
        .Underline = xlUnderlineStyleNone
        .ColorIndex = xlAutomatic
    End With
    With ActiveCell.Characters(Start:=19, Length:=1).Font
        .Name = "Symbol"
        .FontStyle = "Regular"
        .Size = 10
        .Strikethrough = False
        .Superscript = False
```

```
    .Subscript = False
    .OutlineFont = False
    .Shadow = False
    .Underline = xlUnderlineStyleNone
    .ColorIndex = xlAutomatic
End With
With ActiveCell.Characters(Start:=20, Length:=1).Font
    .Name = "Arial"
    .FontStyle = "Regular"
    .Size = 10
    .Strikethrough = False
    .Superscript = False
    .Subscript = True
    .OutlineFont = False
    .Shadow = False
    .Underline = xlUnderlineStyleNone
    .ColorIndex = xlAutomatic
End With
With ActiveCell.Characters(Start:=21, Length:=1).Font
    .Name = "Arial"
    .FontStyle = "Regular"
    .Size = 10
    .Strikethrough = False
    .Superscript = False
    .Subscript = False
    .OutlineFont = False
    .Shadow = False
    .Underline = xlUnderlineStyleNone
    .ColorIndex = xlAutomatic
End With
Range("T4").Select
ActiveCell.FormulaR1C1 = "Strain Amplitude (e0)"
With ActiveCell.Characters(Start:=1, Length:=18).Font
    .Name = "Arial"
    .FontStyle = "Regular"
    .Size = 10
    .Strikethrough = False
    .Superscript = False
    .Subscript = False
    .OutlineFont = False
    .Shadow = False
    .Underline = xlUnderlineStyleNone
    .ColorIndex = xlAutomatic
End With
With ActiveCell.Characters(Start:=19, Length:=1).Font
    .Name = "Symbol"
```

```
    .FontStyle = "Regular"
    .Size = 10
    .Strikethrough = False
    .Superscript = False
    .Subscript = False
    .OutlineFont = False
    .Shadow = False
    .Underline = xlUnderlineStyleNone
    .ColorIndex = xlAutomatic
End With
With ActiveCell.Characters(Start:=20, Length:=1).Font
    .Name = "Arial"
    .FontStyle = "Regular"
    .Size = 10
    .Strikethrough = False
    .Superscript = False
    .Subscript = True
    .OutlineFont = False
    .Shadow = False
    .Underline = xlUnderlineStyleNone
    .ColorIndex = xlAutomatic
End With
With ActiveCell.Characters(Start:=21, Length:=1).Font
    .Name = "Arial"
    .FontStyle = "Regular"
    .Size = 10
    .Strikethrough = False
    .Superscript = False
    .Subscript = False
    .OutlineFont = False
    .Shadow = False
    .Underline = xlUnderlineStyleNone
    .ColorIndex = xlAutomatic
End With
Range("T5").Select
ActiveCell.FormulaR1C1 = "Dynamic Modulus (|E*|) (MPa)"
Range("T6").Select
ActiveCell.FormulaR1C1 = "Phase Angle (d) (Degrees)"
With ActiveCell.Characters(Start:=1, Length:=15).Font
    .Name = "Arial"
    .FontStyle = "Regular"
    .Size = 10
    .Strikethrough = False
    .Superscript = False
    .Subscript = False
    .OutlineFont = False
```

```
    .Shadow = False
    .Underline = xlUnderlineStyleNone
    .ColorIndex = xlAutomatic
End With

Range("T7").Select
ActiveCell.FormulaR1C1 = "Elastic Modulus (E') (MPa)"

Range("T8").Select
ActiveCell.FormulaR1C1 = "Loss Modulus (E") (MPa)"

'Set some formats...
Range("Q1:V1").Merge
With Range("Q1")
    .Font.Bold = True
    .Font.Underline = True
    .Font.Size = 16
    .HorizontalAlignment = xlCenter
End With
Range("T3:T10").Font.Bold = True
Range("Q3:Q10").Font.Bold = True
Range("Q1").EntireColumn.AutoFit
Range("R1").EntireColumn.AutoFit
Range("T1").EntireColumn.AutoFit
Range("U1").EntireColumn.AutoFit

'Start Filling in Values...
Range("R4").Value = Module2.Frequency
Range("R5").Value = Module3.NumberOfCycles
Range("R6").Value = Date
Range("R6").NumberFormat = "mmmm d, yyyy"
Range("R4:R6").HorizontalAlignment = xlLeft

Range("U3").Value = Range("J3").Value
Range("U4").Value = Range("K3").Value
Range("U5").Value = Range("M3").Value
Range("U6").Value = Range("L3").Value
Range("U7").Value = Range("N3").Value
Range("U8").Value = Range("O3").Value
Range("U6").NumberFormat = "0.000"

Range("Q9").Value = "Signal Equations:"
Range("Q10").Value = Module2.Equations(1)
Range("Q10").Activate
Call FormatEquation
Range("Q11").Value = Module2.Equations(2)
```

```
    Range("Q11").Activate
    Call FormatEquation
    Range("Q12").Value = Module2.Equations(3)
    Range("Q12").Activate
    Call FormatEquation
    Range("Q10").Font.Bold = False
    Range("Q9").Font.Underline = True

    'The Phase Angle Chart....
    With Range("Q34")
        .Value = "Phase Angle Chart"
        .Font.Size = 14
        .Font.Bold = True
    End With
    Union(Range("C3", Range("C3").End(xlDown)), Range("L3",
Range("L3").End(xlDown))).Select
    DataCells = Selection.Address
    Charts.Add
    ActiveChart.Location Where:=xlLocationAsObject, Name:="Output"
    ActiveChart.ChartType = xlXYScatterLines
    ActiveChart.SetSourceData Source:=Worksheets("Output").Range(DataCells),
PlotBy:=xlColumns

    With ActiveChart
        .HasTitle = False
        .Axes(xlCategory, xlPrimary).HasTitle = True
        .Axes(xlCategory, xlPrimary).AxisTitle.Characters.Text = "Time (s)"
        .Axes(xlValue, xlPrimary).HasTitle = True
        .Axes(xlValue, xlPrimary).AxisTitle.Characters.Text = "Phase Angle (Degrees)"
    End With
    ActiveChart.PlotArea.Interior.ColorIndex = xlNone
    ActiveChart.Legend.Delete
    ActiveChart.Axes(xlValue).MinimumScale = 0
    ActiveChart.Axes(xlCategory).TickLabels.NumberFormat = "0"
    ActiveSheet.ChartObjects(1).Left = Range("Q35").EntireColumn.Left
    ActiveSheet.ChartObjects(1).Top = Range("Q35").EntireRow.Top
    ActiveSheet.ChartObjects(1).Height = 237

    'The dynamic modulus chart...
    With Range("Q14")
        .Value = "Dynamic Modulus Chart"
        .Font.Size = 14
        .Font.Bold = True
    End With
    Union(Range("C3", Range("C3").End(xlDown)), Range("M3",
Range("M3").End(xlDown))).Select
```

```
   DataCells = Selection.Address
   Charts.Add
   ActiveChart.Location Where:=xlLocationAsObject, Name:="Output"
   ActiveChart.ChartType = xlXYScatterLines
   ActiveChart.SetSourceData Source:=Worksheets("Output").Range(DataCells),
PlotBy:=xlColumns

   With ActiveChart
      .HasTitle = False
      .Axes(xlCategory, xlPrimary).HasTitle = True
      .Axes(xlCategory, xlPrimary).AxisTitle.Characters.Text = "Time (s)"
      .Axes(xlValue, xlPrimary).HasTitle = True
      .Axes(xlValue, xlPrimary).AxisTitle.Characters.Text = "Dynamic Modulus (kPa)"
   End With
   ActiveChart.PlotArea.Interior.ColorIndex = xlNone
   ActiveChart.Legend.Delete
   ActiveChart.Axes(xlValue).MinimumScale = 0
   ActiveChart.Axes(xlCategory).TickLabels.NumberFormat = "0"
   ActiveSheet.ChartObjects(2).Top = Range("Q15").EntireRow.Top
   ActiveSheet.ChartObjects(2).Left = Range("Q15").EntireColumn.Left
   ActiveSheet.ChartObjects(2).Height = 237

   ActiveSheet.PageSetup.PrintArea = "Q1:V53"
   ActiveSheet.PageSetup.TopMargin = Application.InchesToPoints(0.75)
   ActiveSheet.PageSetup.BottomMargin = Application.InchesToPoints(0.75)

End Sub

Public Sub FormatEquation()
   'This formats the equations of the signals...
   '
   'D.J. Swan
   'March 23, 2002
   Dim Pos1 As Integer

   If Left$(ActiveCell.Value, 4) = "LVDT" Then
      ActiveCell.Characters(Start:=10, Length:=1).Font.Name = "Symbol"
      ActiveCell.Characters(Start:=11, Length:=1).Font.Subscript = True
   ElseIf Left$(ActiveCell.Value, 2) = "s0" Then
      ActiveCell.Characters(Start:=1, Length:=1).Font.Name = "Symbol"
      ActiveCell.Characters(Start:=2, Length:=1).Font.Subscript = True
   End If
   If UBound(Module2.Solution) > 3 Then
      Pos1 = 0
      For i = 1 To UBound(Module2.Solution) - 3
         Pos1 = InStr(Pos1 + 1, ActiveCell.Value, "*t")
```

```
      ActiveCell.Characters(Start:=Pos1 + 2, Length:=1).Font.Superscript = True
    Next i
  End If
  ActiveCell.Characters(Start:=InStr(1, ActiveCell.Value, "[R2") + 2,
Length:=1).Font.Superscript = True
End Sub
```

2. Module 2

```
'The purpose of this module is to start the interpretation of various
'complex modulus components
Public Time() As Double              'This array contains the list of times to match the
signal.
Public Data() As Double              'This array contains the singal data.
Public Frequency As Double           'This value is set in Userform1.
Public Angular_Frequency As Double   'Alpha = 2 * Pi * F
Public Solution() As Double          'This contains the solution to the regression.
Public BenchmarkPa As Double         'This is the phase angle (in radians) of the
load/stress.
Public PolyNum As Long               'The max exponent for the polynomial fit (ie.
1=Linear)
Public Pi As Double
Public Equations(1 To 3) As String   'This contains the Equations of the final cycles.
Public RSqu(1 To 3) As Double
Public Signal As Integer

Sub Calculate()
  'This subroutine gets the amplitude and phase angle.
  '
  'D.J. Swan
  'March 28, 2001
  Dim TempPA As Double

  Pi = WorksheetFunction.Pi()

  'Do the Linear Regression Calcs
  Call Regression

  TempPA = Solution(UBound(Solution))

  If Module3.BenchMark Then
    BenchmarkPa = TempPA
  Else
    TempPA = TempPA - BenchmarkPa
    'To solve the issue that -Pi=Pi
    If (TempPA) < 0 Then
```

```
            TempPA = TempPA + 2 * Pi
        End If
        'To handle if they are out of phase by 180 degrees...
        If (TempPA) > Pi Then
            TempPA = TempPA - Pi
        End If
    End If
    Solution(UBound(Solution)) = TempPA

End Sub

Function Magnitude(Real As Double, Imaginary As Double) As Double
    'This finds the magnitue in complex space.
    Magnitude = (Real ^ 2 + Imaginary ^ 2) ^ 0.5
End Function

Function Angle(Real As Double, Imaginary As Double) As Double
    'Finds the angle in complex space.
    Angle = WorksheetFunction.Atan2(Real, Imaginary)
End Function

Public Function GetArea(C1 As Integer, C2 As Integer) As Double
    'This finds the area within the average stress-strain loop.
    '
    'D.J. Swan
    'October 2001.
    Dim Data1() As Double
    Dim Count As Long
    Dim j As Integer
    Dim Area As Double
    Dim Cycles As Long

    Cycles = WorksheetFunction.RoundDown(UBound(AllData, C1) * Frequency /
Module3.SampleRate, 0)

    Count = Cycles * Module3.SampleRate / Module2.Frequency
    ReDim Data1(1 To 2, 1 To Count)

    Area = 0
    For i = 1 To Count - 1
        j = i + 1
        Area = Area + Module3.AllData(C1, i) * Module3.AllData(C2, j)
        Area = Area - Module3.AllData(C1, j) * Module3.AllData(C2, i)
    Next i
    Area = Area + Module3.AllData(C1, Count) * Module3.AllData(C2, 1)
    Area = Area - Module3.AllData(C1, 1) * Module3.AllData(C2, Count)
```

```
    GetArea = Abs(Area / 2) / Cycles

End Function

Sub Regression()
    'This function uses a linear regression similar to the
    'Minnesota Method.
    'It will find the least square regression solution to fit
    'a sinusoid shape on a polynomial of degree N.
    '
    'D.J. Swan
    'Sept 24, 2001
    Dim AArray() As Double
    Dim BArray() As Double
    Dim N As Integer
    Dim MaxExponent As Integer
    Dim Pi As Double
    Dim TempArray() As Double
    Dim Temp1 As Double
    Dim Temp2 As Double


    Pi = WorksheetFunction.Pi()
    MaxExponent = PolyNum + 1   'This is the number of terms in the polynmial
                                'that is to be used.  (2=Linear).
    N = MaxExponent + 2

    ReDim AArray(1 To N, 1 To N)
    ReDim BArray(1 To N)
    ReDim TempArray(1 To N, 1 To N)
    ReDim Solution(1 To N)

    'Start with zero values...
    For i = 1 To N
        For j = 1 To N
            AArray(i, j) = 0
        Next j
        BArray(i) = 0
    Next i

    'Generate Matrix...
    For i = 1 To UBound(Data())
        For j = 1 To MaxExponent
            For k = j To MaxExponent
                AArray(j, k) = AArray(j, k) + Time(i) ^ (j + k - 2)
```

```
            Next k
            AArray(j, N - 1) = AArray(j, N - 1) + Time(i) ^ (j - 1) * Cos(2 * Pi * Frequency *
Time(i))
            AArray(j, N) = AArray(j, N) + Time(i) ^ (j - 1) * Sin(2 * Pi * Frequency *
Time(i))
            BArray(j) = BArray(j) + Time(i) ^ (j - 1) * Data(i)
        Next j
        AArray(N - 1, N - 1) = AArray(N - 1, N - 1) + Cos(2 * Pi * Frequency * Time(i)) ^
2
        AArray(N - 1, N) = AArray(N - 1, N) + Cos(2 * Pi * Frequency * Time(i)) * Sin(2 *
Pi * Frequency * Time(i))
        AArray(N, N) = AArray(N, N) + Sin(2 * Pi * Frequency * Time(i)) ^ 2
        BArray(N - 1) = BArray(N - 1) + Cos(2 * Pi * Frequency * Time(i)) * Data(i)
        BArray(N) = BArray(N) + Sin(2 * Pi * Frequency * Time(i)) * Data(i)

    Next i
    'Fill in the bottom half of the matrix.
    For i = 2 To N
        For j = 1 To (i - 1)
            AArray(i, j) = AArray(j, i)
        Next j
    Next i

    'Invert the matrix
    For i = 1 To N
        For j = 1 To N
            TempArray(j, i) =
WorksheetFunction.Index(WorksheetFunction.MInverse(AArray()), i, j)
        Next j
    Next i
    'Multiply for the solution.
    For i = 1 To N
            Solution(i) = WorksheetFunction.Index(WorksheetFunction.MMult(BArray(),
TempArray()), i)
    Next i
    Temp1 = Solution(UBound(Solution) - 1)
    Temp2 = Solution(UBound(Solution))
    Solution(UBound(Solution) - 1) = Magnitude(Temp1, Temp2)
    Solution(UBound(Solution)) = Angle(Temp1, Temp2)
    Call RSquare
    Call WriteEquation
End Sub

Public Sub RSquare()
    'This procedure will calculate the R^2 statistics value for one the
    'linear regression or Minnesota Method curve fit...
```

```
    '
    'D.J. Swan
    'Dec. 16, 2001
    Dim N As Long
    Dim M As Long
    Dim SSR As Double
    Dim SST As Double
    Dim YAverage As Double
    Dim YHat As Double

    M = UBound(Solution())
    N = UBound(Data())

    SSR = 0
    SST = 0
    YAverage = 0

    'Get average
    For i = 1 To N
        YAverage = YAverage + Data(i)
    Next i
    YAverage = YAverage / N

    For i = 1 To N
        'Get predicted value for step i
        YHat = 0
        For j = 1 To M - 2
            YHat = YHat + Solution(j) * Time(i) ^ (j - 1)
        Next j
        YHat = YHat + Solution(M - 1) * Cos(2 * Pi * Frequency * Time(i) - Solution(M))
        SSR = SSR + (YHat - YAverage) ^ 2
        SST = SST + (Data(i) - YAverage) ^ 2
    Next i
    RSqu(Signal) = SSR / SST

End Sub


Public Sub WriteEquation()
    'This procedure writes out the complete equation of the regression.
    '
    'D.J. Swan
    'March 23, 2002
    Dim N As Integer

    N = UBound(Solution)
```

```
    If Signal = 1 Then
        Equations(Signal) = "s0(t) = "
    ElseIf Signal = 2 Then
        Equations(Signal) = "LVDT 1:  e0(t) = "
    ElseIf Signal = 3 Then
        Equations(Signal) = "LVDT 2:  e0(t) = "
    End If
    If N > 2 Then
        Equations(Signal) = Equations(Signal) & Format(Solution(1), "0.000E+00")
    End If
    If N > 3 Then
        For i = 2 To N - 2
            If Solution(i) < 0 Then
                Equations(Signal) = Equations(Signal) & " - "
            Else
                Equations(Signal) = Equations(Signal) & " + "
            End If
            Equations(Signal) = Equations(Signal) & Format(Abs(Solution(i)), "0.000E+00")
& "*t" & (i - 1)
        Next i
    End If
    If N > 2 Then
        If Solution(N - 1) < 0 Then
            Equations(Signal) = Equations(Signal) & " - "
        Else
            Equations(Signal) = Equations(Signal) & " + "
        End If
    End If
    Equations(Signal) = Equations(Signal) & Format(Abs(Solution(N - 1)), "0.000E+00")
& "*Cos(" & Frequency & "*t*360" & Chr$(176) & " - " & Format(Solution(N) * 180 /
Pi, "0.00") & Chr$(176) & ")"
    Equations(Signal) = Equations(Signal) & " [R2=" & Format(RSqu(Signal), "0.000") &
"]"
End Sub
```

4. Module 3

```
'This module is for solving complex modulus test using the userforms.
Public Frequency As Double              'This value is set in Userform1
Public Angular_Frequency As Double      'Alpha = 2 * Pi * F
Public Sensors(1 To 3, 1 To 4) As Double
Public Pi As Double
Public TimeShift As Double
Public BenchMark As Boolean
Public SampleRate As Double
Public AllData() As Double              'This will read in all information to be processed.
```

```
Public Time_C As String
Public Sensor1_C As String
Public Sensor2_C As String
Public Sensor3_C As String
Public NumberOfCycles As Integer

Public Sub Start()
   Call Module1.Setup
   UserForm1.Status.Caption = ""
   Call UserForm1.Interface
End Sub


Public Sub Complex_Modulus()
   'This Macro will actually get the Rquired numbers for the Triaxial Output.
   '
   'D.J. Swan
   'March 27, 2001
   Dim Repeat As Long
   Dim SheetName As String
   Dim PercentComplete
   Dim DelayTime As Double
   Dim RepeatNo As Integer

   Application.ScreenUpdating = False
   DelayTime = 10 / Module2.Frequency
   RepeatNo = WorksheetFunction.RoundDown((UserForm1.Stop_Time -
UserForm1.Start_Time) / DelayTime, 0)
   NumberOfCycles = 10 * RepeatNo
   UserForm1.Stop_Time = UserForm1.Start_Time + DelayTime

   SheetName = ActiveSheet.Name
   Pi = WorksheetFunction.Pi()

   For Repeat = 1 To RepeatNo

      BenchMark = False

      'Read the data selected from Userform1
      Call ReadAllData(Time_C, Sensor1_C, Sensor2_C, Sensor3_C,
UserForm1.Start_Row)

      'Calculate some sampling constants
      Module2.Angular_Frequency = 2 * Pi * Module2.Frequency   'Changes Frequency
into Angular Frequency
```

```
        SampleRate = (UBound(AllData, 2) - 1) / (AllData(1, UBound(AllData, 2)) -
AllData(1, 1))

        'Define the Load/Stress Curve (Sensor 1)
        BenchMark = True
        Call Get_Data(1, 2)
        Module2.Signal = 1
        Call Module2.Calculate
        Sensors(1, 1) = Module2.Solution(1)
        Sensors(1, 2) = Module2.Solution(2)
        Sensors(1, 3) = Module2.Solution(UBound(Solution()) - 1)
        Sensors(1, 4) = Module2.Solution(UBound(Solution()))

        'This finds the phase lag for the other sensors
        Pi = WorksheetFunction.Pi()
        BenchMark = False
        For i = 1 To 2
          Call Get_Data(1, 2 + i)
          Module2.Signal = i + 1
          Call Module2.Calculate
          Sensors(i + 1, 1) = Module2.Solution(1)
          Sensors(i + 1, 2) = Module2.Solution(2)
          Sensors(i + 1, 3) = Module2.Solution(UBound(Solution()) - 1)
          Sensors(i + 1, 4) = Module2.Solution(UBound(Solution()))
        Next i

        Call Triaxial_Output

        UserForm1.Start_Time = UserForm1.Start_Time + DelayTime
        UserForm1.Stop_Time = UserForm1.Stop_Time + DelayTime
        Worksheets(SheetName).Activate
        'This provides an update as to the approximate amount done.
        PercentComplete = WorksheetFunction.RoundDown(Repeat / RepeatNo * 100, 0)
        UserForm1.Status = Str$(PercentComplete) & "% Complete"
        UserForm1.Repaint
    Next Repeat

    Call TitleOutput
    Call Module1.OutputPage
    Range("A1").Activate
    Worksheets(SheetName).Activate
    Application.ScreenUpdating = True

End Sub

Public Sub TitleOutput()
```

```
Worksheets("Output").Activate

Range("A2").Value = "Start Time"
Range("B2").Value = "Stop Time"
Range("C2").Value = "Average Time"
Range("D2").Value = "s0"
Range("E2").Value = "e0"
Range("F2").Value = "d"
Range("G2").Value = "s0"
Range("H2").Value = "e0"
Range("I2").Value = "d"
Range("J2").Value = "s0"
Range("K2").Value = "e0"
Range("L2").Value = "d"
Range("M2").Value = "|E*|"
Range("N2").Value = "E'"
Range("O2").Value = "E""

Range("D1").Value = "LVDT 1"
Range("D1:F1").Merge
Range("G1").Value = "LVDT 2"
Range("G1:I1").Merge
Range("J1").Value = "Complex Modulus"
Range("J1:O1").Merge

Range("D2").Select
ActiveCell.FormulaR1C1 = "s0"
With ActiveCell.Characters(Start:=1, Length:=1).Font
   .Name = "Symbol"
End With
With ActiveCell.Characters(Start:=2, Length:=1).Font
   .Subscript = True
End With

Range("E2").Select
ActiveCell.FormulaR1C1 = "e0"
With ActiveCell.Characters(Start:=1, Length:=1).Font
   .Name = "Symbol"
End With
With ActiveCell.Characters(Start:=2, Length:=1).Font
   .Subscript = True
End With

Range("F2").Select
ActiveCell.FormulaR1C1 = "d"
```

```
With ActiveCell.Characters(Start:=1, Length:=1).Font
   .Name = "Symbol"
End With

Range("G2").Select
ActiveCell.FormulaR1C1 = "s0"
With ActiveCell.Characters(Start:=1, Length:=1).Font
   .Name = "Symbol"
End With
With ActiveCell.Characters(Start:=2, Length:=1).Font
   .Subscript = True
End With

Range("H2").Select
ActiveCell.FormulaR1C1 = "e0"
With ActiveCell.Characters(Start:=1, Length:=1).Font
   .Name = "Symbol"
End With
With ActiveCell.Characters(Start:=2, Length:=1).Font
   .Subscript = True
End With

Range("I2").Select
ActiveCell.FormulaR1C1 = "d"
With ActiveCell.Characters(Start:=1, Length:=1).Font
   .Name = "Symbol"
End With

Range("J2").Select
ActiveCell.FormulaR1C1 = "s0"
With ActiveCell.Characters(Start:=1, Length:=1).Font
   .Name = "Symbol"
End With
With ActiveCell.Characters(Start:=2, Length:=1).Font
   .Subscript = True
End With

Range("K2").Select
ActiveCell.FormulaR1C1 = "e0"
With ActiveCell.Characters(Start:=1, Length:=1).Font
   .Name = "Symbol"
End With
With ActiveCell.Characters(Start:=2, Length:=1).Font
   .Subscript = True
End With
```

```
    Range("L2").Select
    ActiveCell.FormulaR1C1 = "d"
    With ActiveCell.Characters(Start:=1, Length:=1).Font
        .Name = "Symbol"
    End With

    Range("A1:O2").Select
    Selection.Font.Bold = True
    Columns("A:A").EntireColumn.AutoFit
    Columns("B:B").EntireColumn.AutoFit
    Columns("C:C").EntireColumn.AutoFit
    Columns("A:C").Select
    Selection.NumberFormat = "0.000"
    Columns("A:O").Select
    With Selection
        .HorizontalAlignment = xlCenter
    End With

End Sub

Public Sub Triaxial_Output()
    'This outputs the results of the algorithms.
    'This also calculates several common complex modulus
    'values.
    '
    'D.J. Swan
    'March 27, 2001
    Dim Pi As Double

    Pi = WorksheetFunction.Pi()
    Worksheets("Output").Activate

    Range("3:3").Insert
    Range("3:3").Font.Bold = False

    'Display Time
    Range("A3").Value = AllData(1, 1)
    Range("B3").Value = AllData(1, UBound(AllData, 2))
    Range("C3").Value = (AllData(1, 1) + AllData(1, UBound(AllData, 2))) / 2

    'Compex Modulus
    Range("D3").Value = Abs(Sensors(1, 3)) * 2
    Range("E3").Value = Abs(Sensors(2, 3)) * 2
    Range("F3").Value = Sensors(2, 4) * 180 / Pi
    Range("G3").Value = Abs(Sensors(1, 3)) * 2
    Range("H3").Value = Abs(Sensors(3, 3)) * 2
```

```
    Range("I3").Value = Sensors(3, 4) * 180 / Pi
    Range("J3").Value = Abs(Sensors(1, 3)) * 2
    Range("K3").Value = "=average(E3,H3)"
    Range("L3").Value = "=average(F3,I3)"
    Range("M3").Value = "=J3/K3"
    Range("N3").Value = "=M3*cos(radians(L3))"
    Range("O3").Value = "=M3*sin(radians(L3))"

End Sub

Public Sub ReadAllData(C1 As String, C2 As String, C3 As String, C4 As String,
Start_Row As String)
    'This subroutine will read in all information from the data file.
    '
    'Written by D.J. Swan
    'August 8, 2001
    Dim Current_Row As Long
    Dim Current_Cell As String
    Dim Item_Count As Long

    'Modify these parameters depending on data format.
    'This data sets up the required parameters
    Current_Row = Start_Row
    Current_Cell = C1 & Current_Row
    Item_Count = 0

    'This loops until we are out of data.
    Do While Range(Current_Cell).Value <> "" And Range(Current_Cell).Value <=
UserForm1.Stop_Time
        If Range(Current_Cell).Value >= UserForm1.Start_Time And
Range(Current_Cell).Value <= UserForm1.Stop_Time Then
            Item_Count = Item_Count + 1
            ReDim Preserve AllData(1 To 4, 1 To Item_Count)
            AllData(1, Item_Count) = Range(C1 & Current_Row).Value
            AllData(2, Item_Count) = Range(C2 & Current_Row).Value
            AllData(3, Item_Count) = Range(C3 & Current_Row).Value
            AllData(4, Item_Count) = Range(C4 & Current_Row).Value
        End If
        If Range(Current_Cell).Value < UserForm1.Start_Time Then
            UserForm1.Start_Row = Current_Row
        End If
        Current_Row = Current_Row + 1
        Current_Cell = C1 & Current_Row

    Loop
```

```
End Sub

Public Sub Get_Data(C1 As Integer, C2 As Integer)
    'This procedure sets up two columns for use in Module2 calcs...
    '
    'Written by D.J. Swan
    'August 8, 2001
    Dim ItemCount As Long

    ItemCount = UBound(AllData, 2)
    ReDim Module2.Time(1 To ItemCount)
    ReDim Module2.Data(1 To ItemCount)

    For i = 1 To ItemCount
        Module2.Time(i) = AllData(C1, i)
        Module2.Data(i) = AllData(C2, i)
    Next i
End Sub
```

A.4 Torsional Complex Modulus Program

Modify of stresses and strain calculation in Module 1 of previous program:

```
Sub Setup()
    'This procedure will arrange the laboratory data output
    'into a format that is readable by the analysis software.
    'It also will add the required "Output" worksheet.
    '
    'D.J. Swan
    'August 10, 2001
    Dim OrigName As String
    Dim RowCount As Integer
    Dim EndRow As String
    Dim StartRow As String
    Dim Pi As Double
    Dim Lo As Double
    Dim Ro As Double
    Dim Jp As Double

    Application.ScreenUpdating = False
    Pi = WorksheetFunction.Pi()


    Range("I4").Value = "Time (sec)"
    Range("I6").Formula = "=(A6-$A$6)/1000"
```

```
    Range("J4").Value = "Torsional Stress (MPa)"
    Range("J6").Formula = "=ABS(C6-$C$6)*50/(Pi()/2*50^4)"
    Range("K4").Value = "Torsional Strain 1"
    Range("K6").Formula = "=ABS(D6-$D$6)*50/107.68/150"
    Range("L4").Value = "Torsional Strain 2"
    Range("L6").Formula = "=ABS(E6-$E$6)*50/107.68/150"

    Selection.Copy
    RowCount = 6
    StartRow = "A6"

    Do While Range(StartRow) <> ""
        RowCount = RowCount + 1
        StartRow = "A" & RowCount

    Loop
    RowCount = RowCount - 1
    EndRow = "L" & RowCount
    Range("I6:L6").Select
    Selection.AutoFill Destination:=Range("I6" & ":" & EndRow)

    Range("4:4").Font.Bold = True
    Columns("A:L").EntireColumn.AutoFit
    Range("B6").Activate
    ActiveWindow.FreezePanes = True

    OrigName = ActiveSheet.Name
    Worksheets.Add
    ActiveSheet.Name = "Output"
    Worksheets(OrigName).Activate
    Application.ScreenUpdating = True
End Sub
```

APPENDIX B
DESCRIPTION OF SUPERPAVE IDT
COMPLEX MODULUS PROGRAM

The complex modulus data file has to follow a predefined data format. A visualized procedure has been developed that guides the user through the process of obtaining information and properly interpreting data from the complex modulus test using indirect tension test (IDT).

1. Data Format

In order for the software to properly interpret data, six input data fields are required, namely, two strains from horizontal strain gages, two strains from vertical gages, force, and time. During the complex modulus test, 50 data points are recommended in each cycle. 100 loading cycles are recommended at a given frequency.

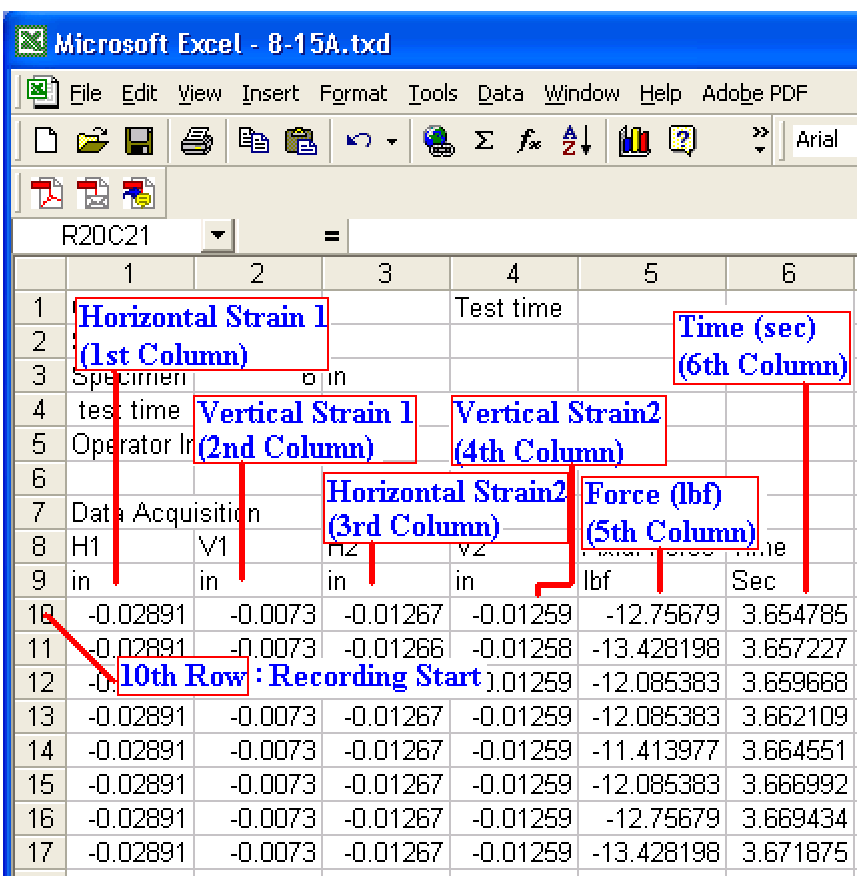

2. File Extension Name and Data Location

Change the extension name to 'txd' and then save into ITLT_dynamic\data folder.

Example: I75-1C.data → I75-1C.txd

3. Report_generator.xls

In the ITLT_dynamic folder, there are four files. Among them, open the 'Report_generator' file with Excel (Note: the computer will ask whether you allow the file to open or not because the program includes a macro. Click 'enable macro'.), and then click 'ctrl+z'. This function eliminates unnecessary lines that might be included in data. When you store the analyzed data, leave the file format as text.

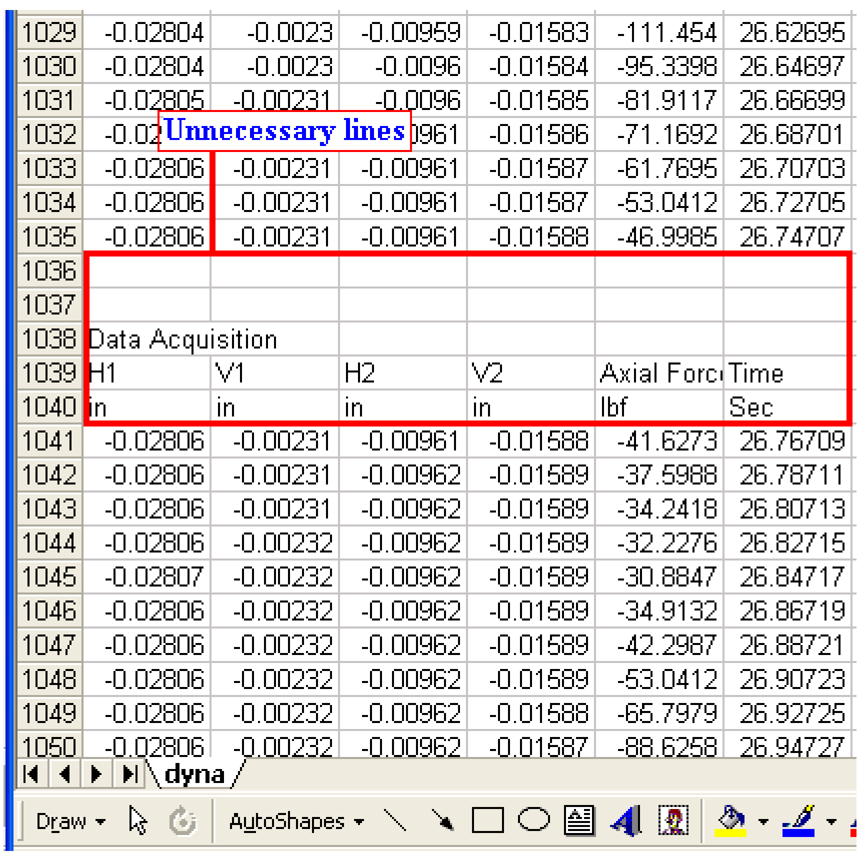

1029	-0.02804	-0.0023	-0.00959	-0.01583	-111.454	26.62695
1030	-0.02804	-0.0023	-0.0096	-0.01584	-95.3398	26.64697
1031	-0.02805	-0.00231	-0.0096	-0.01585	-81.9117	26.66699
1032	-0.02[illegible]	[illegible]	[illegible]961	-0.01586	-71.1692	26.68701
1033	-0.02806	-0.00231	-0.00961	-0.01587	-61.7695	26.70703
1034	-0.02806	-0.00231	-0.00961	-0.01587	-53.0412	26.72705
1035	-0.02806	-0.00231	-0.00961	-0.01588	-46.9985	26.74707
1036						
1037						
1038	Data Acquisition					
1039	H1	V1	H2	V2	Axial Forc	Time
1040	in	in	in	in	lbf	Sec
1041	-0.02806	-0.00231	-0.00961	-0.01588	-41.6273	26.76709
1042	-0.02806	-0.00231	-0.00962	-0.01589	-37.5988	26.78711
1043	-0.02806	-0.00231	-0.00962	-0.01589	-34.2418	26.80713
1044	-0.02806	-0.00232	-0.00962	-0.01589	-32.2276	26.82715
1045	-0.02807	-0.00232	-0.00962	-0.01589	-30.8847	26.84717
1046	-0.02806	-0.00232	-0.00962	-0.01589	-34.9132	26.86719
1047	-0.02806	-0.00232	-0.00962	-0.01589	-42.2987	26.88721
1048	-0.02806	-0.00232	-0.00962	-0.01589	-53.0412	26.90723
1049	-0.02806	-0.00232	-0.00962	-0.01588	-65.7979	26.92725
1050	-0.02806	-0.00232	-0.00962	-0.01587	-88.6258	26.94727

4. Parameter.exe

In the ITLT_dynamic folder, there are four files. Among them, is the executable file 'Parameters.exe' which provides the input frame. Click onto 'Parameters.exe', and fill out the specimen information and testing conditions, and then click onto the 'Run' command button. Make sure that you do not leave any blanks. The following example guides you through the input process. In addition, if you want to input the Poisson's ratio manually, fill out the right side of the input frame.

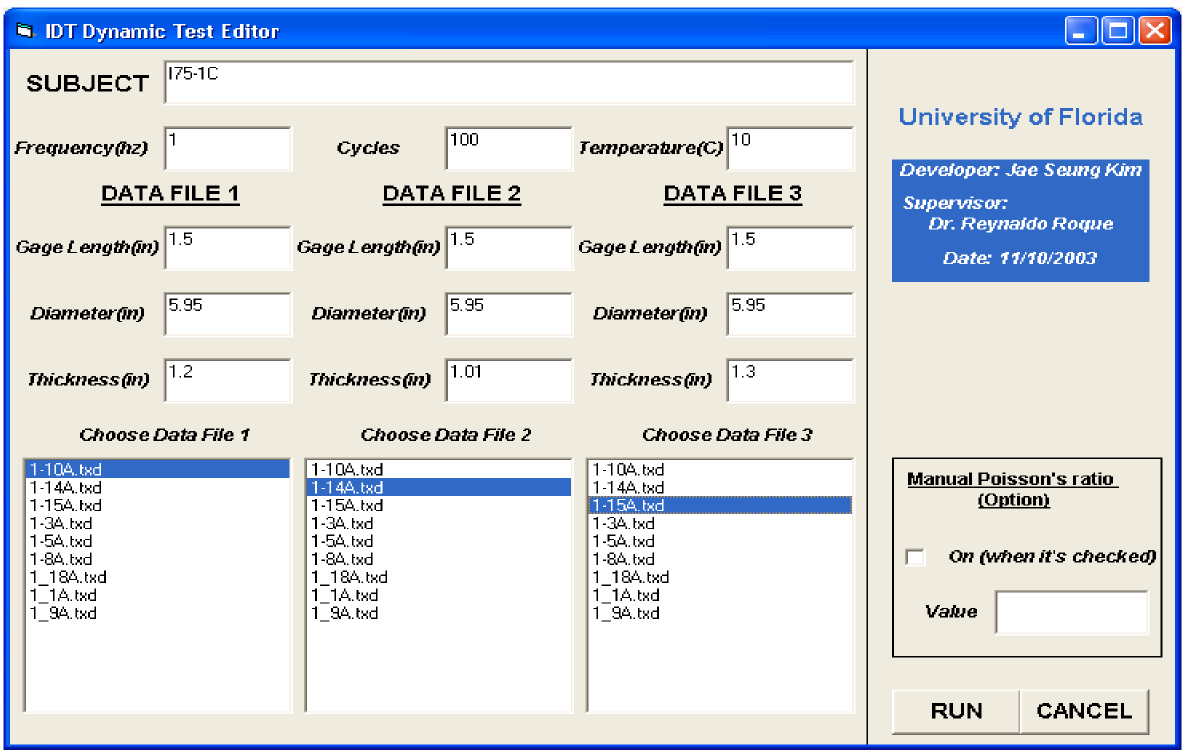

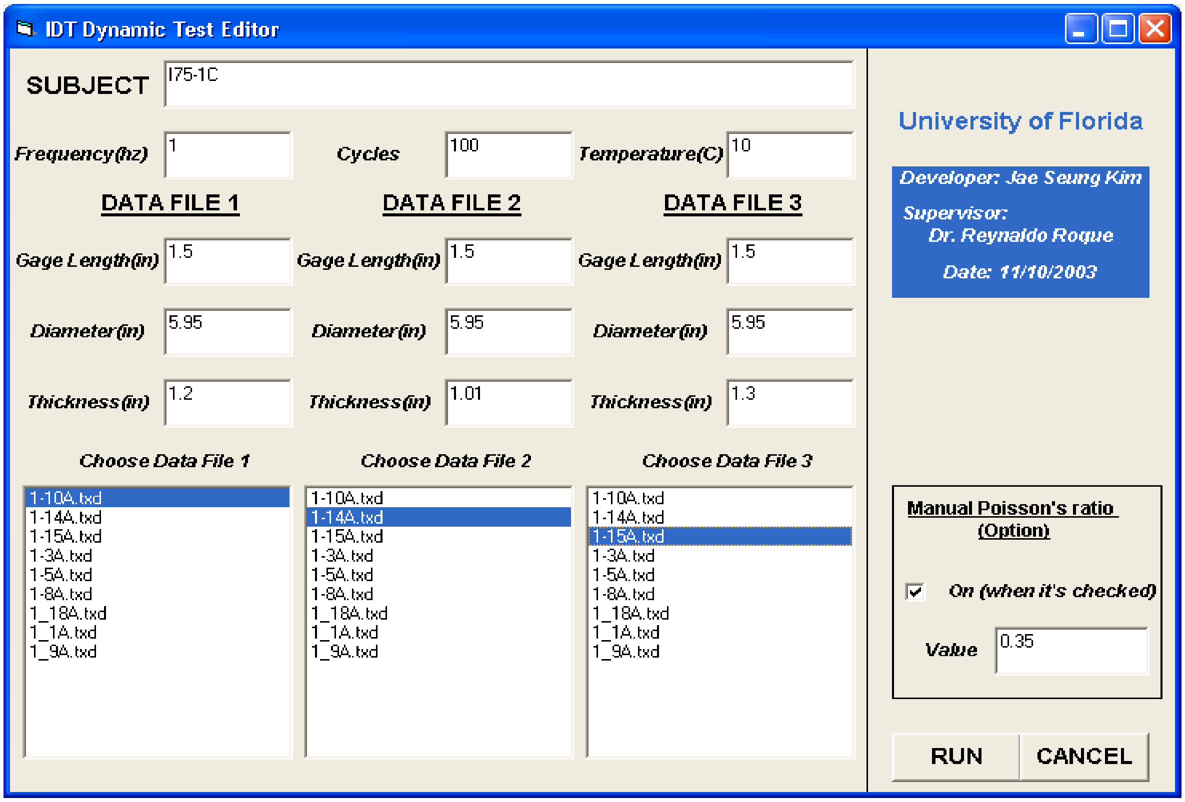

5. ITLT_dynamic.exe

In the ITLT_dynamic folder, there are four files. Among them is the 'ITLT_dynamic.exe' file, which is the executable program for calculating the parameter, phase angle, dynamic modulus (|E*|), storage modulus (E′), and loss modulus (E″) from complex modulus test. This program was directly connected with the 'Parameter.exe' program, so you do not need to run it again. You can get the output file from ITLT_dynamic\out folder. The extension name will be '~.dym'.

1-10A.dym
****

Total Number of Mixtures in Experiment = 3
Test Data Path = C:\Documents and Settings\Owner\Desktop\ITLT_dynamic\data

****

Name of Specimen = I75-1C

****

*********** DYNAMIC PARAMETERS **********

HORIZONTAL DYNAMIC PARAMETERS

CYCLES	PHASE ANGLE(deg)	|E*|(psi)	E'(psi)	E"(psi)
100	13.11	1492306	1453382	338612

VERTICAL DYNAMIC PARAMETERS

CYCLES	PHASE ANGLE(deg)	|E*|(psi)	E'(psi)	E"(psi)
100	12.35	1537487	1501920	328789

CYCLES		POISSON'S RATIO
100	CALCULATED:	0.36
	USED:	0.36

NORMALIZED DEFORMATIONS(micro-strain)

CYCLES	FACE	HI	FACE	VI
100	5	47	5	97
	*6	52	*6	102
	*4	66	*3	105
	*2	67	*2	122
	*1	72	*1	128
	3	76	4	150

(*) - Faces used to calculate Poissons Ratio

NORMALIZED PHASE ANGLES(degree)

CYCLES	FACE	HI	FACE	VI
100	5	10.54	5	8.82
	*1	11.35	*2	10.10
	*2	12.16	*1	12.87
	*6	14.19	*4	12.88
	*4	14.75	*6	13.54
	3	20.70	3	22.00

(*) - Faces used to calculate Phase angle

DISSIPATED ENERGY PER CYCLE

2.077636e-003 (lbf*in/in^3)
1.432480e-002 (KJ/m^3)

PROPERTIES OF SPECIMENS

	SPECIMEN 1	SPECIMEN 2	SPECIMEN 3
FILE NAME	1-10A.txd	1-14A.tx	1-15A.txd
FRIQUENCY(hz)	1.00	1.00	1.00
TEMPERATURE(C)	10	10	10
DIAMETERS(inches)	5.95	5.95	5.95
THICKNESSES(inches)	1.20	1.01	1.30
STRESS(lbf)		65.95	
STRAIN(microstrain)		44.19	

6. Dyna_history.exe

This program provides the following parameters versus number of loading cycles: phase angle, |E*|, E′, and E″. It divides tested data into 10 sets of data and provides complex moduli in each set of data point. Click onto ‘Dyna_history.exe’, which is among four files in ITLT_dynamic folder, and move to ITLT_dynamic\out folder, and then you can get the following output file. The extension name will be ‘~.dyh’.

****

Total Number of Mixtures in Experiment = 3
Test Data Path = C:\Documents and Settings\Owner\Desktop\ITLT_dynamic\data

****

Name of Specimen = I75-1C

****

*********** DYNAMIC PARAMETERS **********

HORIZONTAL DYNAMIC PARAMETERS

CYCLES	PHASE ANGLE(deg)	|E*|(psi)	E'(psi)	E"(psi)
1	14.08	1496067	1451117	363971
11	12.83	1463586	1427055	324959
21	13.87	1467801	1424976	351968
31	14.05	1481471	1437155	359640
41	13.72	1460701	1419006	346507
51	13.47	1489292	1448347	346818
61	13.19	1475297	1436366	336681
71	12.48	1486494	1451368	321244
81	13.34	1476703	1436887	340598
91	12.03	1475142	1442772	307335

VERTICAL DYNAMIC PARAMETERS

CYCLES	PHASE ANGLE(deg)	|E*|(psi)	E'(psi)	E"(psi)
1	12.74	1541215	1503243	340003
11	12.65	1507924	1471299	330324
21	12.39	1512267	1477036	324525
31	12.51	1526330	1490110	330538
41	12.64	1504933	1468457	329330
51	12.78	1533540	1495525	339339
61	12.29	1519984	1485152	323536
71	12.32	1531427	1496182	326663
81	12.14	1521440	1487394	320062
91	12.36	1519805	1484599	325226

CYCLES		POISSON'S RATIO
1	CALCULATED:	0.37
	USED:	0.37
11	CALCULATED:	0.35
	USED:	0.35

21	CALCULATED:	0.35
	USED:	0.35
31	CALCULATED:	0.36
	USED:	0.36
41	CALCULATED:	0.34
	USED:	0.34
51	CALCULATED:	0.31
	USED:	0.31
61	CALCULATED:	0.35
	USED:	0.35
71	CALCULATED:	0.36
	USED:	0.36
81	CALCULATED:	0.35
	USED:	0.35
91	CALCULATED:	0.34
	USED:	0.34

NORMALIZED DEFORMATIONS(micro-strain)

CYCLES	FACE	HI	FACE	VI
1	5	49	5	93
	*6	54	*3	104
	*2	66	*6	106
	*1	68	*2	121
	*4	72	*1	127
	3	76	4	149
11	5	48	5	95
	*6	52	*6	105
	*2	65	*3	108
	*4	68	*2	122
	*1	72	*1	128
	3	76	4	149
21	5	48	5	96
	*6	52	*6	105
	*2	65	*3	107
	*4	67	*2	122
	*1	73	*1	128
	3	77	4	150
31	5	48	5	96
	*6	53	*6	104
	*2	65	*3	107
	*4	70	*2	121

	*1	70	*1	127
	3	75	4	150
41	5	47	5	96
	*6	52	*6	105
	*2	66	*3	107
	*4	68	*2	123
	*1	70	*1	128
	3	77	4	151
51	5	47	3	87
	*6	51	*5	96
	*4	55	*6	104
	*3	63	*4	122
	*2	66	*2	123
	1	72	1	128
61	5	47	5	97
	*6	51	*6	104
	*2	66	*3	106
	*4	68	*2	123
	*1	72	*1	128
	3	78	4	151
71	5	48	5	97
	*6	53	*6	103
	*2	67	*3	106
	*4	69	*2	122
	*1	71	*1	128
	3	75	4	151
81	5	46	5	97
	*6	52	*6	103
	*2	66	*3	106
	*4	66	*2	122
	*1	70	*1	128
	3	77	4	150
91	5	47	5	97
	*6	52	*6	102
	*2	65	*3	105
	*4	66	*2	122
	*1	70	*1	128
	3	76	4	150

(*) - Faces used to calculate Poissons Ratio

NORMALIZED PHASE ANGLES(degree)

CYCLES	FACE	HI	FACE	VI
1	5	10.70	5	9.83
	*2	12.18	*2	10.64
	*1	12.68	*1	12.84
	*6	14.99	*4	13.39
	*4	16.47	*6	14.11
	3	23.44	3	23.94
11	5	11.08	5	9.35
	*1	11.28	*2	10.64
	*2	12.07	*1	12.93
	*6	13.25	*4	13.28
	*4	14.71	*6	13.77
	3	21.86	3	22.88
21	5	10.43	5	9.39
	*2	13.07	*2	10.25
	*1	13.34	*1	12.38
	*6	14.22	*4	13.15
	*4	14.87	*6	13.79
	3	22.16	3	22.42
31	5	12.09	5	9.10
	*1	12.76	*2	10.38
	*2	13.24	*1	12.76
	*6	14.16	*4	13.00
	*4	16.03	*6	13.89
	3	21.39	3	22.72
41	5	10.94	5	9.38
	*2	12.65	*2	10.51
	*6	13.27	*1	12.89
	*1	13.33	*4	13.31
	*4	15.64	*6	13.85
	3	21.66	3	22.71
51	5	10.41	5	9.28
	*1	11.68	*2	10.50
	*2	12.26	*1	13.06
	*6	13.98	*4	13.66
	*4	15.94	*6	13.91
	3	22.27	3	22.47

61	5	9.82	5	8.92
	*1	12.01	*2	9.95
	*2	12.23	*1	12.61
	*6	13.40	*4	12.91
	*4	15.12	*6	13.68
	3	20.74	3	21.93
71	5	10.60	5	8.86
	*6	10.61	*2	10.15
	*2	12.22	*4	12.60
	*1	12.42	*1	12.61
	*4	14.67	*6	13.90
	3	19.53	3	21.92
81	5	8.68	5	9.09
	*2	11.40	*2	10.35
	*1	12.97	*4	12.47
	*6	14.40	*1	12.48
	*4	14.58	*6	13.28
	3	20.27	3	21.64
91	5	9.56	5	8.89
	*1	11.32	*2	10.17
	*2	11.45	*1	12.40
	*6	12.24	*4	12.99
	*4	13.09	*6	13.87
	3	20.54	3	22.04

(*) - Faces used to calculate Phase angle

CYCLES	DISSIPATED ENERGY PER CYCLE
1	2.303682e-003 (lbf*in/in^3)
	1.588333e-002 (KJ/m^3)
11	1.998320e-003 (lbf*in/in^3)
	1.377794e-002 (KJ/m^3)
21	2.159466e-003 (lbf*in/in^3)
	1.488900e-002 (KJ/m^3)
31	2.232863e-003 (lbf*in/in^3)
	1.539505e-002 (KJ/m^3)
41	2.113871e-003 (lbf*in/in^3)
	1.457463e-002 (KJ/m^3)
51	1.813679e-003 (lbf*in/in^3)
	1.250488e-002 (KJ/m^3)

61	2.087679e-003 (lbf*in/in^3)
	1.439404e-002 (KJ/m^3)
71	2.033886e-003 (lbf*in/in^3)
	1.402316e-002 (KJ/m^3)
81	2.076466e-003 (lbf*in/in^3)
	1.431674e-002 (KJ/m^3)
91	1.832621e-003 (lbf*in/in^3)
	1.263548e-002 (KJ/m^3)

PROPERTIES OF SPECIMENS

	SPECIMEN 1	SPECIMEN 2	SPECIMEN 3
FILE NAME	1-10A.txd	1-14A.txd	1-15A.txd
FRIQUENCY(hz)	1.00	1.00	1.00
TEMPERATURE(C)	10	10	10
DIAMETERS(inches)	5.95	5.95	5.95
THICKNESSES(inches)	1.20	1.01	1.30

APPENDIX C
PERFORMANCE TEST DATABASE

C.1 General Description

The database is in written in Microsoft Access, and currently includes:

- Mixture Name
- Mixture Type
- Aggregate Type
- Aggregate Size Distribution
- Specimen Type (Field vs. Laboratory)
- Mixture Design Information
- Mixture Volumetrics
- Superpave IDT Test Results (Resilient Modulus, Creep Compliance, Creep Compliance Parameters, Strength, Fracture Energy, Complex Modulus)
- Triaxial Complex Modulus Test Results
- Other Performance Test Information

C.2 Importing Superpave IDT Test Data

In order to enter data into the database, the following procedure needs to be followed:

For Superpave IDT Test Results:

1) To enter values from the raw Superpave IDT test data files, an Excel macro was developed. The name of the Excel spreadsheet containing the Macro is: IDT11.xls. This macro automates input data from text file into Excel. Once data is in Excel, the user can paste the data directly into the Access database. To copy and paste the data into Access, a macro was also written, entitled “Copy” shown below. Hence, for input: use the “Input Button” – Get Data from Text file.

For copying and pasting, use “Copy Button” – Copy Data in Clip Board to make entries in Access Database

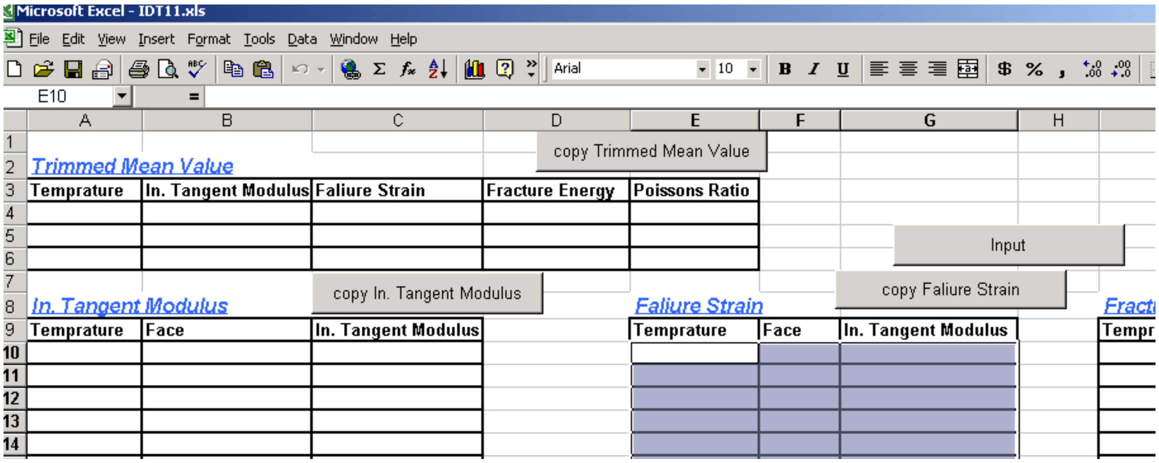

C.3 Entering Non-Superpave IDT Test Data

In order to enter Non-Superpave IDT Test Data Into Database, follow instructions below:

- To enter data in database, double click enable the Access database file
- Click on input
- To enter data click on right click button and then paste. Make sure that data is pasted in last line (See the figure below).

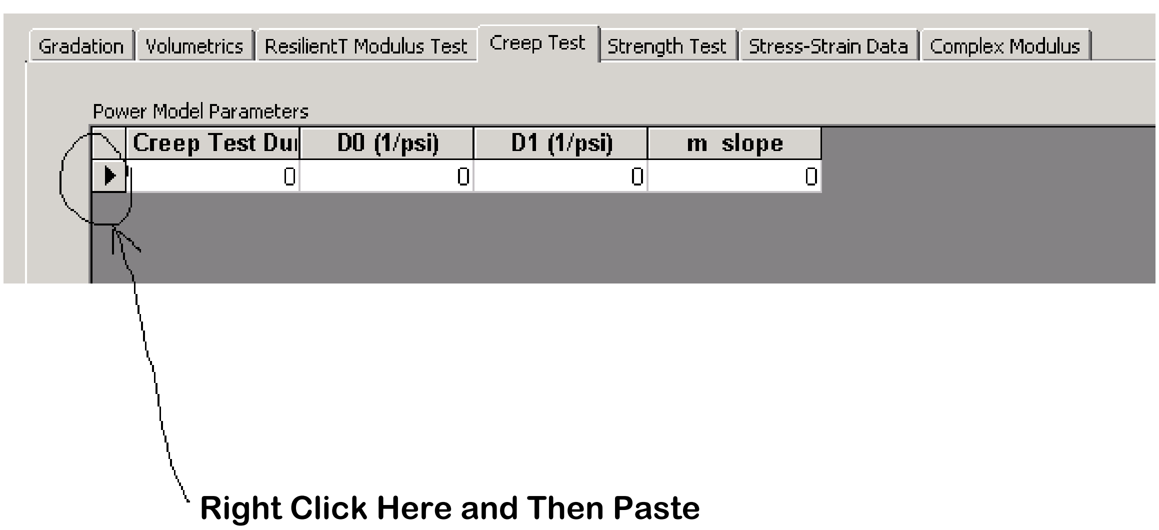

C.4 Perform Search

In order to request a search within the database, the user must specify the search criteria from the Windows-based menu below: